DESIGN, DEVELOPMENT AND OPTIMISATION OF A NOVEL THERMO-SYPHON SYSTEM FOR DOMESTIC APPLICATIONS

A THESIS SUBMITTED IN PARTIAL FULFILMENT OF THE REQUIREMENTS FOR THE DEGREE OF DOCTOR OF PHILOSOPHY AT THE UNIVERSITY OF HUDDERSFIELD

By

Basim Freegah
B.Eng. University of Technology, Baghdad, Iraq, 1998
M.Sc. University of Technology, Baghdad, Iraq, 2000

School of Computing and Engineering
University of Huddersfield
UK
August 2016

ABSTRACT

In order to decrease reliance on fossil fuels, renewable energy has become an important topic of research in recent years. The development in the renewable energy source will help in meeting the requirements of limiting greenhouse-gas effects, and conserve the environment from pollution, global warming, ozone layer depletion, etc. There are various naturally available renewable energy sources. One of these sources is solar energy. Solar energy is available in abundance throughout the world and is the cleanest of all known energy sources. There are various devices that can be used to harness solar energy. One of such devices is a thermo-syphon. Thermo-syphon converts the solar energy obtained from the Sun into thermal energy of a working fluid. This thermal energy in the working fluid can be used for various industrial and household activities. In a closed loop thermo-syphon system, the working fluid circulates within the thermo-syphon loop via natural convection phenomenon and does not need any external devices, such as a pump. Therefore, it is considered to be one of the most efficient devices for the heat transfer. Moreover, the absence of a pumping device reduces the manufacturing and maintenance costs of a thermo-syphon system.

The heat exchange process in the thermo-syphon is a complicated process, which considers the heat convection phenomenon. Therefore, to understand the natural convection process in the thermo-syphon and their effect on the thermal performance of the system a Computational Fluid Dynamics (CFD) based techniques have been used. Numerical results obtained have been verified against the experimental results, and they match closely with each other. The comparison between the CFD and experimental result, suggest that CFD can be used as an effective tool to analyse the performance of a thermo-syphon with reasonable accuracy. In order to investigate the flow structure within the thermo-syphon system, detailed qualitative and quantitative analyses have been carried out in the present study. The qualitative analysis of the flow field includes descriptions of the velocity magnitude and the static temperature distributions contours within the closed loop thermo-syphon system. Furthermore, the variation in the temperature of water within the storage tank, temperature of the working fluid, heat transfer coefficient, wall shear stress, and local velocity and temperature distribution of the working fluid within thermo-syphon loop have been quantified as a function of time. In addition, numerical studies have been conducted to identify the effects of various geometrical parameters, which include the number of the riser pipes, length-to-diameter ratio of the riser pipe on the thermal performance of a closed loop thermo-syphon system. Moreover, a further investigation has been carried out to analyse the effect of various heat flux conditions and different transient thermal loadings on the thermal performance of a closed loop thermo-syphon system. Based on these

analyses some novel semi-empirical relations have been developed to predict the thermal performance of the thermo-syphon, which is one of the focal points of this research.

Another goal of the current study is to improve the thermal performance characteristic of thermo-syphon solar water heating system using an enhancement device to improve the heat transfer. This aspect of the work focuses on the increasing energy conversion from the riser pipes to the working fluid within the thermo-syphon loop. This is accomplished by increasing the surface area of riser pipes by employing several design modifications, such as straight, wavy and helical pipes, within the riser pipes, while maintaining the amount of the working fluid constant within the closed loop thermo-syphon system. In this study, a comparative analysis has been carried out for these new design modifications to identify the best in terms of heat transfer coefficient, heat gain in collector etc., as an indication of thermal performance. According to the findings of this analysis, the model comprising of pipe inside the riser pipe depict better thermal performance as compared to other models. After defining the best design modification, a further detailed investigation has been carried out between the traditional and modified design (straight pipe inside the riser pipe) using experimental and numerical method.

Established methods regarding the design process of thermo-syphons are very limited, and they are severely limited in estimating important design parameters, such as useful heat gain and heat transfer coefficient, which have a significant impact on the thermal performance of thermo-syphon system/loop. A design methodology has been developed to enrich the design process of a closed loop thermo-syphon solar water heating system. The developed methodology is more efficient and reliable since it is capable of estimating various geometrical and thermal parameters, such as collector area, diameter and length of the riser pipes, distance between the centers of the riser pipes, heat transfer coefficient, temperature of the working fluid and the mass flow rate. This design methodology is user friendly and robust.

DECLARATION

- The author of this thesis (including any appendices and/or schedules to this thesis) owns any copyright in it (the "Copyright") and he has given The University of Huddersfield the right to use such Copyright for any administrative, promotional, educational and/or teaching purposes.

- Copies of this thesis, either in full or in extracts, may be made only in accordance with the regulations of the University Library. Details of these regulations may be obtained from the Librarian. This page must form part of any such copies made.

- The ownership of any patents, designs, trademarks and any and all other intellectual property rights except for the Copyright (the "Intellectual Property Rights") and any reproductions of copyright works, for example graphs and tables ("Reproductions"), which may be described in this thesis, may not be owned by the author and may be owned by third parties. Such Intellectual Property Rights and Reproductions cannot and must not be made available for use without the prior written permission of the owner(s) of the relevant Intellectual Property Rights and/or Reproductions.

ACKNOWLEDGEMENTS

In the beginning, I would like to pay my undivided gratitude to almighty Allah for providing me the opportunity to be on this planet and take a part in the advancement of the human race with my best capability. Thereafter, I am highly indebted to my parents for their constant encouragement and support in all stages of my life. My words fall short to thank them.

I would like to express my deep thanks and sincere indebtedness to Prof. Rakesh Mishra for supervising this research and for his efforts to put the research work on the right path. I would like to thank all my colleagues at the Energy, Emissions and Environment Research group at the University of Huddersfield. In addition, I would like to acknowledge the considerable amount of help and support provided by my co-supervisor Dr. Taimoor Asim to complete this thesis.

Sincere gratitude should got to the Establishment of Martyrs who funded my scholarship without whose support I could not achieve this study. Warm thanks should also go to the Iraqi Cultural Attaché in London who took care of my paper work during my study and offered me helps when I needed.

At last but not least, I wish to thank my wife and my family, for their devoted care, quiet sacrifices, and indispensable role as a wife and mother during the previous years of my study.

CONTENTS

LIST OF FIGURES

LIST OF TABLES

NOMENCLATURE

A	Area	m^2
C_1	Cost of piping material	£/ton
C_2	Cost of absorber plate	£/60L
C_3	Cost of insulation material	£/m^3
C_4	Cost of aluminium	£/m^3
C_5	Cost of the tank	£/60L
$C_{Operation}$	Operational cost	£
C_p	Specific heat	J/kg.ºC
$C_{Personal}$	Personal cost	£
C_T	Capacity of the tank	L
$C_{Manufacture}$	Manufacturing cost	£
C_{Total}	Total cost	£
$C_{Maintenance}$	Maintenance cost	£
D	Diameter of the riser pipe	m
Eu	Estimated standard uncertainty	
F'	Collector efficiency factor	
F_R	Heat removal factor of the fluid heater	
h	Heat transfer coefficient	W/m^2.ºC
$H.G_{tank}$	Heat gain in the storage tank	W
h_w	Convective heat transfer coefficient of environment	W/m^2.ºC
I_{BN}	Normal beam radiation	W/m^2
I_T	Solar radiation intensity	W/m^2
K	Thermal conductivity	W/m.ºC
k	Glass extinction coefficient	
k_b	Thermal conductivity of the plate	W/m.ºC
k_f	Thermal conductivity of the working fluid	W/m. ºC
k_{ins}	Thermal conductivity of the insulator	W/m.ºC
k_t	Thermal conductivity of the pipe	W/m.ºC
L	Length of the riser pipes	m
L/d	Length-to-diameter ratio of the riser pipes	
LH	Heat load	W
l_{ins}	Thickness of the insulator	m
Lioc	Meridian of location	º
Lst	Standard meridian for time zone	º

m_w	Mass of water within the tank	kg
$\dot{m}$	Mass flow rate	kg/s
n	Number of samples	
N	Day number of the year	
N_g	Number of glass covers	
np	Number of riser pipes	
N_p	Number of people	
Nu	Nusselt number	
Pr	Prandtl number	
q	Heat flux	W/m^2
q_{back}	Energy loss from rear of the flat plate collector	W/m^2
q_{conv}	Energy loss from the flat plate collector by convection	W/m^2
q_{loss}	Energy loss from the flat plate collector	W/m^2
q_{max}	Maximum heat flux	W/m^2
q_r	Energy loss from the flat plate collector by radiation	W/m^2
Q_{sides}	Energy loss from sides of the flat plate collector	W/m^2
q_{top}	Energy loss from top of the flat plate collector	W/m^2
q_u	Useful heat flux	W/m^2
Q_u	The useful heat	W
Ra	Rayleigh number	
Re	Reynolds number	
s	Surface area	m^2
s_x	Sample standard deviation	
t	Time	s
T^+	Dimensionless temperature	
T_1	Temperature of hot side	ºC
T_2	Temperature of cold side	ºC
T_{fi}	Initial temperature of working fluid	ºC
THg	Glass cover thickness	m
T_i	Temperature of the working fluid at the inlet of collector	ºC
T_{in}	Initial temperature of the working fluid	ºC
T_{it}	Temperature of water at inlet of the tank	ºC
T_{iw}	Initial temperature of water within the tank	ºC
T_o	Temperature of working fluid at the outlet of collector	ºC
T_{ot}	Temperature of water at outlet of the tank	ºC
T_{ow}	Final temperature of water within outlet of the tank	ºC
T_p	Plate temperature	ºC
T_{pm}	Mean plate temperature	ºC

τ_w	Wall shear stress	Pa
U	Overall heat loss	$W/m^2.^oC$
u	Velocity of working fluid	m/s
u*	Frictional velocity	
U_b	Heat loss through the bottom	$W/m^2.^oC$
U_e	Heat loss through the edges	$W/m^2.^oC$
U_t	Overall heat loss through the top	$W/m^2.^oC$
V	Wind velocity	m/s
V_p	Volume of hot water used by each person	L
w	Distance between the centre of two riser pipes	m
$\bar{x}$	Mean value	
x_i	Sample value	

GREEK SYMBOLS

α	Thermal diffusivity	m^2/s
α_p	Absorber plate absorptance	
β	Tilt angle of collector	^{o}
β'	Thermal expansion coefficient	$^oC^{-1}$
δ	Pipe thickness	m
$\int$	Declination angle	^{o}
ε	Correction factor of the earth's orbit	
ε_g	Emissivity of the glass cover	
ε_p	Absorber plate emissivity	
ε_p	Emissivity of absorbing plate	
η_c	Efficiency of the collector	
θ_1	Incidence angle	^{o}
θ_2	Refraction angle	^{o}
ρ	Surrounding's reflectivity	
ρ_1	Reflectivity of the perpendicular components	
ρ_2	Reflectivity of the parallel components	
σ	Stefan-Boltzmann constant	$W/m^2.K^4$
τ_1	Transmittance of the perpendicular component	
τ_2	Transmittance of the parallel component	
τ_g	Transmittance absorptance	
Φ	Latitude angle of the geographic location	^{o}
ω	Hour angle	^{o}
μ	Dynamic viscosity	kg/m.s

SUBSCRIPTS

a	Air
b	Bottom
BN	Normal beam
c	Collector
e	Edge
conv	Convection
f	Fluid
fi	Inlet fluid
g	Glass
H	Hydraulic
i	Inner
it	Inlet tank
in	Initial
ins	Insulation
iw	Initial water
max	maximum
o	Outer
ow	Outlet water
ot	Outlet tank
p	Pressure
pm	Mean plate
P	Person
r	Radiation
R	Removal
t	Tank
u	Useful
x	Sample
wf	Working fluid
w	Wall

CHAPTER 1

INTRODUCTION

Solar energy is one of the most important sources of renewable energy that is available in abundance throughout the world. One of the systems that utilises the solar energy to heat water is solar water heating system. The present chapter briefly introduces the solar water heating systems, specifically passive solar water heating systems. In addition, this chapter provides an introductory discussion regarding the thermal analysis of a closed loop thermo-syphon system (passive). Enhancement techniques of heat transfer as well have been presented in the present chapter. Furthermore, this chapter includes the main researcher aims of this study.

1.1. Solar Energy

The depletion of fossil fuels is escalating the global fuel prices. Furthermore, the drive to preserve the environment, by reducing the amount of greenhouse gases and other pollutants from the fossil fuels, is demanding the development and research on the alternative energy sources. One of the alternative sources of energy is solar energy. This type of energy is available in abundance throughout the world and is the cleanest of all known energy sources. Figure 1-1 depicts the mean day-to-day global solar energy (irradiation) in the winter (January) and the summer (July) seasons respectively, in U.K. It can be clearly seen that the solar radiation varies significantly over the seasons. The maximum solar radiations observed in July and January are 21MJ/m^2 and 3.5MJ/m^2, whereas the observed minimum solar radiations are 12MJ/m^2 and 1MJ/m^2 respectively. Furthermore, it can also be noted that the south region has more solar radiation compared to the north regime. In recent decades, the world has witnessed substantial developments in the field of solar energy as it has been proven to be more efficient in terms of energy extraction. Solar energy plays a vital role in various aspects of life. In just one second, the sun provides about 13 million times more energy than that is generated by all the electricity consumed in one year [1]. It has more advantages in comparison with fossil fuels in terms of environmental effect. It is more environment-friendly. Furthermore, one of the greatest benefits of solar energy is its conversion capability, which means that it can be transformed into any other types of energy, such as heat, electric etc., with relatively simple installation [2]. Whereas other forms of renewable energy sources, like wind turbine, require more complex initial installation.

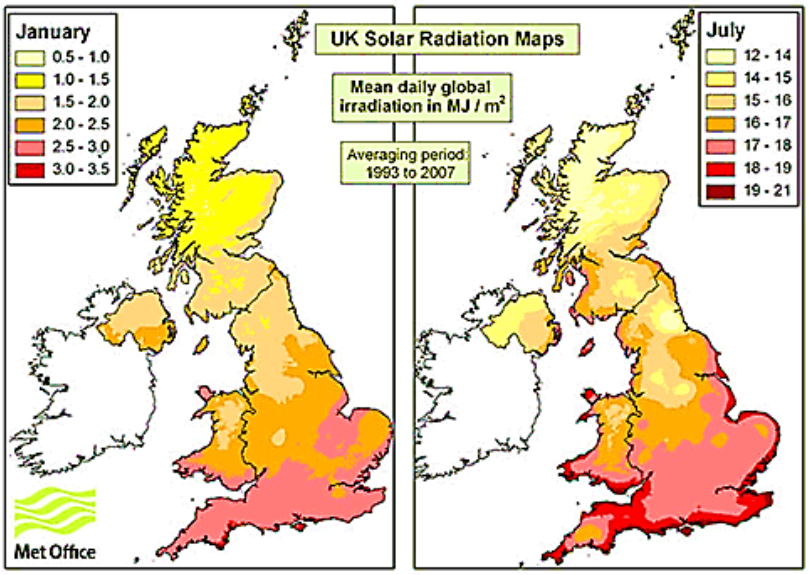

Figure 1-1 Solar radiation across the UK [3]

The energy within the solar rays is capable of starting natural convection within closed mechanical systems containing a suitable working fluid. One such system is commonly known as

solar water heater system, which converts solar energy into internal energy of a fluid, commonly water.

1.2. Solar Based Water Heating Systems

Over the past few decades, a prolific increase has been witnessed in research and development in the field of solar water heating systems and the associated technologies. The demand of hot water, due to population explosion, for day-to-day usage and other industrial applications is urging for effective development and harness of solar energy.

Based on the operational principles, a solar water heater can be divided into two types [4]:

- Active solar water heating systems
- Passive solar water heating systems

In an active system, the working fluid is circulated using an external device (power source), such as a pump, whereas a passive system is based on natural convection within the working fluid. Figure 1-2 shows a passive solar water heating system. This study focuses on passive system as it does not require any external device such as pump and hence making the system less complicated and less expensive to maintain.

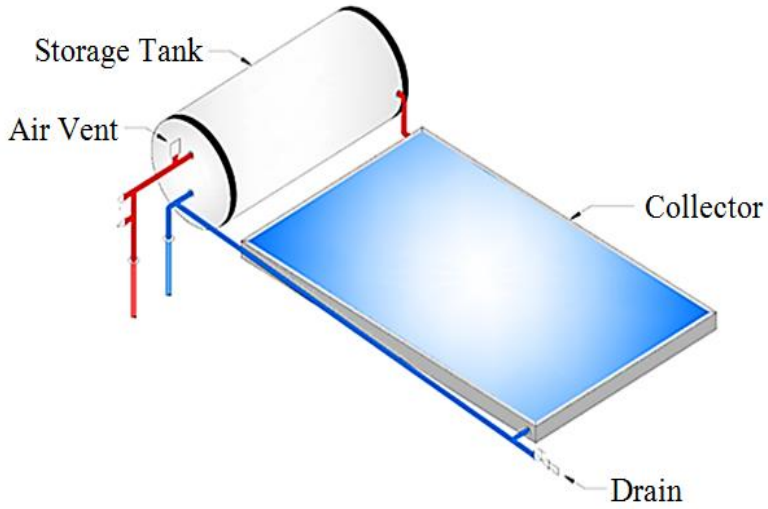

Figure 1-2 Passive solar water heater [5]

The amount of hot water generated by a solar water through system relies on a number of parameters, for example size and type of the system, availability of solar energy at the site, insulation and orientation of the collector etc. [6]

1.3. History of Solar Water Heating Systems

In the past, people had been using different fossil fuels, such as wood, coal etc. to heat water for their daily usage. The development of technology encouraged people to use natural gas for the same purpose. Although application of gasses as heat source has been shown to be more efficient, but it is expensive [7]. The coal and natural gas have to go through various refinements to make them useable, and hence it makes them expensive. Alternatively, the demand for other available energy sources has increased, which are comparatively less expensive and safer to use. One of the most important alternative sources is solar energy, which is used to heat water by solar water heating system. The preliminary design of solar water heating system consisted of a metal tank, which has been painted black. The tank was placed in a location to absorb most intensity of the solar energy. After a certain period of time, the hot water inside the tank can be used for domestic applications. The primary drawback of this system is the amount of time required to heat the water, often a whole day. Moreover, there were no proper insulations in the system to maintain the temperature of water for a long time. Due to the lack of insulation, the absorbed heat dissipated rapidly [7].

Over the years, the design of these hot water metal tanks has improved. In 1981, Clarence Kemp patented a tank design, in which metal panel was added on the tank to increase the heat transfer surface area and hence increase the amount of heat transfer to the working fluid, as shown in Figure 1-3 [7]. At the beginning of the 20^{th} century, various designs were proposed and constructed, having similar heating and storage units, which were exposed to external weather conditions.

In 1909, William Bailey proposed a solar water heater design, which could work through day and night. The design had a solar collector unit and water storage tank placed separately. Since the water storage tank was separate, it could be placed indoor, reducing the impact of external environmental conditions. It helped to maintain the fluid temperature in the tank for a longer time, whereas, the solar collector was kept outside facing south. The solar collector consisted of a coiled pipe inside a glass-covered box. The collector was mounted below the storage tank to allow natural convection taking place in the system [8]. Other designs emerged in the following years, for instance in Japan, a solar water heater with a basin, which was covered by a glass. By the 1960's, more than 100,000 collectors of this type had been in use.

Figure 1-3 Prototype solar water collector [7]

Prior to 1990s, in Australia, sales of the solar water heating systems increased due to the rising oil prices. However, in the late 1990s, the Australian solar water heater market shrank because of the discovery of Natural Gas in previously fuel-short regions, such as the Northern Territory and Western Australia. Despite this, exports level of Sol-Hart, which was one of the Australian leading manufacturers of solar water heaters, remained 50% of the sales [9]. At the same time Large scale promotion of this equipment has begun. The implication of solar energy to heat water was widely used in Greece, and small units of $2m^2$ were installed in majority of the households. In 2001, Greece was the first place in Europe, and 2nd in the World, for keeping the highest rate of m^2 per capita of solar collectors installed, as shown in Figure 1-4 [9].

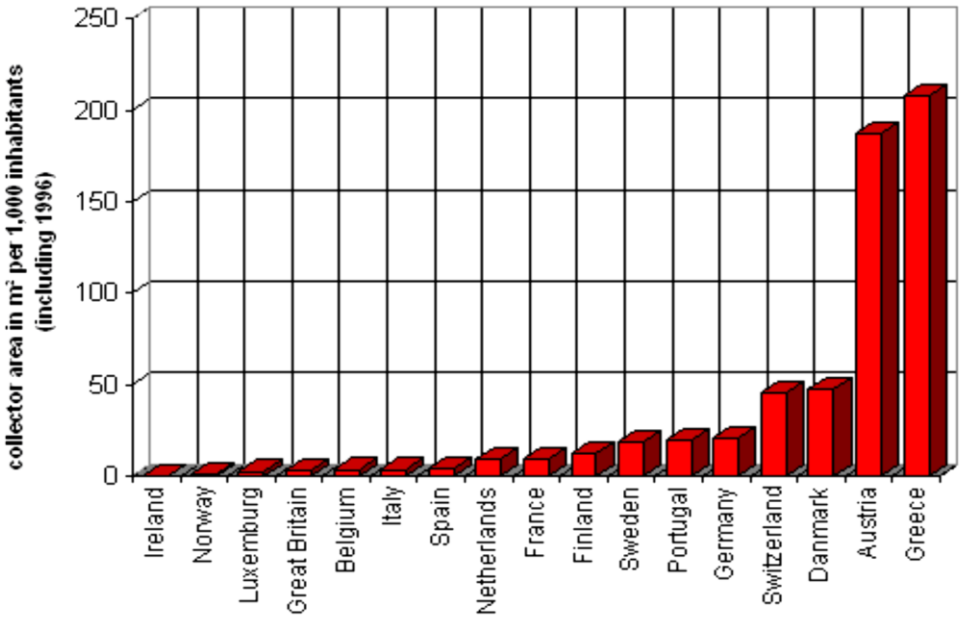

Figure 1-4 Solar collectors in m^2 installed per capita [9]

1.4. Thermo-syphon

A closed loop thermo-syphon system is complicated system with complicated fluid flow characteristics. To understand the fluid flow behaviour in the thermo-syphon, it is necessary to understand the geometrical feature of the system, which has significant impact on the system performance. Thermo-syphon can be denoted as a system that is used to heat water by using solar energy and transfer this heat by working fluid from the solar collector (hot side) to the condenser (cooler side) based on the thermo-syphon principle. The working principle of thermo-syphon states that the working fluid is driven by natural convection due to the temperature difference in the collector. After the collector, the fluid passes through a condenser, where the temperature of the fluid decreases. Subsequently, the fluid flows downwards by the gravity through the return loop.

The temperature of the working fluid increases in the collector, which is exposed to the solar rays. The rise in the temperature of working fluid affects the flow within the thermo-syphon loop. Temperature differences within working fluid cause a density variation, which lead to natural circulation of the working fluid within the closed loop thermo-syphon system.

1.4.1. Thermo-syphon Loop

Thermo-syphon loop solar water heating system commonly consists of three sections, namely solar collector, condenser and connecting pipes (upriser and downcomer), which forms the thermo-syphon loop. The solar collector is one of the main components of thermo-syphon solar hot water systems that is exposed to the solar radiation. It can be considered as a heat exchanger that absorbs thermal energy from the Sun and transfers it to the working fluid within the thermo-syphon. There are several types of solar collectors, like flat-plate, unglazed, flat plate air heating, evacuated and reverse flat-plate collectors [2]. This study will be focused on the first type i.e. flat-plate solar collectors due to its various advantages over other types, such as the capability to collect both beam and diffused radiation [10], ability to work on a wide range of climates [11], low manufacturing cost, and ease of installation. Furthermore, according to Figure 1-5 that depicts the efficiency of different types of solar panels with respect to the temperature difference between the collector and ambient, indicates that the flat-plate solar panel provides better efficiency over a wider temperature difference.

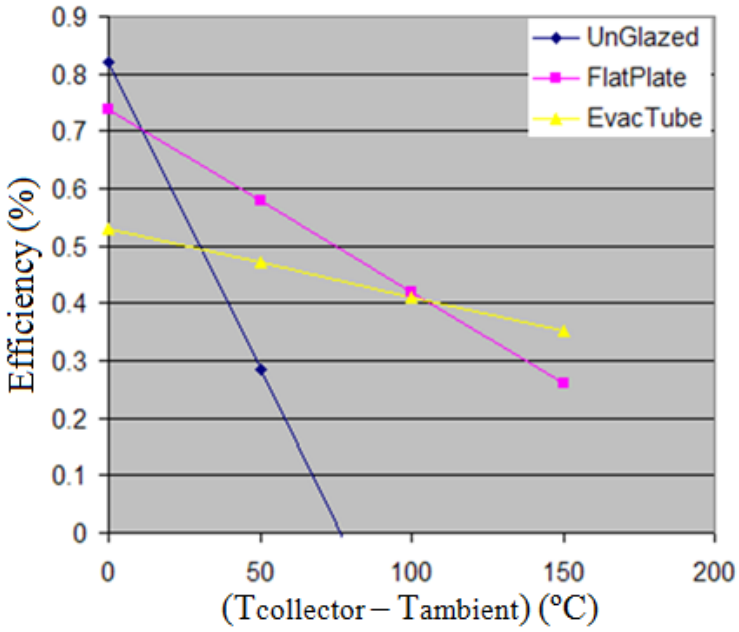

Figure 1-5 Solar collector Efficiency aginst temperature difference between the collector and ambient [12]

Flat-plate solar collectors mainly consist of riser pipes, absorber plate, glazing cover and insulation. These components are assembled in a proper frame as shown in Figure 1-6. The condenser can be considered as a heat exchanger, that is positioned inside the water storage tank and it collects energy from the collector. Finally, the connecting pipes are the pipes through which the working fluid propagates. It is normally assumed that there is no heat transfer taking place through the connecting pipes, and hence they are considered adiabatic.

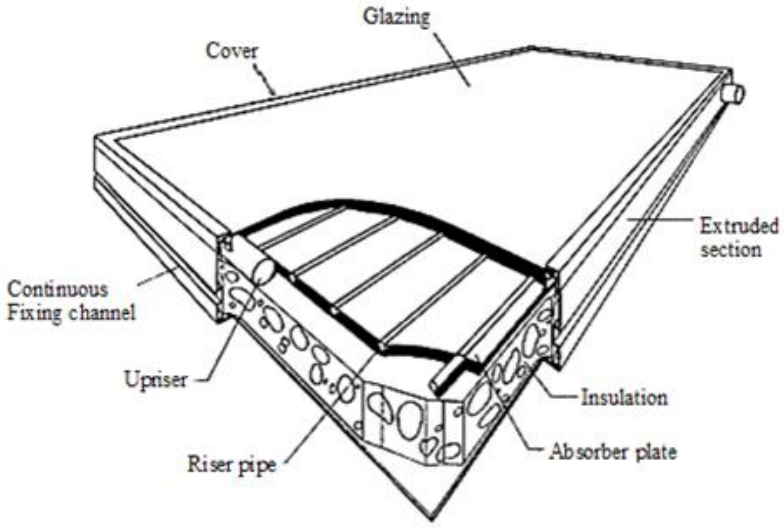

Figure 1-6 A flat plate solar collector [13]

1.4.2. Working Fluid

The working fluid is an essential element of the thermo-syphon system. The main purpose of the fluid is to collect heat energy from the collector and transfer it to the water within the storage tank. It is crucial to select a suitable working fluid for an efficient solar water heating system. The working fluid should be chosen such that it has high specific heat capacity, high thermal conductivity, low viscosity, low thermal expansion coefficient, anti-corrosive properties and low cost [14]. Furthermore, the selection of the working fluid depends on the application as well. For example, fluid with a low boiling point should be chosen for a heating system, whereas, for a cooling system, the boiling point of the fluid should be high.

1.4.3. Storage Tank

This part of thermo-syphon solar water heating system can be defined as a component for storing hot water, which is then used for domestic purposes. Since the solar energy can only be captured during the daytime, and the amount of energy collected depends on the climate as well, it is important to store the hot water in an well-insulted and isolated place (like storage tank) to meet the demand of hot water. Furthermore, the place of storage tank should be above the collector and it should include the exchanger coil to transfer the heat from working fluid to the water within it.

1.5. Types of Thermo-syphons

Based on the working fluid, the thermo-syphon solar water heating systems can be categorised into two groups i.e. single phase and two phase solar water heating systems, as shown in Figure 1-7 and Figure 1-8 respectively. Single phase systems can be further divided into two types, namely open loop and closed loop thermo-syphon solar water heating systems. Almost all of the single phase solar water heater systems use water as the working fluid. The drawback of single phase solar water heating system with water as the working fluid are i) reversed cycle during the night ii) frost formation in extremely cold weathers and iii) low heat capacity and corrosion.

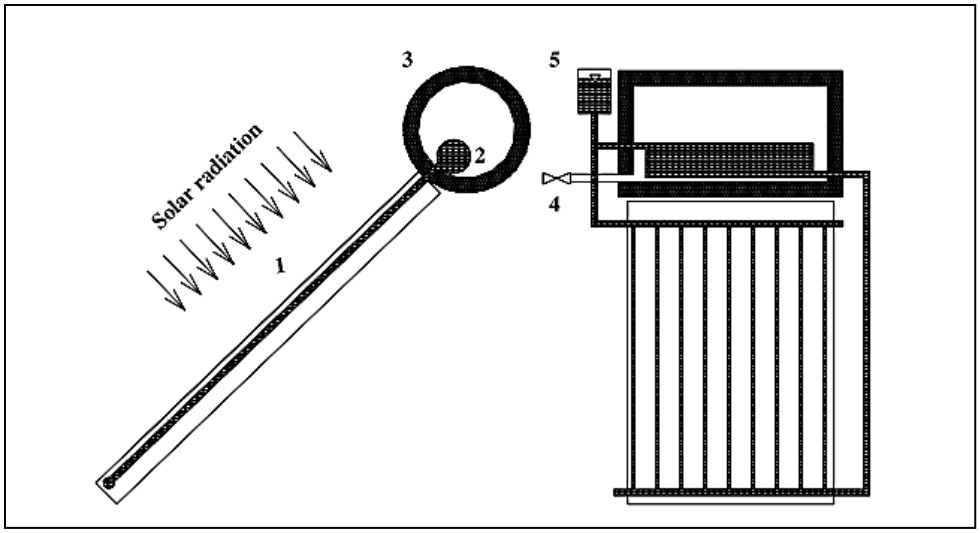

Figure 1-7 Components of a single phase thermo-syphon solar hot water system
1) Solar collector 2) Condenser 3) Storage tank 4) Cold water inlet 5) Expansion tank [15]

A few decades ago, to solve the drawbacks of the single phase solar water heater system, and improve the efficiency of the system, a new system was proposed, which is known as two phase solar water heating system [16]. The two phase solar water heating system consists of working fluid that can change its phases with incorporated environment conditions (temperature, pressure), within thermo-syphon loop. This working fluid undergoes a phase change or evaporation upon exposure to solar radiation. One of the most important consideration in thermo-syphon systems is the heat transfer performance, which is a function of several factors, such as working fluid's properties, geometry and orientation of the thermo-syphon, gravitational effects and operating temperature [17].

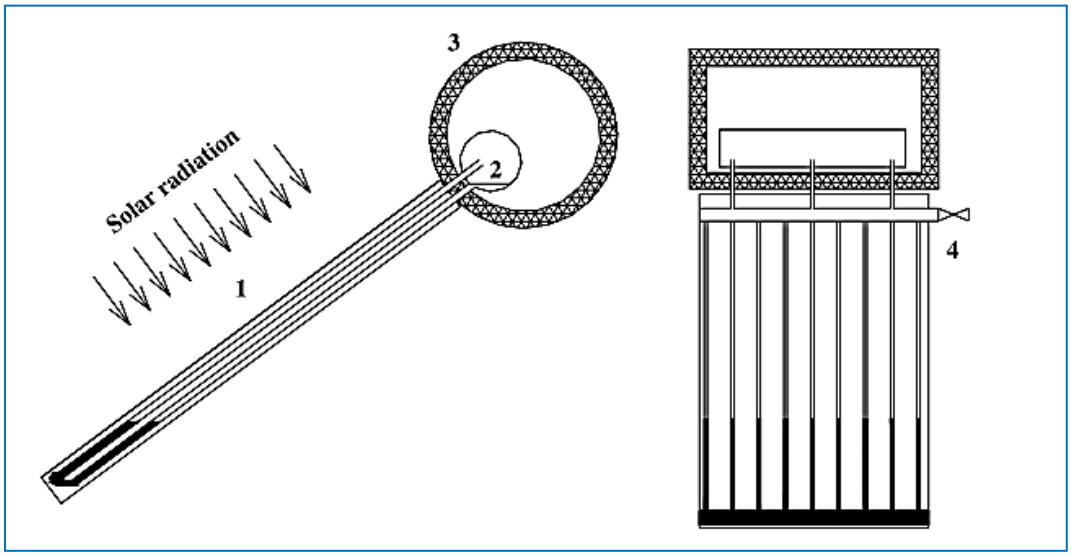

Figure 1-8 Components of a twophase thermo-syphon solar hot water system
1) Solar collector 2) Condenser 3) Storage tank 4) Working fluid inlet valve [15]

1.6. Advantages of Thermo-syphon

The important advantages of thermo-syphon are as follows: [15]:

1. Due to natural circulation of the working fluid within the thermo-syphon loop, it avoids using a conventional pump, which keeps the complexity and costs of a thermo-syphon system low
2. It has higher efficiency as compared to the conventional heat pipe systems
3. It is quite reliable and hence it is often used in parts of nuclear power plants
4. It has high compactness and high heat recovery effectiveness

Due to various advantages, the thermo-syphon solar water heating system is popular throughout the world. There are two primary engineering applications of thermo-syphon systems, i.e. heating and cooling of water. Thermo-syphon can be used for heating water for domestic and industrial use as shown in Figure 1-9 and in geothermal systems. The primary reason for using passive solar water heating systems is that, this system is simple and does not need pump or controller. However, in this type of system, the storage water tank should be situated above or beside the collector [18].

Figure 1-9 Thermo-syphon for domestic applications [19]

A closed loop thermo-syphon system can also be implemented in cooling applications as well, such as emergency cooling systems for electric machines or equipment of a nuclear reactor [20], as shown in Figure 1-10. Thermo-syphon systems are widely used to cool electronic devices because it does not need any external device to recirculate working fluid and has a simple design. Thermo-syphon systems used to cool electronic devices consist of three sections namely evaporator, adiabatic section and condenser. When heat is applied to the evaporator, working fluid will evaporate. Thereafter, the fluid moves towards the condenser. In the condenser, the fluid is cooled. The working fluid returns to the evaporator by gravity [21].

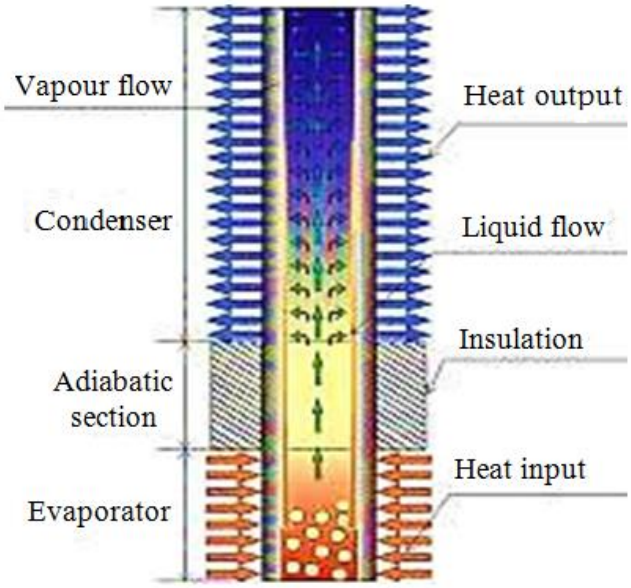

Figure 1-10 Thermo-syphon for cooling electronic devices applications [22]

1.7. Heat Transfer Modes

Heat is a form of energy that reflects the motion of atoms within an object, which is invisible but can be felt. Heat transfer occurs when there is a difference in temperature between two bodies. The heat transfer will navigate from the higher temperature to lower temperature until the system achieves a thermal equilibrium. In the mechanical science, the heat transfer process can be classified into three main sectors namely conduction, convection and radiation. However, it is not mandatory to have a system with all these three processes. Depending on the application, it is possible to have only one or two type of heat transfer processes.

1.7.1. Heat Conduction

It is one of few ways of thermal energy transmission. It is due to heat transfer through which the exchange of thermal energy takes place between atoms of the same material without these atoms being transmitted. Figure 1-11 illustrates the process of thermal conduction. Fourier's Law could be used to calculate conduction rate, which states that the thermal flow rate with respect to time across the surface of a substance is proportional to the thermal gradient and the surface area. Eq. (1.1) below shows this relationship [23].

$$Q_{cond} = KA\frac{(T_1 - T_2)}{\Delta x} \tag{1.1}$$

where K denotes the thermal conductivity, A surface area of wall, T_1 temperature of hot side, T_2 temperature of cold side and Δx the thickness of wall.

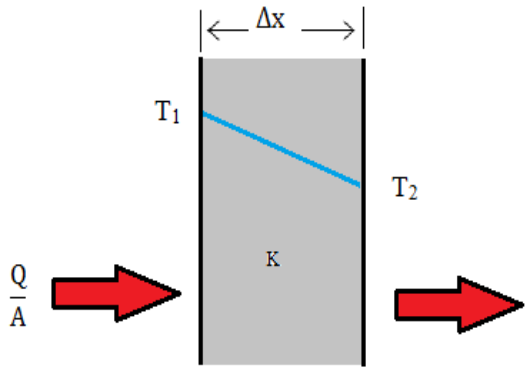

Figure 1-11 Thermal conduction process [24]

1.7.2. Heat Convection

This is also one of few ways of thermal energy transmission in the medium, especially in fluids (liquids and gases). Because of the high temperatures in the fluid, a decrease in its density is noticed, causing a rise up or spread in the fluid particles, which would then be replaced by another more dense fluid. Liquid from this bottom-up movement works in such a way that brings about thermal transmission. This process is called as convection. This type of heat transfer consists of two mechanisms: diffusion and energy transferred by mass or macroscopic motion of the fluid. Figure 1-12 depicts the convection processes that occur on a plate. The rate of heat transfer by convection is calculated by using Eq. (1.2) [23].

$$Q_{conv} = Ah(T_p - T_a) \tag{1.2}$$

where A denotes surface area of wall, h the heat transfer coefficient, T_p plate temperature and T_a air temperature.

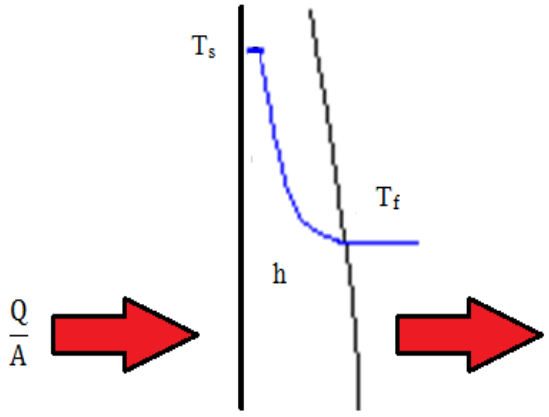

Figure 1-12 Thermal convection process [24]

There are two forms of thermal convection namely:

- Natural convection or free: the fluid movement caused by temperature difference and the difference in density under natural conditions, where there are no external influences to force the fluid movement, such as thermo-syphon
- Forced convection: the fluid movement, as a result of the force or catalyst molecules such as pumps

1.7.3. Radiation

Radiation is one of the ways of transmission of thermal energy in the material, occurring in all kinds of material. This process describes emissions from the material in a vacuum or any other heat transfer media (solid or fluid) in the form of photons and electromagnetic waves. There are many practical applications of heat transfer by radiation, and one of these applications is the solar energy. Figure 1-13 depicts the distribution of radiation energy on a translucent cover. The heat flux from the radiation can be calculated from the Stefan-Boltzmann law, which states that the heat radiated from a black body per unit time is proportional to the product of the fourth power of the absolute temperature and the surface area. The mathematical representation of the Stefan-Boltzmann law is presented in Eq. (1.3) [23].

$$Q_{rad} = \sigma A(T_p{}^4 - T_a{}^4) \tag{1.3}$$

where σ denotes the Stefan-Boltzmann constant, A surface area, T_p plate temperature and T_a is the air temperature.

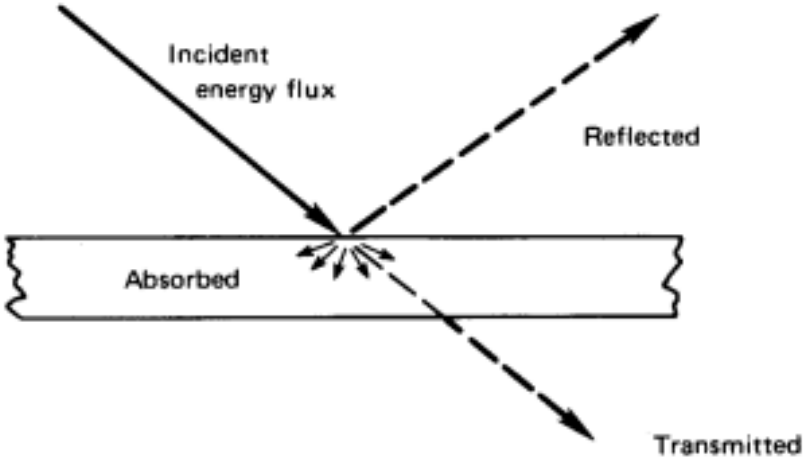

Figure 1-13 Thermal radiation process [23]

1.8. Thermal Analysis of a Closed Loop Thermo-syphon

In order to analyse the performance output of a thermo-syphon loop, several parameters should be considered. These parameters are the solar radiation intensity, transmittance of the glass cover, the overall heat loss coefficient, heat transfer coefficient, heat-removal factor, collector efficiency factor, useful gain, total gain and the loss of energy. The details of these parameters is discussed in the following sub-sections.

1.8.1. Solar Radiation Intensity

The solar radiation intensity (I_T) comprises of three components, namely beam radiation (I_B), diffused radiation (I_D) and reflected radiation (I_R), which can be represented as [25]:

$$I_T = I_B + I_D + I_R \tag{1.4}$$

where,

$$I_B = I_{BN} \cos(\theta_1) \tag{1.5}$$

$$I_D = I_{BN} * C \left[\frac{1+\cos\beta}{2}\right] \tag{1.6}$$

and,

$$I_R = I_{BN} * \rho[\sin\alpha + C] \left[\frac{1+\cos\beta}{2}\right] \tag{1.7}$$

Here, I_{BN} is the normal beam radiation, θ_1 is the incident angle between the solar beam and the normal to the inclined surface, β is the angle of the collector and ρ is the surroundings' reflectivity. I_{BN} and ρ can be further represented as:

$$\rho = \frac{\rho_1+\rho_2}{2} \tag{1.8}$$

and,

$$I_{BN} = \frac{A}{e^{B/\sin\alpha}} \tag{1.9}$$

The $\cos\theta_1$ term in equation 1.5 can be extended to:

$$\cos(\theta_1) = \sin(\Phi - \beta)\sin\int + \cos(\Phi - \beta)\cos\int\cos\omega \tag{1.10}$$

where Φ is the latitude angle of the geographic location and α is the solar altitude angle. $\sin\alpha$ term in equation 1.7 can be extended to[26]:

$$\sin\alpha = \sin\Phi\sin\int + \cos\Phi\cos\int\cos\omega \tag{1.11}$$

where ∫ is the declination angle and ω is the hour angle, given as follows [27]:

$$\omega = \pm(\text{Solar Time} - 12) * 15$$

and,

$$\int = 23.45 \sin\left[\frac{360}{365}(284 + \text{N})\right] \quad (1.12)$$

where N is the day number of the year.

The solar time can be calculated as [26]:

$$\text{Solar Time} = \text{Standard Time} + 4(\text{Lst} - \text{Lioc}) + \text{E} \quad (1.13)$$

where,

$$\text{E} = 9.87\sin(2\Upsilon) - 7.53\cos(\Upsilon) - 1.5\sin(\Upsilon) \quad (1.14)$$

and,

$$\Upsilon = \frac{360}{365}(\text{N} - 81) \quad (1.15)$$

Lst and Lioc in equation 1.13 are standard meridian for time zone (in º) and meridian of location (in º) respectively.

The coefficients A, B and C represent the values of the apparent solar radiation intensity, the atmospheric air extinction and diffused radiation respectively. These three coefficients are calculated using the following relations for any day of the year:

$$\text{A} = 1158\left[1 + 0.066\cos\left((360/365) * \text{N}\right)\right] \quad (1.16)$$

$$\text{B} = 0.175[1 - 0.2\cos(0.93 * \text{N})] - 0.0045[1 - \cos(1.86 * \text{N})] \quad (1.17)$$

$$\text{C} = 0.0965\left[1 - 042\cos\left((360/365) * \text{N}\right)\right] - 0.0075[1 - \cos(1.95 * \text{N})] \quad (1.18)$$

The three coefficients above are function of the day number of the year.

1.8.2. Transmittance-Absorptance Product

The transmittance-absorptance is a product of the glass cover transmittance and the absorber plate absorptance. The absorber plate absorption depends on the absorber plate coating and it can be considered constant. Hence, the variation in the transmittance-absorption is caused by the variation in the glass cover transmittance only. Moreover, the glass cover transmittance is a function of several other variables, such as the inclination angle of the solar radiation on the glass cover, glass type, glass thickness and the purity of iron oxides.

The transmittance of the glass cover is the average of two components resulting from a process called Polarization [26]:

$$\tau_g = \frac{\tau_1+\tau_2}{2} \tag{1.19}$$

In the above equation, the term τ_1 represents the transmittance of the perpendicular component, whereas, the term τ_2 defines the transmittance of the parallel component. Each term can be represented by the Stokes equations, which are as follows[6]:

$$\tau_1 = \frac{\tau\,(1-\rho_1)^2}{1-(\rho_1)^2\,(\tau)^2} \tag{1.20}$$

$$\tau_2 = \frac{\tau\,(1-\rho_2)^2}{1-(\rho_2)^2\,(\tau)^2} \tag{1.21}$$

where τ is the glass transmittance for one interface, which can be calculated by Bouguer`s Law as:

$$\tau = e^{-kL} \tag{1.22}$$

where k is the glass extinction coefficient, and L is the distance travelled by the light through the glass, calculated as:

$$L = \frac{THg}{\cos(\theta_2)} \tag{1.23}$$

THg is the glass cover thickness and θ_2 is the refraction angle, which is the angle between the refracted light inside the glass material and the line perpendicular to the glass surface. It is computed as [13]:

$$\theta_2 = \sin^{-1}\left[\frac{\sin(\theta_1)}{n}\right] \tag{1.24}$$

where n is the refractive index of the transparent material (n = 1.526 for glass) and ρ_1 is the reflectivity of the perpendicular components, which is given as:

$$\rho_1 = \frac{\sin^2(\theta_1-\theta_2)}{\sin^2(\theta_1+\theta_2)} \tag{1.25}$$

while ρ_2 is the reflectivity of the parallel components, which is given as:

$$\rho_2 = \frac{\tan^2(\theta_1-\theta_2)}{\tan^2(\theta_1+\theta_2)} \tag{1.26}$$

1.8.3. Overall Collector Heat Loss Coefficient

The overall heat loss from the collector takes place from the top and bottom surfaces of the collector, along with the edges. The heat loss through the edges is relatively small, and can be neglected. The overall heat loss coefficient through the top surface has a significant effect on the performance of the collector, which is evaluated by considering both convection and radiation from the absorber plate to atmosphere through the glass cover. The overall heat loss is a function of several parameters, such as the absorber plate temperature (Tp), atmospheric temperature (Ta), number of glass covers (Ng), emissivity of glass covers (ε_g), absorber plate emissivity (ε_p), tilt angle of the collector (β) and the convective heat transfer coefficient (h_{fi}). Typical values of the overall heat loss coefficient range from 2 to 10W/m^2.ºC [28]. The value of the overall heat losses from the collector can be estimated as [6]:

$$U = U_t + U_b + U_e \tag{1.27}$$

where U_e is the heat loss through the edges, U_b is the heat loss through the bottom surface and U_t is the overall heat loss through the top surface of the collector.

As the heat loss through the edges is negligibly small, Eq. (1.27) can be rewritten as:

$$U = U_t + U_b \tag{1.28}$$

The heat loss through the bottom surface of the collector can be calculated as:

$$U_b = \frac{k_s}{l_s} \tag{1.29}$$

The heat loss through the top surface can be estimated by:

$$U_t = \left[\frac{N_g}{\frac{c_p}{T_{pm}}\left(\frac{T_{pm}- T_a}{N_g+f}\right)^e} + \frac{1}{h_w}\right]^{-1} + \left[\frac{\sigma(T_{pm}+ T_a)(T_{pm}{}^2+T_a{}^2)}{\left[\varepsilon_p+0.00591N_g h_w\right]^{-1}+\left[\frac{2N_g+f-1+.0133\varepsilon_p}{\varepsilon_g}\right]}\right] \tag{1.30}$$

where k_s is the thermal conductivity of the insulator, l_s is the thickness of the insulator, V is the wind velocity, ε_p is the emissivity of the absorbing plate, ε_g is the emissivity of the glass cover, T_{pm} is the mean plate temperature and σ is the Stefan $-$ Boltzmann constant ($5.67 \times 10^{-8} \frac{W}{m^2K^4}$).

$$c_p = 520(1 - 0.00005\beta^2) \tag{1.31}$$

$$f = \left(1 + 0.089\, h_w - 0.1166\, h_w\, \varepsilon_p\right)\left(1 + 0.07866N_g\right) \tag{1.32}$$

$$e = 0.43\left[1 - \left(\frac{100}{T_{pm}}\right)\right] \tag{1.33}$$

h_w is the convective heat transfer coefficient of environment, which is given as:

$$h_w = 2.8 + 3V \tag{1.34}$$

From Eq. (1.34), it can be noticed that the heat transfer coefficient of environment depends on the velocity of air.

1.8.4. Mean Temperatures

The mean temperatures of the absorber plate (T_p) and the working fluid (T_m) are computed as [29]:

$$T_p = T_m + \left(\frac{I_T\,\varepsilon_p\,\varepsilon_g}{U}\right)\,(1 - F_R) \tag{1.35}$$

$$T_m = T_{fi} + \left(\frac{Q_u}{A_c U F_R}\right)\left(1 - \frac{F_R}{\dot{m}\,C_p}\right) \tag{1.36}$$

where F_R is the heat removal factor for the fluid, and can calculated as:

$$F_R = \frac{\dot{m}\,C_p}{A_c U}\left[1 - \exp\left(\frac{A_c U F'}{\dot{m}\,C_p}\right)\right] \tag{1.37}$$

where $\dot{m}$ is the mass flow rate and A_c is the collector area, which can be calculated as:

$$A_c = np * w * L \tag{1.38}$$

where np is the number of riser pipes, W is the distance between the centres of two-riser pipes and L is the length of the riser pipes individually.

Collector efficiency factor (F') can be computed as:

$$F' = \left[\frac{\frac{1}{U}}{w\left[\frac{1}{U[D_o + (w - D_o)F]} + \frac{1}{\pi D_i h_{fi}} + \frac{2\delta}{k_b D_o}\right]}\right] \tag{1.39}$$

where,

$$F = \frac{\tanh\left[\frac{M(w - D_o)}{2}\right]}{\frac{M(w - D_o)}{2}} \tag{1.40}$$

where D_o is the outlet diameter and k_b is thermal conductivity of the plate.

$$M = \sqrt{\frac{U}{k_t \delta}} \tag{1.41}$$

where δ is pipe thickness and k_t is thermal conductivity of the pipe.

For laminar flow, the Nusselt number (Nu)can be computed as [28]:

$$N_u = \frac{h_{fi} D_i}{k_f} = 3.656 \tag{1.42}$$

where h_{fi} is the heat transfer coefficient of the working fluid, D_i is the inner diameter and k_f is the thermal conductivity of the working fluid.

1.8.5. The Useful Energy

The useful energy gained by the working fluid, can be calculated as [25]:

$$Q_U = Q_T - Q_L \tag{1.43}$$

where Q_T represents the total gain of energy, which can be calculated as:

$$Q_T = A_c F_R I_T \tau_g \alpha_p \tag{1.44}$$

While, Q_L represent the loss of energy, which can be calculated as:

$$Q_L = A_c F_R U (T_{fi} - T_a) \tag{1.45}$$

Using Eq. (1.44) and (1.45), the useful energy gained can be represented as:

$$Q_U = A_c F_R \left[I_T \tau_g \alpha_p - U (T_{fi} - T_a) \right] \tag{1.46}$$

where τ_g is the transmittance absorptance, α_p is the absorber plate's absorptance, T_{fi} is the initial temperature of the working fluid and T_a is air temperature.

1.9. Heat Transfer Enhancement Techniques

To utilise the solar energy captured by the collector more efficiently, it is crucial to improve the heat transfer in the system. Improvement of heat transfer and hence improvement of the thermal performance of thermo-syphon solar water heating system depends on several key parameters. The amount of heat transfer through any material depends on several parameters, such as temperature variations, overall heat transfer coefficient and surface area, as shown in Eq. (1.47).

$$Q = AU\Delta T \tag{1.47}$$

where U is represent the overall heat transfer coefficient that depends on the type of working fluid, thickness of the material and thermal properties. 'A' signifies the geometrical features of the system and the term ΔT depicts the temperature difference. According to Eq. (1.47) geometrical features and the temperature has significant impact on the amount of heat transfer. Further explanations of these parameters have been included in the following section named as Geometrical Parameter and temperature of the working Fluid in section (1.9.1) and (1.9.2) respectively.

1.9.1. Geometrical Parameters

Geometrical parameters play a vital role in the heat transfer process. Increase in surface area enhances the performance of a thermo-syphon. The surface area of the collector can be increased by increasing the number of riser pipes and/or increasing the length-to-diameter ratio (L/d) of the riser pipes. However, increasing the number of riser pipes and/or their L/d ratio increases the amount of working fluid within the thermo-syphon loop. Increasing the amount of working fluid will require more heat flux to raise the temperature of the working fluid by the same amount, which in-turn will require longer time period to achieve a desired temperature of the working fluid.

1.9.2. Temperature of the Working Fluid

According to the Eq. (1.47), the useful heat flux is a function of the change in the temperature of the working fluid, which is represented as ΔT. This temperature difference can be represented as:

$$\Delta T = T_{wall} - T_{ref} \tag{1.48}$$

where T_{wall} is the collective average static temperature of the riser pipes and T_{ref} is the reference temperature of the working fluid, which can be computed as:

$$T_{ref} = \frac{T_{in}+T_{out}}{2} \tag{1.49}$$

where T_{in} and T_{out} are the temperatures of the working fluid at the inlet and outlet section of the thermo-syphon respectively.

By studying the flow characteristics of the working fluid, the thermal performance of closed loop thermo-syphon can be derived. Once this benchmark performance is established, a further heat transfer enhancement is carried out. For example, increasing the temperature decreases the viscosity of fluid and hence decreases wall shear stress as shown in Eq. (1.50). Therefore, it is important to know temperature distribution and velocity profile to understand the behaviour of fluid.

$$\tau_w = \mu \frac{du}{dy} \quad (1.50)$$

where τ_w is the wall shear stress, μ is the dynamic viscosity of the fluid, du is the velocity of fluid and dy is the height above the boundary.

1.9.3. Enhancement Devices

In case of a thermo-syphon, the fluid flow within the pipes is laminar, hence, the effective heat transfer is quite low. Several techniques have been used to enhance the heat transfer rate [30-34]. In general, there are three techniques for this i.e. passive, active and compound technique. In passive technique, as no external power is consumed, the enhancement in the heat transfer rate depends on the geometrical parameters, such as extended surfaces (fins, louvered strips and winglets), rough surfaces (corrugated tubes) and swirl flow devices (twisted tapes and helical twisted tapes) [35]. Active technique depends on an external power to enhance the heat transfer rate, whereas, compound technique is a combination of both passive and active techniques [35]. As the current study is regarding closed loop thermo-syphons, passive techniques have been looked at in detail for improving the heat transfer rate.

1.10. Motivation

Solar energy is considered as a vital source of energy, which can be harnessed to meet ever-increasing energy requirements in the modern world. Extensive research is being carried out to make solar energy affordable so that present reliance on fossil fuels can be minimised. This would also help in meeting the requirements of limiting greenhouse gas effects, conserving the environment from pollution. The energy contained within the solar rays is capable of starting natural convection within closed loop mechanical systems containing a suitable working fluid. A solar energy extraction system consists of various components. One of such components is the thermo-syphon, which captures the solar energy and converts it to the thermal energy of a fluid. Various attempts have been made to analyse the functional characteristics of such systems. However, full flow field analysis and optimisation of such systems has not been attempted. A better understanding of the interdependence of the geometrical features on the flow structure within the thermo-syphon is essential to develop an efficient closed loop thermo-syphon solar water heating system. Therefore, an extensive study is required illustrating the effects of various geometric parameters, such as number of riser pipes and the length-to-diameter ratio of the riser pipes, on the thermal performance of the system under various operating conditions (heat flux and thermal loading).

The requirements for improving the thermal performance of a thermo-syphon solar water heating system are increasing rapidly with the increasing energy needs. The thermal performance of thermo-syphon solar water heating systems can be improved by increasing the surface area of the riser pipes, which will increase the heat transfer rate in the collector. There are various

configurations of themo-syphons in the published literature that have improved thermal performance of the system. However, these systems have not been systematically investigated and hence need further investigations.

The traditional methodology to design of the thermo-syphon relies on many of the assumptions. In this process, the values of mass flow rate, collector plate temperature and most of the geometrical parameters, such as diameter, length of pipes etc., are assumed. The design specification depends on the experience of the designer and the current methodology appears too restrictive. Therefore, a new methodology is required to enhance the design process by controlling various parameters.

1.11. Research Aims

The primary goal of this study is to improve the performance of a closed loop thermo-syphon solar water heating system. Based on this, the research aims have been broken down into the following:

1. Parametric investigation on the effect of various geometrical and flow related variables of a thermo-syphon on thermal performance
2. Investigate the effect of the riser pipes' configurations (design modifications) on the thermal performance of a closed loop thermo-syphon system
3. Developing a methodology to design a closed loop thermo-syphon solar water heating system

1.12. Organisation of Thesis

This thesis is presented in eight main chapters to illustrate the findings of the research conducted on the aforementioned topic. In addition to that, appendices are included to present the detailed explanation of the underlying processes.

Chapter 1 provides a concise introduction to the subject matter, as it provides an overview of the solar energy, which is one of the most important sources of renewable energy. Furthermore, this chapter focuses on providing details of a solar water heating system, which is commonly known as closed loop thermo-syphon. From this overview, the motivation for carrying out this research has been defined, which identifies key areas to be reviewed in Chapter 2.

Chapter 2 presents a critical review of the research that has been conducted in the field of solar heater thermo-syphon. It includes the review of published literature regarding two-phase flow and single-phase flow systems. Furthermore, a review of available literature for the enhancement of heat transfer in thermo-syphon has also been included. It also comprises of the literature review being carried out on the optimisation techniques for a closed loop thermo-syphon. Details of the scope of research have been provided in the form of specific research aims and objectives.

Chapter 3 provides the fundamentals of Computational Fluid Dynamics. It includes the CFD modelling for the traditional model of thermo-syphon. Then implemented meshing technique for the flow domain has been discussed in detail. Subsequently, suitable boundary conditions and solver settings have been specified.

Chapter 4 describes the experimental facility that has been developed to verify numerical thermo-syphon model by comparing the results obtained from experimental tests with the CFD results and evaluate the effect of enhanced heat transfer for the optimum new model on the thermal performance of thermo-syphon. This chapter provides a detailed description of each component that has been used in the experimental setup to build thermo-syphon solar water heating system. Moreover, uncertainty for experimental results has been estimated.

Chapter 5 shows detailed description of the flow structure and temperature distribution of working fluid within the thermo-syphon solar water heating system. In this chapter, an extensive study has been carried out on the effects of various geometric parameters under various heat fluxes and thermal loadings on the performance of a closed loop thermo-syphon solar water heating system with a view to develop parametric relationship.

Chapter 6 shows detailed description of the flow structure and temperature distribution of the working fluid within the closed loop thermo-syphon solar water heating system for various design modifications. In this chapter, an extensive study has been conducted for all new models of thermo-syphon numerically. Furthermore, the comparison between the traditional and new model (straight pipe) has been carried out numerically and experimentally.

Chapter 7 illustrates the development of a thermo-syphon design methodology. The inputs to this model are number of persons to be served, the initial temperature of working fluid within the thermo-syphon loop and the water temperature within the storage tank, the final temperature generated by the thermo-syphon and location of thermo-syphon (altitude). Whereas, the outputs of the model are thermal and flow parameters of working fluid within thermo-syphon loop and geometrical parameters of thermo-syphon loop, such as the diameter of the riser pipe, number of riser pipes etc. Furthermore, a cost analysis has been included for the thermo-syphon system including the comparison of the traditional and modified models to evaluate the effectiveness of the modifications.

Chapter 8 contains the conclusions and recommendations for future study, mentioning the design evaluation, manufacturing, and test procedures. The results obtained from chapters 5, 6, and 7 have shown that the new model can be utilised to enhance the thermal performance of the system. Furthermore, several recommendations have been included regarding future work.

CHAPTER 2

LITERATURE REVIEW

The previous chapter identifies parameters that have significant influence on the thermal performance of a thermo-syphon. Based on the findings, a detailed literature review is conducted in this chapter in order to define the knowledge gaps. The literature review has been divided into three main research areas i.e. the effects of geometrical parameters on the thermal performance of a closed loop thermo-syphon system, design modification to enhance the thermo-syphon performance and finally the design of thermo-syphons. Based on the reviewed literature, the knowledge gaps have been identified, based on which, the research objectives have been formulated.

2.1. Geometrical Parameters

Over the past couple of decades, many researchers have tried to have a better understanding of the hydrodynamics of thermo-syphons in order to improve their performance output. Majority of these works focus on examining the effects of geometrical parameters on the performance of thermo-syphons.

2.1.1. Geometrical Parameters Corresponding to the system

Varol et al. [36] have conducted a comparative numerical investigation between two types of collectors. In the first type, the collector had a wavy absorber, whereas in the second type, it had a flat absorber. The authors have studied the effects of a number of parameters with different ranges, such as tilt angle, wavelength and aspect ratio having a range of 20º to 60º, 1.33 to 4 and 0 to 4 respectively on the thermal performance of solar water heating system. The results have shown that both the shape and the tilt angle of the collector have a significant effect on natural convection heat transfer inside the solar collectors. Figure 2-1 depicts the variations in the mean Nusselt number for various aspect ratios of the collector. 'L' in Figure 2-1 denotes the length-to-height ratio of the wavy pipe, which is non-dimensional. It can be seen that mean Nu is higher for wavy collector at all the aspect ratios. The study has been conducted under no loading condition and with steady state heat input.

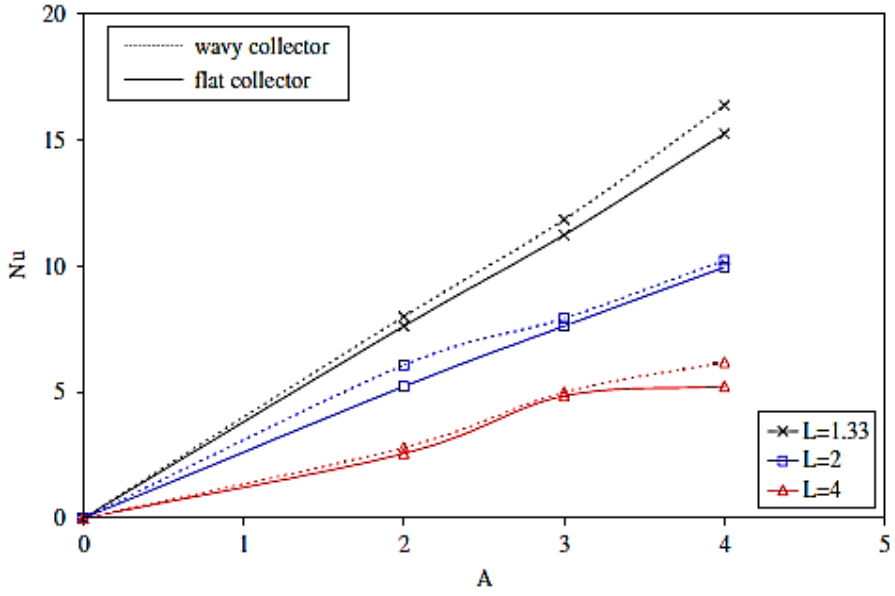

Figure 2-1 Variations of average Nusselt number with respect to aspect ratios (A) of the collector for wavy and flat collectors at ΔT=20ºC and θ=40º [36]

Sivakumar et al. [37] experimentally studied the impact of changing the geometrical parameters, which include the number of riser pipes and their arrangement in a zig-zag pattern. Experiments

have been conducted using copper tubes for header and riser, with different dimensions. The results have shown that increasing the number of riser pipes from 9 to 12 gives efficiency of 59.09%. Moreover, zig-zag configuration of the riser pipes gives an efficiency of 62.90%. Figure 2-2 illustrates the variation in the collector efficiency with respect to time at different dates. In figure, 2-2, case 1 and case 2 denotes 9 and 12 riser pipe respectively, while case 3 denotes zig-zag arrangement. The authors have found that the maximum collector efficiency during the experiments was obtained using zig-zag arrangement of riser pipes at all times, as shown in Figure 2-2. Furthermore, it can be seen clearly from the figure that the maximum collector efficiency was recorded at 13.00 hour for all the experiments. The minimum collector efficiency, at a particular time, has been recorded when 9 riser pipes were used. This study lacks detailed analysis the behaviour of the fluid flow within the riser pipes, such as velocity and temperature distributions.

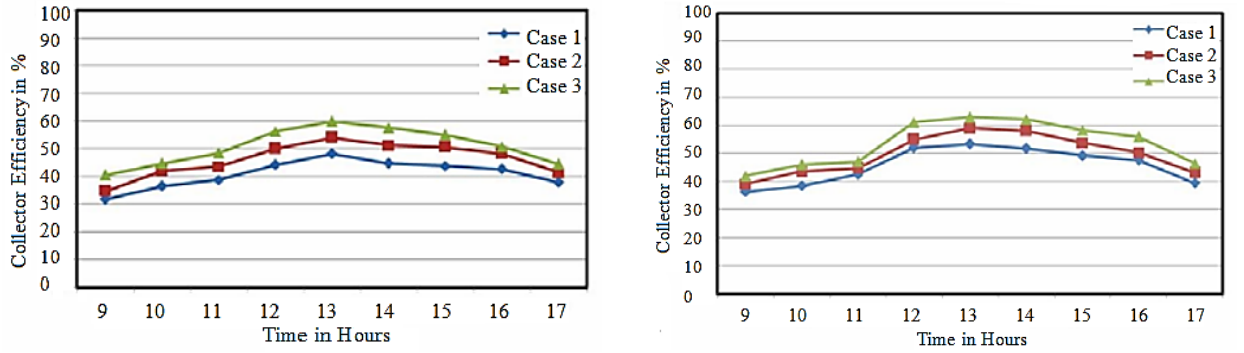

Figure 2-2 Collector efficiency variations on (a) 11th March, 2011 and (b) 18th March, 2011 [37]

Subramanian et al. [38] conducted both numerical and experimental investigation on the solar water heating system in identical conditions for both uniform header and variable header systems. The solar water heater is being designed with different header diameters. The results have indicated that the overall thermal performance decreases for variable header due to non-uniform flow in riser tubes. Furthermore, the results reveal that the overall thermal performance and efficiency are comparatively higher in the uniform header system because of uniform velocity. The study has been conducted under no loading condition and steady state heat input. Furthermore, this study has not considered various important parameters such as heat transfer coefficient, shear stress and pressure drop of the working fluid within the thermo-syphon.

Amori et al. [39] conducted a comparative study between traditional absorber design and new design of solar collectors, which is known as accelerated design, as shown in Figure 2-3, in order to analyse the performance of these two systems. The performance tests have been carried out in identical conditions for both the systems, while maintaining a tilt angle of 33º southern. Furthermore, the authors have also conducted tests on two different types of storage tanks. The results have shown a significant increase in thermal performance for the accelerated design

compared to the traditional design, due to the higher circulation rate of the working fluid with the accelerated absorber. The temperature of the storage tank for both the new and conventional designs has been recorded to be 50ºC and 37ºC respectively. As the collector's cross sectional areas are different for both the designs, the amount of working fluid within the system would be different, the effect of which has not been analysed in detail. Flow field analysis within the closed loop thermo-syphon system would be beneficical to understand the hydrodynamics within it.

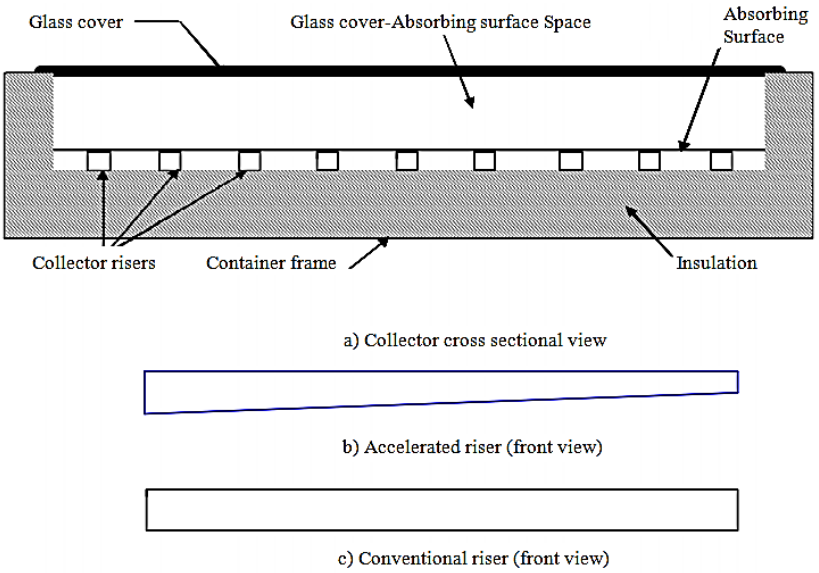

Figure 2-3 Configuration of flat plate collector [39]

El-Din et al. [40] conducted experimental investigations to evaluate the heat transfer properties of a single phase flow within a toroidal type thermo-syphon. The investigation parameters are heated-cooled length ratio, heated length tube diameter ratio, the diameter ratio of the torus-tube and the angle of inclination. The results showed that an increase in heated-cooled length ratio and heated length tube diameter ratio leads to a decrease in the heat transfer rate, whereas, an increase in the torus-tube diameter ratio increases the heat transfer rate by 11%. The reason behind this is the increased exposed surface area to heat flux. Furthermore, it has been observed that the maximum heat transfer rate has been achieved for the tilt angles range of 30º to 45º. This study did not consider the variations in the amount of working fluid in the system, and hence, a further investigation is required in this area.

Balaram [41] has carried out a comparative numerical study on the performance of closed loop thermo-syphon system. An optimization study has also been conducted for several absorber plate shapes. These absorber plates had RPSLT (rectangular profiles with a step change in local thickness), trapezoidal and rectangular as shown in Figure 2-4. The results have shown that the RPSLT profile of the absorber plate is superior to other profiles in terms of performance and difficulties in fabrication. This study has not analysed several parameters that indicate the performance of these systems, like heat gain and heat transfer coefficient in the collector.

Furthermore, a comparative study of performance with respect to traditional model has not been conducted.

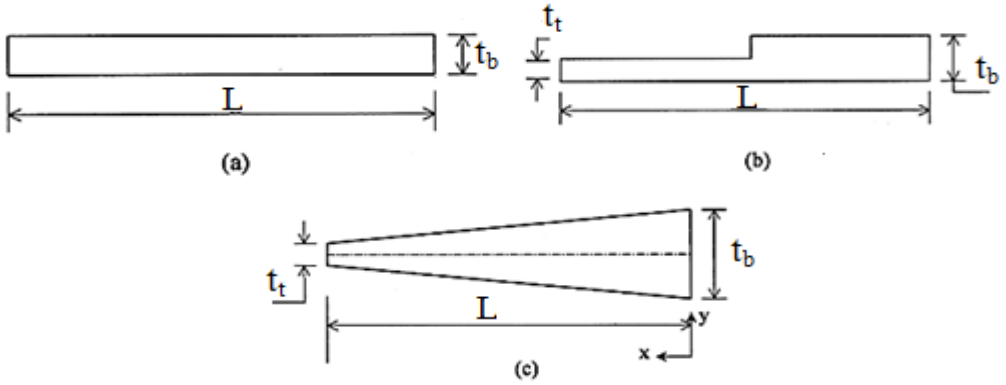

Figure 2-4 Symmetric heat transfer element schematic (a) Rectangular profile (b) RPSLT and (c) Trapezoidal profile [41]

Vishal and Patil [42] conducted a numerical study to investigate the performance of a thermo-syphon system using an elliptical tube instead of a circular pipe. In this study, nine cases have been analysed and compared with the traditional case (circular pipe) depending on the relationship between values of A and B. The values of A and B represent dimensions of the elliptical tube, where A denotes the major axis and B denotes the minor axis of the ellipsoid. The results have shown that B=0.5A gives the maximum outlet and inlet temperatures of water for the same heat flux, in comparison with circular and other elliptical geometries. This is shown in Figure 2-5 where, the variation in temperature at outlet of the collector for different riser pipe configurations. The maximum temperature difference at the outlet of the collector is 4.17ºC between the configurations (elliptical and circular pipes in the riser pipes). However, this study severely lacks in-depth analysis of several important parameters that indicate the performance of solar water heater system, such as heat transfer coefficient and heat gain in the collector.

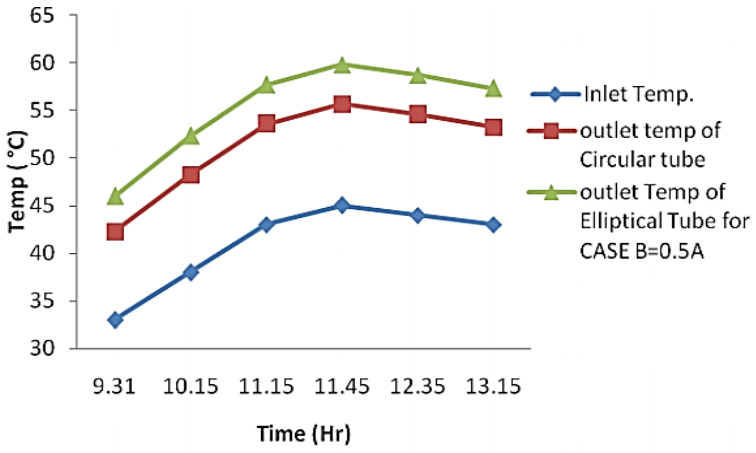

Figure 2-5 Variations of water temperature at the inlet and outlet for elliptical and circular tubes at B=0.5A [42]

A numerical examination of the transient thermal energy behaviour of a wickless heat pipe solar collector was carried out by Hussein et al. [43]. The authors have studied the effects of various parameters, which include the global solar radiation intensity, inlet cooling water temperature, absorber plate material and thickness, the ratio of pitch distance to wickless heat pipe diameter, and the ratio of condenser section length to total wickless heat pipe length on the thermal performance of solar collector. The results have shown that all these parameters have a significant effect on the efficiency of the solar collectors. According to the findings, the efficiency is inversely proportional to the inlet temperature. The efficiency of the system increase from 45% to 70% when the inlet temperature decreases from 363K to 290K. Both these measurements were taken at midday (approximately 12 O'clock). On the other hand, the efficiency of the system increases from 45% to 50% with an increase in solar radiation intensity from 1023W/m^2 to 1123W/m^2. This study did not investigate several important parameters which are indicators of system performance, like heat gain and heat transfer coefficient in collector. Furthermore, this study did not analyse the flow field of the working fluid such as velocity and temperature distribution.

The effect of water storage tank volume and configuration on the performance of a thermo-syphon solar water heating system was investigated numerically by Hasan [44]. According to the Figure 2-6, which illustrate the effect of storage tank configuration on the efficiency of a thermo-syphon solar water heating system, indicates that there is no difference between the performances of vertical and horizontal storage tank systems. The results obtained have demonstrated that using a larger hot water storage tank or smaller collector's area can drastically increase the efficiency of a solar water heating system. The study has been conducted under no loading condition which severely limits its practicability.

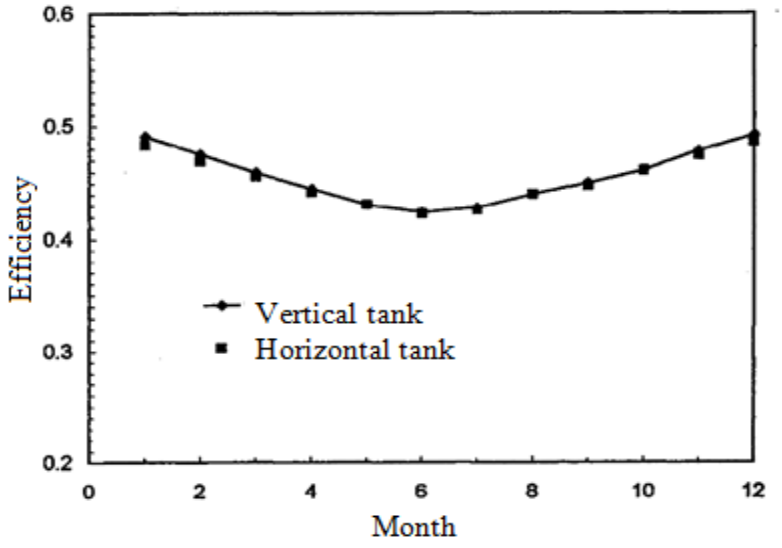

Figure 2-6 Variation of efficiency of thermo-syphon solar water heating system for varying storage tank configurations [44]

Sato et al. [45] have conducted numerical investigations on a modified solar collector by changing the configuration of the riser pipes. This study implemented Computational Fluid Dynamics tools in order to analyse the effects of riser pipe tilt angles, and the location of the downcomer pipe (conventional, lateral and inferior), on the working fluid temperature within the condenser. The study observed that tilt angle of 45º is optimal for the thermo-syphon performance. The study has been conducted under no loading condition and steady heat input.

Alshamaileh [46] conducted a comparative study experimentally between two models one painted with a nickel–aluminium (NiAl) alloy coating and the other with traditional black paint, in order to investigate the performance of these two systems. The performance tests have been conducted in identical conditions for both the models. The tests were carried out in May, July and September of 2008, and March of 2009 as well. The results show that the thermal energy for the new coating (NiAl) was higher as compared to the traditional black painted collector. Furthermore, the average temperature within the collector for new coating (NiAl) increased by 5ºC as compared to the collector with traditional black paint. This is shown in figure 2-7, which indicates the temperature variation in the collector at different time. The study has been conducted under no loading condition and steady heat input. Moreover, details regarding the behaviour of fluid flow within the riser pipes have not been provided, such as velocity and temperature distributions.

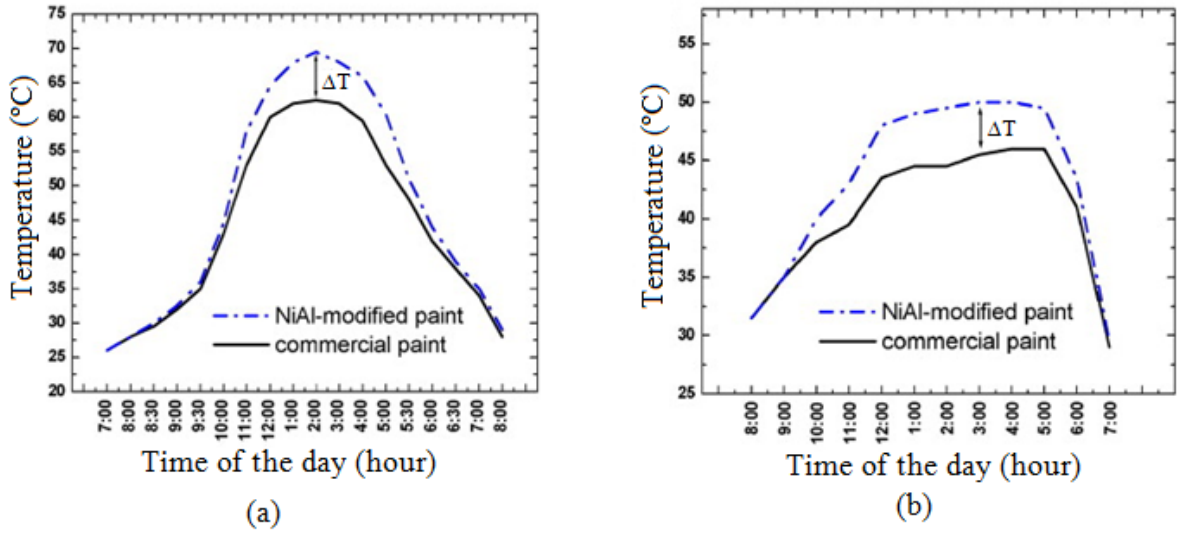

Figure 2-7 Temperature measured in both systems the commercial paint and the NiAl-modified in selected days in (A) July, 2008 and (B) March, 2009

[46]

Zerrouki et al. [47] conducted an analytical study on natural circulation in thermo-syphon domestic flat plate solar water heating system. The actual weather conditions for Algeria have been used in this study. An equation to calculate the mass flow rate of the working fluid within

the closed loop thermo-syphon system has been developed. The effect of height between the water storage tank and the collector has been investigated. Based on the results obtained, it has been shown that the mass flow rate increases with an increase in height between the storage tank and the collector. However, the height between the storage tank and the collector was found to have no considerable effects on the efficiency of the system. Analysis of flow field within thermo-syphon loop, such as velocity and temperature distribution of the working fluid, has not been discussed.

A new design of the solar water heating system has been developed by Abdel Rehim [48]. The new design has a pyramid shaped frustum in order to integrate the collector and the water storage tank into one unit, as shown in Figure 2-8. In this study, a 150L storage tank and a collector with surface area of 1.68m^2 have been used. The results have shown that the new design gives an increased level of performance as compared to the conventional solar water heater. Furthermore, it has been noticed that the water temperature within the storage tank varies with weather conditions; having a range of 40ºC to 60ºC. This performance improvement is due to the increased surface area exposed to Sun rays. Comparisons have been carried out using various levels of working fluid within the system.

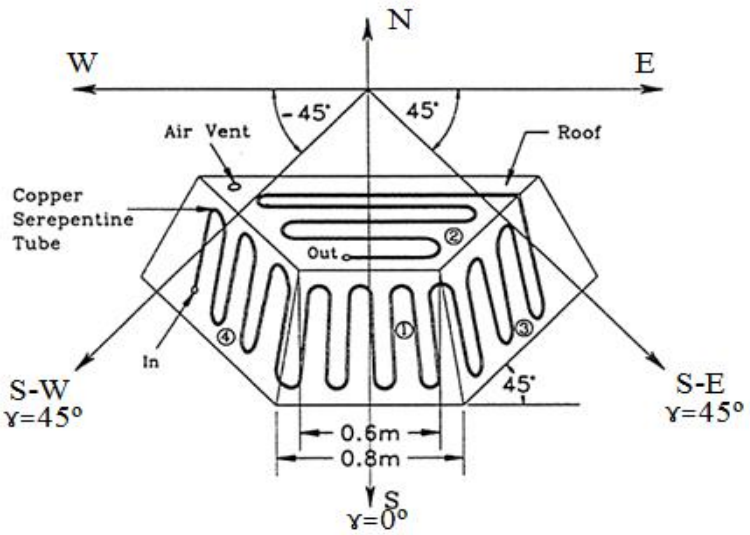

Figure 2-8 A new design of solar water heater with a pyramid shaped frustum [48]

Koff et al. [49] conducted both analytical and experimental studies on thermo-syphon flat-plate solar water heating with a mantle heat exchanger. The effect of using a heat exchanger between the collector and the tank, on the performance of the collector, has been critically analysed. The results depict that the mean daily efficiency of the thermo-syphon, with a mantle heat exchanger, can be up to 50%. This improvement in the performance of the thermo-syphon is due to increased heat energy received by the working fluid, which improves the heat transfer rate between the working fluid and the water within the storage tank. This study did not analyse the working fluid flow behaviour, such as velocity and temperature distribution. Furthermore, the

study did not consider the loading conditions and hence, analysis from this investigation does not represent real world scenarios.

Hussein et al. [50] conducted an analytical study on natural circulation in a closed loop thermo-syphon flat plate solar water heating system. Actual weather conditions for Cairo city have been used with an aim to determine the impact of (i) ratio of storage tank volume to the collector area and (ii) height between the heater storage tank and the collector, on the thermal performance. The results have shown that the ratio of collector area to storage tank volume and the storage tank dimension (height to diameter ratio) ratio have important effects on the thermal performance. The height between the heater tank and the collector has been shown to have limited effects on the heater performance. Nevertheless, the optimum height between the collector and the tank was found to be 0.2m, and the optimum tank dimension (height to diameter ratio) ratio was found to be 1.8. Analyses of the flow field within the closed loop thermo-syphon system, such as velocity and temperature distributions of the working fluid, have not been carried out.

Mathioulakis and Belessiotis [51] numerically and experimentally studied the heat transfer behaviour of a new type of solar water heating system, which consists of a wickless heat-pipe and a tank behind the collector. Ethanol was used as the working fluid, and the study was conducted under the actual operating conditions. The results have shown that the heat transfer behaviour of a new solar water heating system was characterized by high instantaneous efficiencies, with a value of approximately 60%. Furthermore, the results demonstrate that there is no significant difference between the experimental and the numerical results.

2.1.2. Summary of the literature on improving the Thermal Performance of Thermo-syphons based on their geometrical parameters

Literature review regarding the effects of the geometrical parameters on the performance of the thermo-syphon has clearly highlighted some gaps in the knowledge. Based on the discussions, it can be summarised that the published literature has severely limited range of investigation parameters. Furthermore, the previous works lack certain aspects, such as:

1. Most of these studies were conducted at constant heat flux and/or under no loading conditions, and hence these studies do not simulate the real world scenarios
2. Most of these studies lack local flow field analysis, such as temperature and velocity distribution of the working fluid
3. Interdependence of global performance indicators with the local flow field under a variety of flow conditions has not been reported in detail

2.2. Heat Transfer Enhancement

Recently, many researchers have been trying to improve the performance of the thermo-syphon solar collectors. Majority of them have tried to insert devices within the riser pipes or using a refrigerant fluid instead of water to improvement the performance of a closed loop thermo-syphon system.

2.2.1. Using External Devices in order to enhance the Heat Transfer

Iordanou et al. [52] have conducted a numerical study by using the analysis of the CFD model for investigating the effects of placing a metallic mesh inside a riser pipe of a passive solar collector, and the results obtained have been compared with a traditional solar collector. The results have revealed that the use of a metal grid inside the heat pipe leads to increased solar collector temperature. The authors have developed equations to calculate Nusselt number for a certain heat flux, which is a function of Rayleigh number only, as depicted in Eqs. (2.1) and (2.2). However, these derived equations have limited applications, since they are true only for a certain heat flux value. Moreover, these equations do not consider the geometrical parameters and loading conditions on the system.

$$Nu = 0.013(R_a)^{0.285} \qquad \text{when } q=1070 W/m^2 \tag{2.1}$$

$$Nu = 0.007(R_a)^{0.285} \qquad \text{when } q=610 W/m^2 \tag{2.2}$$

Sandhu et al. [53] conducted experimental studies to investigate the effects of inclination angle and insert devices, which include twisted-tape inserts, wire coil inserts and wire mesh inserts on the thermal performance of a flat plate solar collector. The experimental studies were carried out to compare the performance of conventional and novel insert configurations. Water has been used as the working fluid in this study. The results show that the Nusselt number is higher for all the novel insert devices as compared to the conventional system. Hence, the thermal performance for novel insert configurations is found to be better than the conventional system. The reason behind improvement of the thermal performance for insert configurations is the increased Nusselt number (because of higher heat transfer coefficient). The insert devices within the pipe may transform the flow from laminar to turbulent by increasing the Reynolds number, and hence increasing the Nusselt number. Moreover, it has been observed that the tilt angle does not have a significant impact on the Nusselt number, as shown in Figure 2-9, which shows Nusselt number variations against Reynolds number for various collector configurations. However, the amount of working fluid was different in every case and hence, comparison with traditional model is non-conclusive. Furthermore, the effect of insert devices on the temperature of water within the storage tank has not been investigated.

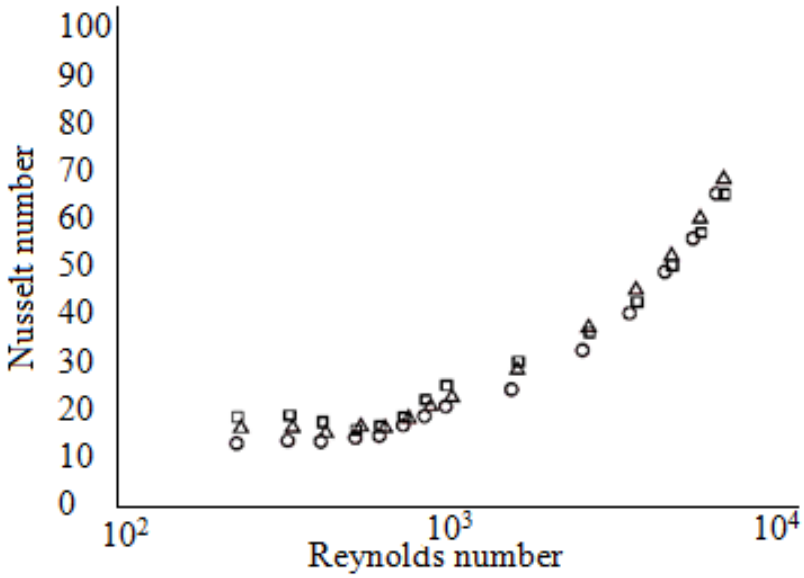

Figure 2-9 Nusselt number variations against Reynolds number for various collector inclinations (o) horizontal (Δ) 30º and (□) 45º [53]

An experimental study on the rate of heat transfer in polypropylene tubes in solar water heaters was conducted by Razavi et al. [54]. The performance was studied under ambient temperatures, within the range of 34ºC to 37ºC. Polypropylene tube was used in solar water heaters in a Reynolds number range of 800-5600. The results show that Eq. (2.3) could be used to predict heat transfer rates in a polypropylene solar heater, in Tehran, where the experiments were performed. However, this equation includes only a limited number of important parameters, and the parameters, which have an effect on the heat transfer coefficient, and hence on the values of Nusselt number, such as thermal loading, number of riser pipes, length of the riser pipes etc., were omitted

$$Nu = 0.0015\ (R_e)^{0.75}\ (P_r)^{1/3} \tag{2.3}$$

Ramasamy and Balashanmugam [55] studied the effect of different shapes of fins on the performance of the solar water heating system. Rectangular and circular fins have been used within the pipe, as shown in Figure 2-10. The results have indicated that the temperature difference at the outlet of the models with and without fins is 7-8ºC. However, the effect of change in the volume of the working fluid within the system has not been considered. Furthermore, the effect of the fins' shape, on the temperature of water within the storage tank, has not been taken into account.

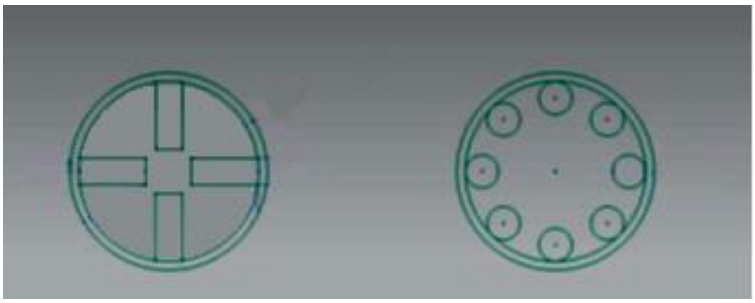

Figure 2-10 Two dimensional sketch of the rectangular and circular fins [55]

Kumar and Prasad [56] have carried out experimental investigations on solar water heating system, having twisted tapes inserted in the tubes. The results have shown that twisted tapes induce swirling flow, which acts as turbulence promoter, leading to increase in the heat transfer. The percentage increase in heat transfer has been recorded to be 18-70%. Pressure drop has also increased between 87-132%, as compared to conventional collectors. Thermal loading conditions, which have significant effects on the performance of a thermo-syphon, have not been investigated in this study.

Hobbi and Siddiqui [57] conducted experimental studies to determine the effects of inserting twisted tape, coil spring wire and conical ridges inside the collector tubes, on the heat transfer enhancement of flat plate solar collectors, as shown in Figure 2-11. The results have shown that the heat transfer rate has not been affected by using the enhancement devices, which have been used in this study. However, the effects of varying amounts of working fluid within the system have not been considered, which is one of the crucial parameters of the thermal performance of a thermo-syphon.

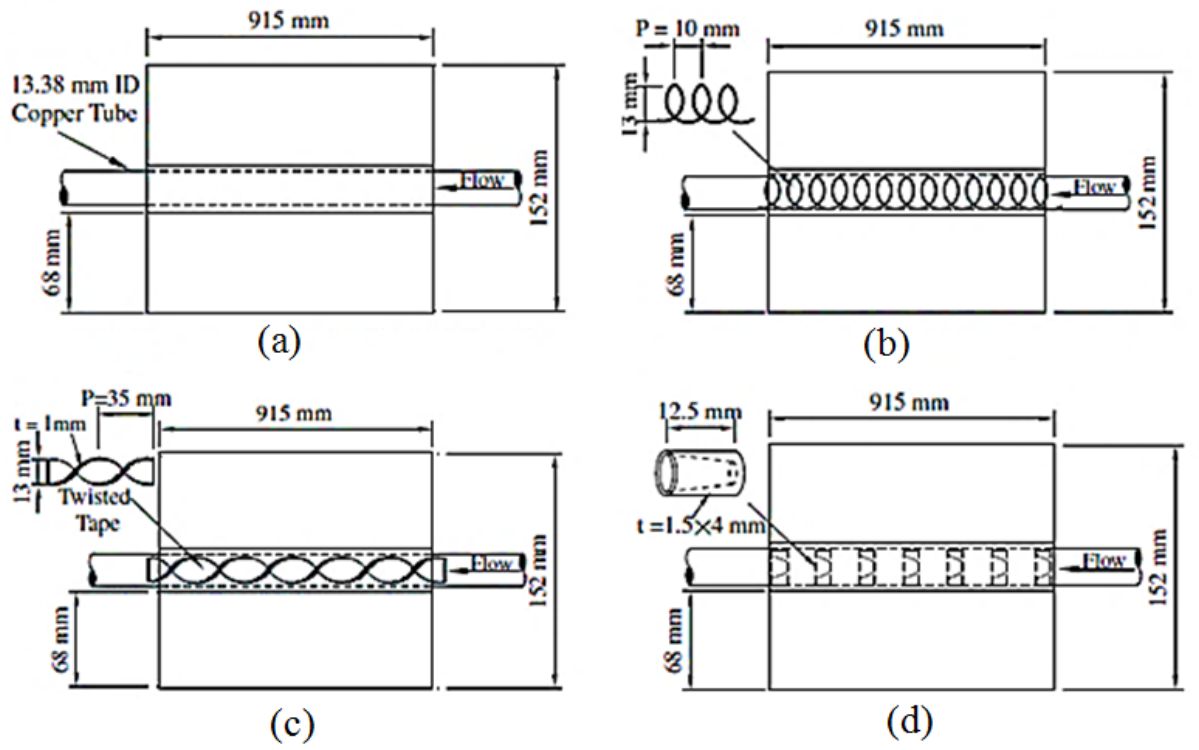

Figure 2-11 Solar collector models (a) base model, (b) coil-spring wir, (c) twised strip and (d) conical ridges [57]

Herrero et al. [58] carried out theoretical investigations on improving the heat transfer of flat plate solar collectors by using wire-coil inserts within the pipe of the collector. This study has been conducted under identical conditions for all the different models. Water and propylene glycol/water mixtures have been used as working fluids. The results have shown that the enhanced collector (with wire-coil inserts within the pipe of the collector) increases the thermal efficiency by 4.5%, as shown in Figure 2-12, which indicates comparison of thermal efficiency between the standard and the enhanced collectors. The comparison between the traditional and the enhanced collector has been conducted under different amounts of working fluid, and hence, this comparison is non-conclusive. Furthermore, this study has been carried out under no load conditions, severely restricting its practicability.

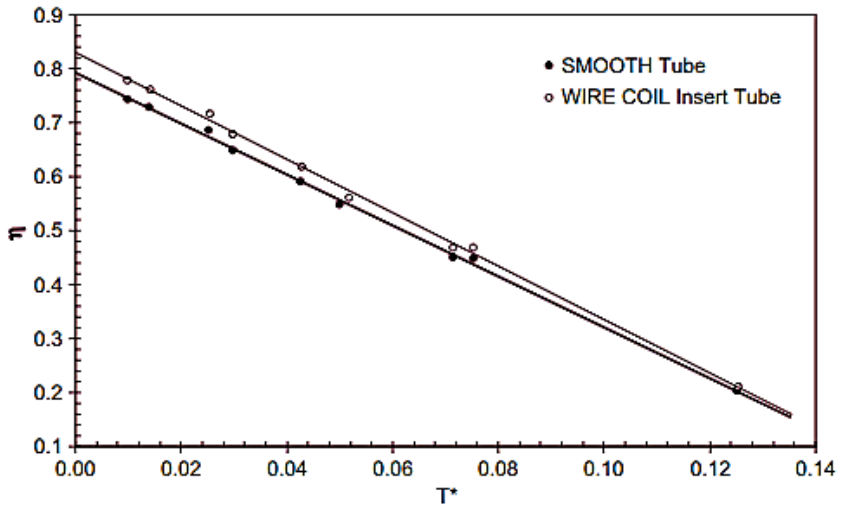

Figure 2-12 Comparison of efficiency between the standard and the enhanced collectors [58]

Jaisankar et al. [59] have conducted experimental study to analyse the performance of a thermo-syphon with respect to heat transfer and friction factor of the solar water heating system using helical and twisted risers, as shown in Figure 2-13. It has been found out that the heat transfer and pressure drop increase as the model changes from Left–Right riser to the helical riser. The experimental data were compared with the data obtained using an empirical equation. Both results match with each other closely . The results have shown that the heat transfer coefficient for traditional model is 2.71 and 3.75 times less as compared with helical and left right twisted pipes respectively. The study, however, has been conducted under no loading, and the effect of varying amounts of the working fluid within the system has not been considered.

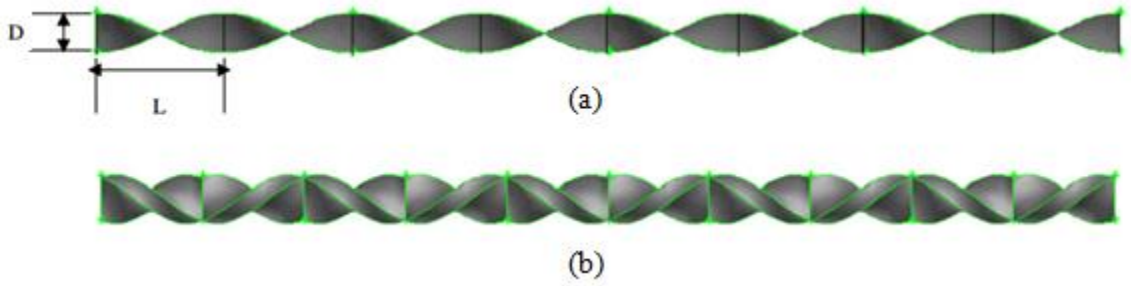

Figure 2-13 Twisted tape geometry with twist ratio 3 (a) Left Right and (b) helical [59]

Viyaykumar et al. [60] conducted experimental studies to investigate the effects of insert coiled wire in juxtaposition with twisted tapes within the riser pipe, on the rate of heat transfer, as shown in Figure 2-14. The wire coil is 5mm in thickness and is made of circular steel, while the steel strip width and thickness are 35mm and 2mm respectively. The effects of spring pitch ratios of 4, 6 and 8 on heat transfer rate have been studied. According to the results found in this

investigation indicates that the heat transfer rate in the collector has increased from 18% to 70%, and hence the thermal performance has increased about 30% as compared to the traditional model, for the same operating conditions. However, the amount of working fluid was different in both the cases, hence; comparison with the traditional model is non-conclusive. Furthermore, the effects of insert devices on the temperature of water within the storage tank, has not been investigated in this study.

Figure 2-14 Riser tube with wire coil and twisted tape [60]

2.2.2. Enhancement of Heat Transfer by changing the Working Fluid

Esen et al. [61] conducted experimental investigations on a two phase closed loop thermo-syphon solar collector with heat pipes. The authors used three refrigerants, namely R-134a, R-407c and R-410A, in similar small-scale two phase thermo-syphon solar heaters. The three systems were tested under the same working conditions in an attempt to find out the most effective refrigerant amongst them, as shown in Figure 2-15 and Figure 2-16 illustrating the daily variations of ambient temperature, average water temperature, solar radiation and collector efficiency for different loadoing conditions. The results show that R-410A as a working fluid is more efficient than other refrigerants for both non-loading and loading operations. However, this study does not present the effects of geometrical parameters on the performance of the thermo-syphon.

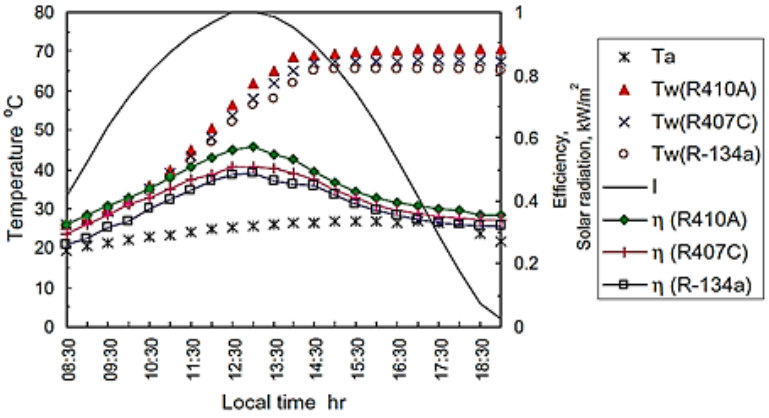

Figure 2-15 Variations of solar radiation, mean tempertaure of water, ambient temperature and efficiency of the collector for every one hour, with different refrigerants under a clear-sky no loading conditions on 10th May, 2003 [63]

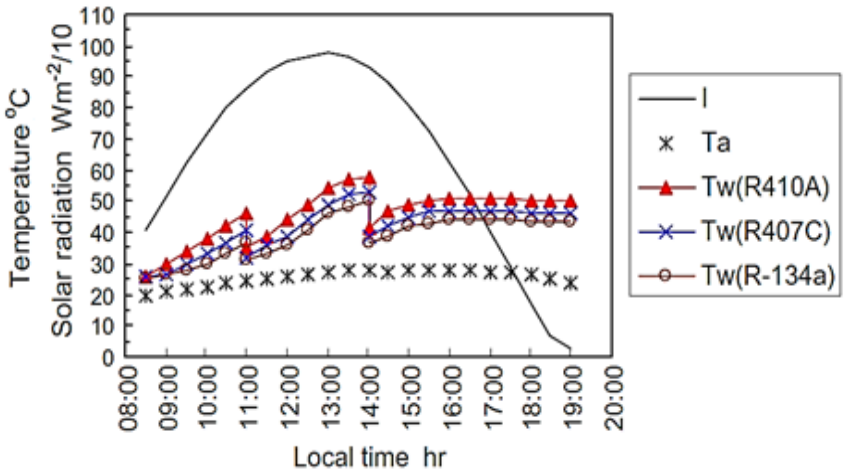

Figure 2-16 Variations of, mean tempertaure of water, temperature of ambient and solar radiation for every one hour, with different refrigerants under a clear-sky no loading conditions on 11th May, 2003 [63]

Lin et al. [62] have studied the thermal performance of a two phase thermo-syphon energy storage system, which can be integrated with building structures. The authors have considered three models, namely heat charge, heat discharge and simultaneous charge and discharge. The performance was studied for all the three models by applying indoor tests with constant intensity of light for several hours, for different fill ratios and loading conditions. Water and alcohol have been used as working fluids. The results have shown that the storage system containing alcohol as the working fluid performs better than water. Furthermore, the system gives optimum heat charge and discharge performance for 35–40% fill ratio, regardless of the working fluid being water or alcohol. The study, however, did not consider the effects of transient heat input (heat

flux), hence, this work does not simulate real world scenarios. As the heat flux depends on intensity of solar energy, it is variable during the day time.

Fanney et al. [63] have conducted experimental studies on the solar domestic water heating systems to find out the impact of irradiance levels on thermal performance of a refrigerant charge (working fluid) inside the pipes of a solar collector. The results indicate that the effects of the irradiance level on thermal performance of refrigerant were limited, and can be considered negligible. However, no information regarding the effect of geometrical parameters on the performance of thermo-syphon system has been provided. Moreover, this work severely lacks the analysis of several important parameters that affect the performance of thermo-syphon, such as heat transfer coefficient, heat gain in collector and heat gain in the storage tank.

Ahmet et al. [15] fabricated and performed comparative tests on single phase and two phase closed loop thermo-syphon solar water heating systems. R-134a has been used as the working fluid in two phase thermo-syphon, while water has been used as the working fluid in single phase thermo-syphon. Tests have been performed under identical working conditions. The results have shown that the final temperature of water within the storage tank, for two phase systems, is higher (about 9ºC) as compared to the single phase thermo-syphon system. This can be clearly seen in Figure 2-17. The authors have not mentioned the value of tilt angle for the solar collector that has been used for this study. Furthermore, the loading patterns have not been studied, along with their impact on the performance of the system.

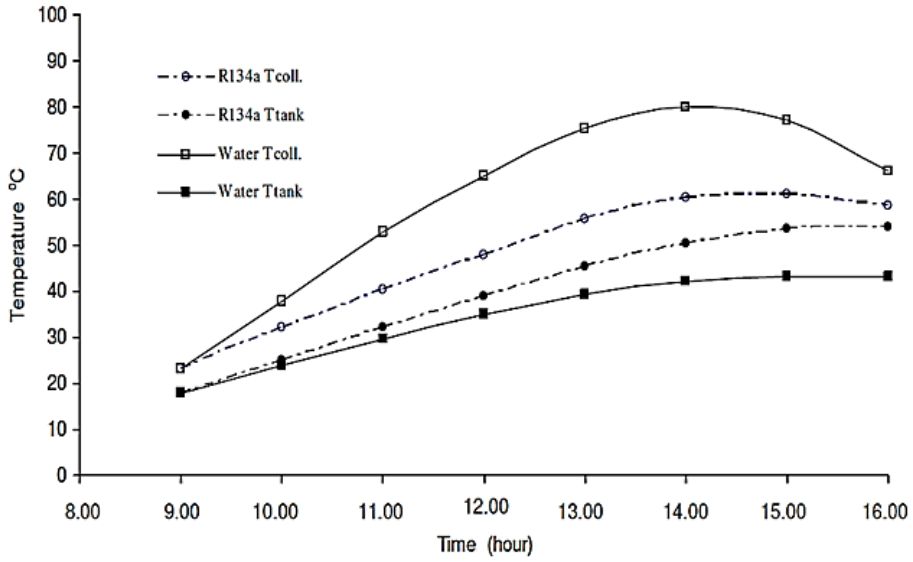

Figure 2-17 Temperature variation within the storage tank and the outlet of the collector for single phase and two phase systems [15]

Abreu and Colle [64] conducted an experimental study to examine the effects of different evaporation lengths, fill ratios of the working fluid, cooling temperature and tilt angle of

collector, on the thermal performance of a two phase closed thermo-syphon system. All the tests were carried out indoors, and an electrical skin heater was used to provide heat flux in place of solar radiation. The results have shown a decrease in thermal resistance of TPCTs (two phase closed thermo-syphon system) with increasing cooling temperatures. This trend has been observed for the lowest fill ratio of the working fluid. Furthermore, the authors have shown that the lowest thermal resistances of TPCTs were achieved for the shortest evaporators. This study, however, has been conducted under no loading conditions, which severely limits its practicability.

Riahi and Taherian [65] carried out experimental investigations on natural circulation of the working fluid, on the performance of a thermo-syphon solar water heating system. Data were collected for several sunny and cloudy days. Dynamic response of the system to variations in solar insulation was studied and analysed. The results have shown that the collector temperature reached 90ºC, and the time at which this temperature was achieved was about one hour after the time for maximum solar irradiation flux. The temperature of the top layer of water was 72ºC on a sunny day. It has been shown that these systems work well both in sunny and cloudy weather conditions. However, in this study, the heat gain in the storage tank and collector has not been investigated.

2.2.3. Summary of the literature on improving the Thermo-syphons' performance based on Heat Transfer enhancement methods

This section of the thesis comprise of a summary of the conducted literature review regarding the effects of the geometrical parameters on the performance of the thermo-syphon. It can be summarised that the published literatures have a limited range of investigations on various parameters such as heat flux and thermal loading conditions. Furthermore, the previous works lack certain aspects, such as:

1- Majority of these studies have not considered the volume change of the working fluid for a modified design of a closed loop thermo-syphon, when comparing with a baseline model. Therefore, the comparison is inconclusive,
2- Most of these studies lack in investigation of parameters such as heat gain in storage tank, heat transfer coefficient and heat gain in the collector. These parameters have ability to provide prediction regarding thermal performance of a closed loop thermo-syphon,
3- Majority of equations, which were developed have limited applications and have not included important parameters such as thermal loading, number of riser pipes and length of the riser pipes, which have an effect on thermal performance of a closed loop thermo-syphon.

2.3. Design of Thermo-syphon Solar Water Heating System

Belessiotis and Mathioulakis [66] developed simple and efficient methodology for the design of thermo-syphon solar hot-water systems. Table 2-1shows specifications of the system that has been presented in this work. This methodology can be used to estimate energy optimization of the system. However, this methodology relies on several hypotheses and constant geometrical parameters of thermo-syphon. Furthermore, in this study the costs of thermo-syphon system design have not been included.

Table 2-1 Specifications of the system [66]

Collector aperture area	2.16 m^2 (1092 mm×1980 mm)
Collector cover material	Single tempered glass, 3 mm thickness
Collector channels	17 tubes of 8 mm internal diameter, 11 cm tube pitch
Collector absorber	Selective painted copper
Collector insulation	40 mm glass wool
Collector slope	45°
Heat transfer fluid	Water–glycol mixture
Storage	Horizontal tank, volume: 162 l, diameter: 53 cm, length: 138 cm
Tank insulation	80 mm polyurethane
Heat exchanger	Double jacket
Connecting pipes	Well insulated tube, 22 mm diameter, total length 1.8 m

Rikoto et al. [67] conducted the design of the solar water heater system for heating 250L of water from 25°C to 70°C. In this study, daily global solar radiation of approximately 750W/m^2 has been assumed in April. Furthermore, all assumptions and design conditions, which have been used in this study, are shown in Table 2-2. The results have reported that to produce 250L of hot water for 7 hours, the system will require a collector with an area of 6m^2. However, in this study the costs of thermo-syphon system design have not been considered. Furthermore, other important specifications regarding geometrical parameter such as diameter, length, and number of riser pipes have not been reported.

Table 2-2 Assumptions and design conditions of the system [67]

Items	Condition or assumptions
Location	Danjawa(Latitude13°N)
Testing period	April, May, and June
Collector inlet temperature	25°C
Collector outlet temperature	70°C
Plate to covers spacing	2.5cm
Collectorto water outlet distance	25cm
Bottom and edge insulation	5cm
Top, edge and bottom loss	Negligible
Collector size	85 x 120 m^2
No. of glass covers	1
Tube spacing	8cm
Orientation	Due south
Mean solar radiation for December	750W/m^2

Agbo et al. [68] carried out numerical and experimental study to design a thermo-syphon solar water heating system, which will be utilized to heat 150L of water, up to 80°C. In this study, value of average daily global solar radiation 15MJ/m^2 per day has been assumed, and the efficiency of collector is 60%. The results have shown that to produce this amount of hot water per day, collector will need an area of 3.4m^2. However, this study did not mention other important specifications regarding geometrical parameter such as diameter, length, and number of riser pipes. Furthermore, in this study the costs of thermo-syphon system design have not been investigated.

2.3.1. Summary of Literature regarding Design of the Thermo-syphon Solar Water Heating System

Literature review is presented above about the design of the thermo-syphon solar water heating system. It can be summarised that the methodologies included in the published literature are severely limited in scope and application. Furthermore, the previous works that have been carried out in order to design the thermo-syphon lack certain aspects such as:

1- Majority of these studies depend on several hypotheses and constant geometrical parameter of thermo-syphon such as diameter, length, and number of riser pipes,
2- Most of these analyses conducted on the aforementioned literature assumed a constant or no loading on the system. However, the loading of the system will vary based on the number of users of the system and their availability to use the facility. Henceforth, to design an efficient solar water heating system, various parameters need to be considered, that capture the real life situation,
3- Majority of these studies regarding thermo-syphon solar water heating system design lack the costs optimisation.

2.4. Scope of Research

It has been noticed from the review of the published literature that the current knowledge base regarding the flow diagnostic within a thermo-syphon is fairly limited and major gaps exist in linking local flow features with global performance indicators. This information is of utmost importance to the thermo-syphon designers. Furthermore, the practical use of thermo-syphon involves a broad range of operating conditions in which the heat flux input and the thermal loading conditions constantly vary. Based on the research and studies that have been reviewed in this chapter, the scope of the research regarding a closed loop thermo-syphon has been decided.

The first research area in this study is to identify the effect of geometrical parameters on the thermal performance of the thermo-syphon under different heat flux and variety of thermal loading conditions. The practical use of thermo-syphon involves a broad range of operating conditions with varying heat fluxes. In the present study, detailed numerical investigations are

proposed to be conducted on the velocity magnitude and static temperature profiles of the working fluid within the riser pipes of a thermo-syphon.

The second research area presented, in this study, is an investigation on heat transfer enhancement. To achieve that, different models are proposed to be systematically tested in this study. The aim of this research area is to increase the surface area of riser pipes to improve the heat transfer and hence improve the thermal performance of the thermo-syphon solar water heating system. A comparative analysis has been carried out to identify the model that provides better thermal performance. Subsequently, the thermal performance of the best model has been further analysed to investigate the effect of amount of working fluid. Furthermore, the comparison between baseline model and the best new model has been carried out. It is proposed to develop a modified system with better heat transfer characteristics. It is also proposed to test the best model experimentally.

The third research area of this study is to develop design methodology of a closed loop thermo-syphon solar water heating system. Relation between various parameters has been established by analysing the numerical result of the thermo-syphon models. These parameters (number of riser pipe, length to diameter ratio of the riser pipe, heat flux, thermal loading, and time) have significant impact on the performance characteristics of the thermo-syphon. The derived relations between the parameters have been embedded in the thermo-syphon designing process. This methodology will also help to develop a more efficient system, since it considers most of the real life situations. In addition, an optimisation model has been proposed to model an efficient thermo-syphon.

2.5. Specific Research Objectives

In this work, an attempt will be made to achieve a better understanding of the flow structure within a thermo-syphon by analysing the natural convection phenomenon and its impact on the thermal performance of thermo-syphon. After a careful review of the aforementioned literature, following objectives are defined to achieve the aims of this project:

1. To determine the effect of the number of riser pipes on the performance of thermo-syphon
2. To establish the effect of length to diameter ratio (L/d) of the riser pipes on the performance of thermo-syphon
3. To determine the effect of a closed wavy tube inside the riser pipe on the performance of thermo-syphon
4. To determine the effect of a closed helical tube inside the riser pipe on the performance of thermo-syphon
5. To determine the effect of a closed straight tube inside the riser pipe on the performance of thermo-syphon with same amount of working fluid

6. To formulate the effect of a closed straight tube inside the riser pipe on the performance of thermo-syphon with larger amount of working fluid
7. To formulate the effect of a closed straight tube inside the riser pipe on the performance of thermo-syphon with smaller amount of working fluid
8. To analyse the effect of transient heat fluxes on the performance of thermo-syphon
9. To establish the effect of transient thermal loading conditions on the performance of thermo-syphon
10. Development of semi-empirical relations for the Nusselt number, Reynolds number, plate temperature and temperature of working fluid at inlet and outlet of the collector
11. Development of a design methodology for a thermo-syphon system based on optimum thermal performance and cost consideration

For successful completion of the project and achieving all the above-mentioned aims and objectives, a combination of experimental and numerical investigations have been carried out. The following chapter will provide a detailed explanation of the numerical method that has been adopted in this study.

CHAPTER 3

NUMERICAL MODELLING

According to research objectives that have been identified in the previous chapter and to have a better understanding of the flow structure within a thermo-syphon, this study uses Computation Fluid Dynamics (CFD) based technique. By using CFD, a virtual domain of working fluid has been developed to investigate the natural convection phenomenon within the thermo-syphon. This technique has been used to predict the temperature and velocity distribution of working fluid within the thermo-syphon. This chapter illustrates a brief introduction to the numerical modelling and the justification for the solver selection and the boundary conditions.

3.1. Introduction to CFD

Computational fluid dynamics (CFD) is a technique, which can be used to analyse fluid flow behaviour of systems for different applications. In this study, the CFD has been used to understand the flow characteristics in a solar water heating system. A 3D CFD analysis of the system considers the complexity of the system and provides close to real life results based on the inputs. However, for a complex system, the computational time increases significantly. Never the less, for understanding the flow behaviour, CFD is more beneficial as compared to the experimental work since through the CFD a detailed investigation can be conducted on the flow structure and other phenomenon in the system in a cost effective manner. There are several software packages available for this type of analysis, which have a wide range of applications for both academic and industrial research problems. For example, since more than five decades, the CFD has been utilised to analyse the flow phenomenon in the aircraft and jet engines industries. Recently, CFD has been applied in the design of IC engines. Moreover, in recent years, there have been applications of this method in various other sectors, which include internal combustion engines, gas turbines, and furnaces combustion chambers. Furthermore, automotive manufacturers regularly using CFD, to enhance the design of their product by predicting the drag forces caused by the airflow over the vehicle. CFD is rapidly becoming a dynamic tool in industrial processes and products designing.

The CFD helps to analyse a system with various parameters and configurations, whereas for, experimental investigation the level of cost increase with the number of configurations and the number of measurands becomes prohibitive. In addition, there are additional costs in the experimental investigations, such as labour cost, manufacturing cost, energy consumption and experimentation time. On the other hand, CFD codes can be used to produce exceedingly large volumes of result almost at no extra expense. In addition, CFD makes the parametric studies more economical to optimise the equipment performance. However, as it is mentioned before, a complex system will increase the computation time of the analysis. Comparing with the other costs and variables, the CFD technique is more effective to analyse system with various configurations.

In the present study, ANSYS fluent package has been used because it is the most-efficient computational fluid dynamics software among the other tools that exist. Fluent can give more capability in terms of analysing and time consumption for those who are interested in the optimisation of systems performance. Furthermore, this package is equipped with different physical models, which are well validated. That means fluent can provide accurate results in reasonable time for a very wide range of CFD applications.

3.2. Working of CFD Code

The CFD codes are developed based on implementing the numerical algorithms, which can solve the fluid flow problem numerically. All the CFD commercial packages provide a simple use of their interface to do the analysis. Most of the packages follow similar steps such as the inputting of parameters, obtaining, and analysing the results. Most of the CFD packages can be divided into three main components, through which the fluid flow problem is analysed.

1. Pre – Processor
2. Solver
3. Post – Processor

In the first stage (i.e pre – processing), a user can prepare the object for solution. This can be done by defining the geometry of the model. Then, the geometry is divided into a number of non-overlapping smaller suitable regions of a suitable size. This process is called meshing. Selecting either the chemical or physical phenomena modelling, defining the properties of the fluid and also specifying the appropriate boundary cell conditions which coincide with or touch the boundary of the domain, are included in the pre – processing stage [69].

There are three distinctive numerical solution techniques. They include finite element, finite difference, and finally, the spectral methods. There is also the finite volume method, which is a special finite difference formulation, is very much essential to the most well recognized CFD codes.

Due to the fact that there is quite an increase in the engineering workstations popularity, with many having outstanding graphic capabilities, recent packages of CFD are now well equipped with versatile data tools of visualisation. Such visualization tools include grid display, domain geometry, shaded and line contour plots, vector plots, 3D and 2D surface plots, tracking of particle, view manipulations, etc. In recent version, some of these facilities have included also dynamic result display through animations. In addition to introducing graphics, all the codes produce alphanumeric output that are reliable and have facilities for data export to manipulate further externally to the CFD codes. As with most other CAE branches, CFD codes graphics output capabilities have sort of transformed how its ideas are being communicated to the non – specialists.

3.3. Governing Equations of Fluid Flow

The mathematical equations governing the transport are based on the three fundamental physics principles. They include:

1- The fluid mass is conserved
2- The time rate of momentum change is equal to the sum of the fluid particle forces. (Newton's second law)
3- The rate of energy change inside the fluid particle equal to sum of the net flux of heat and rate of work done on the fluid particle (Thermodynamics first law)

The flow fluid is assumed to be continuum. In analysing the flow of fluid at macroscopic length scales, the molecular motion and molecular structure may be ignored. The fluid behaviour is described in terms of the pressure, temperature, velocity, density, etc., which are the macroscopic properties of the fluid. The smallest possible fluid elements are the points in a fluid or fluid particles whose individual molecules do not influence its macroscopic properties.

3.3.1. Law of Conservation of Mass

The mass conservation for a fluid element can be denoted as follows [70]

$$\text{Rate of change of mass in fluid element} = \text{Net rate of flow of mass into the fluid element} \quad (3.1)$$

For liquids, as the density remains constant, the equation of mass conservation can be expressed as:

$$\text{Div u} = 0 \quad (3.2)$$

Eq. (3-2) describes the net mass flow, across the boundaries, out of the system. The equation above can also be expanded fully as can be seen in Eq. (3.3).

$$\frac{\partial \mathrm{u}}{\partial \mathrm{x}} + \frac{\partial \mathrm{v}}{\partial \mathrm{y}} + \frac{\partial \mathrm{w}}{\partial \mathrm{z}} = 0 \quad (3.3)$$

Eq. (3.3) represents the mass conservation law for an incompressible, unsteady, and Three-dimensional fluid flow.

3.3.2. Law of Conservation of Momentum

The second law of Newton's states that the time rate of a fluid particle momentum change is equal the total forces on the particle [71]:

$$\text{Rate of momentum change in fluid element} = \text{Sum of the forces acting on the fluid element} \quad (3.4)$$

Forces exerted on a fluid particle are of two types, the body forces and the surface forces. Viscous force and pressure are amongst the surface forces while that of the body forces include electromagnetic, centrifugal, gravity and coriolis forces. It is quite a common practice in fluid dynamics to highlight the contributions of each type of forces.

According to the momentum conservation law, the rate of momentum change of a particle in the x-direction is equal to the sum of the rate of shear stress change and the component of other body forces acting in the x-direction. The momentum conservation law for x direction can be presented as follows.

$$\rho g_x + \frac{\partial \sigma_{xx}}{\partial x} + \frac{\partial \tau_{yx}}{\partial y} + \frac{\partial \tau_{zx}}{\partial z} = \rho \left(\frac{\partial u}{\partial t} + u \frac{\partial u}{\partial x} + v \frac{\partial u}{\partial y} + w \frac{\partial u}{\partial z} \right) \quad (3.5)$$

The momentum equation components for y and z directions can be written as:

$$\rho g_y + \frac{\partial \sigma_{xy}}{\partial x} + \frac{\partial \tau_{yy}}{\partial y} + \frac{\partial \tau_{zy}}{\partial z} = \rho \left(\frac{\partial v}{\partial t} + u \frac{\partial v}{\partial x} + v \frac{\partial v}{\partial y} + w \frac{\partial v}{\partial z} \right) \quad (3.6)$$

$$\rho g_z + \frac{\partial \sigma_{xz}}{\partial x} + \frac{\partial \tau_{yz}}{\partial y} + \frac{\partial \tau_{zz}}{\partial z} = \rho \left(\frac{\partial w}{\partial t} + u \frac{\partial w}{\partial x} + v \frac{\partial w}{\partial y} + w \frac{\partial w}{\partial z} \right) \quad (3.7)$$

The sign that is associated with the normal viscous stresses is opposite to the sign associated with that of pressure. This is because the normal sign convention allows the tensile stress to be a positive normal stress, thereby allowing the pressure, by normal definition a normal force that is compressive, having a minus sign alongside it.

3.3.3. Law of Conservation of Energy

The first law of thermodynamics can be used to derive the equation of energy. It states that the rate of energy change in fluid particle is equal to sum of the rate of heat addition to the fluid particle and the rate of work done on the particle:

$$\text{The rate of energy change} = \text{Rate of heat addition} + \text{Rate of work done} \quad (3.8)$$

The energy in the fluid particle is conserved, by calculating the total heat gain by the fluid element and the work done on the element or by the element. The mathematical representation of the energy conservation law is as follows [72]:

$$\frac{\delta(E_T)}{\delta t}+\frac{\delta(uE_T)}{\delta x}+\frac{\delta(vE_T)}{\delta y}+\frac{\delta(wE_T)}{\delta z} = -\frac{\delta(uP)}{\delta x}-\frac{\delta(vP)}{\delta y}-\frac{\delta(wP)}{\delta z}-\frac{1}{Re.\,Pr}\left[\frac{\delta q_x}{\delta x}+\frac{\delta q_y}{\delta y}+\frac{\delta q_z}{\delta z}\right] + \frac{1}{Re}\left[\frac{\delta}{\delta x}\left(u\tau_{xx}+v\tau_{xy}+w\tau_{xz}\right)+\frac{\delta}{\delta y}\left(u\tau_{xy}+v\tau_{yy}+w\tau_{yz}\right) + \frac{\delta}{\delta z}\left(u\tau_{xz}+v\tau_{yz}+w\tau_{zz}\right)\right] \quad (3.9)$$

where E_T represent total energy

3.3.4. Equations of State

Three-dimensional fluid motions can be described by a five partial differential equation system. This five partial differential equation include momentum equation in x, y and z direction, energy equation and mass conservation equation. Density, Temperature, internal energy, and pressure are four thermodynamic variables that are also unknown. Before we can obtain any relationships among any of the thermodynamic variables, thermodynamic equilibrium assumption has to be made.

Fluid particle properties rapidly change from one place to another within a flow field and the fluid can adjust itself thermodynamically to the new conditions so fast that these alterations are taking place instantly. Hence, making the fluid always to be in a state of thermodynamic equilibrium. However, there is only one exception. They are some specific flow, having resilient shockwaves, and can be often approximated well enough by making equilibrium assumptions. A thermodynamic equilibrium system can be described by using only two state variables. Equations of state can be used to relate two state variables, which are temperature and density, the other state variables. Eq. (3.10) and (3.11) are given as the equations of state [73]:

$$p = p\,(\rho,T) \quad (3.10)$$

and

$$i = i\,(\rho,T) \quad (3.11)$$

At low-speed flow, gases and liquids act as fluids that are incompressible. Without variations in density, mass conservation equation, energy equation, and momentum equations have no linkage between them. Therefore, momentum and mass conservation equations are often used to solve the fluid flow field along with the ideal gas law. However, the energy equation is implemented only for a situation where the heat transfer is considered.

3.3.5. Navier – Stokes Equations

In a typical Newtonian fluid, the viscous stresses are proportional to the fluid deformation rate. Since we know that liquids in general are incompressible, the viscous stresses, therefore, are twice the size of the linear deformation local rate, and then multiplied by the dynamic viscosity. These equations are given below [74]:

$$\rho g_x - \frac{\partial p}{\partial x} + \mu\left(\frac{\partial^2 u}{\partial x^2} + \frac{\partial^2 u}{\partial y^2} + \frac{\partial^2 u}{\partial z^2}\right) = \rho\left(\frac{\partial u}{\partial t} + u\frac{\partial u}{\partial x} + v\frac{\partial u}{\partial y} + w\frac{\partial u}{\partial z}\right) \quad (3.12)$$

$$\rho g_y - \frac{\partial p}{\partial y} + \mu\left(\frac{\partial^2 v}{\partial x^2} + \frac{\partial^2 v}{\partial y^2} + \frac{\partial^2 v}{\partial z^2}\right) = \rho\left(\frac{\partial v}{\partial t} + u\frac{\partial v}{\partial x} + v\frac{\partial v}{\partial y} + w\frac{\partial v}{\partial z}\right) \quad (3.13)$$

$$\rho g_z - \frac{\partial p}{\partial z} + \mu\left(\frac{\partial^2 w}{\partial x^2} + \frac{\partial^2 w}{\partial y^2} + \frac{\partial^2 w}{\partial z^2}\right) = \rho\left(\frac{\partial w}{\partial t} + u\frac{\partial w}{\partial x} + v\frac{\partial w}{\partial y} + w\frac{\partial w}{\partial z}\right) \quad (3.14)$$

3.4. Pre-Processing

The CFD analysis contains two main stages and they are pre-processing and post processing. Pre-processing is divided in to two further stages as creating the geometrical model and meshing the geometric model [75-79]. The thermo-syphon geometry can therefore be created and then meshed suitably in order to proceed with analysing the model further.

3.4.1. Thermo-syphon Geometry

In order to analyse the thermal performance of a closed loop thermo-syphon system, geometrical features of thermo-syphon system has been modelled as shown in Figure 3-1. The model consists of several inclined riser pipes connected at the top to the upriser and at the bottom to the downcomer. An internal diameter of 13.6mm has been used for riser pipes, with a thickness of 0.7mm. These dimensions are considered based on standard dimensions of the UK copper pipe. In this work, the upriser and downcomer diameters and thickness were kept as same as the riser pipe. The reason behind that is to avoid losses, due to increase in the upriser and downcomer diameters with respect to the diameter of the riser pipe that leads to increase in the amount of losses in the flow such as increase in heat loss and friction loss (between inner surface and working fluid). The contribution of these losses will reduce the thermal performance of a closed loop thermo-syphon system. The inner diameter of the condenser is kept at 20.2mm, with thickness of 0.9mm. The model has been investigated under various lengths to diameter ratios of riser pipes L/d = 50, 75 and 100 for different heat flux values being applied to the riser pipes, simulating the effect of the solar rays on these pipes. The whole model is made with a 53º inclination, which is the latitude of the site of the Huddersfield city. Recently, several researchers

have studied the effect of number of riser pipes on the thermal performance of a closed loop thermo-syphon system. However these studies were very limited [37]. In order to analyse the effect of the number of riser pipes on the thermal performance output of a closed loop thermo-syphon extensively, five, seven, and nine riser pipes have been modelled separately in the thermo-syphon model.

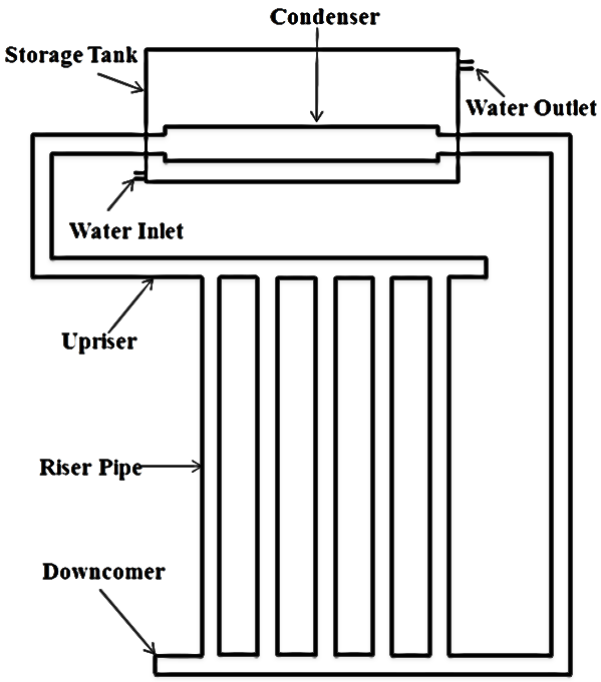

Figure 3-1 The geometry of the thermo-syphon

3.4.2. Meshing of the Flow Domain

The next step after completing the geometric modelling is creating mesh of the flow domain. Meshing is important [80] for generating the flow field solution at mesh point. The hybrid meshing is used for 3D simulations for the flow domain, which consists of two different meshes, namely hexagonal and tetrahedral as shown in Figure 3-2 [81]. Hexagonal mesh elements give more accurate results due to lower diffusion [82]. In order to capture the fluid flow phenomena accurately in the boundary layer region, mesh elements should be concentrated in this region. For this purpose, inflation layers have been implemented on the walls. For the mesh independence test, three and ten layers of inflation have been implemented with first layer thickens of 0.7mm and growth rate of 1.2 [83]. The mesh independence test indicates that three layers of inflation are sufficient for this study.

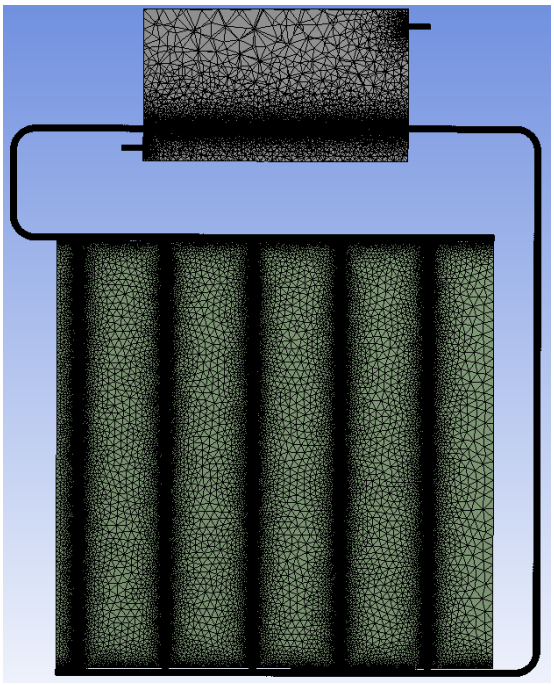

Figure 3-2 Mesh of thermo-syphon numerical model

3.4.3. Details of Calculation Method for y+

y+ can be defined as a non-dimensional distance from the wall. It indicates the size of the first cell height from the wall. A lower y+ value helps to predict the flow characteristics close to the wall more accurately and hence provide better results in comparison with higher y+ value. Since, the current study deals with the heat transfer, first the dimensionless temperature should be calculated using following equation [84]:

$$T^{+} = \frac{T_w - T}{T^{*}} \tag{3.15}$$

where T_w the wall temperature at a certain point and T is the fluid temperature.

T* can be determined as follow:

$$T^{*} = \frac{(\alpha)*(q)}{(k)*(u^{*})} \tag{3.16}$$

where q, α, k and u^{*} denotes the wall heat flux, thermal diffusivity, thermal conductivity and dimensionless velocity respectively. The dimensionless velocity can be estimated as follow

$$u^{*} = \sqrt{\frac{\tau_w}{\rho}} \tag{3.17}$$

where ρ denotes the density, while t_w denotes the wall shear stress. The wall shear stress can be calculated using the following:

$$\tau_w = \frac{\mu u}{y} \tag{3.18}$$

where μ denotes the dynamic viscosity, u denotes the velocity of fluid and y denotes the distance from the wall.

To calculate y+ following equation can be used [85]:

$$y^+ = \frac{T^+}{P_r} \tag{3.19}$$

where P_r denotes the Prandtl number

- **Sample Calculation of y+**

The y+ value of the model can be calculated by following the steps mentioned below.

1- Calculate reference temperature (T_{ref})

$$T_{ref} = \frac{T_w + T}{2} = \frac{18.478 + 17.681}{2} = 18.079^oC$$

2- Values of the properties of fluid are given by [86] at a reference temperature. These values are($\mu = 0.00102 kg/m.s$, $\rho = 998 kg/m^3$, $k = 0.602 W/m.K$, $\alpha = 1.48E\text{-}07 m^2/s$, $P_r = 6.94$)

Calculated wall shear stress, based upon the velocity (u) retrieved from a solution of the flow field, which is $3.08 \times 10^{-4} m/s$. In this simulation, the first layer thickness(y) was defined as 0.0007m. Hence,

$$\tau_w = \frac{\mu u}{y} = \frac{0.00102 * 0.000308}{0.0007} = 0.000448 W/m^2$$

3- Calculate u^*

$$u^* = \sqrt{\frac{\tau_w}{\rho}} = \sqrt{\frac{0.000448}{998}} = 0.00067$$

4- Calculate T^*

$$T^* = \frac{(\alpha)*(q)}{(k)*(u^*)} = \frac{(1.48E-07)*(198.636)}{(0.602)*(0.00067)} = 0.072854$$

5- Calculate T^+

$$T^+ = \frac{T_w - T}{T^*} = \frac{18.478-17.681}{0.072854} = 10.94933$$

Calculate y +

$$y+ = \frac{T^+}{P_r} = \frac{10.94933}{6.94} = 1.578$$

It is commonly accepted in CFD that the laminar sub layer to be in the region, where y+ < 10 [84]. By using the similar steps as shown in example above, the value of y+ for other cases was estimated. Table 3-1 summarises the value of y+ for all cases, which is considered in this study.

Table 3-1 The value of y+

Number of riser pipe	L/d	Heat flux	Thermal loading	y+
5	75	15th of March	Weekday	1.578
7	75	15th of March	Weekday	1.419
9	75	15th of March	Weekday	1.293
5	50	15th of March	Weekday	1.368
5	100	15th of March	Weekday	2.058
5	100	15th of June	Weekday	2.2
5	100	15th of September	Weekday	1.81
5	100	15th March	weekend	1.967

3.5. Solver Execution

The solver used in the present study is called Fluent, which is an integral part of CFD package Ansys 14. The details of the solver settings used in the present study have been presented in the following section.

3.6. Selection of the Physical Models

The working of a closed loop thermo-syphon system was modelled as follows:

1. Three dimensional Navier-Stokes equations, along with the energy and the continuity equations, have been solved numerically. In the CFD, an iterative approach has been adopted to simulate the transient flow of water in the thermo-syphon
2. Radiation: In fluent there are five models regarding radiation namely [87]
    - P1 Model

- Discrete Ordinate Model
- Surface to surface model
- Discrete transfer Radiation Model
- Rosseland Model

All models mentioned above have certain advantages and limitations. The Discrete Ordinate Model has technical CPU limitation [88]. However, it considers Scattering Coefficient of the species. The Scattering Coefficient for radiation captures a cloudy day environment condition. Therefore, for this study the Discrete Ordinate Model has been used.

3. Boussinesq approximation has been used to model the generated buoyant forces being more accurately. This approximation ignores the density differences, except where they appear in terms multiplied by g i.e. the acceleration due to gravity, since it is sufficiently small to be neglected. The essence of the Boussinesq approximation is that the difference in inertia is negligible, but gravity is sufficiently strong to make the specific weight appreciably different. In the Present study, the Boussinesq approximation approach has been used for several reasons as follow:

- The Boussinesq approximation is valid when the density variation is very small [89]
- The Boussinesq approximation leads to reduce complexity of variations in density of fluids [90-96]

4. Thermal expansion coefficient of water can be calculated by using Eq.(3.20) [97]

$$\acute{\beta} = (0.8\,T^{0.5348} - 1.9114) * 10^{-4} \tag{3.20}$$

where T is temperature of working fluid (°C)

5. The wall of the pipe can be considered smooth when the thickness of the laminar sub-layer is higher than the roughness [98-101]. In this study, the effect of the roughness has been ignored due to the flow within the pipe being laminar.

3.6.1. Material Properties and Operating Conditions

In the present study, the investigations have been carried out in a closed loop thermo-syphon system. The fluid medium within the thermo-syphon has been defined as liquid-water with an initial density of 998.2kg/m^3, dynamic viscosity of 1.003*10^{-3}kg/m.s, thermal conductivity of 0.6W/m.ºC and specific heat of 4.182kJ/kg.ºC. The material for the thermo-syphon pipe that has been used in the current study is copper.

The operating conditions being specified in to the solver are the operating pressure of 101.3kPa (i.e. atmospheric pressure) and turning the gravitational acceleration of 9.81m/s^2 on for the investigations carried out in a closed loop thermo-syphon system.

3.6.2. Boundary Conditions

In this study, the performance of a closed loop thermo-syphon solar water heating system has been analysed under various thermal loading conditions for three weather conditions (March, June, and September) in Huddersfield. The results presented here correspond to seven hours of continuous operation of the thermo-syphon. Because a closed loop thermo-syphon solar water heating system relies on the solar energy. Therefore, it is necessary to calculate the solar heat flux received by the system. The solar radiation intensity, on an inclined surface of the solar collector can be defined as function of solar angle, tilt angle of system and location (local latitude). In this current study, the transient effects of the heat flux and thermal loading on the system have been investigated by altering the boundary condition of the system through a User Defined Function (UDF). APPENDIX A illustrates the used UDF implemented in this transient study. Heat flux exposed to the riser pipes has been calculated using Eq. (3.21). The uprisers and downcomers are assumed to be well insulated and the thermal losses from these components are ignored [102-104] for all the cases under the present study. The reasons behind this assumption are, firstly the o thermal losses are small as the surface area of these parts are small, secondly, it is expected that this loss will be same for all the configurations tested and hence will not affect final optimized outcome. Thermal loading data has been obtained from Aung et al. [105].

$$q = I_T \varepsilon \tau [\sin\delta \sin(\theta - \propto) + \cos\delta \cos(\theta - \propto) \cos\omega] \tag{3.21}$$

where I_T is solar radiation intensity, δ is the inclination angle, θ is tilt angle of thermo-syphon, $\propto$ is local latitude and ω is the hour angle of the sun and ε denotes the correction factor of the earth's orbit and can be calculated by equation (3.22) [106].

$$\varepsilon = \left[1 + 0.033 \cos\left(\frac{360 N_d}{365}\right)\right] \tag{3.22}$$

N_d denotes the day number, and τ denotes the atmospheric transmittance. τ value varies with location and elevation and is typically between 0 and 1, according to Sen [107] . At very high elevations with clear air, the value of τ can be considered as high as 0.8, whereas for a clear sky with high turbidity, it can be as low as 0.4.

Figure 3-3 depicts the variations in heat flux inputs on different days of the year in Huddersfield, from 9am to 4pm. The three days shown cover a wide variety of seasons encountered in a solar year. It can be seen that during the morning period, the heat flux increases until midday, then decreases throughout the afternoon. This trend is the same for all the three days.

Figure 3-4 depicts the findings of a research conducted by Aung et al. [105], which demonstrate the variations in thermal loadings, from 9am to 4pm, over weekdays (WD) and weekends (WE). It can be clearly seen that the thermal loading is higher during the morning period as compared to the afternoon.

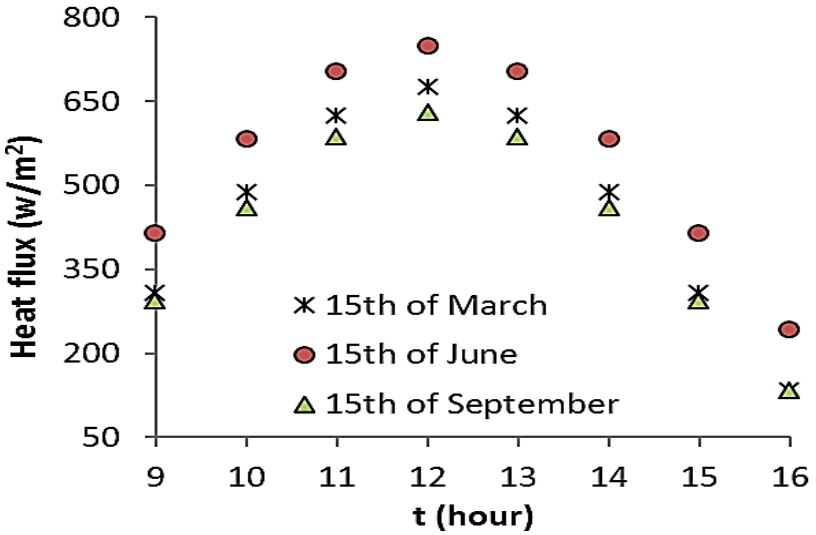

Figure 3-3 Heat fluxes, as a function of time, for various days of the year

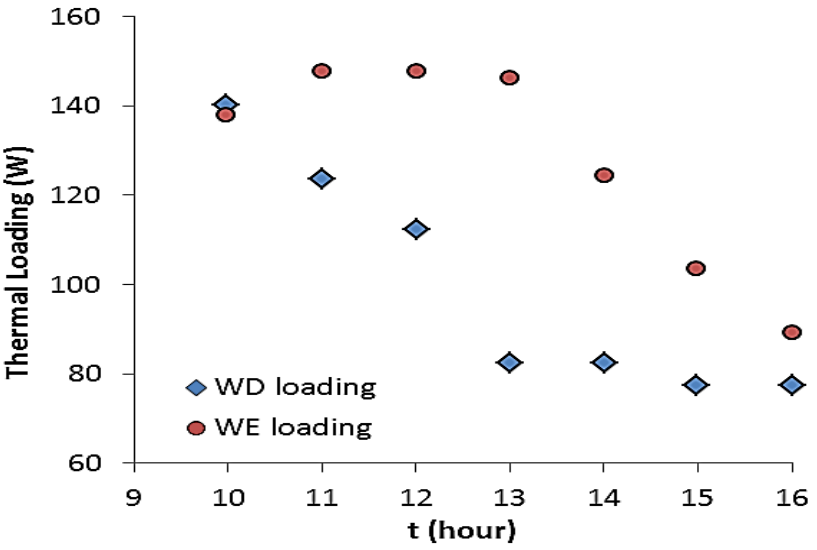

Figure 3-4 Thermal loading during a weekday and weekend [105]

Furthermore, a program has been created by using MATLAB code as shown in APPENDIX B. This program can be used to calculate the solar radiation intensity for any day of the year and at any hour on the day and any location of the world with reasonable accuracy.

Using multiple regression analysis on the data generated from the Eq. (3.21) for heat flux, three equations have been developed for measuring heat flux (corresponding to 15th March 15th June and 15th September). Thermal loading data have been obtained from [97] and two equations to measure the transient thermal loading (representing weekday and weekend loading conditions) have been developed. All these equations above are listed in Table 3-2. Those expressions have been used to define the transient boundary condition of heat flux and thermal loading via a user-defined function (UDF) as included in appendix A.

Table 3-2 Set of equations for heat flux and thermal loading

Type	Equations	Data
Heat Flux (W/m^2)	$HF = HF_{max}\left[3.702\left(t/t_{max}\right)^4 - 6.381\left(t/t_{max}\right)^3 + 0.472\left(t/t_{max}\right)^2 + 1.949\left(t/t_{max}\right) + 0.453\right]$	15th March
	$HF = HF_{max}\left[2.484\left(t/t_{max}\right)^4 - 4.281\left(t/t_{max}\right)^3 - 0.103\left(t/t_{max}\right)^2 + 1.667\left(t/t_{max}\right) + 0.556\right]$	15th Jun
	$HF = HF_{max}\left[3.674\left(t/t_{max}\right)^4 - 6.333\left(t/t_{max}\right)^3 + 0.494\left(t/t_{max}\right)^2 + 1.913\left(t/t_{max}\right) + 0.461\right]$	15th September
Thermal Loading (W)	$TL = TL_{max}\left[-4.173\left(t/t_{max}\right)^4 + 8.06\left(t/t_{max}\right)^3 - 4.22\left(t/t_{max}\right)^2 - 0.192\left(t/t_{max}\right) + 0.995\right]$	Working Day
	$TL = TL_{max}\left[0.887\left(t/t_{max}\right)^4 - 0.55\left(t/t_{max}\right)^3 - 1.62\left(t/t_{max}\right)^2 + 0.797\left(t/t_{max}\right) + 0.997\right]$	Week End

where, t is instantaneous time and t_{max} is maximum time of operation

In the present work, a number of statistical analysis tests have been used to ensure the validity of the regression models. These statistical analysis tests are namely F-value, Durbin-Watson statistic, standard error, t-Test value, Lilliefors test, Chi-square and p-value. A brief description is provided for each test. Appendix C shows the important features of the considered tests and their significance.

Several statistical tests have been undertaken to justify the usefulness of the developed equations using multiple regression analysis. Table 3-3shows that the derived equations have achieved the acceptable criteria in all the tests. That means the equations can be used with confidence for further applications.

Table 3-3 The proposed statistical tests and thier acceptance criteria

Type of test	Acceptance criteria		H.F (15^{th} March)	H.F (15^{th} March)	H.F (15^{th} March)	TL (WD)	TL (WE)
F-value	If (F < F critical) is accepted [108]	F	1.0020	1.0017	1.0025	1.0364	1.1186
		F critical	4.2838	4.5108	4.3641	4.2838	4.2031
Durbin-Watson statistic	Less than 2 is accepted [109]		1.8085	1.3457	1.7017	0.2742	0.3798
Standard error	Regression		57.1552	51.339	52.508	8.03E-05	7.90E-05
	Numerical data		57.0963	51.376	52.441	8.15E-05	7.41E-05
	Percentage error (%)		0.103	0.072	0.127	1.472	6.612
t-Test	Closed to zero [110]		0.00065	0.00078	0.00218	0.02124	0.0525
Lilliefors test	If 0= accepted 1= rejected [111]		0	0	0	0	0
Chi-square	Less than 0.05 is accepted [112]		0.012	0.009	0.009	0.03	0.02
P-value	More than Chi-square is accepted [112]		1	1	1	1	1

3.6.3. Solver Setting

Working by natural convection has been chosen for solver setting in FLUENT. In this study, the following solver settings have been used:

1. Double Precision Transient solver because it provides more precise results [113]. Pressure-Based solver has been used as the flow is subsonic and incompressible flow [114]. This work was carried out under transient simulation conditions hence, PISO algorithm with a neighbour correction for pressure – velocity coupling was used [115] for this transient simulations with large time step size.
2. To construct the values of gradients, as in secondary diffusion terms and velocity gradients, at the cell face, Green-Gauss node based methodology has been used in the present study [115]. Green-Gauss Node Based has been selected because this option is more suitable than the cell-based gradient option for unstructured meshes, as it provides more accurate results [116]
3. The solver stores the calculated values at the centre of cell. However, for convective terms in momentum equation, face values are also required. These values are taken by using Upwind spatial discretisation scheme which interpolates the cell centre values . The Second Order Upwind discretization method has been chosen as it predicts results with a

better accuracy. In this process, Tylor series expansion has been implemented for the cell centred solution at the cell centroid and therefore improves the accuracy [115]. The Body Force Weighted method has been selected, because, present study has been conducted with natural convection [117]

3.6.4. Convergence Criteria

The convergence criteria indicate the convergence of the solution. It is, therefore, essential to consider this factor. The default convergence criterion for the continuity and temperatures in three dimensions and the laminar parameters in Ansys 14 is 0.001.

This chapter provided a detailed explanation of the CFD models used in this study, such as geometry, mesh generation and solver setup. In order to verify the numerical model, an experimental setup was built with the same geometrical features used the CFD models. In the next chapter, the experimental setup and procedure used to collect the data is described in detail.

CHAPTER 4

EXPERIMENTAL SETUP

The previous chapter presented the methodology of the CFD modelling implemented in this study, which includes the governing equations, geometry creation, mesh adoption, and justification of applied boundary conditions. The numerical results are proposed to be verified against the experimental findings. This chapter provides a detailed description of the experimental setup by describing the equipment used and the justification of the setup and the test procedure. Furthermore, it also includes the instrumentation calibration procedure and the method of estimating the uncertainties in the experiment.

4.1. Introduction

The experimental setup of a closed loop thermo-syphon solar water heating system has been developed in the fluids lab at University of Huddersfield. There are two main aims of the experimental work, the first aim is to verify numerical thermo-syphon models predictions by comparing the results obtained from experimental tests with the CFD results. The second aim is to evaluate enhanced heat transfer for the optimum new model on the thermal performance of thermo-syphon as compared to traditional model that has been mentioned in previous chapter. This work is conducted to achieve objective five, which is to determine the effect of a closed straight tube inside the riser pipe on the performance of thermo-syphon with same amount of working fluid. A prototype model of this configuration has been developed for the experimental work. The characteristics of the baseline model have been mentioned in section (3.4.1)

4.2. Thermo-syphon Components

Like any test rig, a closed loop thermo-syphon solar water heating system consists of several components. The following sections provide an extensive description of the components used during this experimental work.

4.2.1. Casing Collector

Figure 4-1 shows the casing of the thermo-syphon set up. Casing was carefully designed to hold the collector and other components at the required location. Wood was chosen as the preferred material to build the casing after careful consideration, as it is inexpensive, strong, easy to manufacture, requires low maintenance and has low heat conductivity. The casing holds the riser pipes and the upriser, which is placed at 53º with the ground. The dimensions of the casing are defined based on literature regarding the experimental work [39]. In this study, the dimensions of the casing are 1100 mm x 1200mm x 180mm in length, height and depth respectively, while a wooden sheet with a thickness of 18mm was used for the rear of the casing.

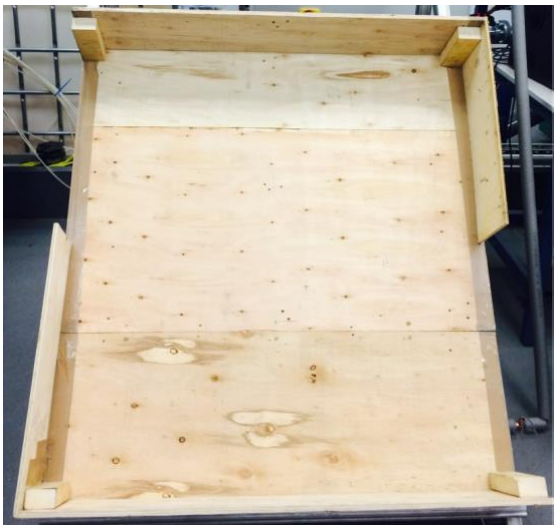

Figure 4-1 The casing of thermo-syphon

4.2.2. Insulation

Celotex PIR GA4075 insulation board was used to insulate the back and the sides of the wooden thermo-syphon casing mentioned in section 4.2.1 in order to reduce the heat loss of thermo-syphon. The Celotex PIR boards are specially made for cut-to-fit applications and have excellent lower overall heat transfer coefficient values with having just a single layer of insulation while having a core comprising of polyisocyanurate (PIR), hence providing lower heat loss. Thickness of insulation used is 50mm [118] as shown in Figure 4-2.

Figure 4-2 Insulation

4.2.3. Collector

The collector consists of several inclined riser pipes connected at the upper end to the upriser, and at the lower-end to the downcomer, as shown in Figure 4-3. An external diameter of 15mm has been selected for the riser pipes, upriser and the down comer, with a wall thickness of 0.7mm based on standard dimensions of the UK copper pipe. In this experimental work, the length-to-diameter ratio of the riser pipes is 75. Copper has been selected as the pipe material for its material characteristics, which suits the current purpose such as low cost, high thermal conductivity and well machinability.

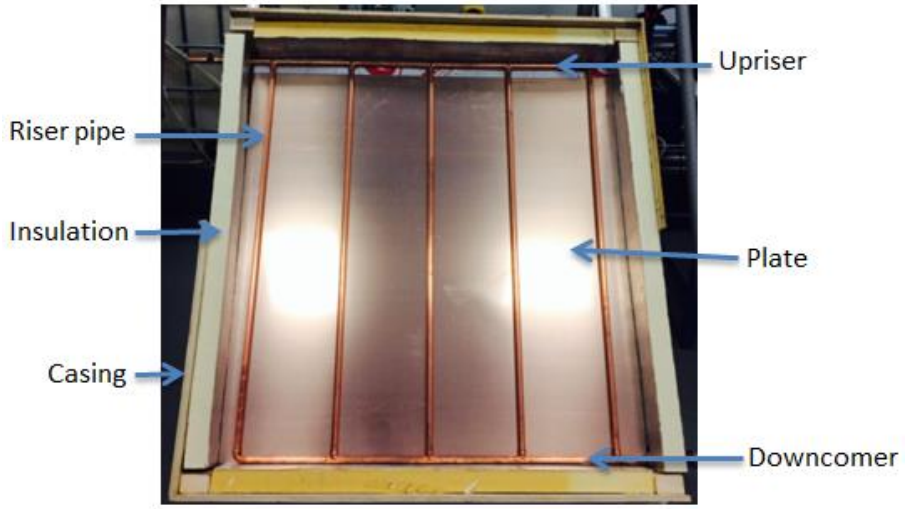

Figure 4-3 Collector of thermo-syphon

Black paint has been used for painting collector in order to increase the heat absorption and reduce the heat emission, as shown in Figure 4-4.

Figure 4-4 Black painting of collector of thermo-syphon

4.2.4. Halogen Floodlight

Four 500W Linear Halogen R7s Bulbs with 118mm length have been used in an array formation and evenly spaced over an area of $1m^2$, as shown in Figure 4-5. Each halogen floodlight has been placed inside a 18cm x 16cm casing. The Halogen lights were made from die cast aluminium with a toughened glass diffuser to ensure the safety during the experiment. The light has a handle, which was used to hang it from a support on the top of the collector. Moreover, this handle bar also helps to improve the handling feature.

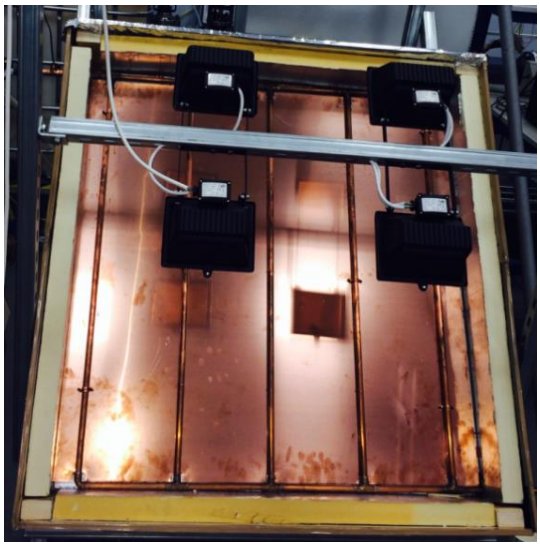

Figure 4-5 Halogen Floodlight

4.2.5. Storage Tank

To store the required amount of hot water, a plastic drum has been used and this is shown in Figure 4-6. This plastic open top drum has a height of 635mm and a diameter of 398mm and can hold 60L of water. In order to reduce the heat loss from the water tank proper insulation has been used. A condenser has been fixed within the water tank so that the heat energy from the working fluid flowing within the condenser will be transferred to the water in the water tank. The condenser was designed and manufactured with an external diameter of 22mm, length of 600mm and a wall thickness of 0.9mm as shown in Figure 4-7. Silicon was used to seal the connections where the pipes are connected with the tank.

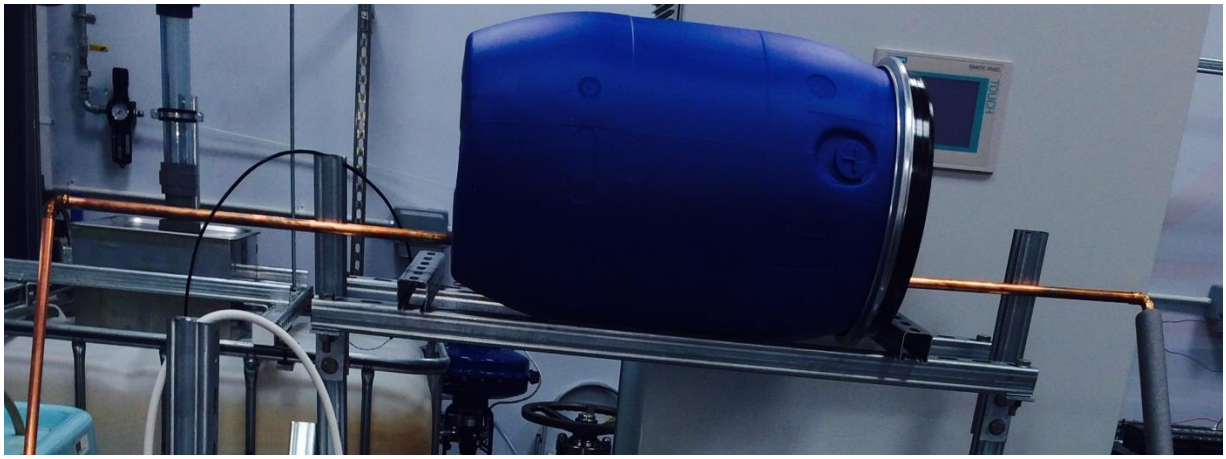

Figure 4-6 Storage tank

Figure 4-7 Condenser

4.2.6. Thermocouple

Thermocouples have been used to measure the temperature of working fluid in inlet to the collector, outlet of the collector, and water in the storage tank, as shown in Figure 4-8. The specifications of thermocouple are:

- Sensor type: Type K (Nickel Chromium/Nickel Aluminium)
- Cable: 4mm O.D. x 1 metre long
- Operating range: -75°C to +250°C

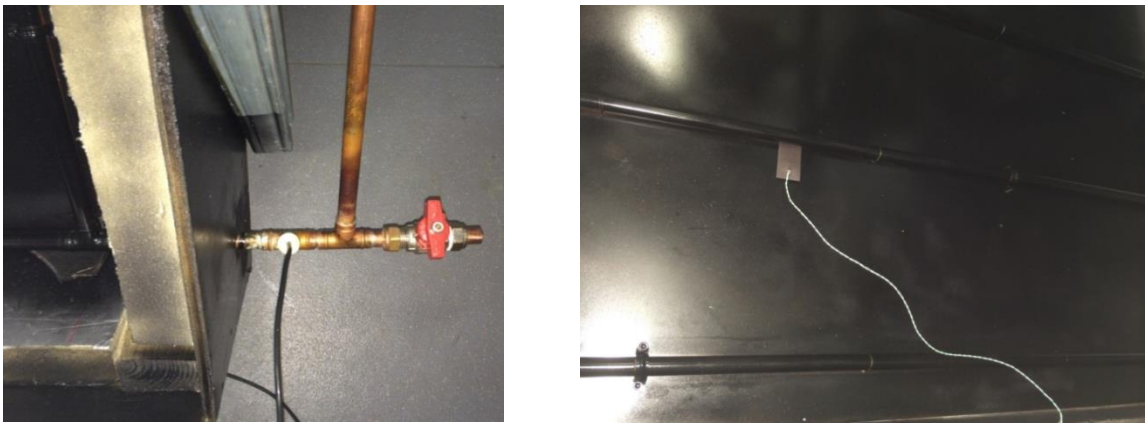

(a) (b)

Figure 4-8 Thermocouple

While the specifications of thermocouple, which are used to measure temperature of the plate as follow below:

Sensor type:	Type K (Nickel Chromium/Nickel Aluminium) to IEC 584
Construction:	Magnetic strip (50 x 25 x 1)mm
Hot junction:	Positioned/seated in the magnetic strip for surface measurement
Cable:	1/0.3mm Teflon® insulated twisted pair
Temperature range:	-50ºC to +150ºC

4.2.7. Temperature Measurement

Temperatures have been measured at the inlet and outlet of the collector, plate, and water storage tank using a Pico device, as shown in Figure 4-9.

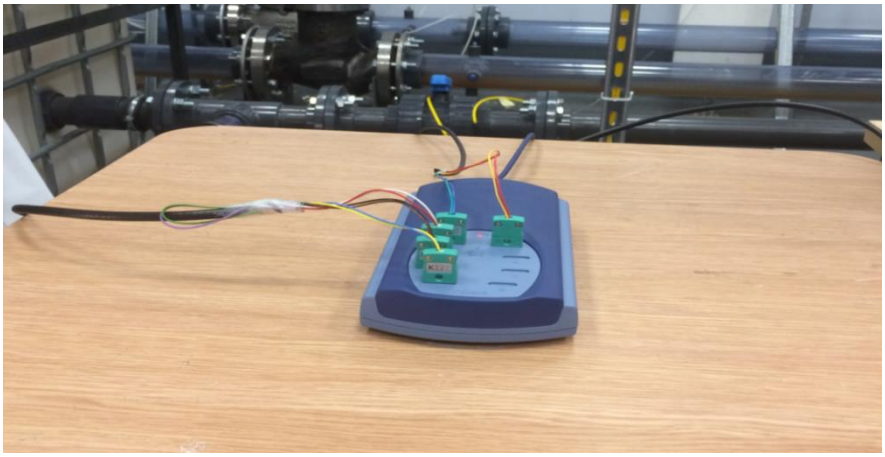

Figure 4-9 Data logger

The implementation of TC-08 is comparatively easy. The temperature can be measured and recorded simply by connecting the TC-08 with the thermocouple and a USB port on computer. The signal output from this device is temperature directly as shown in Figure 4-10. Table 4-1 summarises the specifications of the Data Logger.

Table 4-1 Specifications of the data logger

Number of channels (single unit)	8
Maximum number of channels (using up to 20 TC-08s)	160
Conversion compensation	100ms per thermocouple channel + 100ms for cold junction compensation
Temperature accuracy	sum of +-0.2% of reading and ±0.5ºC
Voltage accuracy	sum of +-0.2% of reading and ±10µv
Overvoltage protection	
Maximum common-mode voltage	±7.5 V
Input impedance	2 MΩ
Input range (voltage)	±70 mV
Resolution	20 bits
Noise-free resolution	16.25 bits
Thermocouple types supported	B, E, J, K, N, R, S, T
Input connectors	Miniature thermocouple
Operating temperature	0 to 50°C
Operating temperature for stated accuracy	20 to 30°C
Operating humidity	5 to 80 %RH non-condensing
Storage humidity	5 to 95 %RH non-condensing
Water resistance	Not water-resistant
PC interface	USB 1.1
Power requirements	Powered from USB port
Compliance	European EMC and LVD standards FCC Rules Part 15 Class

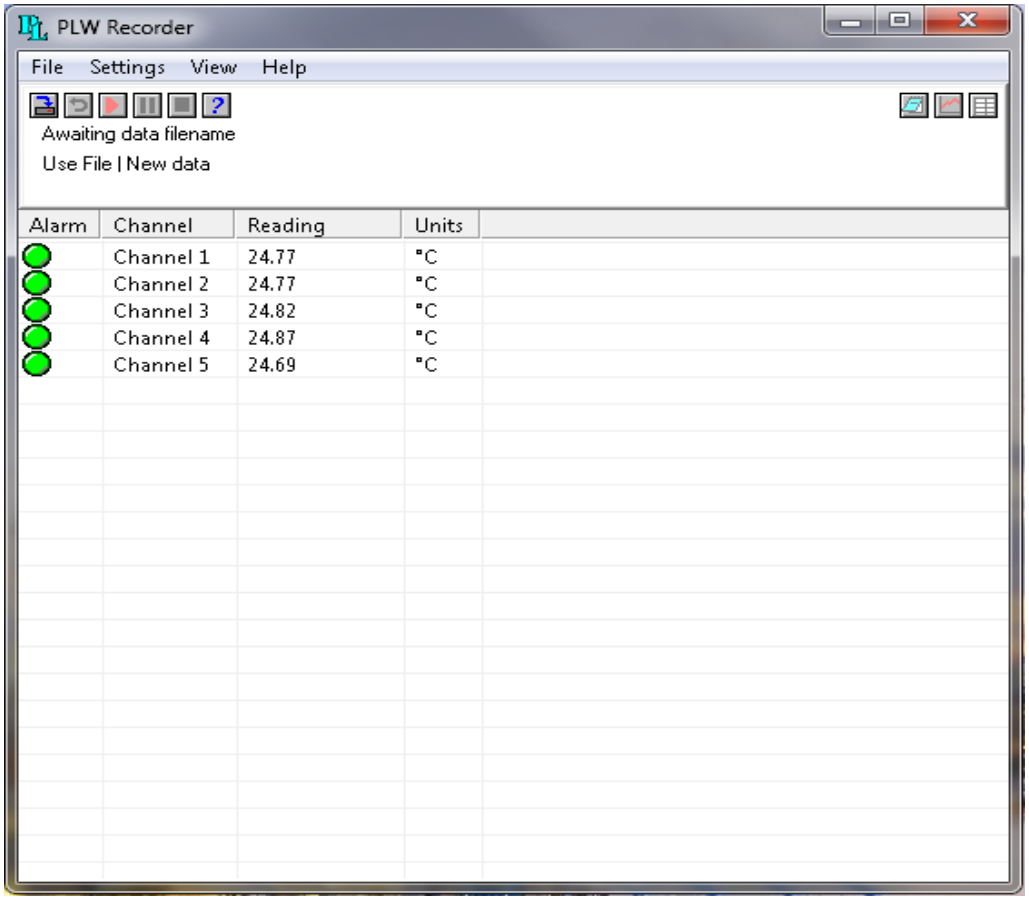

Figure 4-10 The signal output

4.3. Thermocouple Calibration

In this study, thermocouple has been calibrated against glass thermometer [119]. The equipment used to calibrate the thermocouples is thermometer, power supply and kettle. The Procedure of calibrating the thermocouple as follow:

1- Connect thermocouples with data logger
2- Connect the data logger with computer
3- Fill the kettle with water and heat it up to the boiling point
4- Put both thermometer and thermocouples inside the kittle as shown in Figure 4-11

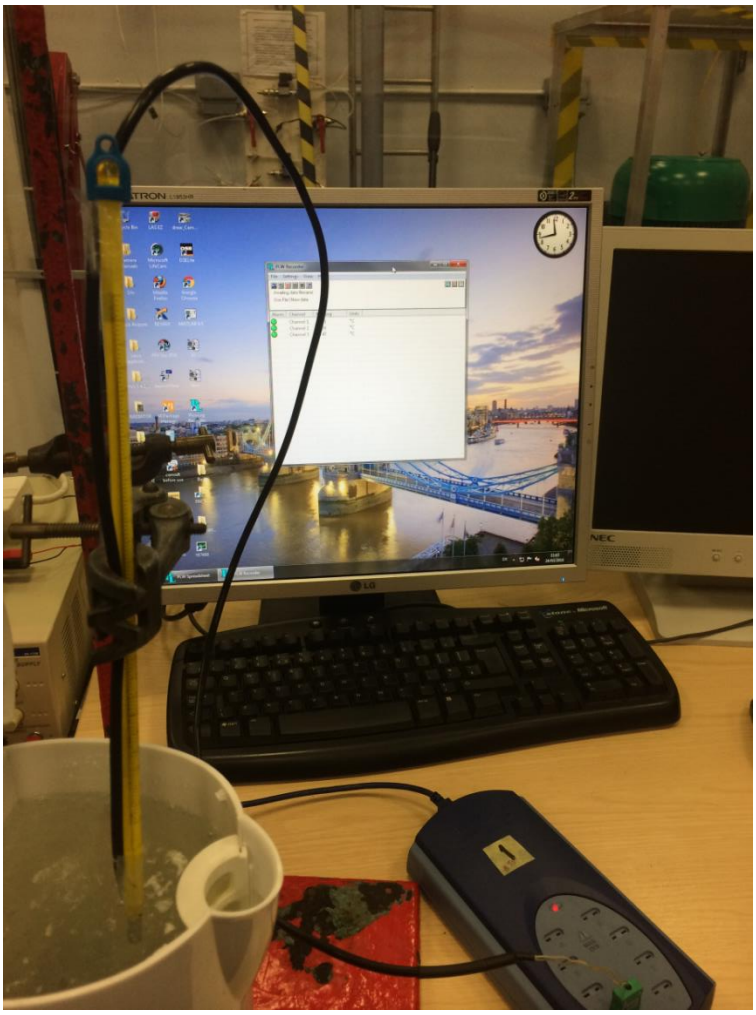

Figure 4-11 Thermocouple calibration

5- Record the data from both thermometer and thermocouple for several reading
6- Repeat step 4 several time
7- Take the average value of data for both thermometer and thermocouple
8- Finally, take the different between them

All the data regarding calibration of thermocouples can found in appendix D.

4.4. Experimental Procedure

Figure 4-12 depicts the adopted experimental test rig setups for both models, in the present study.

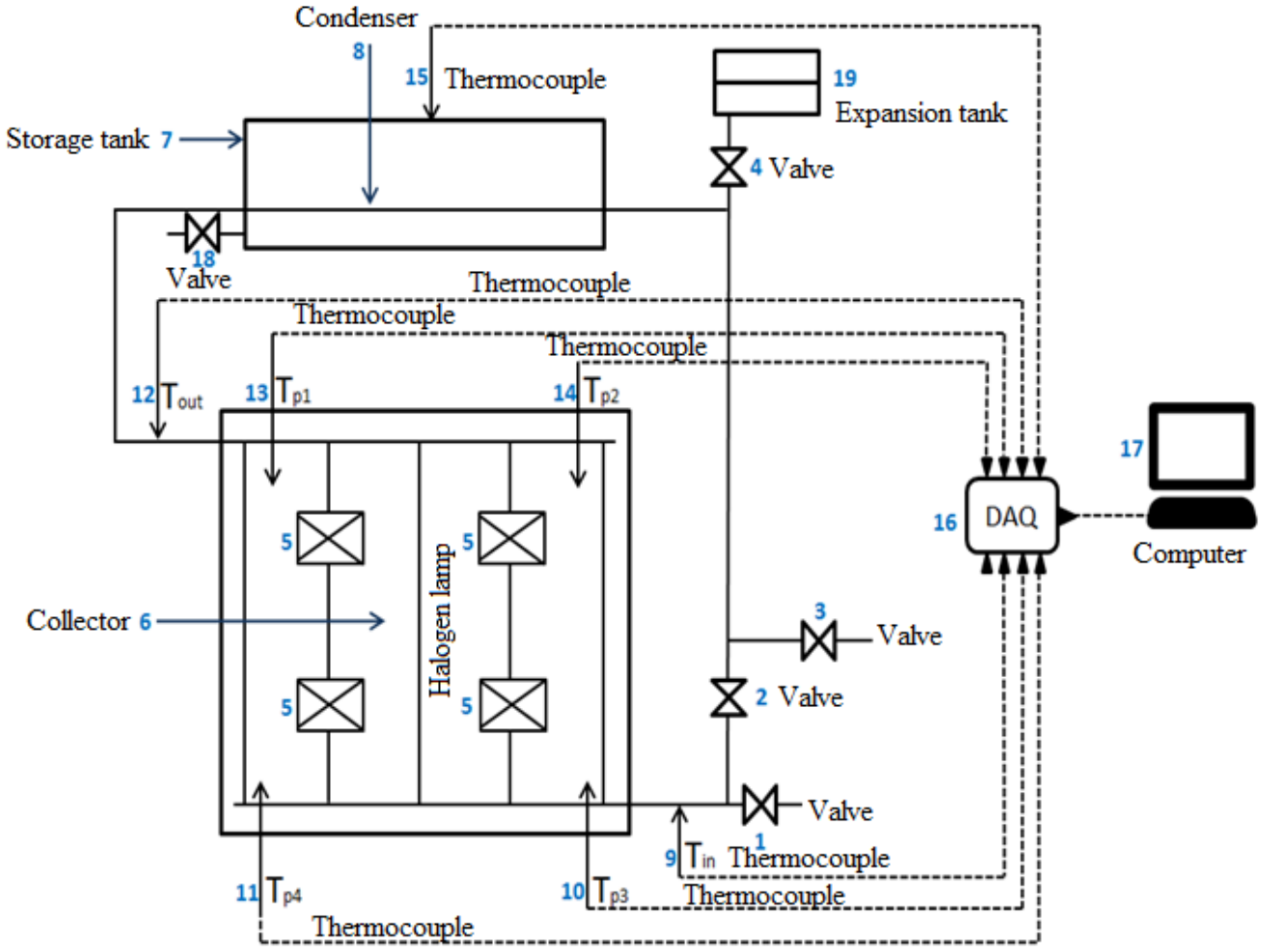

Figure 4-12 Schematic of the experimental setup

Figure 4-12 shows the schematics of the test rig setup with the location of the equipment used. For example, 1, 2, 3, 4 and 18 represent the location of the valves, 5 is halogen lamp, 6 is collector, 7 is the storage tank, and 8 is the condenser. Moreover, 9 and 12 are thermocouples that measure the temperature of working fluid at the inlet and outlet of collector respectively. 10, 11,13, 14 are thermocouples that measure the temperatures at the plate, 15 is thermocouple that measure the water temperatures at the storage tank, 16 is data logger, 17 is computer and 19 is expansion tank. All the thermocouples have been connected to a data logger and a computer has been used to record and save the temperature data.

The experimental work was conducted according to the procedure below:

1. Fill the storage tank with water by valve number 18
2. Fill the thermo-syphon loop with working fluid. In order to ensure that there is no air within the thermo-syphon loop and it is completely filled, the following steps were adopted:

    - Open valves number 1, 2 and 3 and keep valve number 4 closed
    - When the working fluid comes out from valve 3, valves number 2 was closed
    - Wait till the working fluid comes out from valve 3 again, then open valves number 2 and 4
    - When the working fluid comes out from valve 4, close valves number 1, 3 and 4

3. Prepare computer or laptop to record the data
4. Connect thermocouples with data logger and connect the data logger with computer
5. Connect halogen lamps plug to electricity socket (220 – 240V)
6. Prepare the data logger software
7. Turn on halogen lamps
8. Start the test

4.5. Calculation of Useful Heat Flux

In order to calculate the amount of heat flux that the collector is exposed to, a Martindale LM92 Lux Meter device has been used. The device is chosen due to its user-friendly interface and wide range applications. The specifications of this device are as below:

- A measurement range ranging from 200 Lux to 200, 000 Lux
- Low cost light meter with a resolution of 0.1 Lux

The heat flux in (W/m^2) is equal to the illuminance Ev in lux (lx) times 0.0079 [120]. In this study, average heat flux has been used [121].

$$HF\ (W/m^2) = Ev(lx) \times 0.0079 \tag{4.1}$$

The formula below can be used to calculate useful heat flux:

$$q_u = HF - q_{loss} \tag{4.2}$$

The energy loss from the flat plate collector happens from three sides namely top, back and sides:

$$q_{loss} = q_{top} + q_{back} + q_{saids} \quad (4.3)$$

The loss of energy through the top for flat plate collectors without glazing is as below [121]:

$$q_{top} = q_{conv} + q_r \quad (4.4)$$

where q_r is heat reflected from plate to ambient by radiation, can calculate by:

$$q_r = \sigma \left({T_p}^4 - {T_a}^4 \right) \quad (4.5)$$

where σ is the Stefan-Boltzmann constant = $5.76*10^{-8}$ (W/m^2K^4).

q_{conv} is the heat energy reflected from pleat to ambient by convection, can estimated by [122]:

$$N_u = 1 + 1.44\left[1 - \frac{1708[\sin(1.8\beta)]^{1.6}}{R_a \cos\beta}\right]\left[1 - \frac{1708}{R_a \cos\beta}\right] + \left[\left(\frac{R_a \cos\beta}{5830}\right)^{1/3} - 1\right] \quad (4.6)$$

$$N_u = \frac{q_{conv}\, L}{(T_b - T_a)k} \quad (4.7)$$

where,

N_u is Nusselt number
β is tilt angle of collector
R_a is Rayleigh number
q_{back} is heat energy loss from back, can calculated by:

$$q_{back} = U\, \Delta T \quad (4.8)$$

where,

U is overall heat transfer coefficient ($W/m^2.^oC$), which is calculated by Eq. (4.9).

$$U_{back} = \frac{k_{ins}}{l_{ins}} \quad (4.9)$$

where,

k_{ins} is the thermal conductivity of insulation
l_{ins} is the thickness of insulation

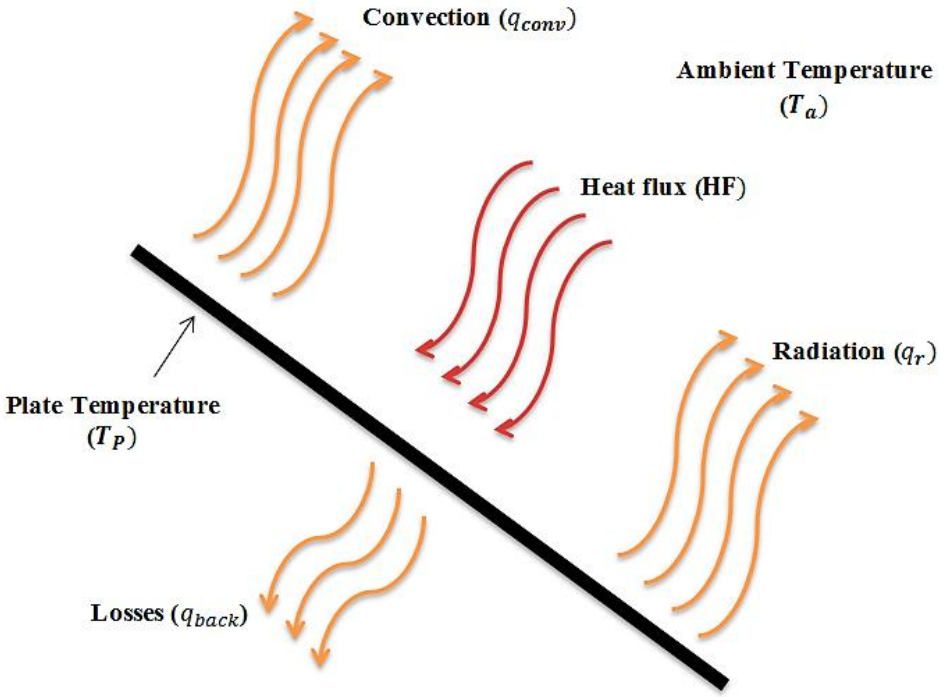

Figure 4-13 Processes of heat balance

Table 4-2 Characteristics parameters

	Symbol	Value	Unites
Length of collector	L	1	m
Lux	Ev	25250	lx
The Stefan-Boltzmann constant	σ	$5.76x10^{-8}$	W/m^2K^4
The tilt angle of collector	β	53	
Temperature of plate	T_p	70	ºC
Ambient temperature	T_a	25	ºC
Thickness of insulation	x	0.05	m
Thermal conductivity of insulation	k	0.02	W/m.K

According to values in Table 4-2 and using equations above in this chapter, can calculate useful heat flux as below:

To calculate average heat flux that obtained from halogen lamp, Eq. (4.1) can be used.

$$HF\ (W/m^2) = 25250 \times 0.0079 = 199.47 W/m^2$$

Using Eq. (4.5), it can be estimated the energy loss per meter square from the plate to ambient by radiation:

$$q_r = 5.76 * 10^{-8} * (70^4 - 25^4)$$
$$q_r = 1.36 W/m^2$$

The energy loss per meter square from the plate to ambient by convection can be evaluated by using Eq. (4.6) and (4.7).

$$R_a = \frac{(9.81 * .00312 * (70-25) * 1^3}{1.77^{-5} * 2.49^{-5}} = 3.12 * 10^9$$

$$N_u = 1 + 1.44\left[1 - \frac{1708[\sin(1.8*53)]^{1.6}}{3.12*10^9*\cos 53}\right]\left[1 - \frac{1708}{3.12*10^9*\cos 53}\right] + \left[\left(\frac{3.12*10^9*\cos 53}{5830}\right)^{1/3} - 1\right] = 2.634$$

$$q_{conv} = \frac{2.634*(70-25)*0.02}{1} = 2.37 W/m^2$$

To establish the heat loss from backside, Eq. (4.8) and Eq. (4.9) can be used.

$$U_{back} = \frac{0.02}{0.05} = 0.4\ W/m^2.K$$
$$q_{back} = 0.4 * (70 - 25) = 18 W/m^2$$

Finally, the useful heat flux can be calculated by using Eq. (4.2), (4.3) and (4.4).

$$q_{top} = 2.371 + 1.36 = 3.73 W/m^2$$
$$q_{loss} = 3.731 + 18 = 21.73 W/m^2$$
$$q_u = 199.47 - 21.731 = 177.74 W/m^2$$

4.6. Development an Equation to Predict Mass Flow Rate within Thermo-Syphon Loop

The flow rate within the thermo-syphon is very slow and therefore it is rather difficult to measure the velocity of the flow. However, it is important to measure the velocity of the flow in order to control the mass flow rate through the pipes. There are many devices to measure the flow velocity through a thermo-syphon. These devices can be put into two categories as internal and external. Internal devices are cheaper than external devices, but using these can have a negative impact on the flow field, which will develop an obstruction in the flow and adding resistance to the flow within a thermo-syphon and hence severely affecting the performance. On the other hand, the external devices do not affect the flow inside a thermo-syphon, but are considerably more expensive than internal devices. So, during this particular study, the velocity of the flow within thermo-syphon loop has been controlled using the procedure explained below:

1. Open the valve (valve number 4 as shown in
2. Figure 4-12 Schematic of the experimental setup
3.) and close it after one hour. Record the opening time and the closing time of the valve. Using this data, calculate the volume of water released from the valve using the Eq. (4.10)

$$V = \pi r^2 H_{wf} \tag{4.10}$$

where H_{wf} is high of working fluid in expansion tank and r is radius of expansion tank

4. Next convert the volume of water released from the valve into mass (kg) using the following Eq. (4.11)

$$m=V*\rho \tag{4.11}$$

5. Then divide the mass (kg) by time (s) to obtain the mass flow rate (kg/s) using Eq. (4.12)

$$\dot{m} = \frac{m}{t_{wf}} \tag{4.12}$$

where t_{wf} is the time duration between opening and closing the valve number 4

6. Repeat the procedure above after every hour and recorded the findings
7. The table summarises the experimental results for three experiments

Table 4-3 The amount of mass flow rate against different values of the working fluid properties

Time (minutes)	T_{in}(ºC)	T_{out}(ºC)	T_{ref}(ºC)	T_w(ºC)	ṁ(kg/s)	μ (kg/m.s)	Di (mm)	Ra E+07
30	35.98	47.75	41.865	66.31	0.003450	0.000614	13.6	1.97
60	38.16	49.68	43.92	68.01	0.003408	0.000591	13.6	1.99
90	39.19	50.65	44.92	68.365	0.003331	0.000581	13.6	1.95
120	40.08	51.38	45.73	68.68	0.003272	0.000572	13.6	1.93
150	40.73	51.93	46.33	69.15	0.003256	0.000566	13.6	1.94
180	41.48	52.56	47.02	69.475	0.003213	0.00056	13.6	1.92
210	41.99	53.2	47.595	69.6	0.003159	0.000554	13.6	1.89
240	42.55	53.47	48.01	69.38	0.003083	0.00055	13.6	1.84
270	43.07	53.98	48.525	69.845	0.003077	0.000545	13.6	1.85
300	43.52	54.43	48.975	69.98	0.003039	0.000541	13.6	1.83

8. Based on the data presented in Table 4-3, and using multiple variable regression analysis, semi-empirical correlation for the prediction of the mass flow rate of

working fluid within the thermo-syphon loop, has been developed. This correlation is a function of the Rayleigh number, inner diameter of the upriser pipe (D_i) and dynamic viscosity (μ) of working fluid.

$$\dot{m} = 2.64 * 10^{-9} * D_i * \mu * {R_a}^{1.502} \quad (4.13)$$

$$\dot{m} = 2.64 * 10^{-9} * D_i * \mu * \left(\frac{g*\beta*(T_w - T_{ref})*{D_i}^3}{\alpha*\nu}\right)^{1.502} \quad (4.14)$$

For more details regarding how Eq. (4.13) has been developed, see appendix E

In the present work, a number of statistical analysis tests have been used to ensure the validity of the regression models. These statistical analysis tests are namely F-value, Durbin-Watson statistic, standard error, t-Test value, Lilliefors test, Chi-square and p-value. A brief description is provided for each test. Appendix C shows the important features of the considered tests and their significance.

Several statistical tests have been undertaken to justify the usefulness of the developed equations using multiple regression analysis. Table 4-4 shows that the derived equation for the mass flow rate has achieved the acceptable criteria in all the tests. That means the equation can be used with confidence for further applications.

Table 4-4 The proposed statistical tests and thier acceptance criteria for mass flow rate

Type of test	Acceptance criteria		Mass flow rate(kg/s)
F-value	If (F < F critical) is accepted [108]	F	1.0014
		F critical	2.9782
Durbin-Watson statistic	Less than 2 is accepted [109]		1.7528
Standard error	Regression		0.01776
	Experimental		0.01778
	Percentage error (%)		0.11
t-Test	Closed to zero [110]		0.00037
Lilliefors test	If 0= accepted If 1= rejected [111]		0
Chi-square	Less than 0.05 is accepted [112]		0.0324
P-value	More than Chi-square is accepted [112]		1

Figure 4-14 depicts the comparison between experimental data and predicated data from Eq. (4.14) for mass flow rate of working fluid within the thermo-syphon loop. It can be clearly seen that the data from experimental test and predicted data from equation have the same trend and there is a good agreement between them. These values refer that the developed equations here

depict no significant difference to the available data and they have the same trend. Hence, the prediction equation developed here represent mass flow rate of working fluid within thermo-syphon loop with reasonable accuracy.

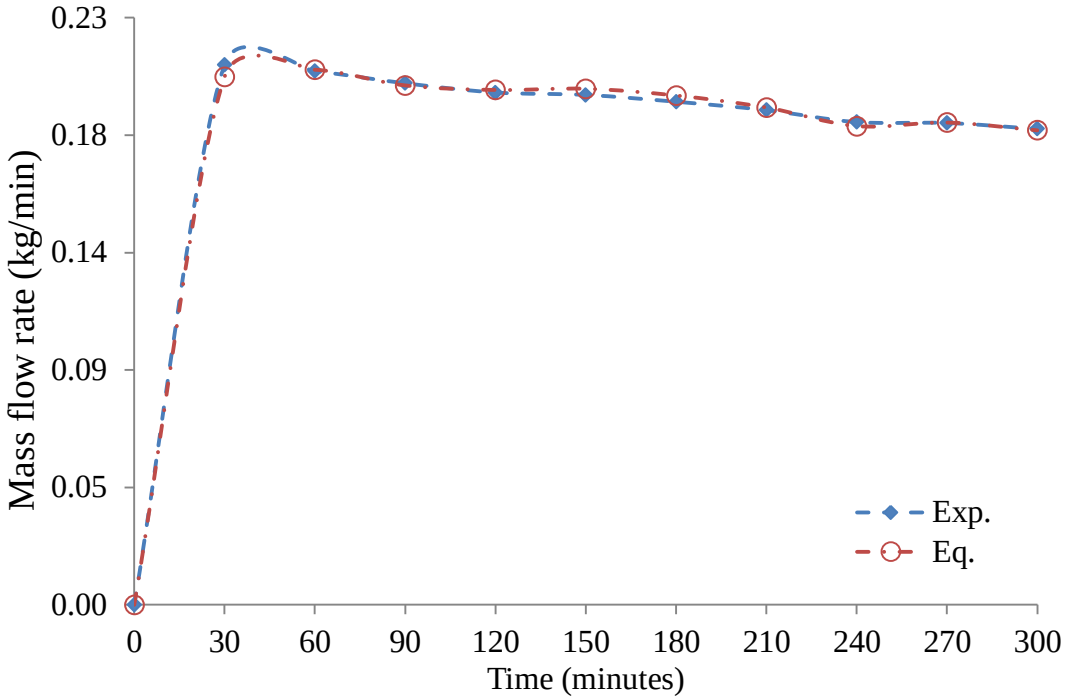

Figure 4-14 Comparison between experimental and predicted data for mass flow rate of working fluid

4.7. Estimating Uncertainty

Uncertainty of measurement can be defined as the amount of errors or fluctuations in the measurement mainly due to human error. For the experiment performed above, such human errors can be reflected in measuring the temperature and mass flow of working fluid within the thermo-syphon system. These measuring errors are brought in by different instruments, which does not necessarily operate under ideal measuring conditions.

In order to estimate uncertainty first, the sample mean should be computed. The sample mean, $\bar{x}$ is obtained by taking the average of the sampled values. The average value is computed by summing up the values sampled and dividing them by the sample size, n as shown in Eq. (4.14) [123].

$$\bar{x} = \frac{1}{n}\sum_{i=1}^{n} x_i \qquad (4.14)$$

where,

$\bar{x}$ = Mean value
x_i = Sample value
n = Number of sample

After that, we compute the sample standard deviation. The sample standard deviation provides an estimate of the population standard deviation. The sample standard deviation, S_x, is computed by taking the square root of the sum of the squares of sampled deviations from the mean divided by the sample size minus one as below [124]:

$$s_x = \sqrt{\frac{1}{n-1}\sum_{i=1}^{n}(x_i - \bar{x})^2} \tag{4.15}$$

The value n-1 is the degrees of freedom for the estimate, which signifies the number of independent pieces of information that go into computing the estimate. In a case of Absence of any systematic influences during sample collection, the sample standard deviation will approach its population counterpart as the sample size or degrees of freedom increases. The degrees of freedom for an uncertainty estimate are useful for establishing confidence limits and other decision variables.

Finally, from Eq. (4.16) the estimated standard uncertainty can be calculated.

$$Eu = \frac{s_x}{\sqrt{n}} \tag{4.16}$$

Based on the results, which have been obtained from experimental tests, are included in APPENDIX F and the above-mentioned equations Eq. (4.14), (4.15) and (4.16) are used to calculate the value of uncertainty in this experiment work.

A sample calculation of the uncertainty in the measurement is shown below. Based on this calculation procedure the uncertainty of other measurements are calculated which are shown the Table 4-5 In this study, for test number 1 depicted in APPENDIX F, the mean outlet temperature can be calculated by:

Mean value:

$$\overline{T_{out}} = \frac{1}{300}\sum_{i=1}^{300} T_i = \frac{1}{300}(15251.81) = 50.84^{o}C$$

Sample standard deviation:

$$s_x = \sqrt{\frac{1}{300-1}\sum_{i=1}^{300}(T_i - \overline{T_{out}})^2} = \sqrt{\frac{1}{300-1}\sum_{i=1}^{300}(6524.24)} = 4.671^oC$$

Estimated standard uncertainty:

$$Eu = \frac{s_x}{\sqrt{n}} = \frac{4.671}{\sqrt{300}} = 0.269^oC$$

Furthermore, estimated standard uncertainty for all tests can be calculated using same procedure above.

The mean estimated standard uncertainty $1/n_t \sum_{i=1}^{n} Eu = \frac{0.269+0.308+0.232+0.451}{4} = 0.315^oC$

where n_t is number of tests

Table 4-5 The estimated standard uncertainty

	Thermocouple at inlet collector(ºC)	Thermocouple at outlet collector(ºC)	Thermocouple at the storage tank(ºC)	Thermocouple at the wall(ºC)	Mass flow rate(kg/s)
Mean standard uncertainty	0.239	0.315	0.162	0.482	0.000042
Percentage error %	$\pm$0.696	$\pm$0.626	$\pm$0.742	$\pm$0.825	$\pm$0.961

This chapter provided a detailed overview of the experimental work conducted in this study by explaining the equipment and the test rig followed by the experiment procedure and the data acquisition system. After explaining the experimental work, next chapter will illustrate the extensive details of the baseline model. The numerical model of the traditional baseline was verified against the experimental findings by following the procedure and setup mentioned in this chapter.

CHAPTER 5

BASELINE MODEL

This chapter presents the results obtained from Experimental and CFD simulations for different cases that have been discussed in chapter three. In order to understand the natural convection and the complex flow structure happening within thermo-syphon system, a detailed qualitative and quantitative analysis has been conducted. The effects of various geometric parameters and heat flux on the thermo-syphon system performance have been examined under different thermal loading condition. Furthermore, semi-empirical relationships have been developed to estimate the thermo-syphon system performance as a function of the geometrical parameter, operating condition (heat flux, thermal loading) and time.

5.1. Spatial Discretisation

The accuracy of the numerical results depends on the discretization of the domain, which is known as meshing process. Table 5-1 summarise numerical results of water temperature of storage tank with various mesh configurations for five cases which combines different L/d ratio of riser pipe with the number of riser pipes. This analysis has been conducted to ensure the numerical results independence on the mesh quality. According to the results shown in Table 5-1, for case 1 the percentage difference between the results for 2.5 million and 5.2 million is very small and negligible (0.19%). Henceforth it can be considered that the mesh with 2.5 million elements can capture the flow behaviour inside the thermo-syphon with similar accuracy as the mesh with 5.2 million. Therefore, to reduce the computation time and cost, the mesh with lower elements has been used for further investigation. Using the similar methodology, the mesh for other cases has been determined as well.

Table 5-1 Spatial discretisation results

	L/d ratio	N. pipe	N. Element (million)	Temperature of water at the center of the storage tank (ºC)	Difference in Temperature (%)
Case 1	50	5	2.5	15.0725	0.188
			5.2	15.0441	
Case 2	75	5	3.2	15.0948	0.0958
			6.5	15.0803	
Case 3		7	3.8	15.0678	0.1157
			7.8	15.0852	
Case 4		9	4.4	15.0525	0.1677
			9.1	15.0778	
Case 5	100	5	3.8	15.0873	0.1145
			7.8	15.1046	

5.2. Temporal Discretisation

Since the case under study is Transient-State, the time step independence test should be conducted. Otherwise, it can lead to inaccurate results of CFD. Therefore, time-step independence test has been conducted with three different time steps (3s, 6s, and 12s). This test has been conducted on case 2 as mentioned in Table 5-1 under the heat flux condition of 15th March with weekday thermal loading condition. Table 5-2 summarises the result of time steps independence, which shows that the difference in temperature of water within the storage tank is less than 0.6% between the three-time steps under consideration. The temperature of water in the storage tank is an important parameter, which indicates the performance of the system. Hence, it can be concluded that the time step with 12s is capable of predicting the flow features accurately; therefore 12s time step has been chosen for further analysis of thermo-syphon.

Table 5-2 Temporal discretisation results

Time Step (sec.)	Temperature of water at the center of the storage tank (ºC)	Difference in Temperature (%)
3	31.58	0.08
6	31.61	0.58
12	31.79	

5.3. Benchmark Tests

It is essential to verify the numerical model of the system prior to the analysis of the data. The benchmark test is one of the approved methodologies to verify the numerical model of the system. Benchmarking refers to comparing the numerical results against experimental findings. Benchmarking the numerical data with experimental ensure the model's capability to capture the actual physical phenomenon. Table 5-3 contains the physical parameters of a traditional thermo-syphon model that has been used for experimental work.

Table 5-3 Test rig specifications of traditional model of thermo-syphon

Height of casing	1.2	m
Width of casing	1.1	m
Depth of casing	0.18	m
Tilt angle of collector	53º	
Number of riser pipes	5	
Length of the riser pipes	1	m
Inside the riser pipe diameter	0.0136	m
Outside the riser pipe diameter	0.015	m
Riser pipe material	Copper	
Absorber plate length	1	m
Absorber plate width	1	m
Absorber plate thickness	0.0007	m
Absorber plate material	Copper	
Diameter of tank	0.398	m
High of tank	0.635	m
Material of tank	Plastic	
Inside diameter of condenser	0.0202	m
outside diameter of the condenser	0.022	m
Length of condenser	0.6	m
Condenser material	Copper	

In this study, the numerical model has been verified against the experimental findings for the temperature of water within the storage tank, working fluid's temperature at the inlet and outlet of collector and mass flow rate of working fluid within the thermo-syphon loop under constant heat flux.

Figure 5-1 depicts the variations in the experiments and CFD results with respect to the temperature of water within the storage tank, temperature of working fluid for five hours of operation with constant heat flux of 177.74W/m^2 and under no loading from the storage tank. It can be clearly seen that during the first hour of the operation the difference between the experimental and numerical results are very small. However, as the operation time extends the difference between the results starts to increase. The maximum difference between the CFD and experimental result is observed for water temperature in the storage tank with a value of 8.28%. After five hours operation the difference in working fluid temperature at the inlet and outlet of the collector is recorded as 10.17% and 9.86% respectively. Moreover, according to the experimental results, during the first 40minutes operation fluid temperature values both at the inlet and outlet of collector increase rapidly and after that, the increment rate becomes linear with a gradient of 0.101ºC/min (working fluid at outlet) and 0.064ºC/min (working fluid at inlet) respectively. On the other hand, the storage water temperature increases linearly from the beginning, with a gradient of 0.034ºC/min. similar trend has been observed for the numerical investigation. According to the numerical findings, the temperature increment rate after 40minuites becomes linear with a gradient of 0.12ºC/min (working fluid at outlet) and 0.081ºC/min (working fluid at inlet) accordingly. On the other hand, the storage water temperature increases linearly from the beginning, with a gradient of 0.045ºC/min. It is expected to have small discrepancies between the experimental and numerical results because the numerical techniques do not capture all form of losses in the system. The amount of the loss depends on the temperature difference between the ambient and thermo-syphon system, which increases with time. In addition, in the numerical modelling, the ambient temperature is kept constant whereas in real life the ambient temperature will vary with respect to time. Thus, the variation in the ambient temperature during the experiment will also affect the outcome. In CFD the riser pipe has full contact with the collector plate, whereas small gap has been found at some sectors between the riser pipe and collector plate in the experimental setup. This has reduced the contact surface and therefore the amount of heat transfer by conduction. In addition, in CFD both the downcomer and upriser were considered adiabatic, while in experimental there are some losses. Despite the above-mentioned reasons, a good agreement has been observed between the CFD results and the experimental results. The maximum variation between them is recorded as to be less than 11%. Hence, this numerical model can be considered a reliable model for representing a closed loop thermo-syphon solar water heating system.

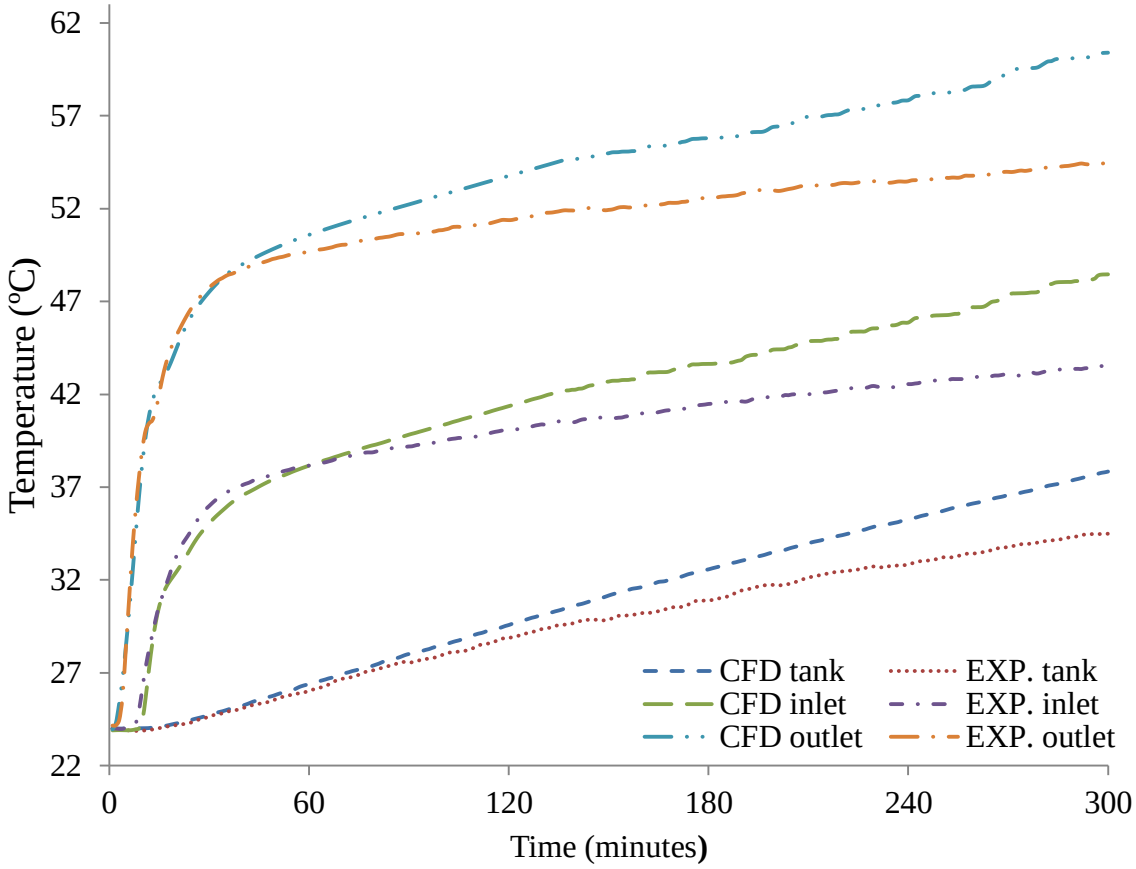

Figure 5-1 Validation of the CFD results with respect to the experimental results for the temperature of water within the storage tank and temperature of working fluid at inlet and outlet of collector

Figure 5-2 depicts the mass flow rate of working fluid within the thermo-syphon loop for both numerical and experimental results for five hours of operation time with a constant heat flux of 177.74W/m^2 (calculated in section 4.5) under no loading from the storage tank. It can be clearly seen that the value of mass flow rate of working fluid within the thermo-syphon loop is higher for CFD, as compared to experimental. The reason behind this difference is the presence of connectors such as fittings, elbows and tees that have been used in the experimental setup, which leads to increase in the resistance of flow fluid and hence decrease in the mass flow rate of working fluid. The difference between the CFD and the experimental results for mass flow rate of working fluid within thermo-syphon loop is recorded as 13.65%. Furthermore, it can be seen from Figure 5-2 that, at the beginning, the mass flow rate increases rapidly and after a while, it stabilises to a constant value because a constant heat flux has been applied on the system.

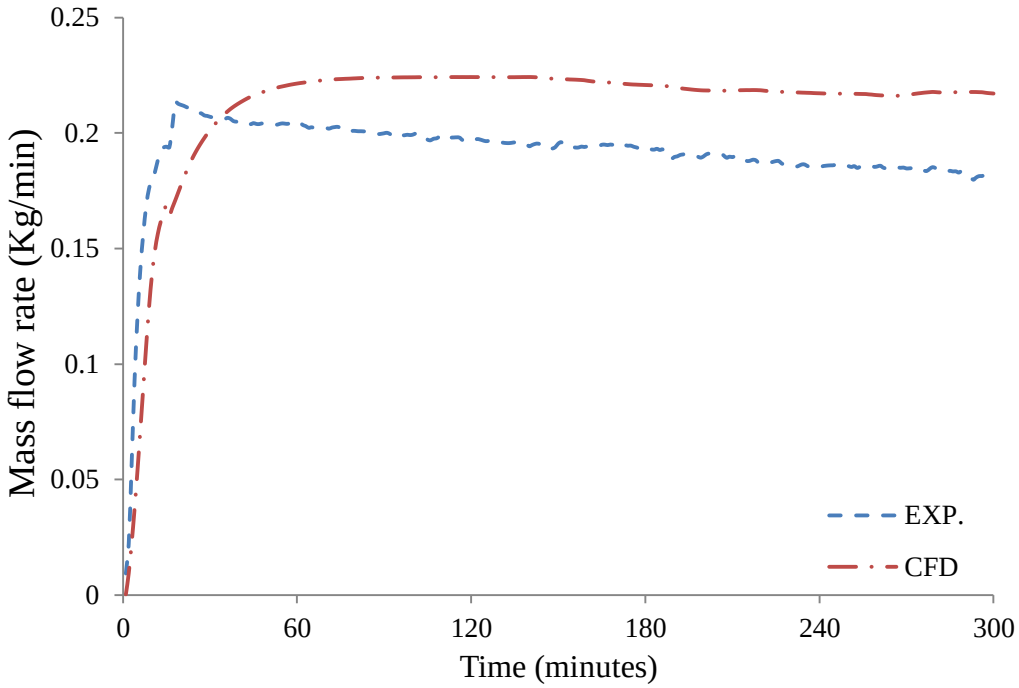

Figure 5-2 Validation of the CFD results with respect to the experimental results for the mass flow rate within the thermo-syphon loop

5.4. Flow Field Analysis

The numerical analysis carried out on the closed loop thermo-syphon solar water heating system depicts the natural convection phenomena, the distribution of temperature and velocity of working fluid within the model. The natural convection phenomenon happens when the working fluid gets heated and the temperature of the working fluid increases consecutively decreasing its density. Hence, the volume of the working fluid increases. The lower density fluid moves towards the top wall of the riser pipe. For example, increasing the water temperature by 8ºC cause the density to decrease by 2.123kg/m^3 [125] Due to the inclination of the riser pipes, the working fluid accelerates along the top wall of the riser pipe and enters the upriser and subsequently into the condenser which is based in the water storage tank.

Figure 5-3 depicts the velocity distribution of the working fluid within the thermo-syphon loop and hot water within the water storage tank at a heat flux corresponding to 15th March under thermal loading condition of weekday. In order to understand the working fluid behaviour within thermo-syphon loop at various heat flux conditions, different times have been chosen on that day. According to the findings, the average velocity of the fluid increases until midday (12 O'clock), achieving a value of 0.0077m/s, since the maximum heat flux is emitted at that time. Subsequently, the average velocity starts to decrease to 0.0057m/s at 16 O'clock. The working fluid attains the highest velocity at the upriser and downcomer, and the average velocity of the

working fluid is measured to be 0.0233m/s, which is equal to the sum of velocities for all riser pipes. There is no significant difference in the average velocity of working fluid, and the approximated value of working fluid in each riser pipe is 0.00466m/s. The total average velocity of the working fluid in the thermo-syphon is measured. Moreover, since the diameter of the condenser is bigger than the diameter of the upriser and downcomer, it can be seen that the velocity in the condenser is lower as compared to the upriser and downcomer. Similar analogy can be applied for bends in the upriser and downcomer where cross sectional area increases thus decreasing the velocity.

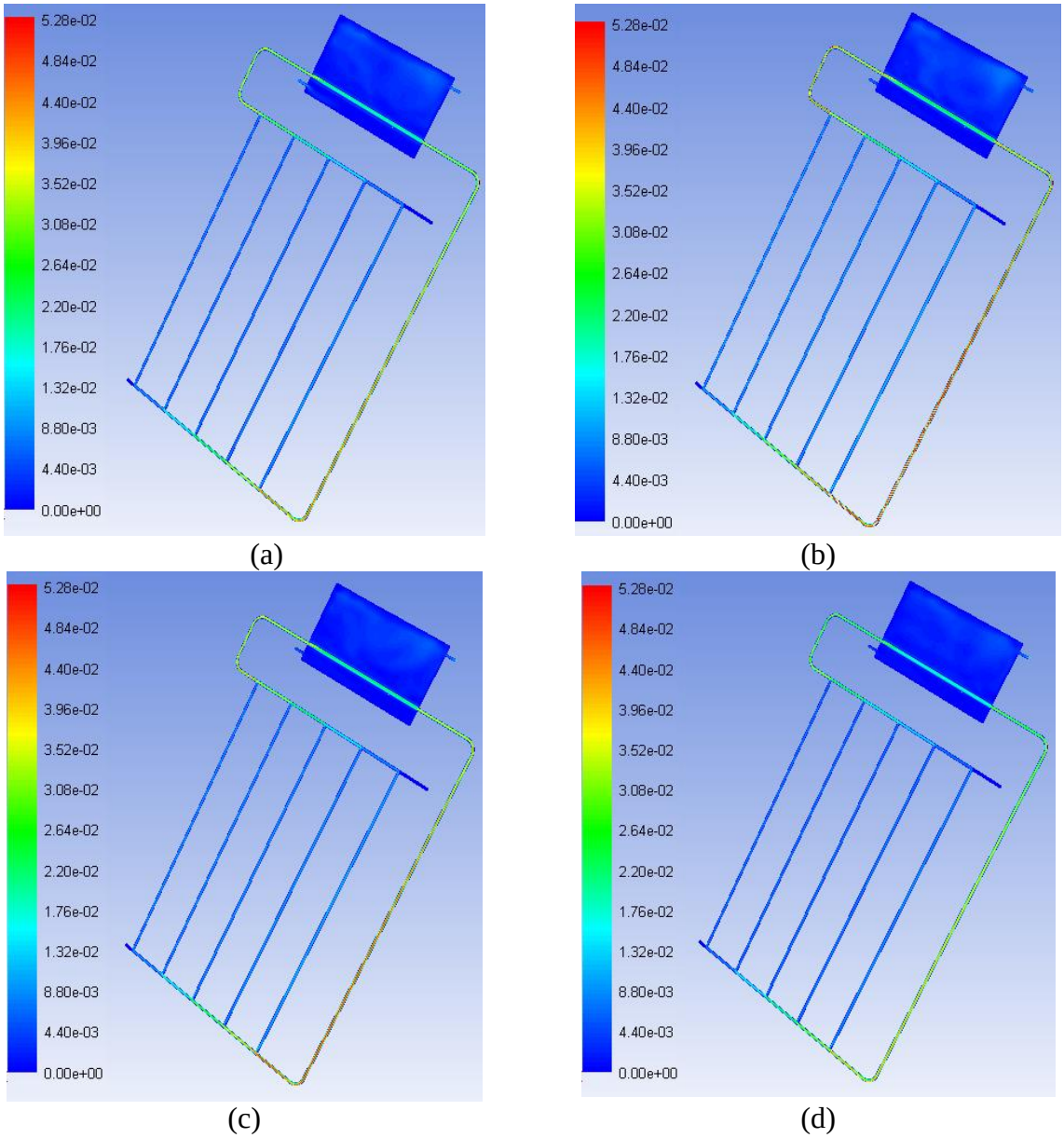

Figure 5-3 Flow velocity variations of the working fluid within thermo-syphon loop and water within the storage tank on 15th March under thermal weekday loading for (a) 10 O'clock (b) 12 O'clock (c) 14 O'clock and (d) 16 O'clock

Figure 5-4 further depicts the natural convection phenomena occurring in the thermo-syphon model considered in the present study, which is represented in a form of temperature distribution in the thermo-syphon system. As mentioned earlier, the working fluid heats up in the riser pipe and moves upward in the pipe to the upriser. Along the riser pipe, more thermal energy of the solar rays is transferred to the working fluid increasing the internal energy and temperature further. It can be seen that the highest temperature of the working fluid is observed at the riser pipes and upriser junction while the lowest temperature of the working fluid is observed at downcomer. In this case, the maximum and minimum average temperatures are measured to be 80.20ºC and 54.74ºC respectively for 12 O'clock heat flux condition. Whilst regarding water within the storage tank, it can be clearly seen that the maximum temperature of water is 29.85ºC at upper section of the storage tank and the minimum temperature of water is 15ºC at the bottom section of the storage tank, where the inlet is located. Furthermore, heat of the working fluid is accumulated along the top wall of the condenser and the water within the storage tank.

It would be prudent at this point to present the mass balance in the thermo-syphon loop in order to analyse its performance. From the current setup and configuration, it is expected not to have any recirculation in the riser pipe. The only way to recirculate the flow is through the recirculating pipe. Which refers that the velocity direction within the riser pipe and the recirculation pipe will be opposite and the total mass flow through all the riser pipes should equate to the mass flow through the recirculating as it is shown in Figure 5-5. Figure 5-5 represents the mass balance in the riser pipes and the recirculating pipe. It can be seen that the sum of the mass flow rates of the working fluid passing at any cross-section of the riser pipes is equal to the mass flow rate of the working fluid through the cross section of the recirculating pipe. Hence, the mass is balanced in the thermo-syphon loop considered in the present study.

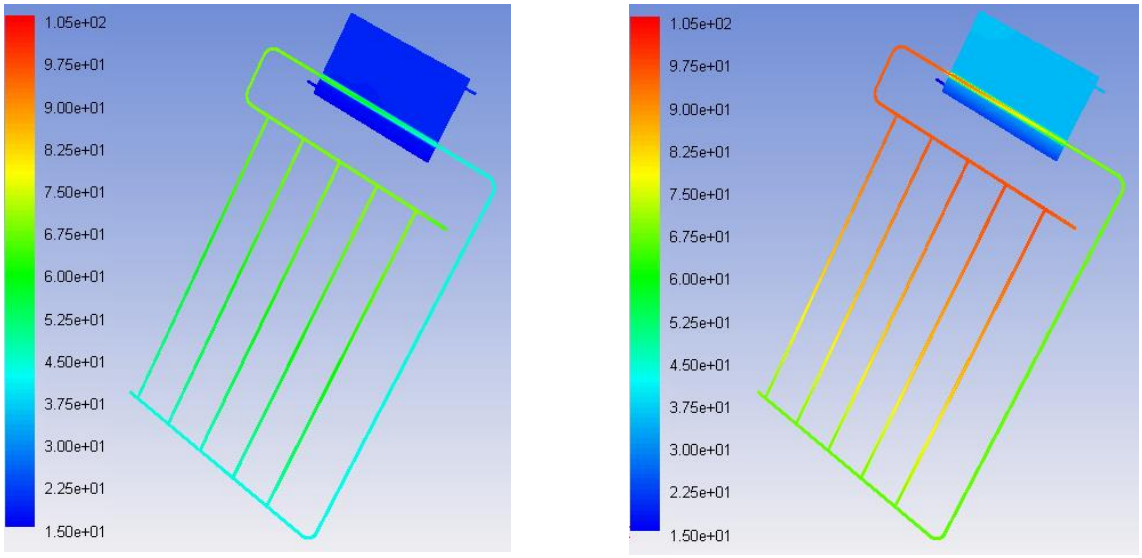

(a) (b)

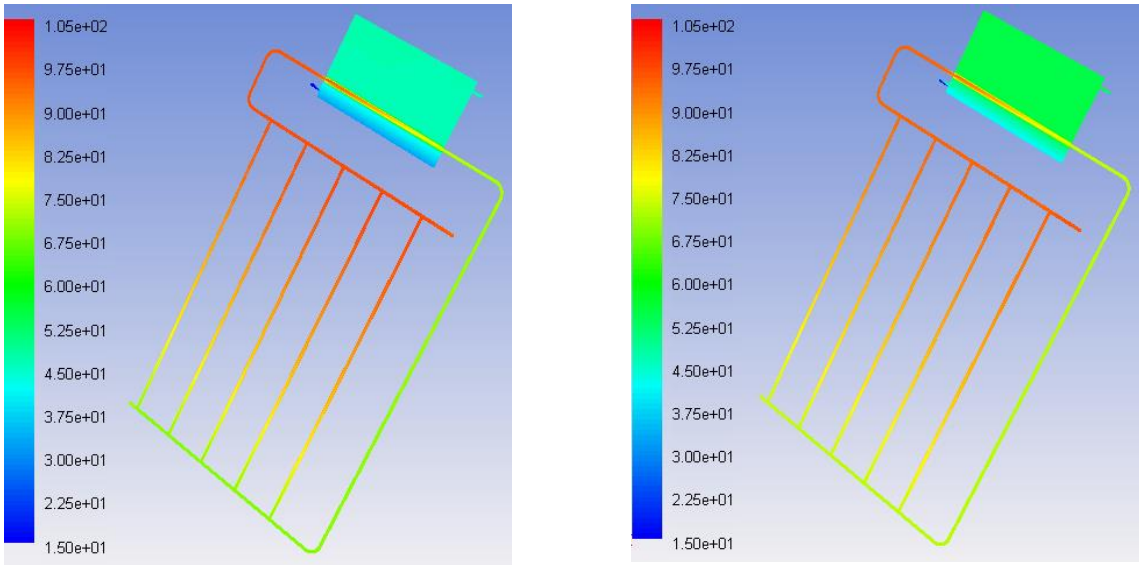

(c) (d)

Figure 5-4 Static temperature distributions of the working fluid within thermo-syphon loop and water within the storage tank on 15th March at midday under thermal weekday loading for (a) 10 O'clock (b) 12 O'clock (c) 14 O'clock and (d) 16 O'clock

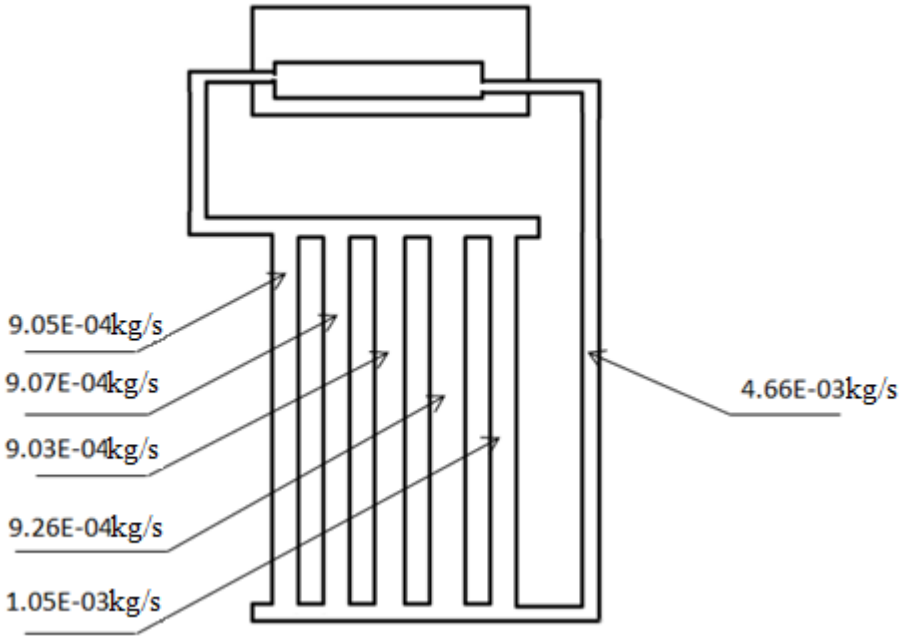

Figure 5-5 Mass balance of the working fluid within the thermo-syphon loop

5.5. Effect of Geometrical Parameters

The thermo-syphon model considered in the presented study has been analysed with different number of the riser pipes and L/d ratios. The following sections show extensively the effects of tilt angle of collector, number of the riser pipes and L/d ratios on the performance of the thermo-syphon characteristic.

5.5.1. Effect of Tilt Angle

There are several factors, which have significant effects on the amount of the solar radiation-reaching the collector. One of the most important factors is the tilt angle of the solar collector. In order to estimate the optimum tilt angle of the collector, many studies have been conducted [126-131]. The majority of these studies have been shown that the optimum tilt angle of the collector is equal to the latitude of the location (site) with angle variation of 10º to 15º, depending on the application. In the present study, simple MATLAB code has been created to investigate and determine the optimum tilt angle for the thermo-syphon. The MATLAB code has been attached in the appendix B. Figure 5-6 depicts that the optimum tilt angle is equal to the latitude of the location.

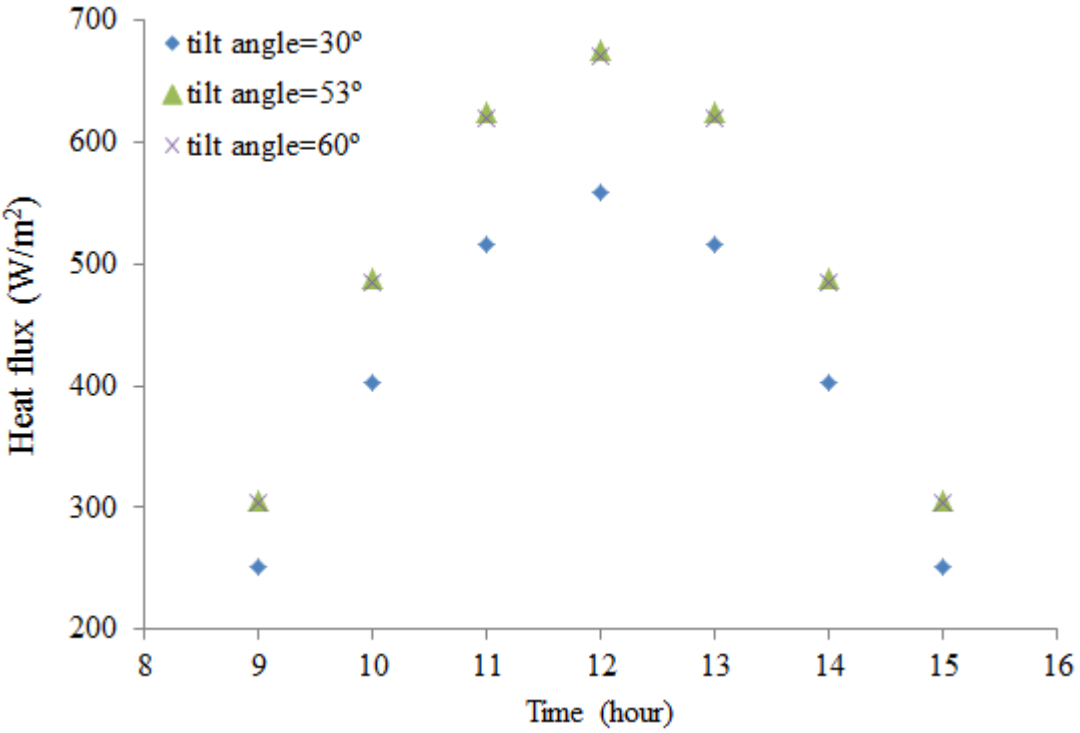

Figure 5-6 Heat flux variations for different tilt angles on 15th March

Based on observation above the tilt angle for the collector has been chosen to be 53º, as the research has been conducted in Huddersfield and the altitude of Huddersfield is 53º.

5.5.2. Effect of Number of Riser Pipes

The following section of this chapter will illustrate the effect of number of riser pipes on the thermal performance of the thermo-syphon. This has been conducted based on numerical results obtained from a configuration, which has been designed with a collector tilt angle of 53º, L/d ratio of 75, and heat flux that represents the 15th March. Based on the conclusion from the previous section (Effect of Tilt Angle), to obtain optimum heat flux the tilt angle of collector has been chosen to be 53º. For L/d ratio, an average of 50, 75, and 100 has been chosen which is equal to 75. Additionally, heat flux obtained on 15th March was chosen since it approximately represents the average value of heat flux obtained in the year. Moreover, the thermal loading used in this particular case represents a weekday, as this provides a general example for hot water consumption. Five, seven, and nine pipes have been used in this analysis to investigate the effect of the number of pipes on the thermo-syphon performance.

Figure 5-7 depicts the static temperature distribution at the cross-section of the storage water tank and the condenser, for (a) five riser pipes, (b) seven riser pipes and (c) nine riser pipes that have been considered in the present study. The thermal loading condition that has been specified represents the weekday with a heat flux of 15th March, and the corresponding L/d ratio has been selected as 75. It can be clearly seen that the hot water occupies the upper section of the tank, while the cold water settles at the bottom of the tank. Due to its lower density, hot water rises within the storage tank and accumulates along the top wall of the storage tank. The same thing happens for working fluid within thermo-syphon loop. As the working fluid flows along the condenser pipe, heat exchange takes place between the working fluid and the storage water. In this process, working fluid transfers the heat to the storage water. Hence the temperature of water in the storage tank increases and moves towards the top. Whereas the temperature of the working fluid decreases and moves toward the bottom of the condenser pipe. Subsequently, the working fluid recirculates via recirculation pipe due to the gravity.

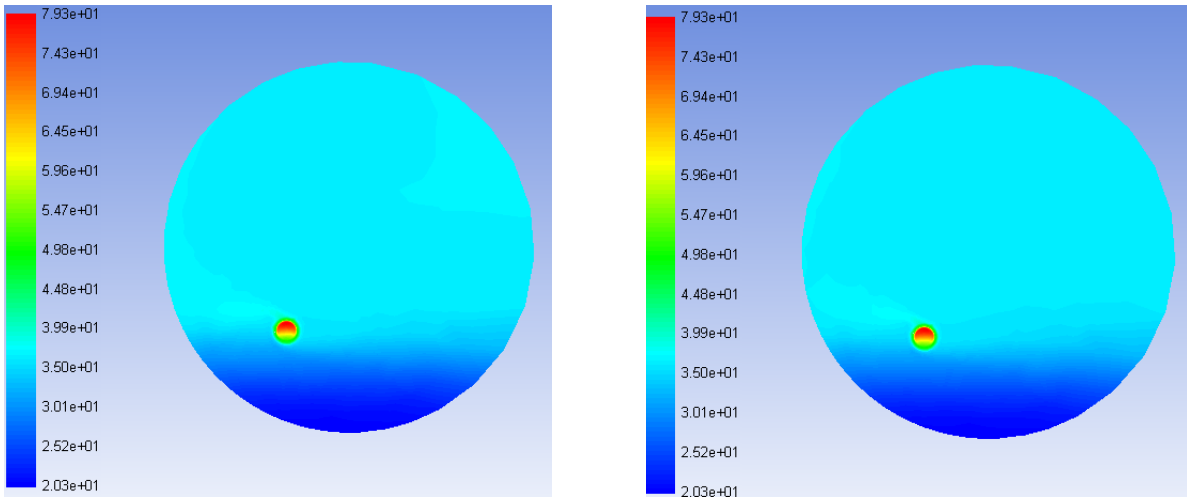

(a) (b)

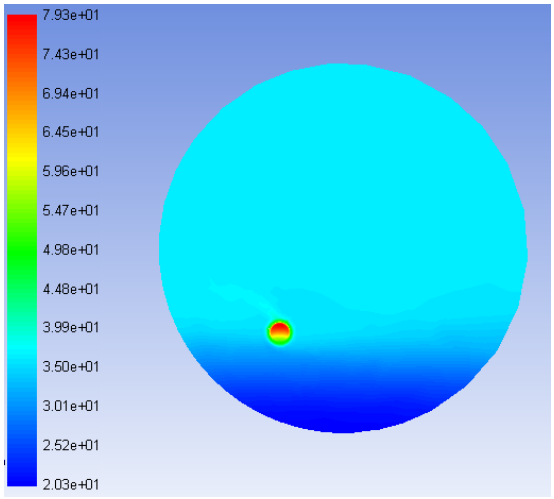

(c)

Figure 5-7 Static temperature distributions within the storage water tank and the condenser for (a) 5 pipes (b) 7 pipes and (c) 9 pipes on 15th March under thermal weekday loading

Figure 5-8 depicts the variation in water's temperature at the centre of the storage tank for a variable number of the riser pipes at a heat flux corresponding to 15th March under thermal loading condition of the weekday. It can be seen that the temperature within the tank is higher for nine riser pipes as compared to five and seven riser pipes. The temperature rise of water within the storage tank after operation time of seven hours were 30.08ºC, 31.53ºC and 33.09ºC for 5, 7 and 9 riser pipes respectively. Since, the surface area which is exposed the heat input is a function of the number and length of riser pipe an increase in the number of riser pipe will lead to increase in the surface area and hence increase in the amount of heat transfer to the working fluid. It is obvious from the fact that more riser pipes will transfer more hot fluid to the condenser thus increase water temperature within the storage tank. It can therefore be concluded that increasing the number of riser pipes increases the temperature of the water within the storage tank.

Figure 5-9 depicts the variation in temperature of working fluid at the centre of the condenser for a variable number of the riser pipes at a heat flux corresponding to 15th March under thermal loading condition of the weekday. It can be seen that the temperature of working fluid within the condenser is higher for nine riser pipes as compared to others for same reasons as above. Increasing the number of the riser pipes from 5 to 7 and from 5 to 9 lead to an increase in temperature of working fluid within the condenser by 5.3% and 10.5% respectively. Furthermore, it can be noted that the working fluid temperature decreases at the end, as the heat flux starts to decrease, which is exposed to the collector.

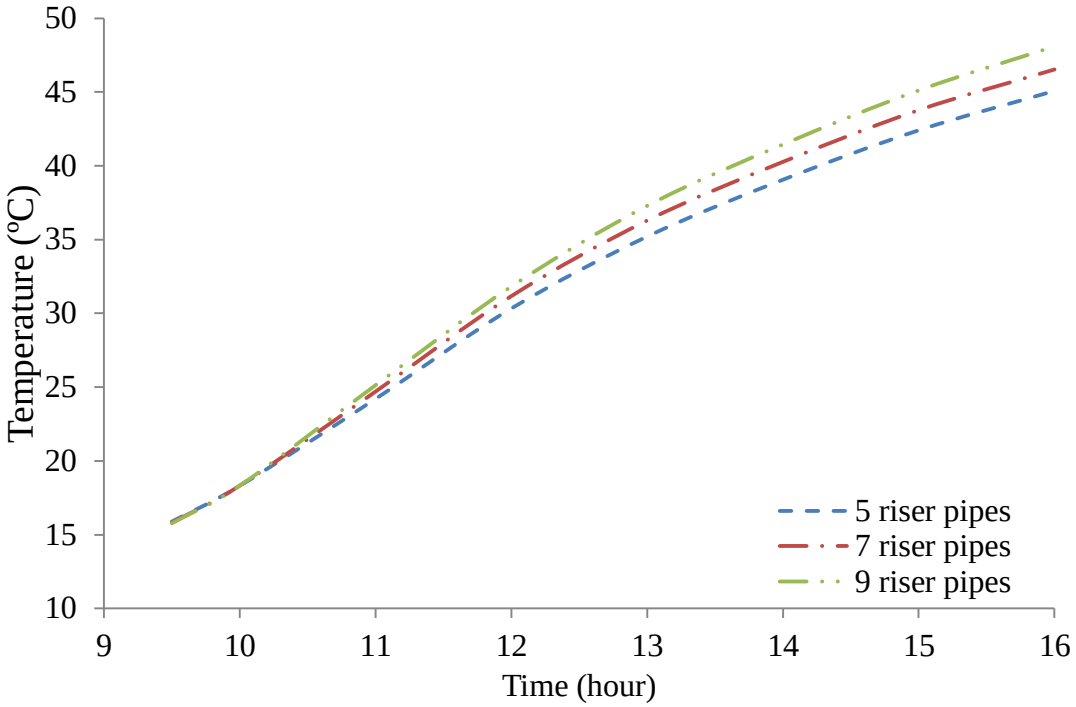

Figure 5-8 Temperature variations at the centre of the storage water tank for various numbers of riser pipes on 15th March under thermal weekday loading

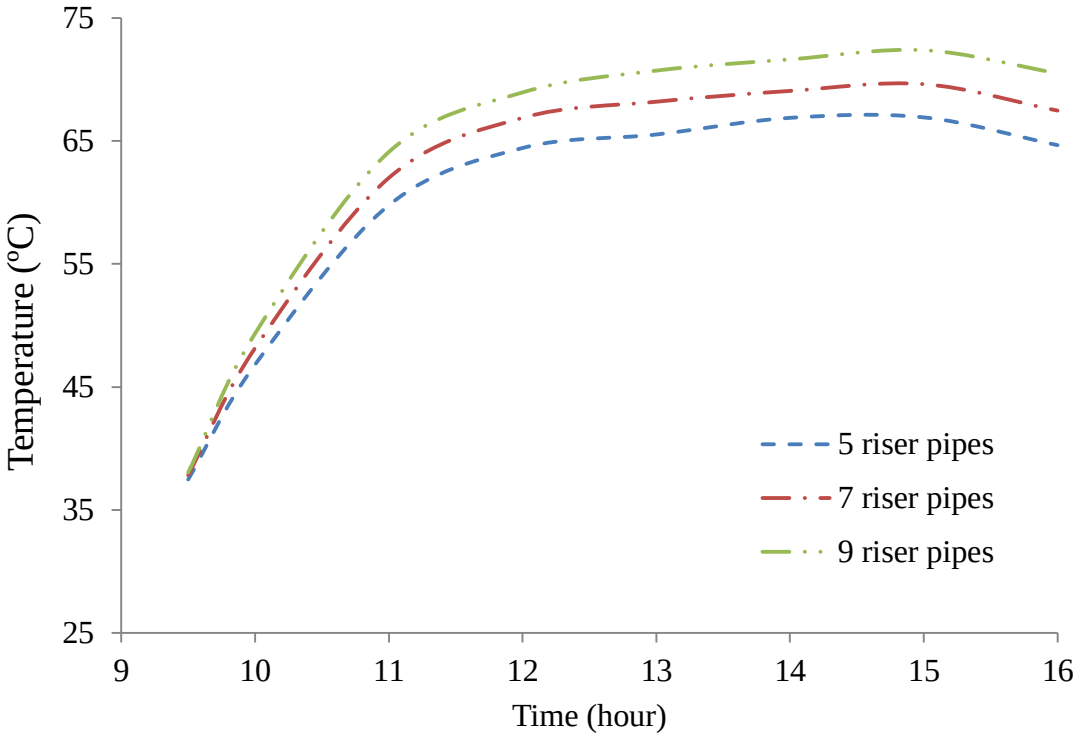

Figure 5-9 Temperature variations of the working fluid within the condenser for various numbers of riser pipes on 15th March under thermal weekday loading

Figure 5-10 depicts the variation in mass flow rate, of working fluid within thermo-syphon loop for variable numbers of riser pipes at a heat flux corresponding to 15th March under thermal loading condition of the weekday. This mass flow rate measured at a cross section of upriser before the condenser. It can be seen clearly that the average mass flow rate changes along with the change in solar heat flux. It can be seen from this figure that the average mass flow rate within the closed loop thermo-syphon follows the changes of irradiance pattern, increasing in the morning and decreasing in the afternoon. This is due to the fact that, the mass flow rate is directly related to the rate of evaporation and condensation. Furthermore, mass flow rate within the closed loop thermo-syphon is higher for nine riser pipes as compared to five and seven riser pipes. The maximum mass flow rate was recorded to be 0.00414kg/s, 0.00427kg/s, and 0.00432kg/s for five, seven and nine riser pipes respectively.

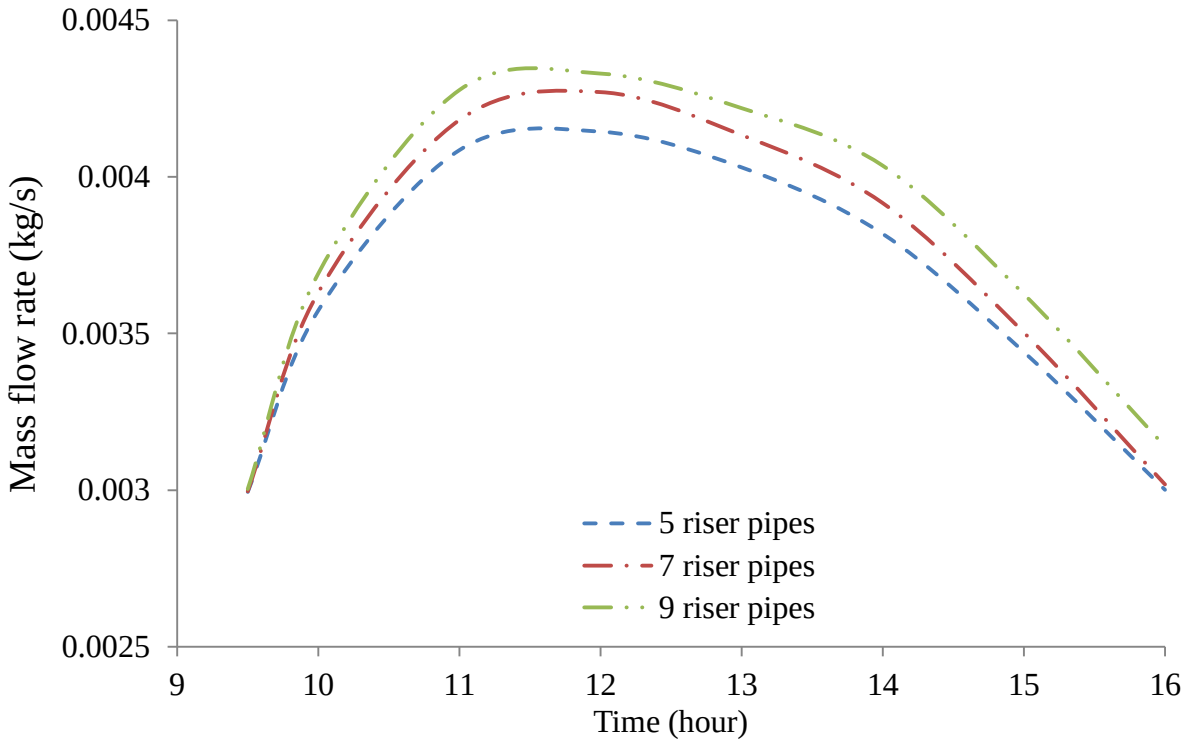

Figure 5-10 Circulating mass flow rate within thermo-syphon loop for various numbers of riser pipes on 15th March under thermal weekday loading

Figure 5-11 depicts wall shear stress variations within the closed loop thermosyphon for variable numbers of riser pipes at a heat flux corresponding to 15th March under thermal loading condition of the weekday. It can be clearly seen that the wall shear stress is higher for nine riser pipes as compared to five and seven riser pipes. The maximum wall shear stress was recorded to be 0.01099Pa, 0.00902Pa and 0.00801Pa for nine, seven and five riser pipes respectively.

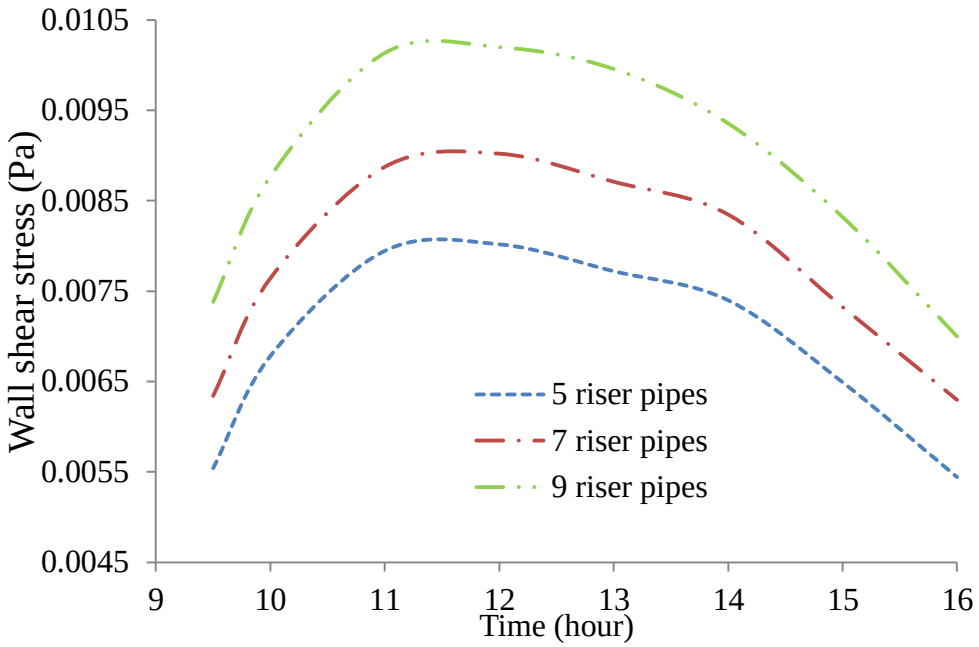

Figure 5-11Wall shear stress variations within thermo-syphon loop for various numbers of riser pipes on 15th March under thermal weekday loading

Figure 5-12 depicts the variations of global heat transfer coefficient of working fluid within thermo-syphon loop for the same conditions as above. This heat transfer coefficient has been calculated using the following expression:

$$h = \frac{q}{\Delta T} \tag{5.1}$$

where q is the heat flux input (in W/m^2) and ΔT can be calculated from Eq.(1.48), which is given by $\Delta T = T_{wall} - T_{ref}$

where T_{wall} is the area-average static temperature of the riser tubes collectively, and T_{ref} is the reference temperature can be calculated from Eq.(1.49), which is given by $T_{ref} = \frac{(T_i + T_o)}{2}$

where T_i and T_o are the area-average static temperatures in the cross-sections of the inlet and outlet of the collector.

It can be clearly seen from Figure 5-12 that the heat transfer coefficient within the collector is highest for nine-riser pipe, as compared to five and seven riser pipe. The increase in the number of riser pipes increases the surface area of the riser pipes exposed to heat flux with constant collector area and hence, increases the amount heat transfer to working fluid. This increased heat transfer increases the working fluid temperature and hence reduce the temperature difference between the surface and working fluid, leading to an increment of heat transfer coefficient. Furthermore, it can be seen that the heat transfer coefficient increases at the beginning with the rising heat flux until

midday. Subsequently as the heat flux, decreases the heat transfer coefficient starts to decrease. It has been noticed that at midday representing the maximum heat flux, the heat transfer coefficient was highest. The highest heat transfer coefficients were recorded to be 44.75W/m^2.ºC, 58.69 W/m^2.ºC and 71.75 W/m^2.ºC for five, seven and nine riser pipes respectively. Therefore, it can be concluded that the number of riser pipes has effect on the heat transfer coefficient of working fluid within the thermo-syphon loop. Similarly, as it was pre-mentioned, the amount of heat transfer is proportional to the heat flux and the above discussion represents that the heat transfer coefficient is proportional to the total heat transfer.

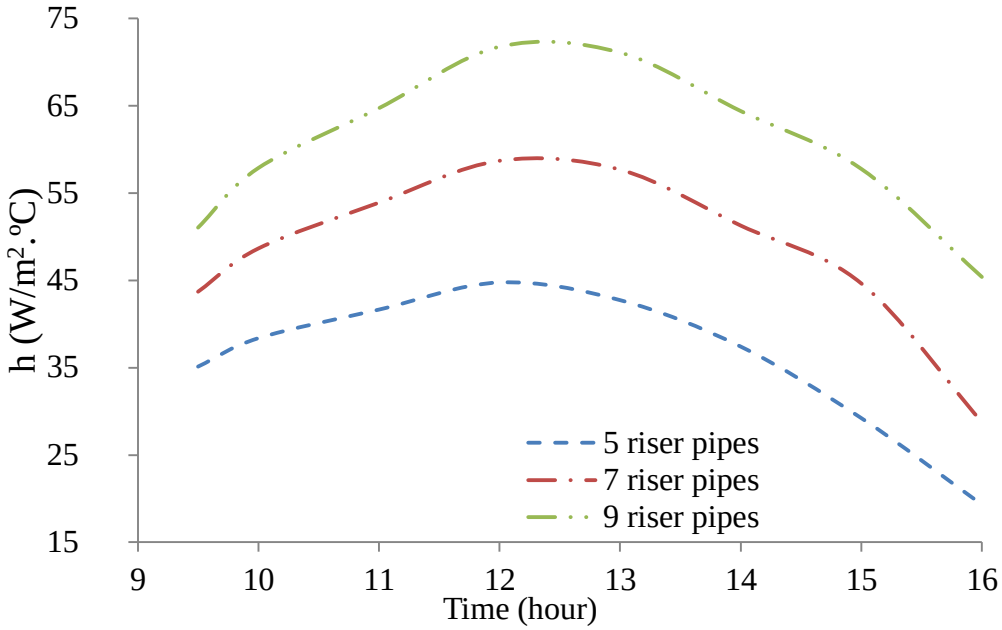

Figure 5-12 Heat transfer coefficient variations within the collector for various numbers of riser pipes on 15th March under thermal weekday loading

Figure 5-13 depicts the flow velocity variations within the cross-section taken along the length of the middle riser pipe in the y-z plane of the thermo-syphon configurations having various numbers of riser pipes at a heat flux corresponding to 15th March under weekday thermal loading condition. In this study, the middle riser pipe has been chosen, because the distance between the middle riser pipe and the downcomer is same for all the configurations and hence, to achieve a more accurate and reliable comparison among the configurations. The scale of the contours has been kept constant for effective comparison purposes. It can be seen that the velocity of the working fluid is higher as it climbs up the riser pipe due to its lower density. This is because the hot water rises up in the riser pipe's cross sections, and then propagates towards the upriser. Furthermore, it can be clearly seen that the velocity of working fluid within the riser pipe is highest for the configuration with five riser pipes as compared to the same of seven and nine riser pipes. It must be noted that increse in number of pipes are for same collector area which sebsequently inputs same amount of

heat for these different configuations. Therefore, it can be concluded that increasing the number of riser pipe has an impact on the velocity of working fluid within the riser pipe.

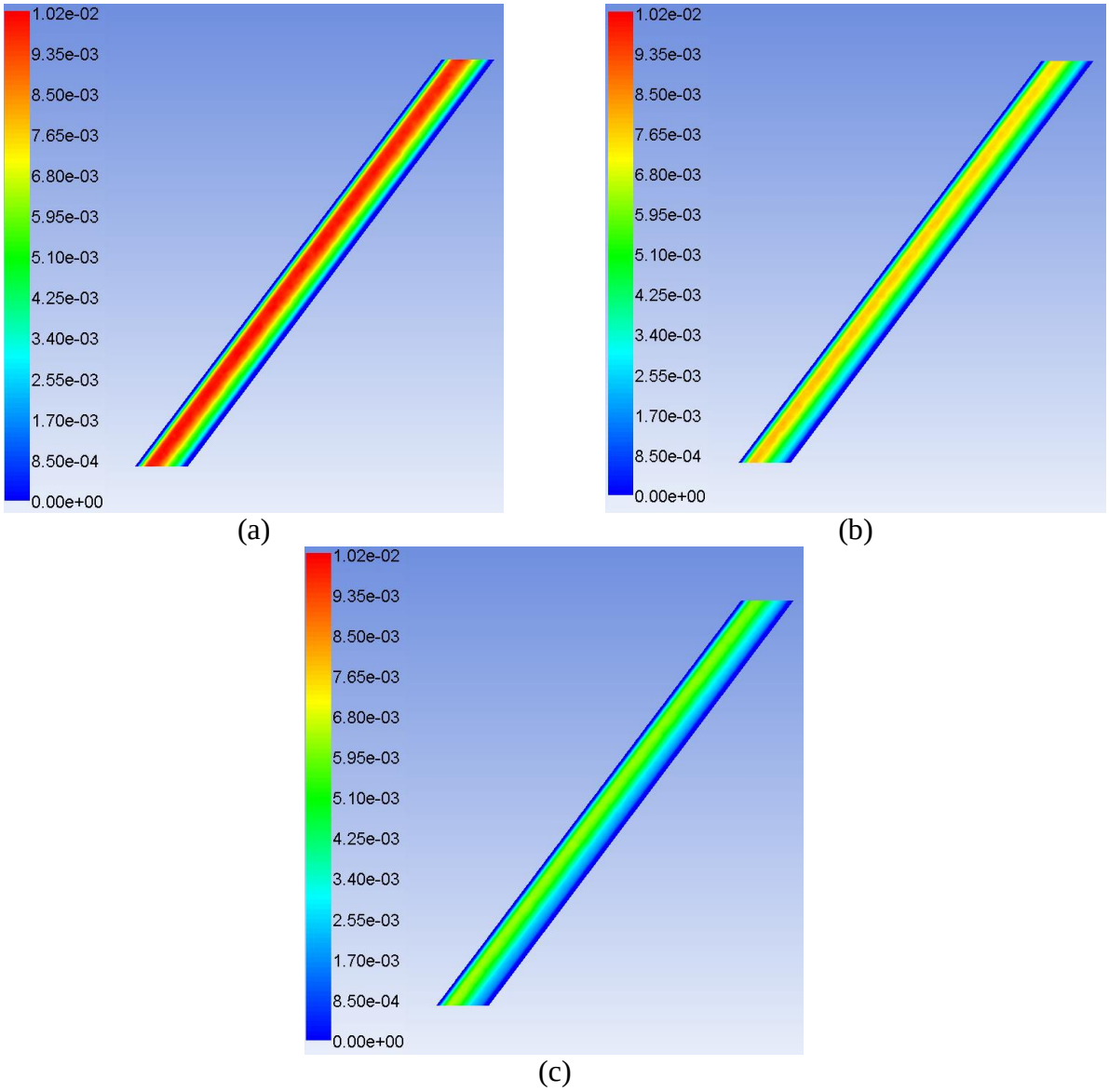

Figure 5-13 Flow velocity variations within the middle riser pipe at 12 O'clock (midday) for (a) 5 pipes (b) 7 pipes and (c) 9 pipes on 15th March under thermal weekday loading

Figure 5-14 depicts the velocity profiles of the working fluid taken at a radial cross-section within the middle riser pipe on the x-y plane for heat flux obtained on 15th March has been applied for the three different number of the riser pipe arrangements, that has been considered in the current study, under working day thermal loading conditions. It can be clearly seen that the velocity of the working fluid is higher at the centre of riser pipe for all cases. Furthermore, an increase in the number of riser pipe decreases the velocity of working fluid within the riser pipe. The recorded

maximum velocity of working fluid within the middle riser pipe for five, seven, and nine riser pipes arrangements were 0.547m/min, 0.406m/min and 0.289m/min respectively. It can be further concluded that increased number of the riser pipes decreases the velocity of working fluid within the riser pipe, and increases the mass flow rate of working fluid within the thermo-syphon loop.

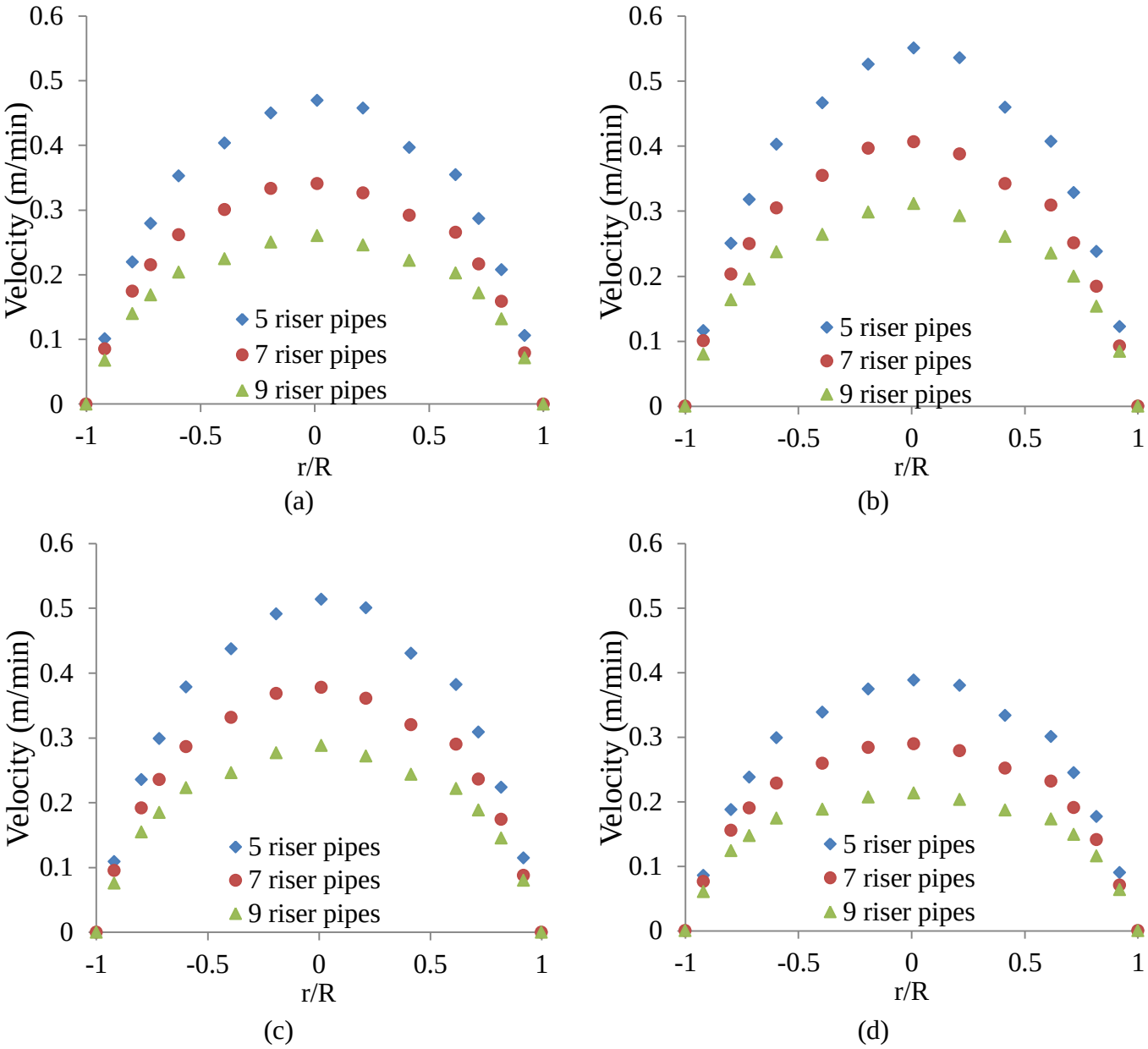

Figure 5-14 Velocity profiles within the middle riser pipe for various number of riser pipes at midday on 15th March under thermal weekday loading for (a) 10 O'clock (b) 12 O'clock (c) 14 O'clock and (d) 16 O'clock

Figure 5-15 depicts static temperature distribution within the cross-section taken along the length of the middle riser pipe in the y-z plane at a heat flux corresponding to 15th March for the three number of the riser pipe (a) 5 riser pipes (b) 7 riser pipes (c) 9 riser pipes considered in the present study. The corresponding thermal loading condition that has been specified is the weekday. It can be clearly seen that the hot water occupies the periphery of riser pipe wall, whereas the cold water is in the centre of pipe. This is because the density of the hot water reduces after absorbing solar energy, which causes it to rise above the denser cold water. It can be further noticed that the temperature within the riser pipe is highest with nine-riser pipe as compared to five and seven the riser pipe. This means that the working fluid's temperature increases with increased number of the riser pipe.

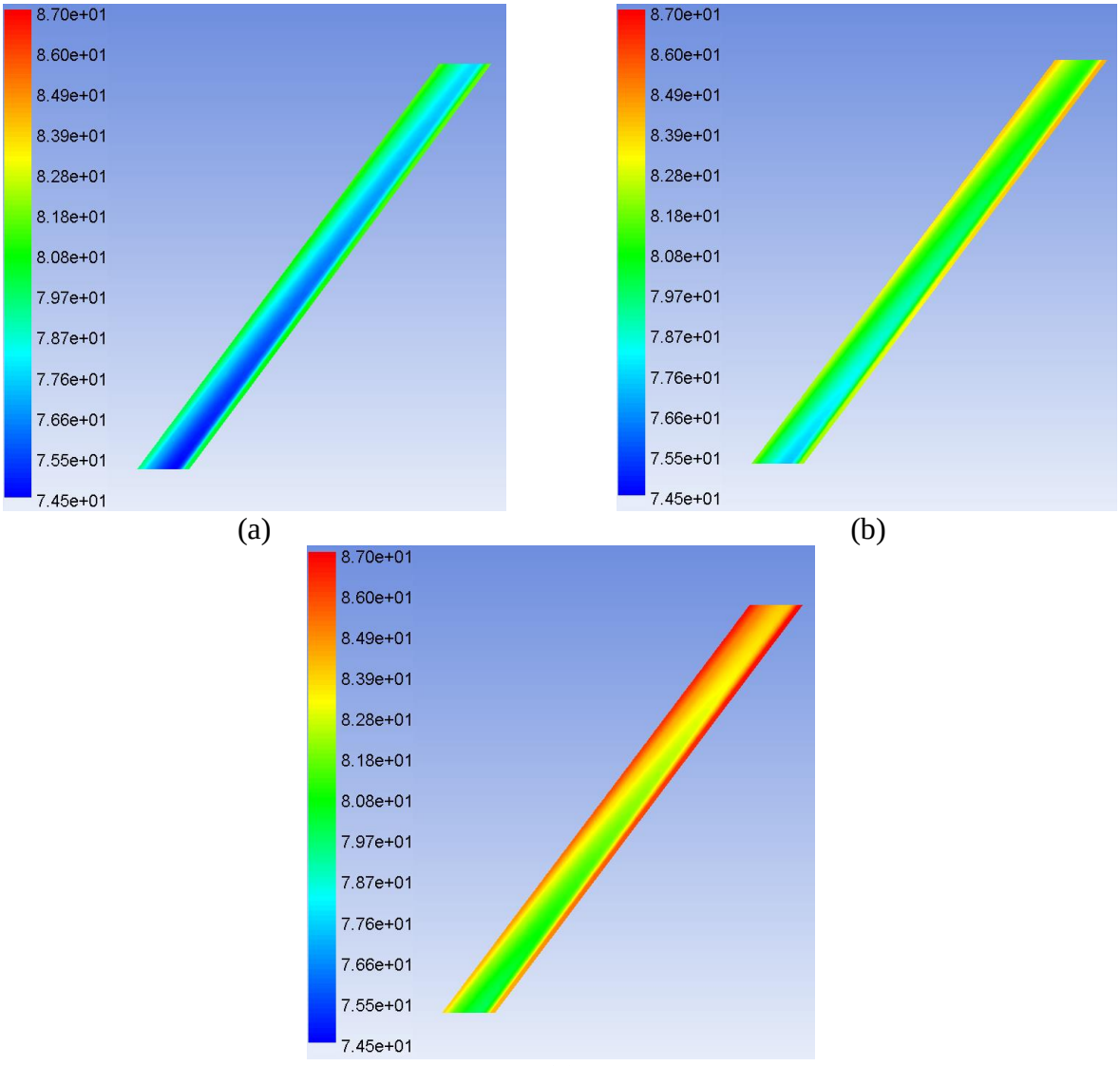

Figure 5-15 Static temperature distribution within the middle riser pipe at 12 O'clock (midday) for (a) 5 pipes (b) 7 pipes and (c) 9 pipes on 15th March under thermal weekday loading

Figure 5-16 depicts the static temperature profiles of the working fluid taken at a radial cross section within the middle riser pipe on the x-y plane at a heat flux corresponding to 15th March for the three number of the riser pipes considered in the present study. The corresponding thermal loading condition that has been specified is that of the weekday. It can be clearly seen that the temperature of working fluid is higher in the near wall regions where the solar heat flux is directly in contact with the riser pipe wall. Furthermore, the temperature of working fluid is higher for nine-riser pipe as compared to five and seven riser pipe. The average temperature value for 5, 7 and 9 riser pipes is 80.02°C, 82.87°C and 85.46°C respectively. It can be further concluded that an increase in number the riser pipe increases the temperature of working fluid within the riser pipes.

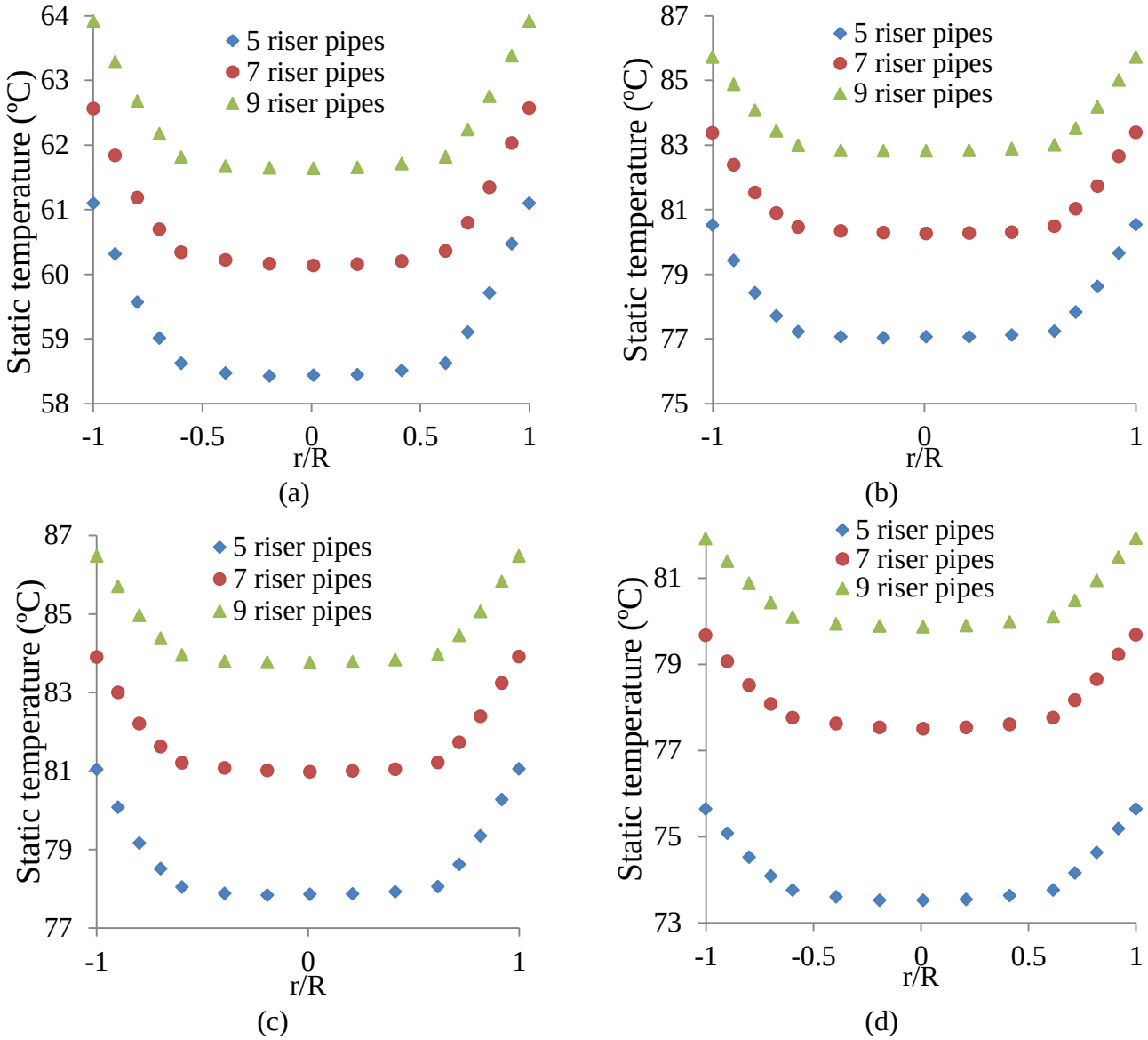

Figure 5-16 Static temperature variations within the middle riser pipe for various number of riser pipes at midday on 15th March under thermal weekday loading for (a) 10 O'clock (b) 12 O'clock (c) 14 O'clock and (d) 16 O'clock

Since the amount of working fluid for 9 riser pipes is larger compared to 5 riser pipes, it needs more energy per unit mass of working fluid to get moving. This effect can also be deduced from fig 5.14 where velocity profile obtained for 9 riser pipes is lower compared to 5 riser pipes.

Based on the aforementioned analysis of effect of riser pipe number on various parameters can be denoted in Table 5-4. It must be noted that the mass flow rate is measured at a cross section of upriser before the condenser.

Table 5-4 The effect of the riser pipe number on various parameters

Number of pipes (np)		5	7	9
Water Temperature within the storage tank (ºC)	Value	30.33	31.17	31.82
	Percentage difference (%)	2.7	2.1	
Mass flow rate within thermo-syphon loop (kg/s)	Value	0.00414	0.00427	0.00433
	Percentage difference (%)	3.1	1.4	
Wall shear stress (Pa)	Value	0.00801	0.00902	0.01099
	Percentage difference (%)	21.0	12.0	
Heat transfer coefficient of working fluid ($W/m^2.ºC$)	Value	44.75	58.69	71.75
	Percentage difference (%)	31.0	22.0	

By studying the Table 5-4 it can be concluded that the storage tank temperature of the thermo-syphon has insignificant improvement with an increase in the number of pipes. A 2.7% increase in water temperature was recorded as the number of pipes was increased from 5 to 7. However, when the number of pipes were increased from 7 to 9 the water temperature increased only by 2.1%. This trend is similar for the other parameters such as mass flow rate and the heat transfer coefficient. Based on above results, increasing the number of pipes more than 5 does not have significant improvement on the storage tank temperature. Therefore, to reduce the complexity of the geometry and the computational cost 5 riser pipes will be chosen for next investigations.

5.5.3. Effect of L/d Ratio

In order to, study the effect of L/d ratio on the performance of thermo-syphon, five riser pipes set has been chosen. This number of the riser pipes is chosen based upon the conclusion of the previous section. In the previous section, it was concluded that the number of the riser pipes have a small effect on the storage tank temperature. Since the scope of the study considers only three number of the riser pipe (five, seven and nine), henceforth to reduce the computation time and complexity of the geometry, five riser pipes have been considered for further investigation, in the following sections.

Figure 5-17 depicts the temperature distribution within the condenser and storage water tank for three different L/d ratios of riser pipes of the thermo-syphon models considered in the present study at a heat flux corresponding to 15th March under thermal loading of working day. It can be clearly seen that the hot water occupies the upper section of storage tank while the cold water is

accumulated at the lower sections. Furthermore, it can be seen that the average temperature of water is higher for L/d ratio =100, as compared to the L/d ratio of 75 and 50. The average temperature of water within the storage tank was 34.60ºC, 30.30ºC and 26.10ºC for L/d=100, 75 and 50 respectively. Whilst the average temperature of working fluid within the condenser was 76.48ºC, 64.43ºC and 52.08ºC for L/d=100, 75 and 50 respectively. This indicates that an increase in the L/d ratio of riser pipes leads to an increase in the average temperature of water within the condenser and hence the temperature of storage water tank. As mentioned in the previous section that the surface area which is exposed the heat input is a function of the number and length of the riser pipe, so, increasing the L/d ratio of riser pipe leads to increase the surface area and hence the heat energy transmitted to working fluid within the thermo-syphon. It is obvious; from the fact that increase L/d ratio of riser pipes transfer more hot fluid to the condenser thus increase water temperature within the storage tank. Thus it can be concluded that an increase in L/d ratio of riser pipes increases the temperature of the water within the storage tank.

Figure 5-18 depicts the variation in water's temperature at the centre of the storage tank for variable length to diameter ratio of the riser pipe at a heat flux corresponding to 15th March under thermal loading of working day. It can be seen that the temperature of the working fluid within the condenser and temperature of water within the storage tank are higher for L/d = 100 as compared to L/d = 75 and L/d=50 of the riser pipes. It is obvious from the fact that longer riser pipes offer more surface area for the solar energy to be converted into the working fluid's internal energy; hence increasing its temperature. At the end of the period of operation, the water temperature within the storage tank is 53.20ºC, 45.80ºC and 37.57ºC for L/d=100, L/d=75 and L/d=50 respectively. Hence, increase in the length of the riser pipes increases the temperature of water within the storage tank.

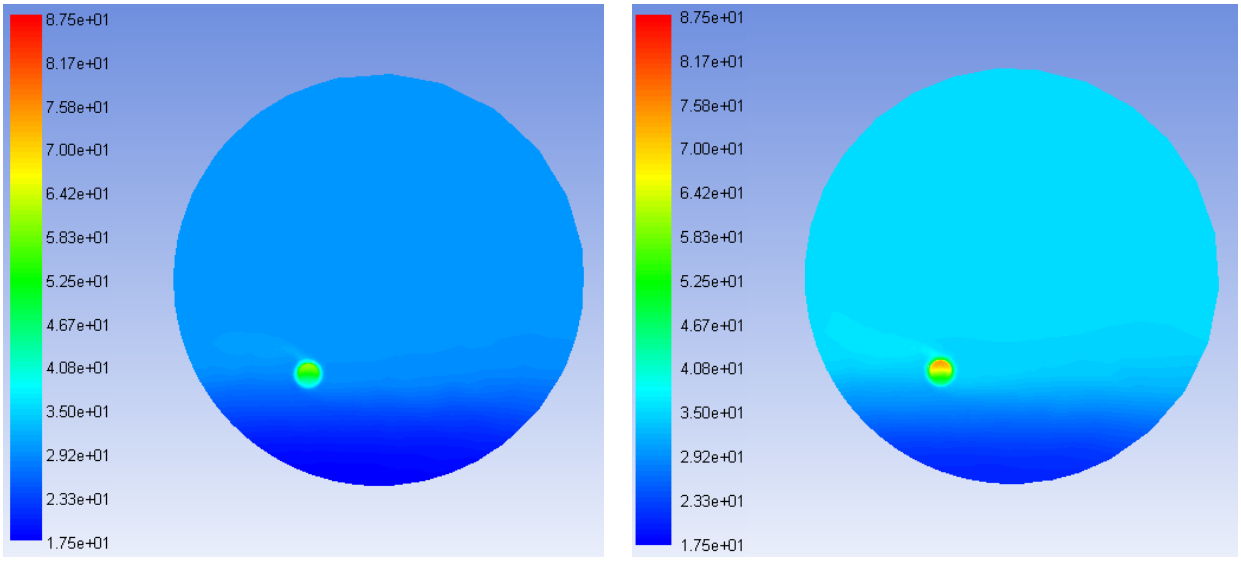

(a) (b)

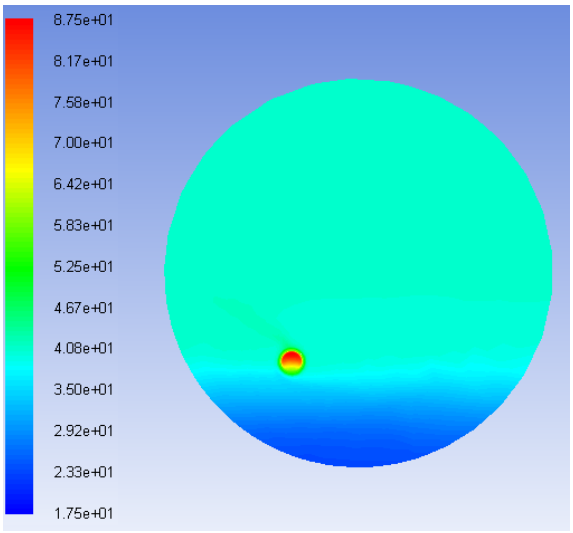

(c)

Figure 5-17 Temperature variations within the condenser and storage water tank for (a) L/d=50, (b) L/d=75 and (c) L/d=100 at midday on 15th March under thermal weekday loading

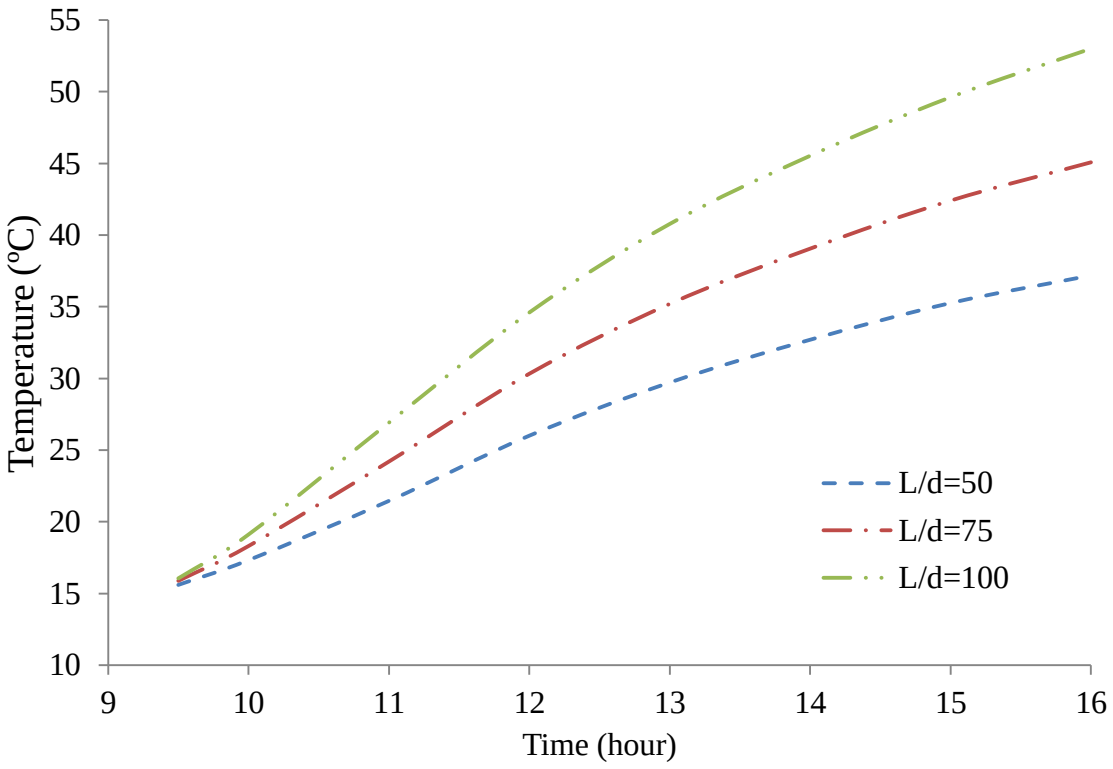

Figure 5-18 Temperature variations within the storage water tank for various L/d ratios of riser pipes on 15th March under thermal weekday loading

Figure 5-19 depicts the variation in working fluid's temperature within the condenser for variable lengths of the riser pipes at a heat flux of 15th March under thermal loading of working day. It can be seen that the temperature within the condenser is higher for L/d = 100 as compared to L/d = 75 and L/d=50 of the riser pipes. Increase L/d ratio of the riser pipes from 50 to 75 and from 50 to 100 lead to increase the temperature of working fluid within the condenser by 22.9% and 42.8% respectively. It is obvious from the fact that longer riser pipes offer more surface area for the solar energy to be converted into the working fluid's internal energy. Hence, increase in the length of the riser pipes increases the temperature of the working fluid within the condenser. Furthermore, the working fluid's temperature within the condenser varies with the similar trend as the heat flux varies with respect to time. During the first three hours from 9-12 O'clock, the heat flux increases and hence the temperature of working fluid. Later on, after 12 O'clock, the heat flux start to decrease and hence the temperature of working fluid within the condenser was decreased. Therefore, even after the heat transfer in the condenser, the working fluid temperature in the condenser increases at the beginning at a rate with a higher gradient. After a certain period of time, it reaches a certain value, when the increment rate is nearly constant and at the late afternoon it starts to decrease

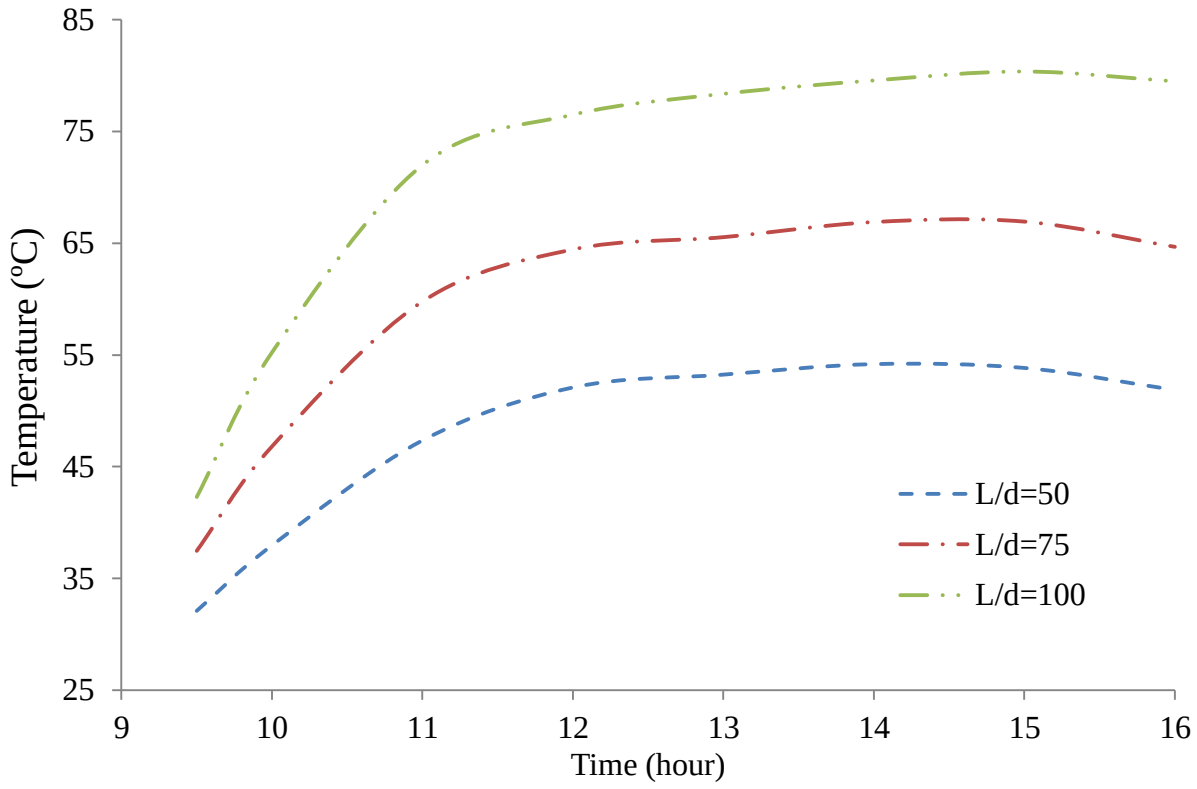

Figure 5-19 Variations in temperature of the working fluid within the condenser for various L/d ratios of riser pipes on 15th March under thermal weekday loading

Figure 5-20 depicts the variation in mass flow rate of working fluid within the thermo-syphon loop for variable length to diameter ratio of riser pipes at a heat flux corresponding to 15th March

under thermal loading condition of the weekday. This mass flow rate measured at a cross section of upriser before the condenser. It can be seen clearly that the average mass flow rate increase with an increase in both riser pipes length and solar heat flux. The maximum average mass flow rate are 0.0034kg/s, 0.0041kg/s and 0.0048kg/s for L/d=50, L/d=75 and L/d=100 respectively.

Figure 5-21 depicts wall shear stress variations within thermosyphon loop for variable length to diameter ratio of riser pipes at a heat flux corresponding to 15th March under thermal loading condition of the weekday. It can be clearly seen that the wall shear stress is higher for L/d=100 as compared to other ratio of the riser pipes. The maximum average wall shear stress are 0.00873Pa, 0.01019Pa and 0.01147Pa for L/d=50, L/d=75 and L/d=100 respectively.

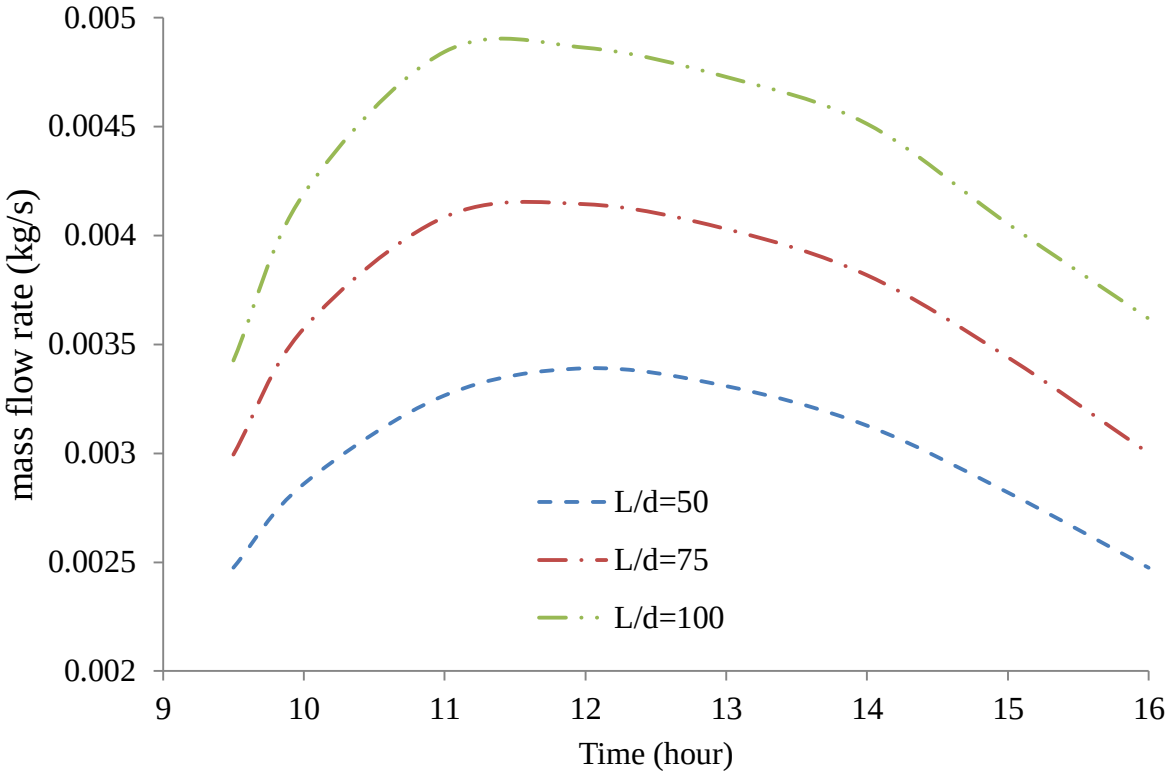

Figure 5-20 Circulating mass flow rate for various L/d ratio of riser pipes on 15th March under thermal weekday loading

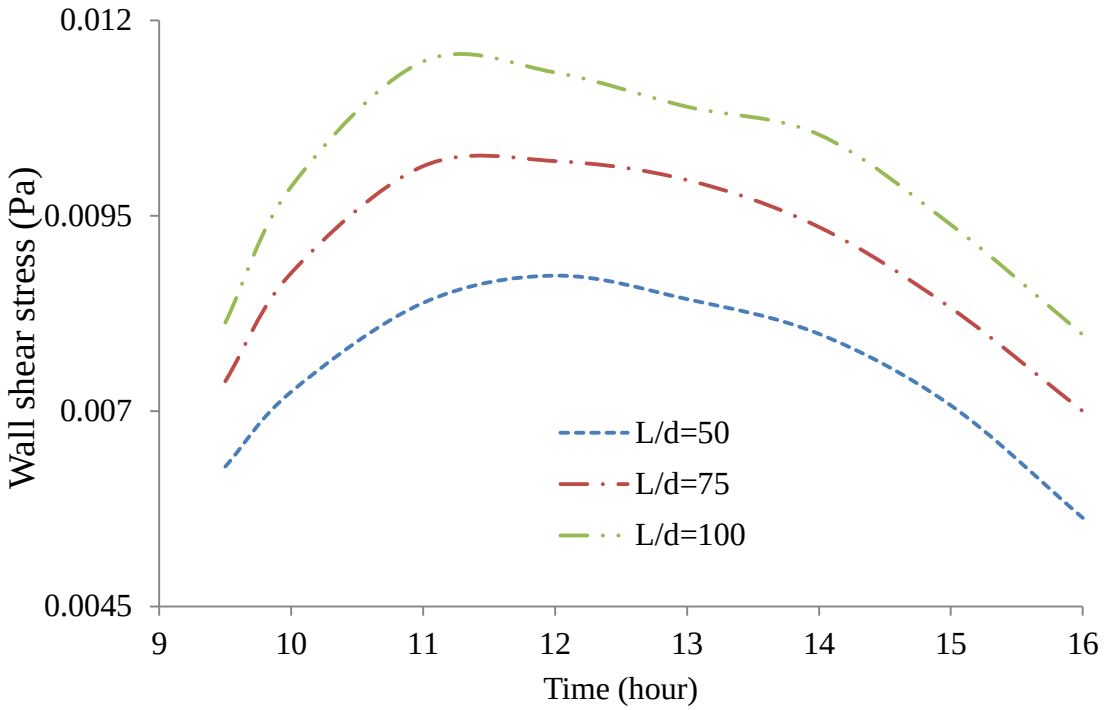

Figure 5-21 Wall shear stress variations within thermo-syphon loop for various L/d ratio of riser pipes on 15th March under thermal weekday loading

Figure 5-22 depicts variations of the heat transfer coefficient within the thermo-syphon for the same conditions as above. It can be clearly seen that the heat transfer coefficient within the collector is highest for L/d ratio of 100, as compared to L/d ratio of 50 and 75. The increase in L/d ratio of riser pipes increases the surface area, which exposed to heat flux and hence increases the amount heat transfer to working fluid. This increased heat transfer increases the working fluid temperature and hence reduce the temperature difference between the surface and working fluid, leading to an increment of heat transfer coefficient. Furthermore, it can be seen that the heat transfer coefficient increases, then decreases, depending on the variation in the heat flux input to the thermo-syphon. It can therefore, be concluded that increasing the length of riser pipe has a significant impact on the heat transfer coefficient of the working fluid within the thermo-syphon loop. Similarly, as it was mentioned above, the amount of heat transfer is proportional to the heat flux and the above discussion represents that the heat transfer coefficient is proportional to the total heat transfer. Hence, combining these two arguments it can be suggested that, if there is a temperature gradient, the heat transfer coefficient is proportional to the heat flux.

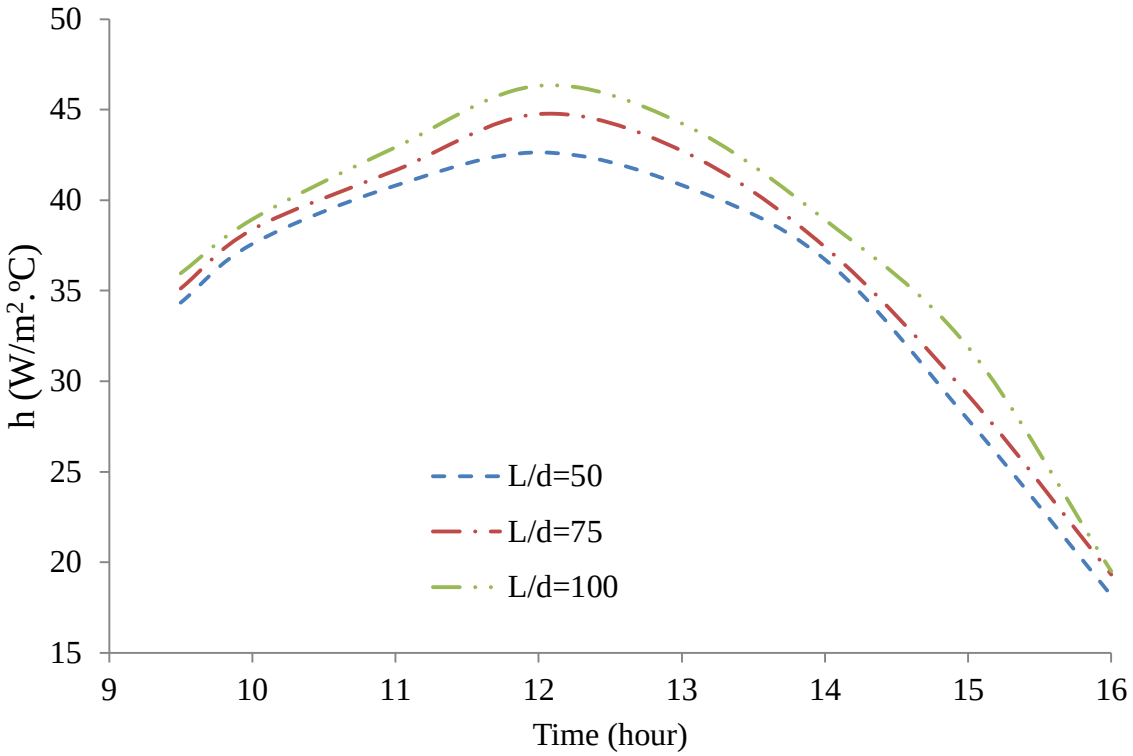

Figure 5-22 Heat transfer coefficient variations within the collector on different days of the year L/d ratio of riser pipe on 15th March under thermal weekday loading

Figure 5-23 depicts the flow velocity variations within the cross-section taken along the length of the middle riser pipe at a heat flux corresponding to 15th March, for the three ratios of L/d of riser pipe considered in the present study. The corresponding thermal loading condition that has been specified is the weekday. It can see be clearly that the velocity of working fluid within the riser pipe is highest for L/d of 100 as compared to L/d of 75 and 50. It can be concluded that increasing the length of riser pipe has a significant impact on the velocity of working fluid within the riser pipe. This is due to the fact that L/d of 100 requires more surface area of collector as compared to L/d of 50.

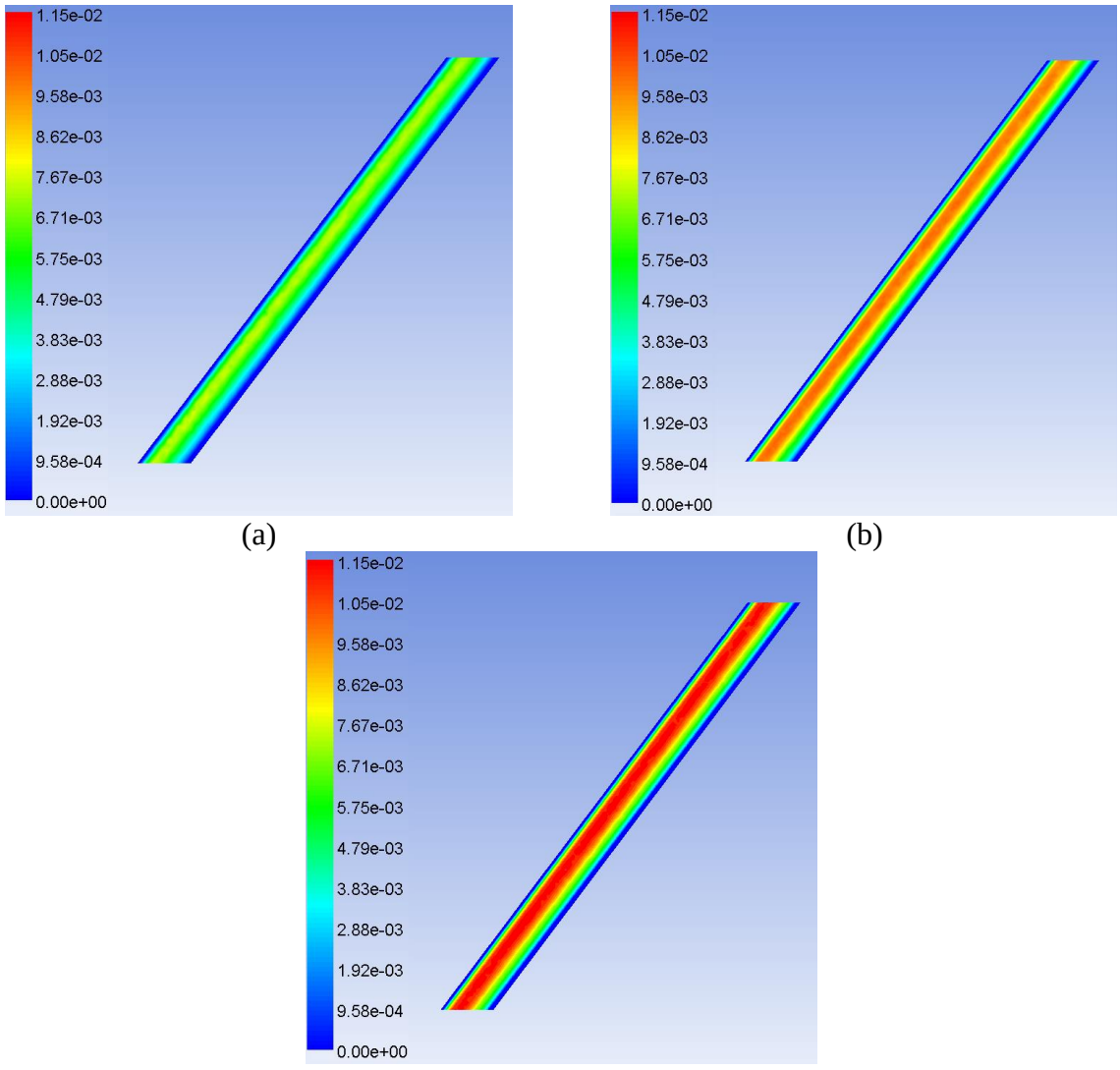

Figure 5-23 Flow velocity variations within the middle riser pipe for (a) L/d=50 (b) L/d=75 and (c) L/d=100 on 15th March under thermal weekday loading

Figure 5-24 depicts the velocity profiles of the working fluid taken at a cross section within the middle riser pipe for the various L/d ratio of riser pipe considered in the present study. It can be clearly seen that velocity of the working fluid within riser pipe is affected by a length to diameter ratio of the riser pipe. Findings show that the velocity is increasing with increase of the L/d ratio. In addition, the velocity of working fluid is higher at the centre of riser pipe for all the cases. Increase L/d leads to increase surface area of collector and hence increased the amount of heat convert to the working fluid within the riser pipe, which lead to increase the velocity of the working fluid. It can be concluded that the velocity of working fluid indicates rate of heat transfer in working fluid. For example, when the velocity within the riser pipe increases, the amount of heat transfer also increases.

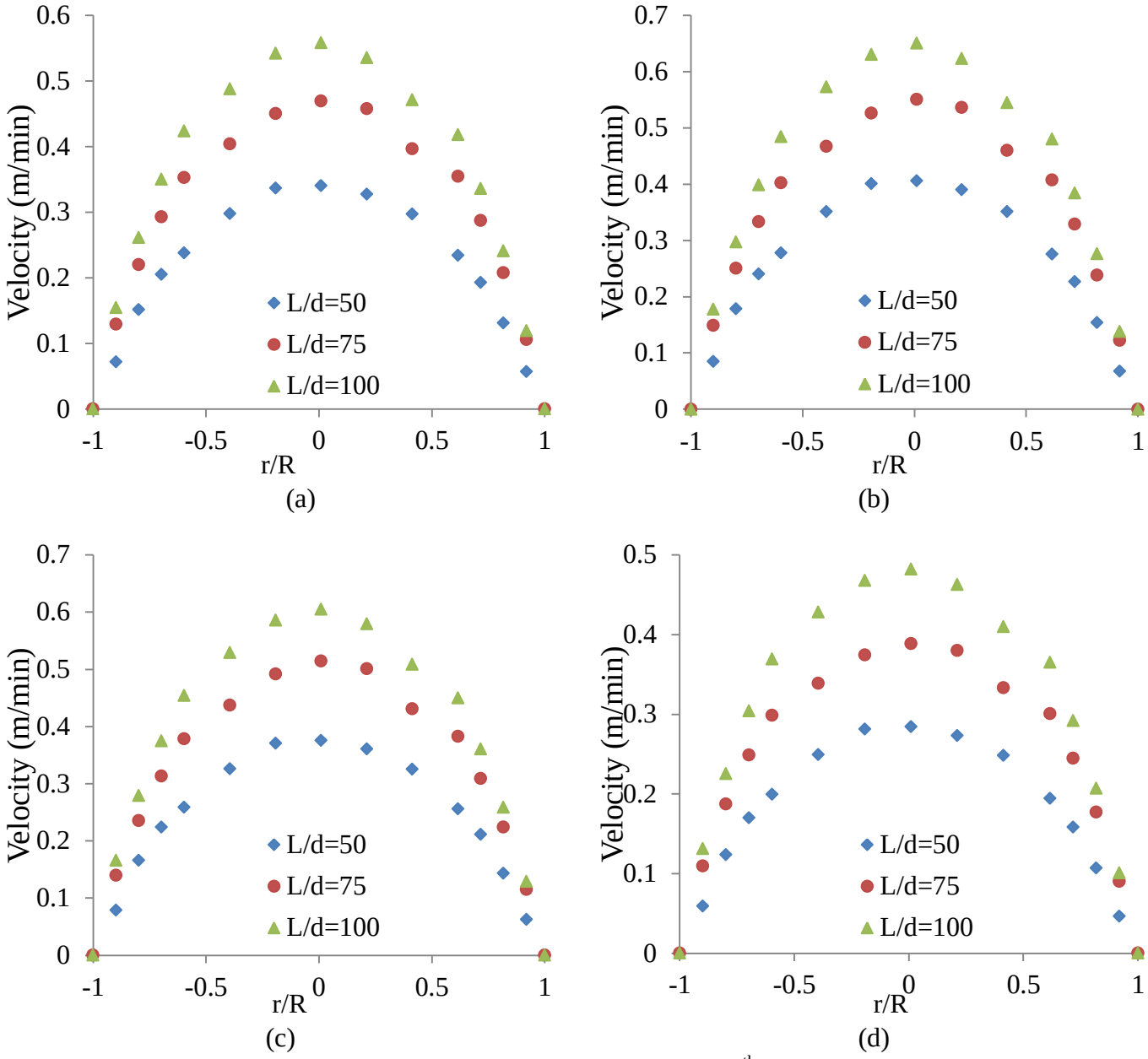

Figure 5-24 Velocity profiles within the middle riser pipe on 15th March for different L/d ratio of riser pipe under thermal weekday loading for (a) 10 O'clock (b) 12 O'clock (c) 14 O'clock and (d) 16 O'clock

Figure 5-25 depicts the variation in static temperature of the working fluid within the cross-section taken along the length of the middle riser pipe on 15th March, for the three L/d ratios of riser pipe considered in the present study. The corresponding thermal loading condition that has been specified is that of the weekday. It can see be clearly that the temperature of working fluid within the riser pipe is highest for L/d of 100 as compared to L/d of 75 and L/d of 50. It can therefore be concluded that increasing the length of riser pipe has a significant impact on the temperature of the working fluid within the thermo-syphon loop.

Figure 5-26 depicts the static temperature profiles of the working fluid taken at a cross-section within the middle riser pipe at a heat flux corresponding to 15th March for the three ratio of L/d of riser pipe considered in the present study. The corresponding thermal loading condition that has been specified is that of the weekday. It can be clearly seen that the temperature of working fluid is higher on L/d=100, as compared to L/d=75 and L/d=50. Furthermore, the temperature of the working fluid is lowest in the centre of riser pipe for all the cases. Exploring the velocity and the temperature profile inside riser pipe it can be concluded that the velocity distribution within the riser pipe is opposite to the temperature profile.

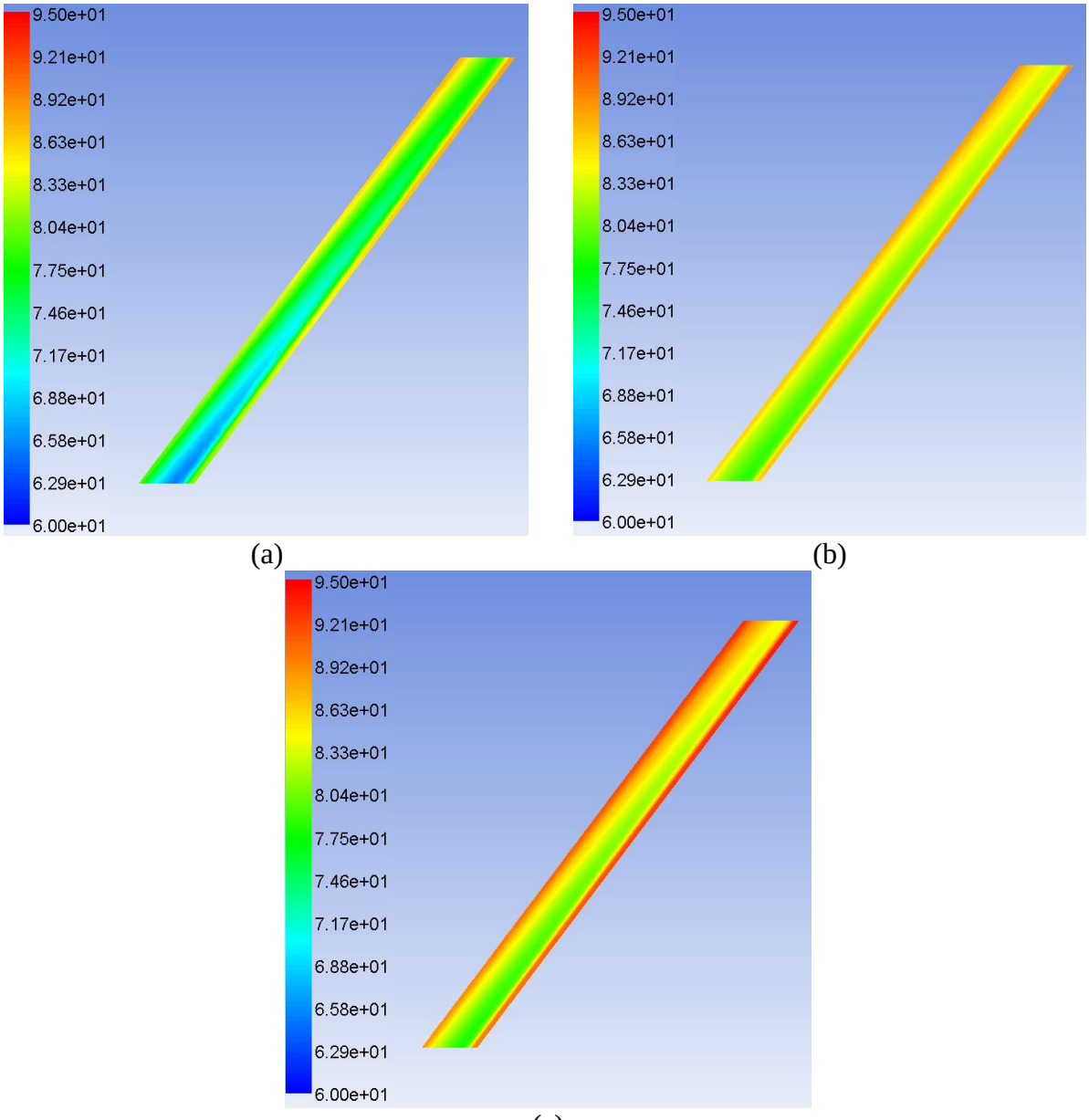

Figure 5-25 Static temperature distributions within the middle riser pipe for (a) L/d=50 (b) L/d=75 and (c) L/d=100 on 15th March under thermal weekday loading

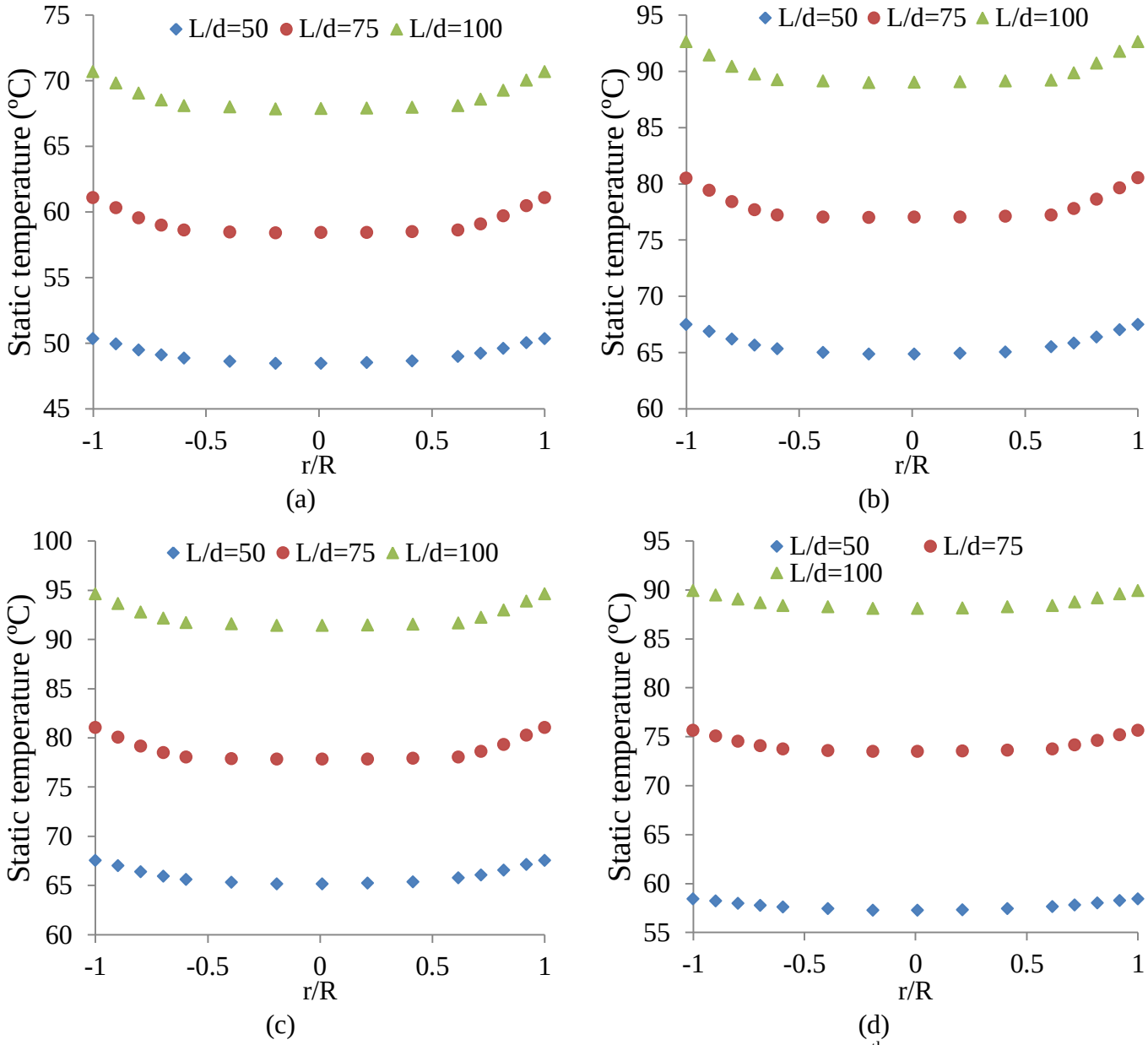

Figure 5-26 Static temperature variations within the middle riser pipe on 15th March for different L/d ratio of riser pipe under thermal weekday loading for (a) 10 O'clock (b) 12 O'clock (c) 14 O'clock and (d) 16 O'clock

Based on aforementioned analysis of effect of L/d ratio of riser pipe on various parameters can be denoted as follows:

Table 5-5 The effect of the length to diameter ratio of the riser pipe on various parameters

L/d		50	75	100
Water Temperature within the storage tank (^{o}C)	Value	26	30.33	34.6
	Percentage difference (%)	16.6	14.0	
Mass flow rate within thermo-syphon loop (kg/s)	Value	0.00339	0.00414	0.00486
	Percentage difference (%)	22.1	17.3	
Wall shear stress (Pa)	Value	0.00873	0.01019	0.01133
	Percentage difference (%)	16.7	11.1	
Heat transfer coefficient of working fluid (W/m^2.^{o}C)	Value	42.63	44.75	46.31
	Percentage difference (%)	4.9	3.4	

By studying the Table 5-5, it can be concluded that the L/d ratio of the riser pipes has significant impact on the performance of a closed loop thermo-syphon system. This can be clearly seen as a 16.6% increase in water temperature was recorded as the L/d ratio of the riser pipes was increased from 50 to 75. However, when the L/d ratio of the riser pipes were increased from 75 to 100 the water temperature increased only by 14.0%. This trend is similar for the other parameters such as mass flow rate, the wall shear stress and the heat transfer coefficient. It can be seen that the L/d ratio of 100 provides the best performance among the other configuration. Therefore, L/d (length to diameter ratio) of 100 will be chosen for next investigations.

5.6. Effect of Heat Flux

To study the effect of heat fluxes on the thermal performance of thermo-syphon, three values of heat flux corresponding to 15th March, 15th June and 15th September have been used in the present study. The reason behind choosing these values are, they represent the different seasons in the year and hence it can simulate the real world operating condition. The analysed thermo-syphon model consists of five riser pipes with an L/d (length to diameter ratio) of 100 at an inclination angle of 53º. This configuration is chosen based upon the conclusion of the previous sections. In the previous sections, it was concluded that the length to diameter ratio has more significant impact on the performance of the thermo syphon. Since the scope of the study considers only three L/d values, henceforth the highest L/d value (100) has been considered for further investigation, in the following chapters. Moreover, another conclusion was that the numbers of riser pipes have a small effect on the storage tank temperature. Henceforth, to reduce the computation time and complexity of the geometry, five riser pipes have been chosen. The thermal loading used in this particular case represents a weekday as this provides a more general background for the use of hot water consumption.

Figure 5-27 depicts static temperature distribution within the cross-section of the storage tank and the condenser for the three days of the year considered in the present study at middle day (12 O'clock). The corresponding thermal loading condition that has been specified is that of the

weekday. It can be further noticed that the temperature within the storage tank and the condenser are highest on 15th June as compared to 15th March and 15th September. The average temperature of working fluid within the condenser for 15th March 15th June and 15th September is 76.48ºC, 84.47ºC and 68.74ºC respectively. While the average temperature of water within the storage tank for 15th March, 15th June and 15th September is 34.60ºC, 37.92ºC and 31.76ºC respectively. This means that the working fluid's temperature increases significantly on the days when the heat flux input to the thermo-syphon is higher. It is evident that more heat flux provided to the riser pipes heats up the working fluid further.

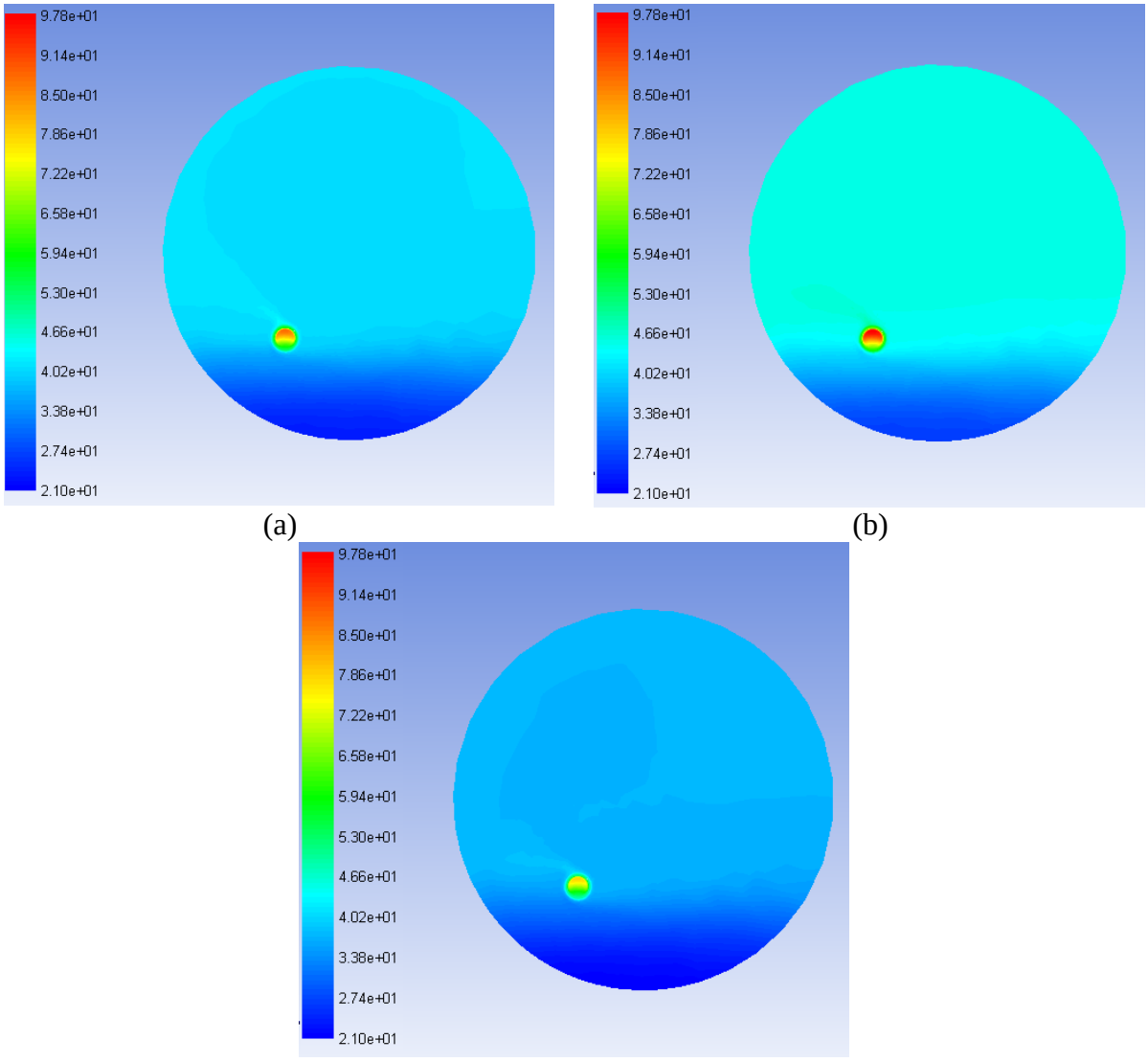

Figure 5-27 Static ttemperature distributions within the storage water tank and the condenser for (a) 15th March (b) 15th June (c) 15th September under thermal weekday loading

Figure 5-28 depicts the variation in working fluid's temperature within the storage water tank for variable amount of heat flux provided to the riser pipes. It can be seen clearly that the temperature within the storage water tank is higher at a heat flux corresponding to 15th Jun as compared to heat flux of other days (15th March, 15th September). This observation indicates that the tank temperature increases significantly during the summer as compared to the winter. It is obvious from the fact that more heat flux provided to the riser pipes heats up the working fluid further. Furthermore, it can be noticed that the final tank temperature around 57.10ºC, 50.21ºC and 47.60ºC with the days of 15th Jun, 15th March, 15th September respectively.

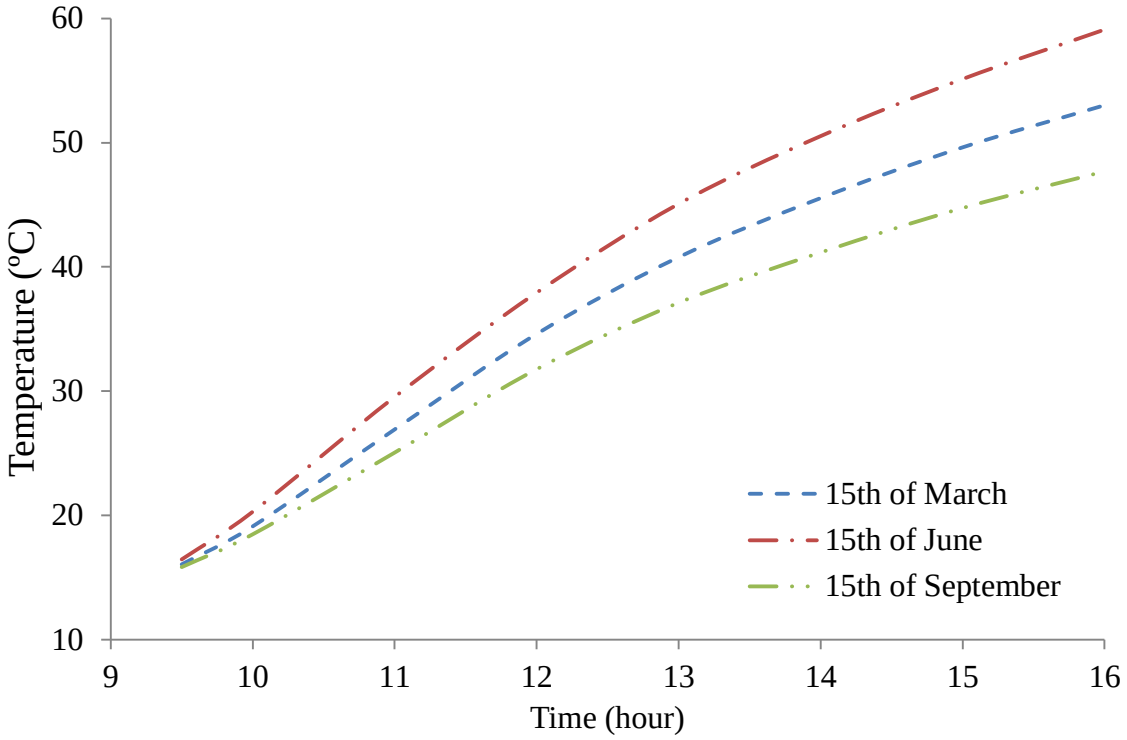

Figure 5-28 Temperature variations within the storage tank for various heat fluxes under thermal weekday loading

Figure 5-29 depicts the variation in working fluid's temperature within the condenser for variable amount of heat flux, which is picked up by riser pipes. It can be seen that the temperature within the condenser is higher at a heat flux corresponding to 15th Jun as compared to heat flux of other days (15th March, 15th September). The maximum temperature of working fluid within the condenser was 89.86ºC, 79.47ºC and 70.73ºC for 15th of June, 15th March and 15th September respectively. Hence, an increase in the amount of a heat flux increases the temperature of the working fluid within the condenser.

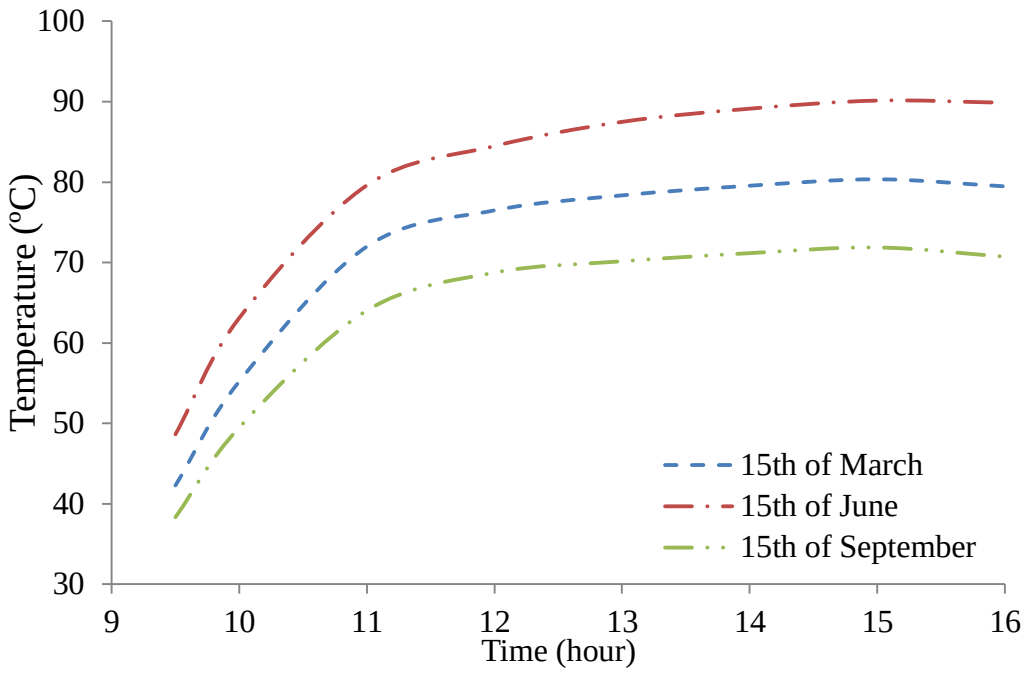

Figure 5-29 Temperature variations within the condenser for various heat fluxes under thermal weekday loading

Figure 5-30 depicts the variation in mass flow rate of working fluid within the thermo-syphon for variable heat flux under the thermal loading condition of weekday that has been considered in present study. This mass flow rate measured at a cross section of upriser before the condenser. It can be seen clearly that the increasing in solar heat flux leads to increase in the mass flow rate within the system because it increases the amount of heat, which is received by the working fluid within the thermo-syphon. The maximum mass flow rate for all cases of solar heat flux has been achieved at local solar noon as follows, 0.00512kg/s, 0.00480kg/s and 0.00451kg/s for days of 15th Jun, 15th March, and 15th September respectively.

Figure 5-31 depicts wall shear stress variations within thermosyphon loop for variable amount of heat flux under thermal loading condition of the weekday. It can be clearly seen that the wall shear stress is higher for June as compared to March and September. The maximum average wall shear stress was 0.01147Pa, 0.01242Pa and 0.01054Pa for 15th March, 15th June and 15th September respectively. This observation indicates that, increasing amount of heat flux will lead to an increase in the velocity of working fluid within the thermo-syphon and as the velocity increases, the wall shear stress starts to increase as well.

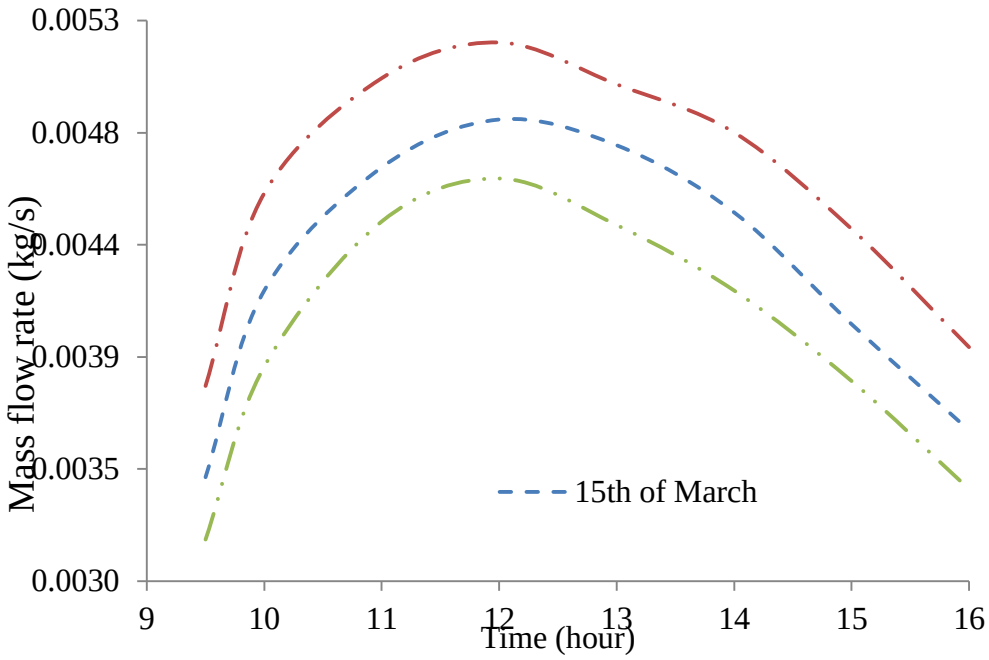

Figure 5-30 Circulating mass flow rate of the working fluid for various heat fluxes under thermal weekday loading

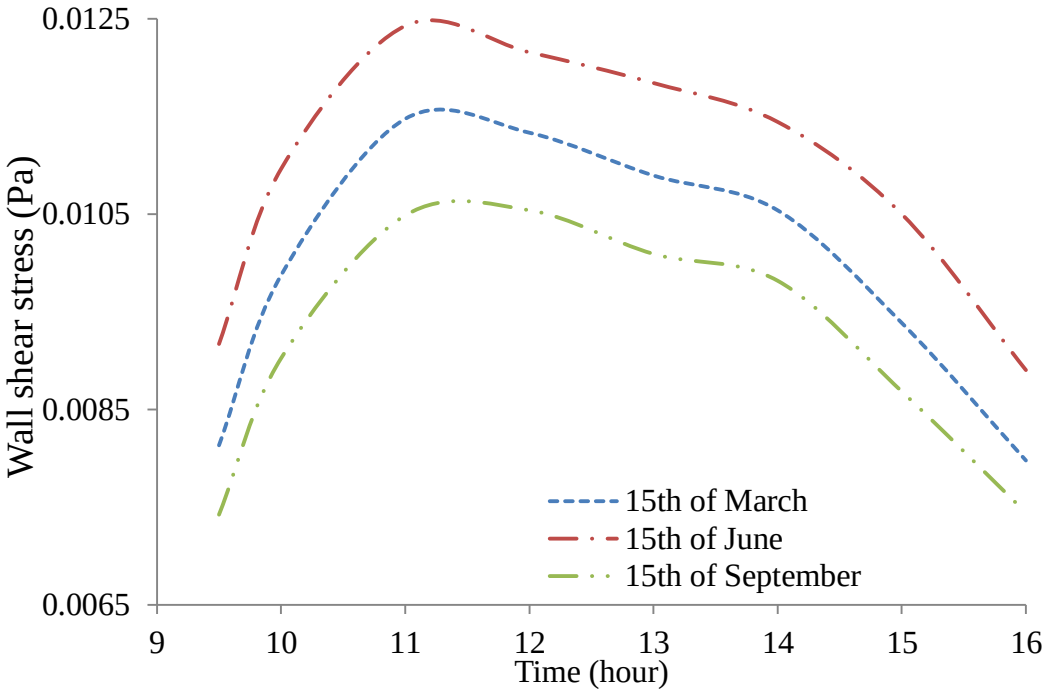

Figure 5-31 Wall shear stress variations within thermo-syphon loop for various heat fluxes under thermal weekday loading

Figure 5-32 depicts the variations of heat transfer coefficient within the thermo-syphon loop for the same conditions as above. It can be clearly seen that the heat transfer coefficient of working fluid is highest on 15th June, as compared to 15th March and 15th September. The maximum value of heat transfer coefficient was 43.47W/m^2.ºC, 47.31W/m^2.ºC and 50.14W/m^2.ºC for 15th September, 15th March and 15th June respectively and happens at midday when the heat flux was maximum. The increase in heat flux input increases the amount heat transfer to working fluid. This increased heat transfer increases the working fluid temperature and hence reduces the temperature difference between the surface and working fluid, leading to an increase in of heat transfer coefficient. Furthermore, it can be seen that the heat transfer coefficient increases, then decreases, depending on the increase and decrease in the heat flux input to thermo-syphon. Similarly, as it was previously mentioned, the amount of heat transfer is proportional to the heat flux and the above discussion represents that the heat transfer coefficient is proportional to the total heat transfer. It can, therefore, be concluded that the heat input has a significant effect on the heat transfer coefficient of working fluid within the thermo-syphon loop.

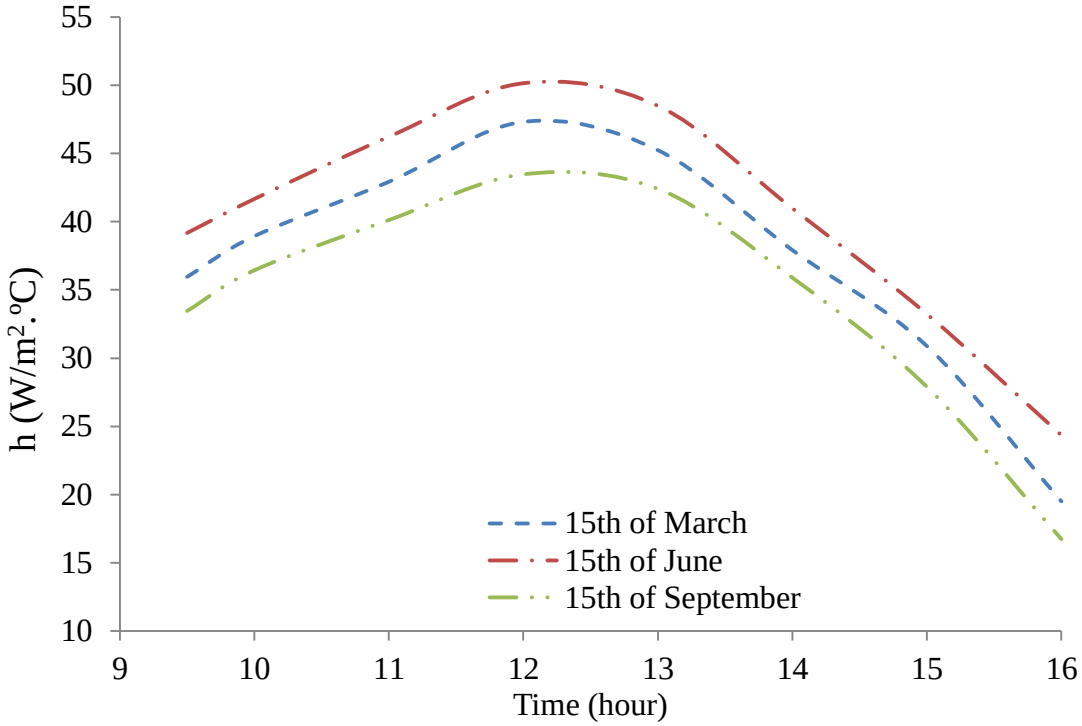

Figure 5-32 Global heat transfer confection for various heat fluxes under thermal weekday loading

Figure 5-33 depicts the flow velocity variations within the cross-section taken along the length of the middle riser pipe, for the three days of the year considered in the present study. The corresponding thermal loading condition that has been specified is that of the weekday. The scale of the contours has been kept constant for effective comparison purposes. It can be clearly seen that the flow velocity is considerably higher at the upper section of the riser pipe. This is because

the hot water rises up in the riser pipe's cross sections, and then propagates towards the upriser. Furthermore, it can be clearly seen that the velocity within the riser pipe is highest on 15th June as compared to 15th March and 15th September. This means that the working fluid's velocity increases significantly on the days when the heat flux input to the thermo-syphon is higher.

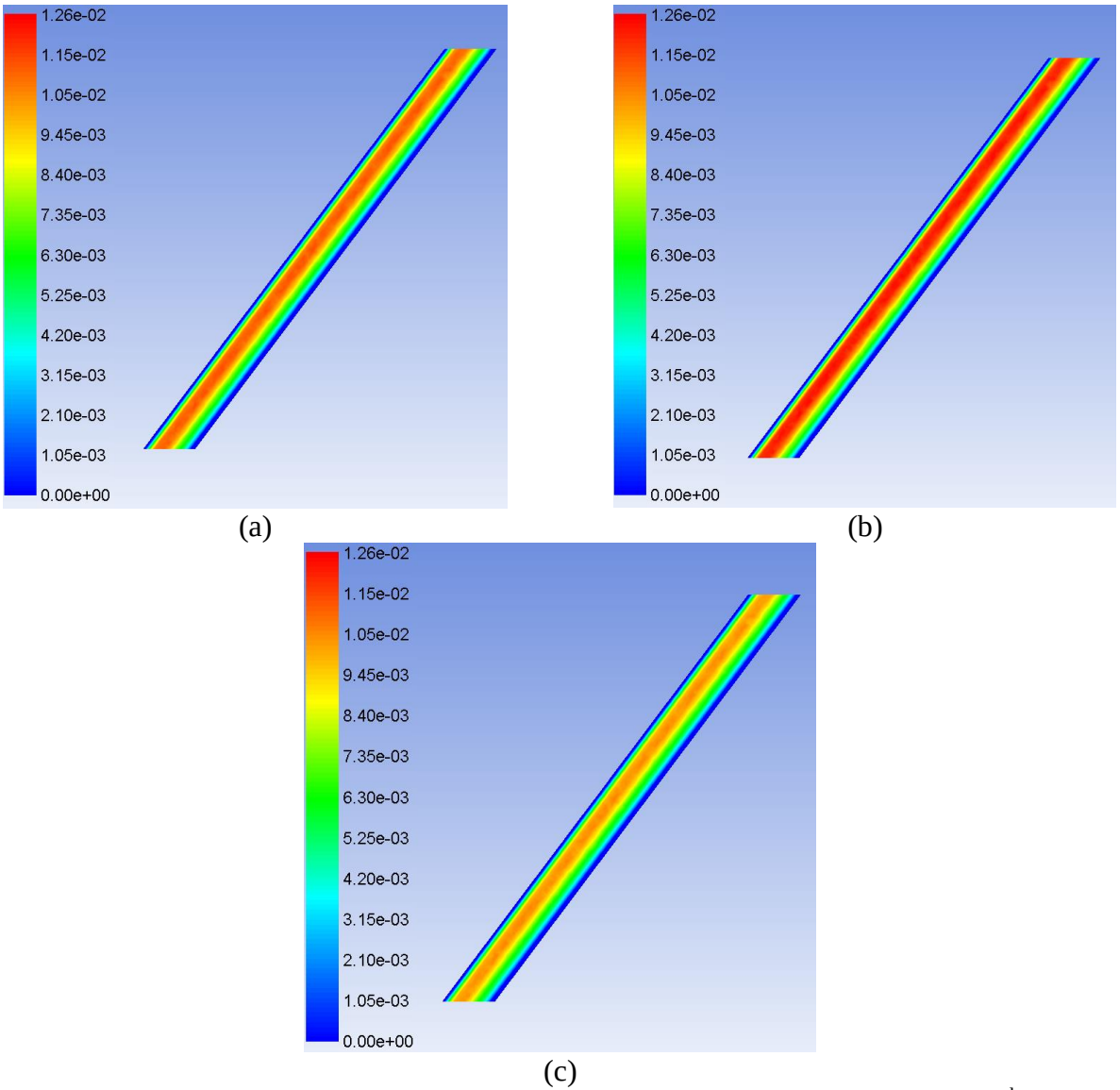

Figure 5-33 Flow velocity variations within the middle riser pipe at midday for (a) 15th March (b) 15th June (c) 15th September under thermal weekday loading

Figure 5-34 depicts the velocity profiles of the working fluid taken at a cross section within the middle riser pipe for the three different days of the year considered in the present study, under working day thermal loading conditions. It can be clearly seen that the velocity of the working fluid is higher at the centre of riser pipe for all cases. Furthermore, increase in heat flux input increases the velocity of working fluid within the riser pipe. It can be further seen that the flow of

the working fluid within the riser pipe is fully developed. It can be concluded that increasing heat input has a significant impact on the velocity of working fluid within the thermo-syphon loop.

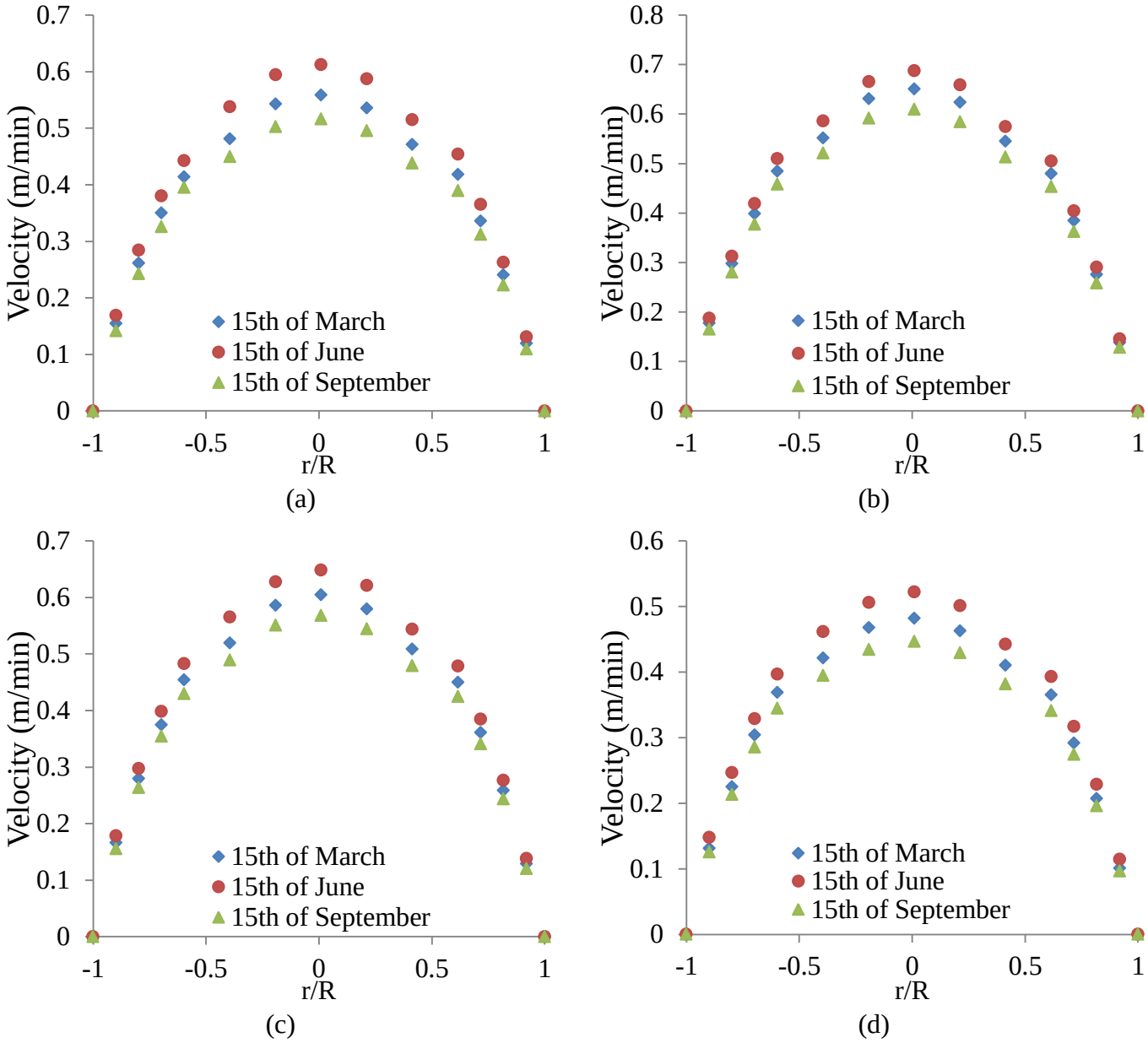

Figure 5-34 Velocity profiles within the middle riser pipe for various heat fluxes under thermal weekday loading for (a) 10 O'clock (b) 12 O'clock (c) 14 O'clock and (d) 16 O'clock

Figure 5-35 depicts static temperature distribution within the cross-section taken along the length of the middle riser pipe for the three days of the year considered in the present study. The corresponding thermal loading condition that has been specified is that of the weekday. It can be clearly seen that the hot water occupies the upper-wall region of the riser pipe, whereas the cold water settles on the bottom of the pipe. This is because the density of the hot water reduces after

absorbing solar energy, which causes it to rise above the more-dense cold water. It can be further noticed that the temperature within the riser pipe is highest on 15th June as compared to 15th March and 15th September. This means that the working fluid's temperature increases significantly on the days when the heat flux input to the thermo-syphon is higher. It is evident that more heat flux provided to the riser pipes heats up the working fluid further.

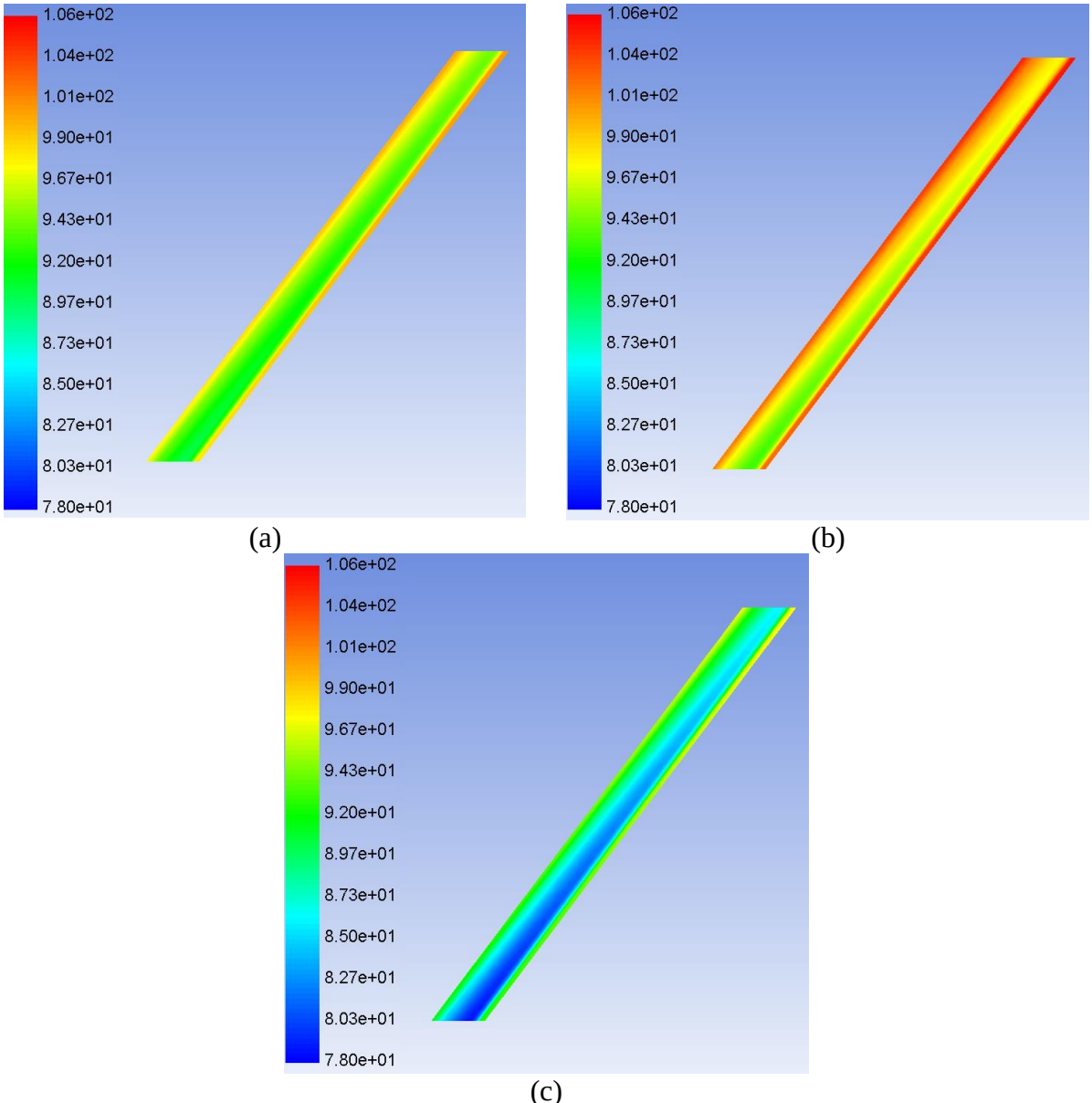

Figure 5-35 Static temperature distributions within the middle riser pipe for (a) 15th March (b) 15th June (c) 15th September under thermal weekday loading

Figure 5-36 depicts the static temperature profiles of the working fluid taken at a cross section within the middle riser pipe. It can be clearly seen that the temperature of working fluid is higher in the near wall regions where the solar heat flux is directly in contact with the riser pipe's wall.

Furthermore, an increase in the heat flux input increases the temperature of the working fluid within the riser pipe. It can be concluded that increasing heat input has a significant impact on the temperature of working fluid within the thermo-syphon loop.

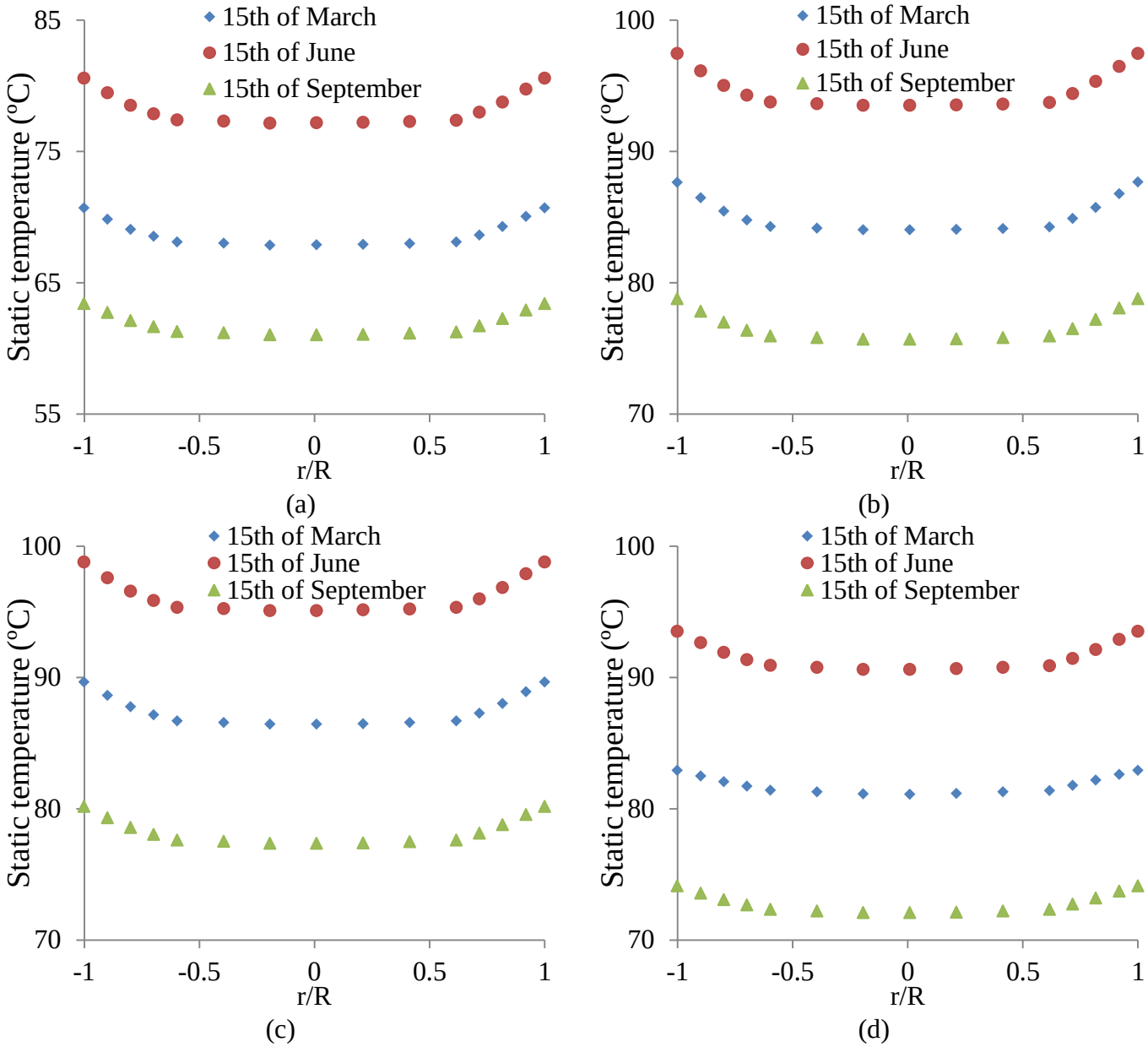

Figure 5-36 Static temperature variations within the middle riser for various heat fluxes under thermal weekday loading for (a) 10 O'clock (b) 12 O'clock (c) 14 O'clock and (d) 16 O'clock

Figure 5-37 depicts the velocity profile of the working fluid within the different riser pipes at a heat flux corresponding to 15th March under thermal loading of the working day. It can be seen clearly that the maximum velocity of working fluid happens in first riser pipe near from return pipe while the minimum velocity happens in fifth riser pipe far away from the return riser pipe.

The average velocity value of working fluid is 0.435m/min, 0.437m/min and 0.502m/min for the left, middle and right riser pipes respectively. This simply means that the average velocity of working fluid decreases with an increase in distance between the riser pipe and the return pipe. The reason behind that is friction, between working fluid and pipe's surface that increases in proportion to length of pipe and opposes the fluid flow. Therefore, fluid tries to flow the less resistant path and escape through the right end pipe with higher velocity. Whereas in the middle riser pipe and the far end pipe (left end pipe) the fluid velocity is comparatively low.

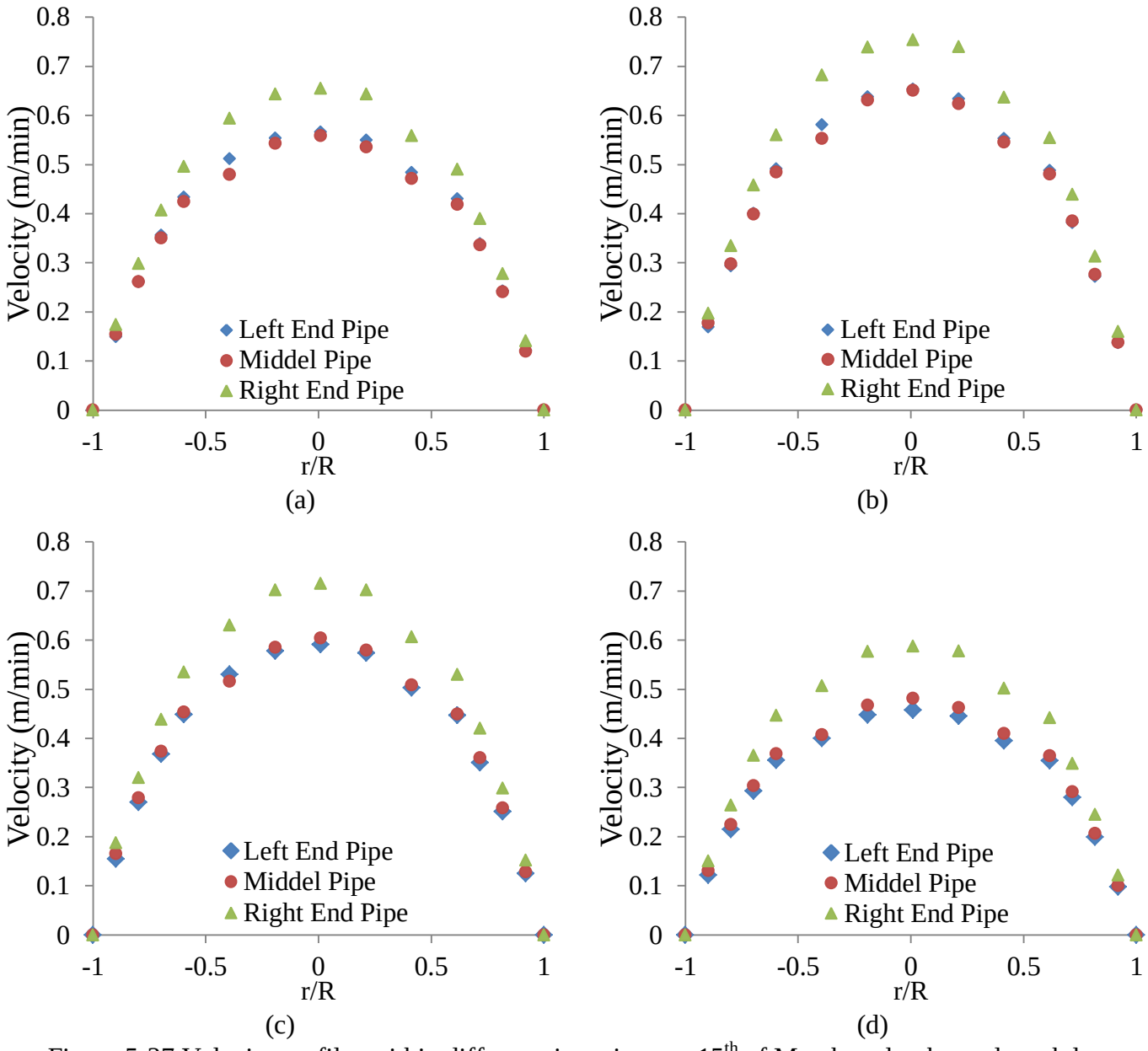

Figure 5-37 Velocity profiles within different riser pipes on 15th of March under thermal weekday loading for (a) 10 O'clock (b) 12 O'clock (c) 14 O'clock and (d) 16 O'clock

Figure 5-38 depicts the static temperature of the working fluid within the different riser pipes at heat flux on the 15th of March under thermal loading of the working day. It can be clearly seen that the minimum temperature of working fluid is attained in fifth riser pipe far away from the return riser pipe. Whilst, the maximum temperature happens in first riser pipe near from return pipe. The average temperature values are 91.39ºC, 93.33ºC and 93.47ºC for left, middle and right riser pipe respectively. This simply means that the temperature of working fluid increases with an increase in distance between the riser pipe and the return pipe.

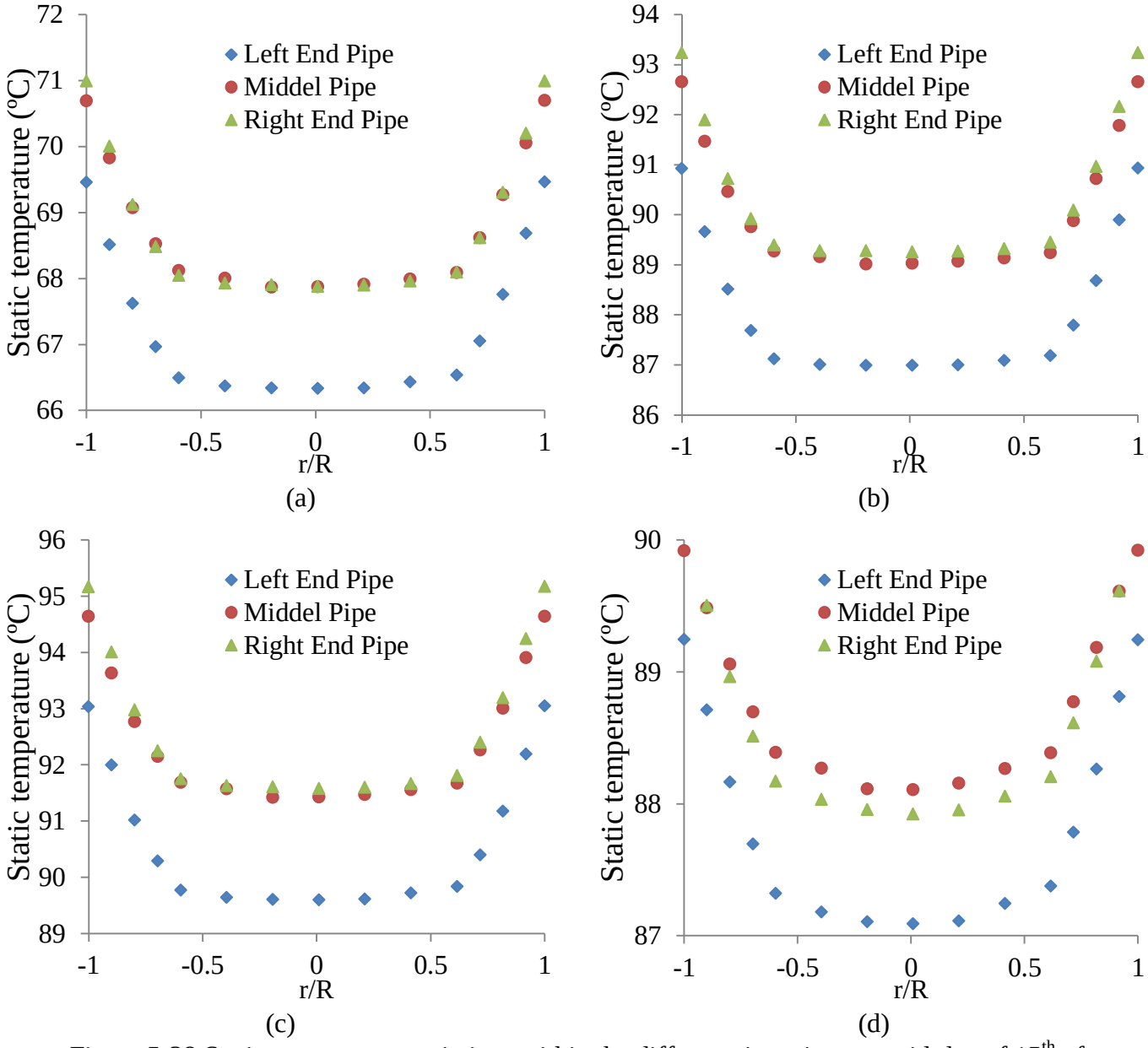

Figure 5-38 Static temperature variations within the different riser pipes on mid-day of 15th of March under thermal weekday loading for (a) 10 O'clock (b) 12 O'clock (c) 14 O'clock and (d) 16 O'clock

Figure 5-39 depicts the velocity profile of working fluid within the middle riser pipe on 15th March under thermal loading. Three locations have been chosen to identify the velocity profile within the middle riser pipe at different time. The location of profile is denoted by Y, which is measured from the riser pipe entrance. It can be clearly seen that the velocity of working fluid within the riser pipe is fully developed for all lengths of riser pipe; this simply mean that the velocity of working is approximately constant throughout the riser pipe. Furthermore, the maximum velocity is attained at the centre of riser pipe while the minimum near the wall.

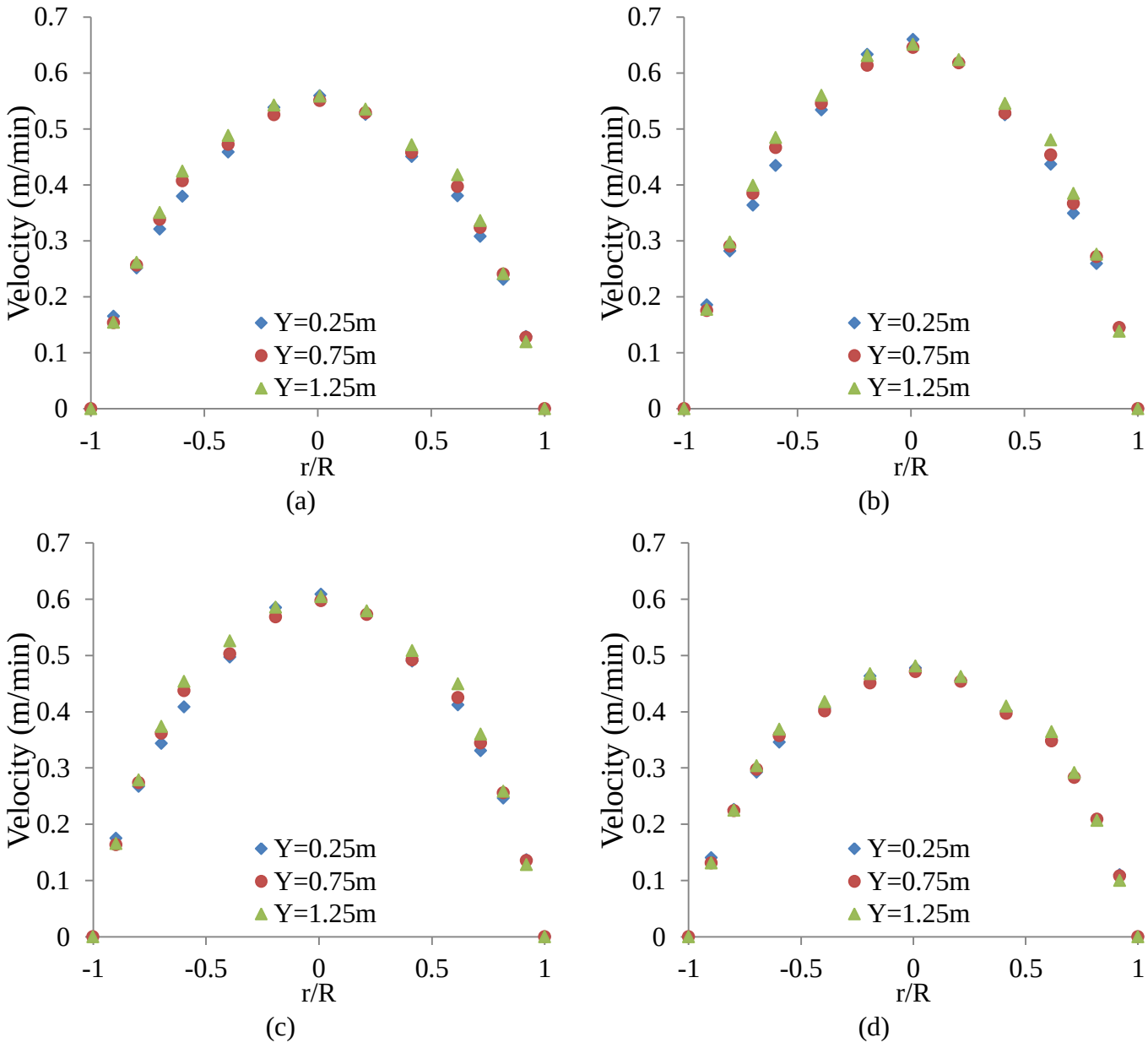

Figure 5-39 Velocity profiles within the middle riser pipe at different crossection of riser pipe on 15th March under thermal weekday loading for (a) 10 O'clock (b) 12 O'clock (c) 14 O'clock and (d) 16 O'clock

Figure 5-40 depicts the static temperature of the working fluid within the middle riser pipe at heat flux on the 15th March under thermal loading of the working day. The location of profile is denoted by Y, which is measured from the riser pipe entrance. It can be clearly seen that the temperature of the working fluid within the riser pipe increase across the length of the riser pipe. Furthermore, the maximum temperature is attained in the region near the wall, while the minimum temperature happens in the centre of the riser pipe.

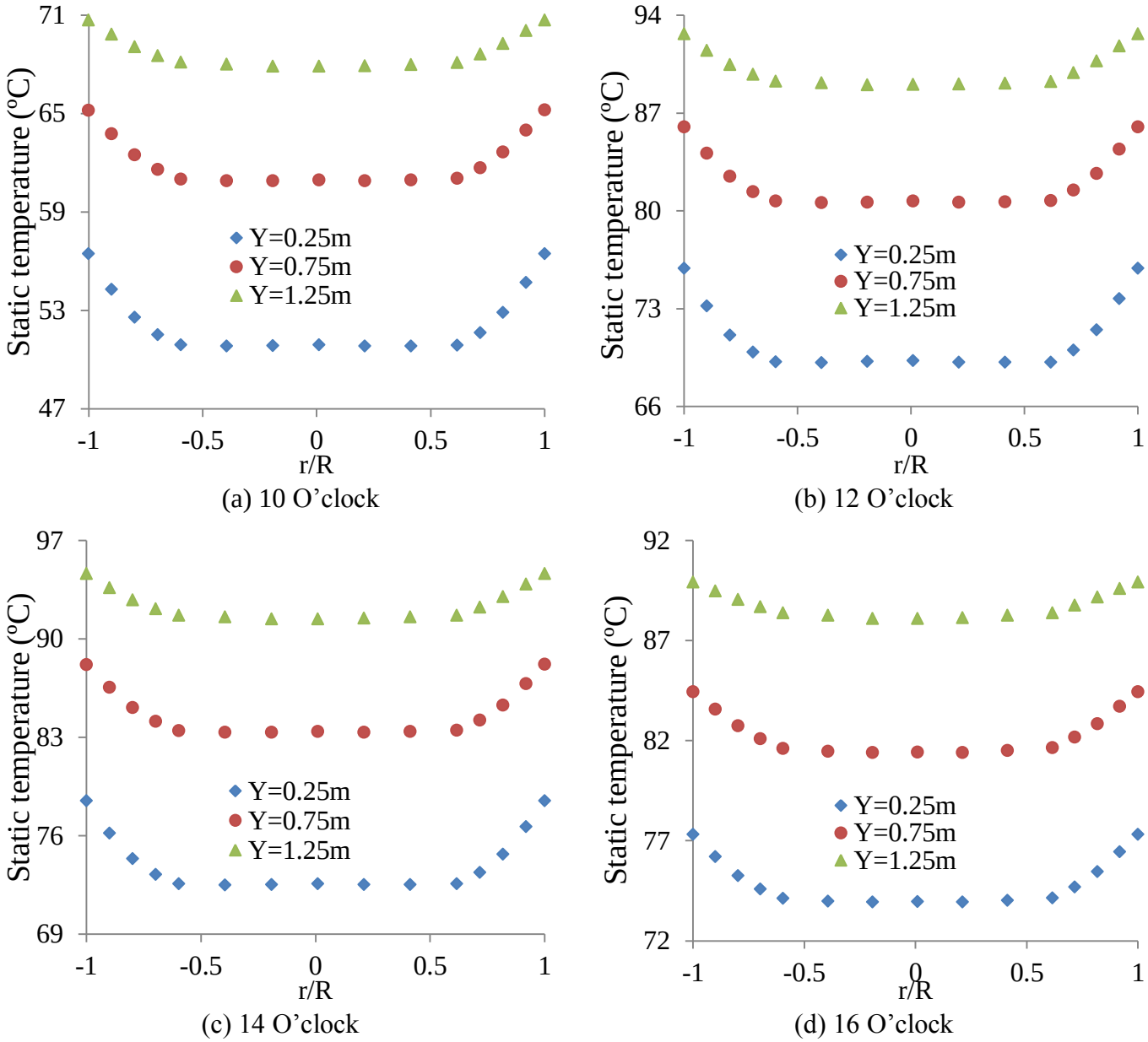

(a) 10 O'clock (b) 12 O'clock

(c) 14 O'clock (d) 16 O'clock

Figure 5-40 Static temperature variations within the middle riser pipe at different crossection of riser pipe on 15th March under thermal weekday loading for (a) 10 O'clock (b) 12 O'clock (c) 14 O'clock and (d) 16 O'clock

Figure 5-41 depicts the velocity profile of working fluid within the middle riser pipe at different hours during a day under thermal loading of the working day. It can be seen that the velocity of working fluid increases, then decreases, depending on the increase and decrease in the heat flux input to the thermo-syphon. The average velocity of working fluid within the riser pipe is 0.39m/min, 0.44m/min, 0.45m/min, 0.43m/min, 0.42m/min, 0.37m/min and 0.33m/min at 10, 11, 12, 13, 14, 15 and 16 O'clock respectively. It is clear that the maximum velocity occurs at midday when the heat flux is maximum and the minimum velocity happen at the end of the day. This simply means that the velocity of working fluid increases significantly with an increase in the heat input. Furthermore, the maximum velocity is attained in the centre of riser pipe while the minimum near the wall.

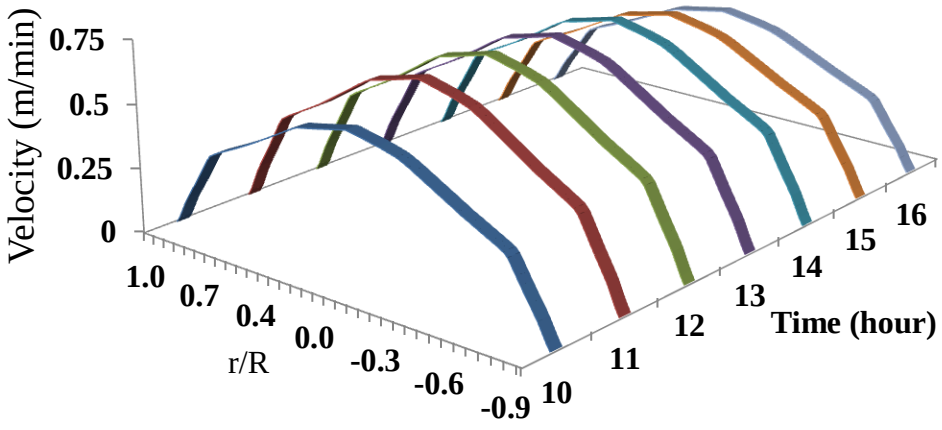

Figure 5-41 Velocity profiles within the middle riser pipe on different hours (heat input) of the day on 15th March under thermal weekday loading

Figure 5-42 depicts the static temperature of the working fluid within the middle riser pipe at different hours during a day under thermal loading of the working day. It can be seen that the temperature of working fluid increases, then decreases, depending on the increase and decrease in the heat flux input to the thermo-syphon. The average temperature of working fluid within the riser pipe increases from an initial temperature (15ºC) to 69.30ºC at 10 O'clock then it increases slightly until it reaches the maximum temperature of 93.59ºC at 14 O'clock after that it starts to decrease slightly until it reaches to 90.49ºC at the end of the day. This simply means that the temperature of working fluid increases significantly with an increase in the heat input. Increase in

the temperature due to increase in heat flux leads to increase in the velocity of working fluid within the riser pipes and it can be noticed that from the interrelation between figure 5-41 and figure 5-42. Moreover, it has been observed that, at the centre of the pipe the temperature is minimum, whereas, near the wall the temperature is maximum.

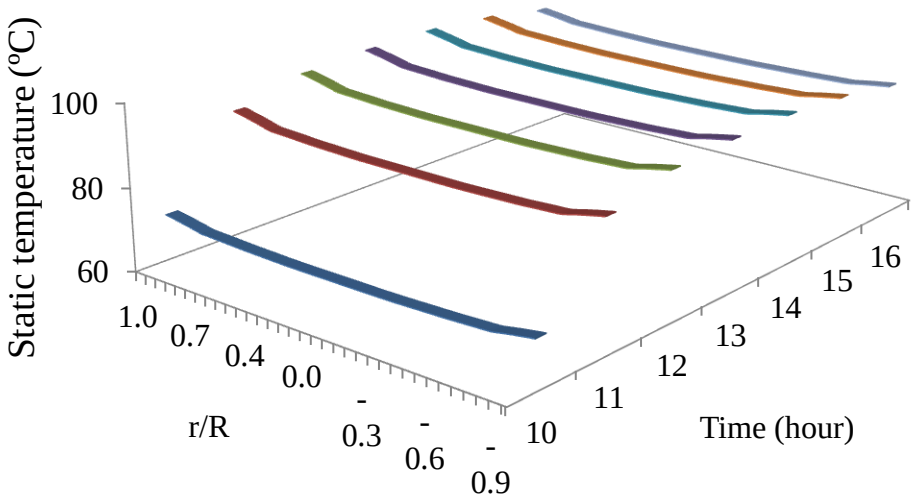

Figure 5-42 Static temperature variations within the middle riser pipe on different hours (heat input) of the day on 15th March under thermal weekday loading

Based on aforementioned analysis of effect of heat flux on various parameters can be summarised as follows:

Table 5-6 The effect of heat fluxes on various parameters

Heat flux		15th September	15th March	15th June
Water Temperature within the storage tank (ºC)	Value	31.76	34.60	37.92
	Percentage difference (%)	9.61	9.57	
Mass flow rate within thermo-syphon loop (kg/s)	Value	0.00454	0.00481	0.00512
	Percentage difference (%)	5.91	6.40	
Wall shear stress (Pa)	Value	0.01054	0.01133	0.01215
	Percentage difference (%)	7.50	7.21	
Heat transfer coefficient of working fluid (W/m^2.ºC)	Value	43.46	47.31	50.14
	Percentage difference (%)	8.82	6.10	

From Table 5-6, it can be concluded that the performance of a closed loop thermo-syphon system is a function of heat flux. This can be clearly seen as a 9.6% increase in water temperature was recorded as heat flux increased during the duration from 15th September to 15th March and, when the heat flux increased within period from 15th March to 15th of June the water temperature increased by 9.57%. This trend is similar for the other parameters such as mass flow rate, the heat transfer coefficient, and the wall shear stress.

5.7. Effect of Thermal Loading

Figure 5-43 depicts the variations in static temperature of the working fluid and water within the cross-section area of the condenser and the storage tank respectively, for the transient thermal loading conditions considered in the present study at mid-point of day (12 O'clock). The corresponding heat flux input of 15th March is used here. It can be noticed that the temperature within the storage tank and the condenser is higher for no loading condition compared to weekday and weekend loading conditions. The maximum working fluid temperature within the condenser for no loading, weekday and weekend loading conditions were recorded to be 94.01ºC, 86.75ºC and 84.85ºC respectively. While the minimum temperature of water within the storage tank for no loading, weekday and weekend loading conditions were 27.84ºC, 23.20ºC and 21.55ºC respectively. Moreover, it has been observed that the weekday and weekend loading condition does not change much (the maximum difference between weekday and weekend thermal loading is about 30W), henceforth the difference in the temperature of the working fluid in the storage tank is insignificant. Furthermore, it can be concluded that the temperature of working fluid and water are affected by thermal loading conditions.

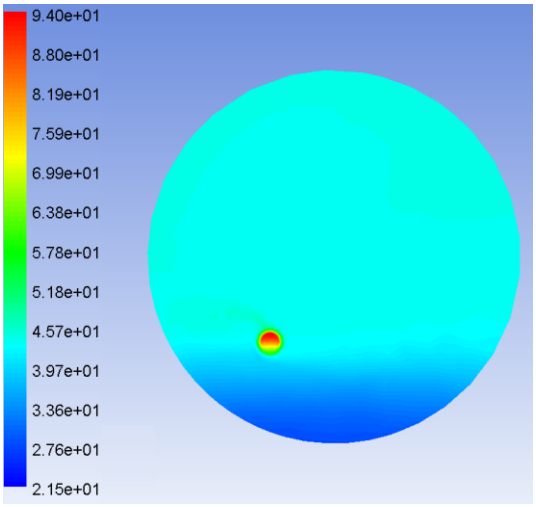

(a)

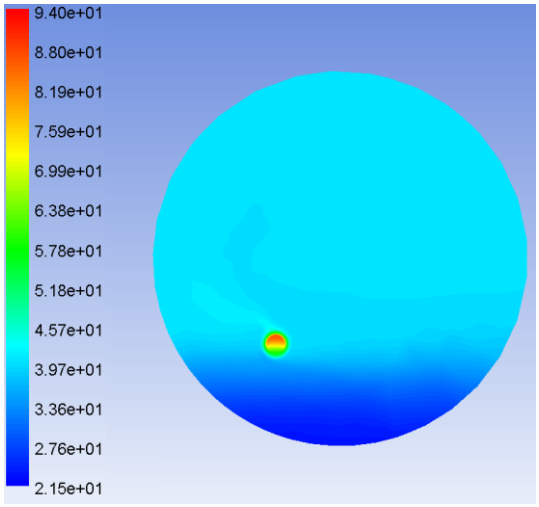

(b)

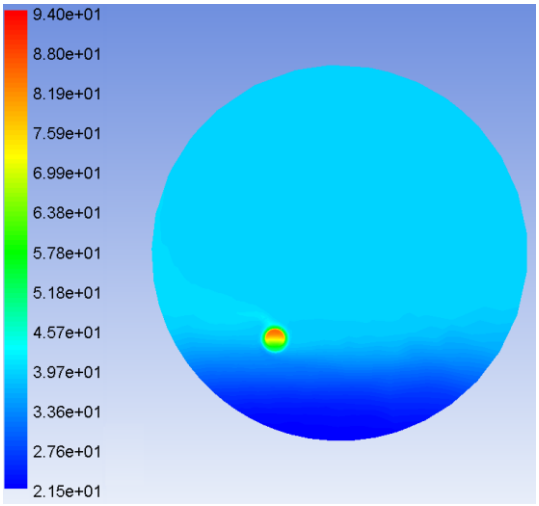

(c)

Figure 5-43 Static ttemperature distributions within the storage tank and the condenser on 15th March under (a) no loading (b) weekday loading and (c) weekend loading

Figure 5-44 depicts the variations in the temperature of water within centre of the storage water tank, for the transient thermal loading conditions considered in the present study on heat flux of 15th March. It can be seen clearly that the temperature within the storage water tank is higher for no loading condition as compared to weekday loading and weekend loading conditions. The temperature of water within the storage tank at end of day for no loading, weekday loading and weekend loading was 60.30ºC, 53ºC and 50.60ºC respectively. Moreover, it has been observed that the static temperature of water is primarily unaffected with the change in thermal loading patterns between weekday loading and weekend loading due to difference between them being quite low (maximum 30W).

Figure 5-45 depicts the variations in the temperature of working fluid within the condenser, for the transient thermal loading conditions considered in the present study at a heat flux corresponding to 15th March. It can be seen clearly that the temperature of working fluid is higher for no loading condition as compared to weekday loading and weekend loading. The maximum temperature within the condenser for no loading, weekday loading and weekend loading was 97.01ºC, 80.35ºC and 77.93ºC respectively. Moreover, it has been observed that the static temperature of working fluid is primarily unaffected with the change in thermal loading patterns between weekday loading and weekend loading due to difference between them being quite low (approximately 30W). Moreover, it can be concluded that an increase in thermal load decreases the temperature of working fluid within the condenser.

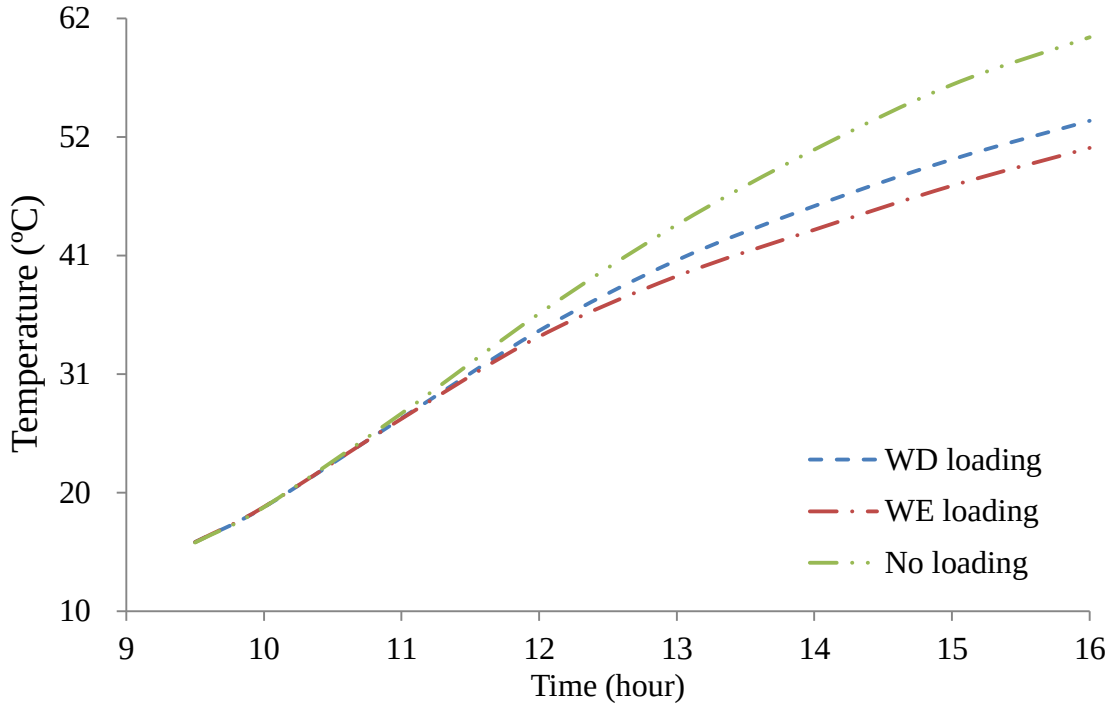

Figure 5-44 Temperature variations within the water storage tank on 15th March under different thermal loading conditions

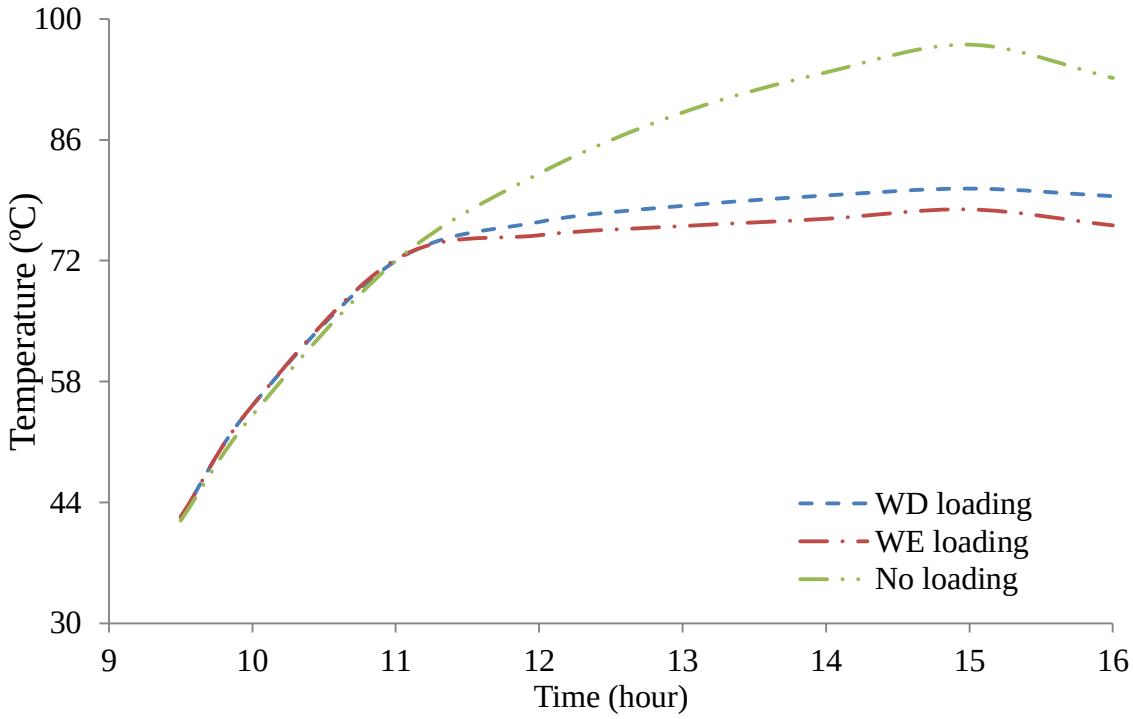

Figure 5-45 Temperature variations within the condenser for various thermal loading conditions on 15th March

Figure 5-46 depicts the variations in mass flow rate of working fluid within the thermo-syphon loop, at a heat flux corresponding to 15th March, for the various thermal loading conditions considered in the present study. It can be seen clearly that the mass flow rate of working fluid is higher for no loading condition as compared to weekday loading and weekend loading. The maximum mass flow rate for no loading, weekday loading and weekend loading was 0.00495kg/s, 0.00481kg/s and 0.00479kg/s respectively. It can be seen clearly that the thermal loading has a small negligible effect on the mass flow rate of working fluid. Furthermore, the mass flow rate of working fluid within the thermo-syphon loop increases and decreases with the increase and decrease in the heat flux input.

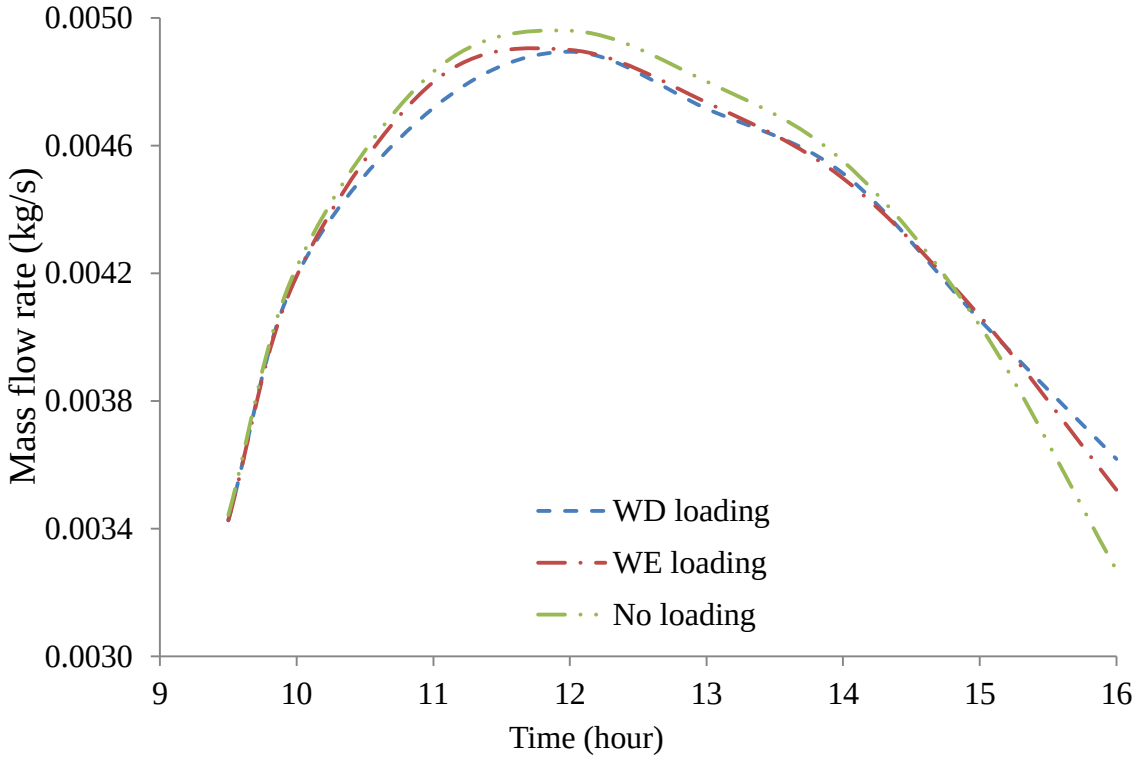

Figure 5-46 Mass flow rate variations of the working fluid within the thermo-syphon loop on 15th March for various thermal loading conditions

Figure 5-47 depicts the variations in heat transfer coefficient of working fluid within the thermo-syphon loop, at a heat flux corresponding to 15th March, for various thermal loading considered in the present study. The heat transfer coefficient depends on the temperature difference between the wall and mean flow. It has been observed that, although the temperature of the wall is high at no loading condition, whereas it (static wall temperature) is comparatively low for weekend and weekday loading condition. However, the temperature difference (ΔT) between the wall and mean flow remains almost same for all the thermal loading conditions. Therefore, the heat transfer coefficient difference among the thermal loading conditions is very small. Never the less, it can be seen that the heat transfer coefficient of working fluid is higher for no loading condition as

compared to weekday loading and weekend loading. Moreover, It can be clearly seen that the heat transfer coefficient within the collector is unaffected by thermal loading due to difference between thermal loading patterns is quite low. Furthermore, it can be identified that the heat transfer coefficient increases and decreases with the increase and decrease in the heat flux input.

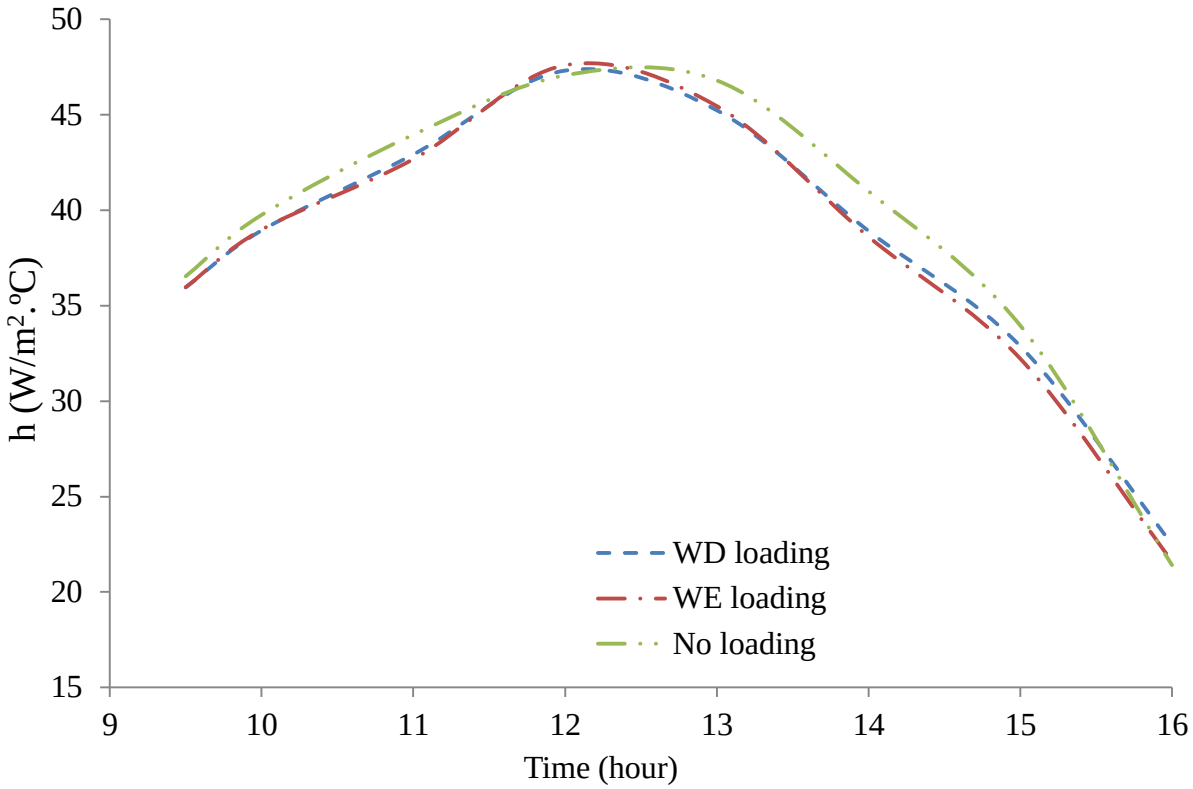

Figure 5-47 Heat transfer coefficient variations within the collector on 15th March for various thermal loading conditions

Figure 5-48 depicts the variation in flow velocity within the cross-section area taken along the length of the middle riser pipe, for the transient thermal loading conditions considered in the present study at middle of the day (12 O'clock). The heat flux input corresponds to 15th March. It can be noticed that the velocity of working fluid is highest for no loading conditions as compared to weekday loading and weekend loading. The average velocity of working fluid for no loading, weekday loading and weekend loading was 0.00487m/s, 0.00473m/s and 0.00478m/s respectively. Moreover, it has been observed that the velocity of working fluid is primarily unaffected with the change in thermal loading patterns between weekday loading and weekend loading since the difference between loading patterns is quite low. Furthermore, it can be concluded that the velocity of working fluid is affected by thermal loading conditions due to aforementioned reasons mentioned for Figure 5-43.

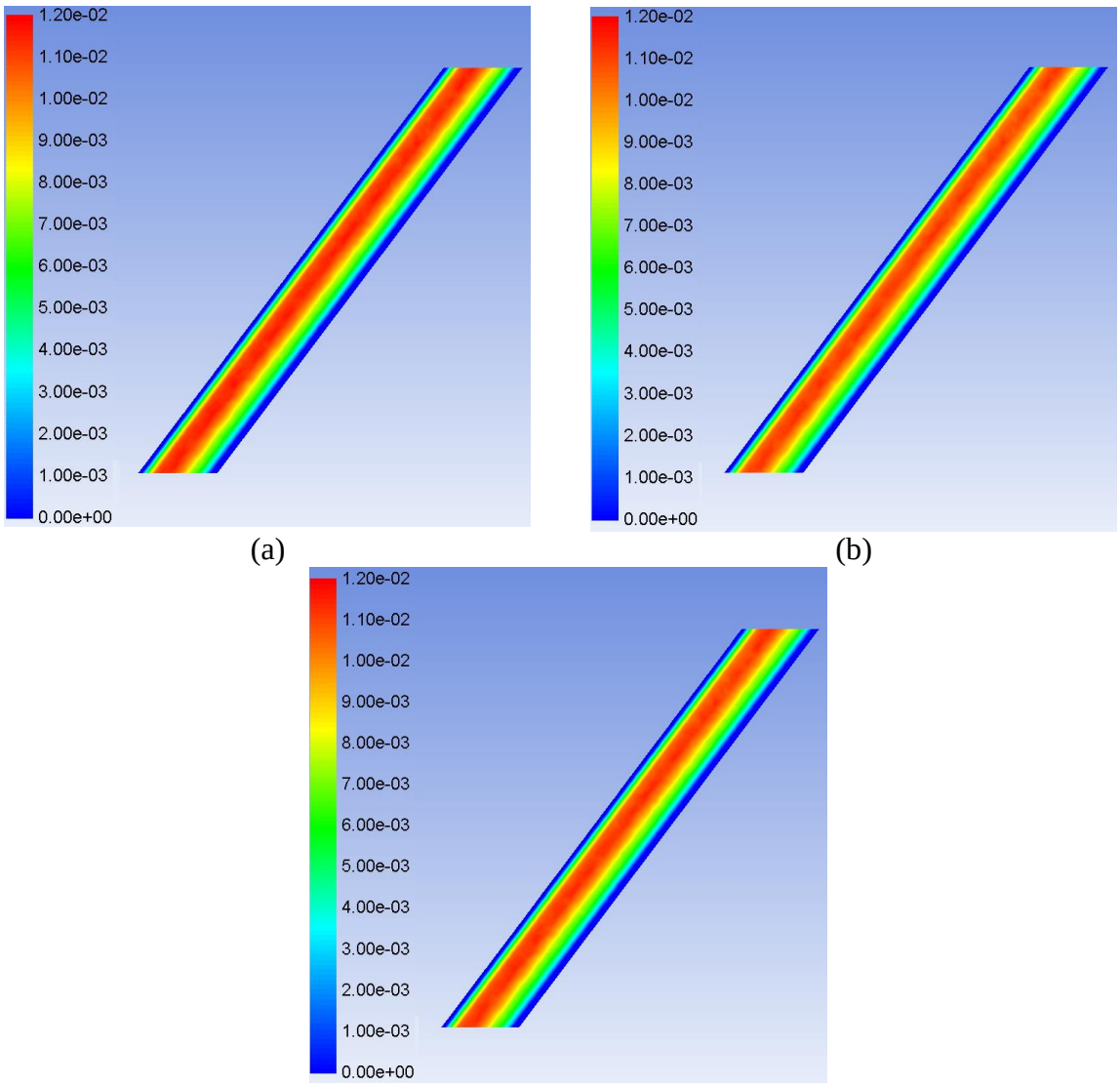

Figure 5-48 Flow velocity variations within the middle riser pipe on 15th March under (a) no loading (b) weekday loading and (c) weekend loading conditions

Figure 5-49 depicts the variation in static temperature of the working fluid within the cross-section area taken along the length of the middle riser pipe, for the transient thermal loading conditions considered in the present study at middle point of the day (12 O'clock). The heat flux input corresponds to 15th March. It can be noticed that the temperature of working fluid is highest for no loading condition as compared to weekday loading and weekend loading. The average temperature of working fluid for no loading, weekday loading and weekend loading was 99.01ºC, 92.95ºC and 90.95ºC respectively. Moreover, it has been observed that the temperature of working fluid is primarily unaffected with the change in thermal loading patterns between weekday loading and weekend loading due to difference between loading patterns is quite low. This is due to the fact that the real-world thermal loading conditions vary only slightly, which results in

insignificant flow variations. Furthermore, it can be concluded that the velocity of working fluid is affected by thermal loading conditions due to aforementioned reasons mentioned for Figure 5-43.

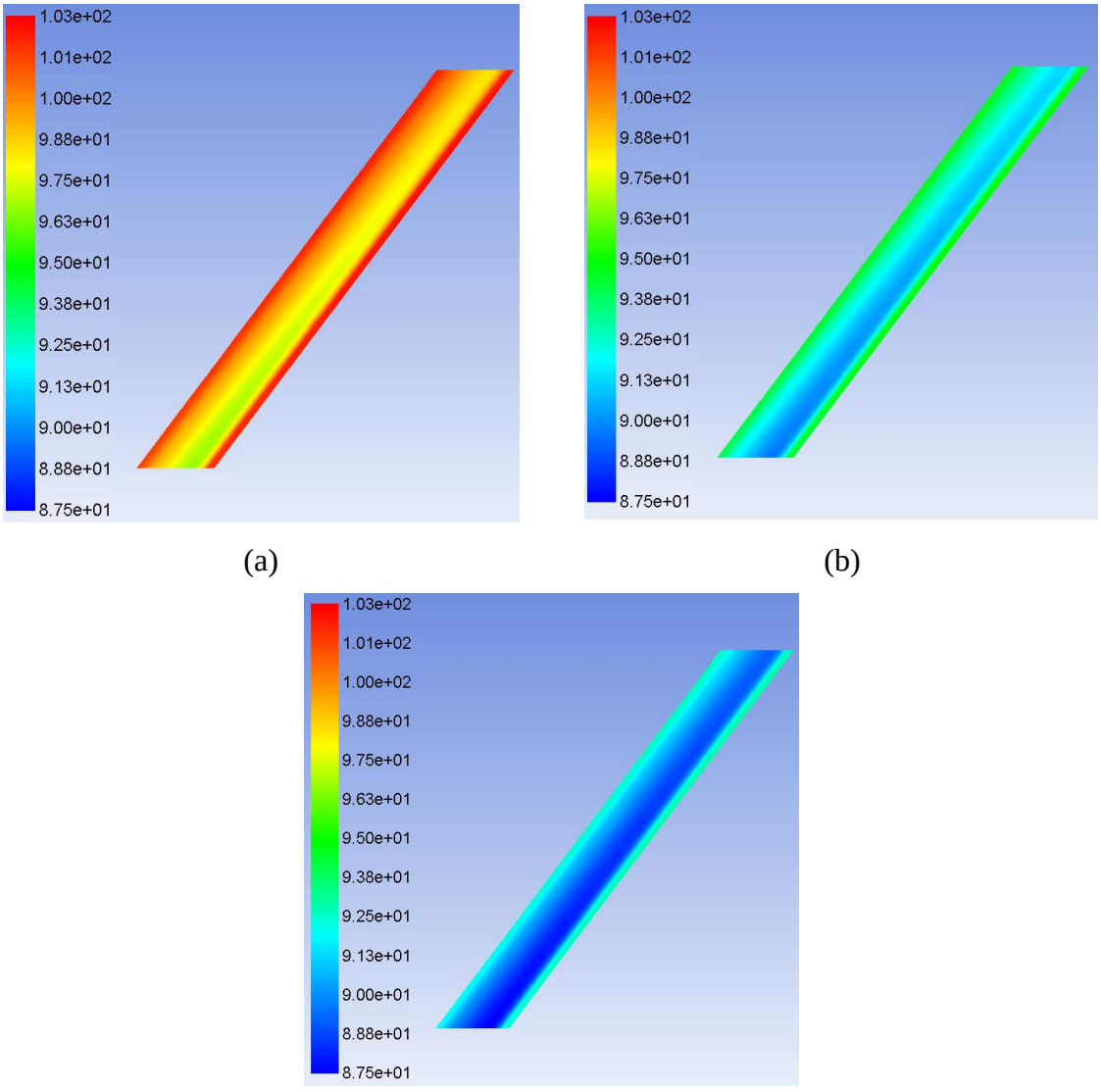

Figure 5-49 Static temperature distributions within the middle riser pipe on 15th March, under (a) no loading (b) weekday loading and (c) weekend loading

Based on aforementioned analysis of effect of thermal loading on various parameters, it can be denoted that thermal loading has significant effect on the storage tank temperature.

5.8. Development of Novel Semi-Empirical Prediction Model

Based on the results, which have been obtained in this chapter, prediction models for the Nusselt number, Reynolds number, collector plate's temperature, and inlet, outlet temperature of working fluid within thermo-syphon loop can be developed. These parameters indicate the thermal performance of the thermo-syphon system. These models will be incorporated in the designing process to ease the thermo-syphon designing process and make it more efficient.
The Nusult number [45] and Reynolds number [47] can be calculated by the following expressions:

$$\mathrm{Nu} = \frac{\mathrm{h\,D}}{\mathrm{k}} \tag{5.2}$$

$$\mathrm{R_e} = \frac{\rho\,\mathrm{V\,D}}{\mu} = \frac{4\dot{m}}{\pi\mu\mathrm{D}} \tag{5.3}$$

According to the literature review, geometrical parameters (the length and number of riser pipes), heat input and loading conditions have a significant impact on the thermal performance of thermo-syphon. So, these parameters have been selected to develop equations that have the ability to provide indications regarding the thermal performance in order to predict the performance of the system. These equations have been developed by using the data that were obtained from CFD simulations carried out in this chapter. These data include the properties of working fluid, mass flow rate of working fluid within thermo-syphon loop, heat flux, and thermal loading.

Some semi-empirical correlations have been developed using multiple variable regression approach for predicting Nussult number, Reynolds number, collector plate's temperature, and inlet, outlet temperature of working fluid as a function of the geometric parameter, heat input variables and different thermal loading, which are discussed in Chapter 3. These prediction models are shown as following.

$$\mathrm{N_u} = \frac{0.136\left(\frac{\mathrm{q}}{\mathrm{q_{max}}}\right)^{0.469}(\mathrm{np})^{0.911}\left(\frac{\mathrm{L}}{\mathrm{d}}\right)^{0.123}\left(\frac{\mathrm{Time_{H.F_{min}}}}{\mathrm{Time_{H.F_{max}}}}\right)^{0.0597}}{\left(1+\frac{\mathrm{TL}}{\mathrm{TL_{avr}}}\right)^{0.0213}} \tag{5.4}$$

$$\mathrm{R_e} = 29.375\left(\frac{\mathrm{q}}{\mathrm{q_{max}}}\right)^{0.233}\left(1+\frac{\mathrm{TL}}{\mathrm{TL_{max}}}\right)^{0.216}(\mathrm{np})^{0.0582}\left(\frac{\mathrm{L}}{\mathrm{d}}\right)^{0.531}\left(\frac{\mathrm{Time_{H.F_{min}}}}{\mathrm{Time_{H.F_{max}}}}\right)^{0.335} \tag{5.5}$$

$$\mathrm{T_{wall}} = \frac{1.839\,(\mathrm{T_{ref}})\left(\frac{\mathrm{q}}{\mathrm{q_{max}}}\right)^{0.0217}}{\left(1+\frac{\mathrm{TL}}{\mathrm{TL_{avr}}}\right)^{0.0184}(\mathrm{np})^{0.0874}\left(\frac{\mathrm{L}}{\mathrm{d}}\right)^{0.0736}\left(\frac{\mathrm{Time_{H.F_{min}}}}{\mathrm{Time_{H.F_{max}}}}\right)^{0.125}} \tag{5.6}$$

$$\frac{T_o - T_i}{T_o - T_{in}} = \frac{0.816\left(\frac{q}{q_{max}}\right)^{0.309}\left(1+\frac{TL}{TL_{avr}}\right)^{0.5091}\left(\frac{Time_{H.F_{min}}}{Time_{H.F_{max}}}\right)^{2.403}}{(np)^{0.0089}\left(\frac{L}{d}\right)^{0.084}} \quad (5.7)$$

$$\frac{T_o + T_i}{T_o + T_{in}} = \frac{1.178(np)^{0.0023}\left(\frac{L}{d}\right)^{0.0255}}{\left(\frac{q}{max}\right)^{0.1316}\left(1+\frac{TL}{TL_{avr}}\right)^{0.3033}\left(\frac{Time_{H.F_{min}}}{Time_{H.F_{max}}}\right)^{1.004}} \quad (5.8)$$

where,

N_u is Nusult number
R_e is Reynolds number
T_{wall} is temperature of plate
q is the heat flux
q_{max} is the maximum heat flux
np is the number of the riser pipes
$\frac{L}{d}$ is the length to diameter ratio of the riser pipe
TL is the thermal loading
TL_{avr} is the average thermal loading
T_i is temperature of working fluid at the inlet of collector
T_o is temperature of working fluid at the outlet of collector
T_{in} is the initial temperature of working fluid
$Time_{H.F_{min}}$ is time, which happens at the minimum incident heat flux
$Time_{H.F_{max}}$ is time, which happens at the maximum incident heat flux

The limitations of the equations above are:

- These equations are applicable only to a closed loop thermo-syphon solar water heating system
- These equations are developed for single-phase thermo-syphon solar water heating system
- These equations are applicable only to passive system

For more details regarding how Eq. (5.4), (5.5), (5.6), (5.7) and (5.8) have been developed, appendix E describes the procedures of the deriving the above mentioned equations.

In the present work, a number of statistical analysis tests have been used to ensure the validity of the regression models. These statistical analysis tests are namely F-value, Durbin-Watson statistic, standard error, t-Test value, Lilliefors test, Chi-square and p-value. A brief description is provided

for each test. Appendix C shows the important features of the considered tests and their significance.

Several statistical tests have been undertaken to justify the usefulness of the developed equations using multiple regression analysis. Table 5-7 shows that the derived equations Nu number, Re number, T_w, T_i and T_o have achieved the acceptable criteria in all the tests. That means the equations can be used with confidence for further applications. As Nusselt number, Reynolds number, collector plate's temperature, and inlet, outlet temperature of working fluid in the thermo-syphon system can be predicted by these equations with reasonable accuracy. Hence, the prediction models presented in this chapter can be used for various heat fluxes, various thermal loading conditions, and a variety of thermo-syphon configuration within the thermo-syphon system. Furthermore, the prediction models developed here can be used directly for designing closed loop thermo-syphon system.

Table 5-7 The proposed statistical tests and thier acceptance criteria

Type of test	Acceptance criteria		Nu	Re	T_{wall}(ºC)	T_i(ºC)	T_o(ºC)
F-value	If (F < F critical) is accepted [108]	F	1.0734	1.1095	1.0295	1.0131	1.1832
		F critical	1.5708	1.5643	1.5643	1.5642	1.5643
Durbin-Watson statistic	Less than 2 is accepted [109]		1.0849	0.9618	1.5601	1.0271	1.2774
Standard error	Regression		0.0377	7.6850	0.0053	0.0231	0.0133
	CFD		0.0364	7.2957	0.0052	0.0229	0.0145
	Percentage error (%)		3.571	5.336	1.923	0.871	8.275
t-Test	Closed to zero [110]		0.0150	0.0332	0.0021	0.0263	0.0292
Lilliefors test	If 0= accepted 1= rejected [111]		0	0	0	0	0
Chi-square	Less than 0.05 is accepted [112]		0.0253	0.0631	0.0564	0.0325	0.0436
P-value	More than Chi-square is accepted [112]		1	1	1	1	1

From the prediction models, it can be seen clearly that the heat flux, number of the riser pipe, L/d ratio and thermal loading have a considerable effect on the Nusselt number, Reynolds number and T_{wall}. Eq. (5.4) demonstrate Nusselt number as a function of geometric parameters (L/d, np), varying heat flux and thermal loading. According to the findings, Nusselt number is proportional to the geometric parameter (L/d, np), varying heat flux and is inversely proportional to the thermal loading. Similarly, according to Eq. (5.5), Reynolds number, is proportional to the geometric parameters (L/d, np), varying heat flux and thermal loading. Moreover, Eq. (5.6), proposes a

proportional relation between the plate temperature with heat flux and inversely proportional to the thermal loading and geometric parameters (L/d, np).

The following section illustrates the accuracy of the developed equations for calculating Nusselt number, Reynolds number of the working fluid and T_w/T_{ref} ratio. To identify the accuracy level of the equations, the calculated data from the equations are ploted against the numerical data from CFD. Figure 5-50, Figure 5-51 and Figure 5-52 depicts the variations in the Nusselt number, Reynolds number of the working fluid and T_w/T_{ref} ratio calculated by the developed equation and that predicted by the CFD. According to the figures, the maximum difference between them is 11% for Reynolds number calculation and most of the points are well below that error margin. In addition, the error margin for Nusselt number of the working fluid and T_w/T_{ref} ratio are 10% and 3% respectively. Therefore, based on this observation it can be concluded that, the developed equations are well capable of predicting Nusselt number, Reynolds number of the working fluid and T_w/T_{ref} ratio with reasonable accuracy.

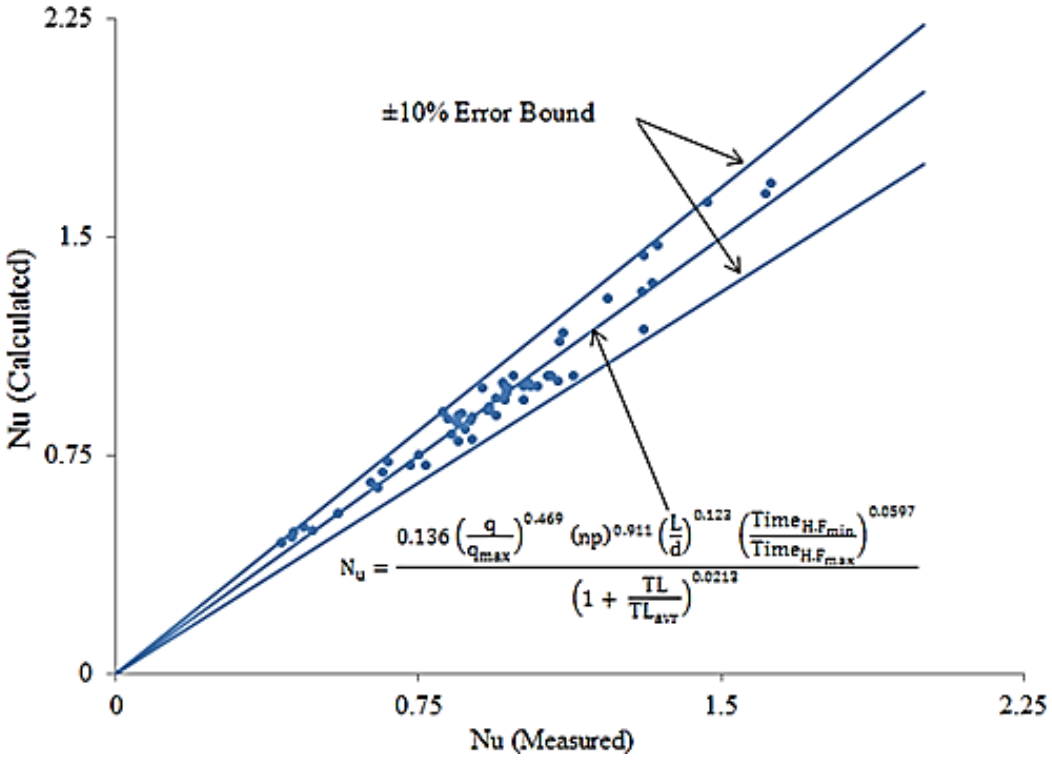

Figure 5-50 Nusselt number variations

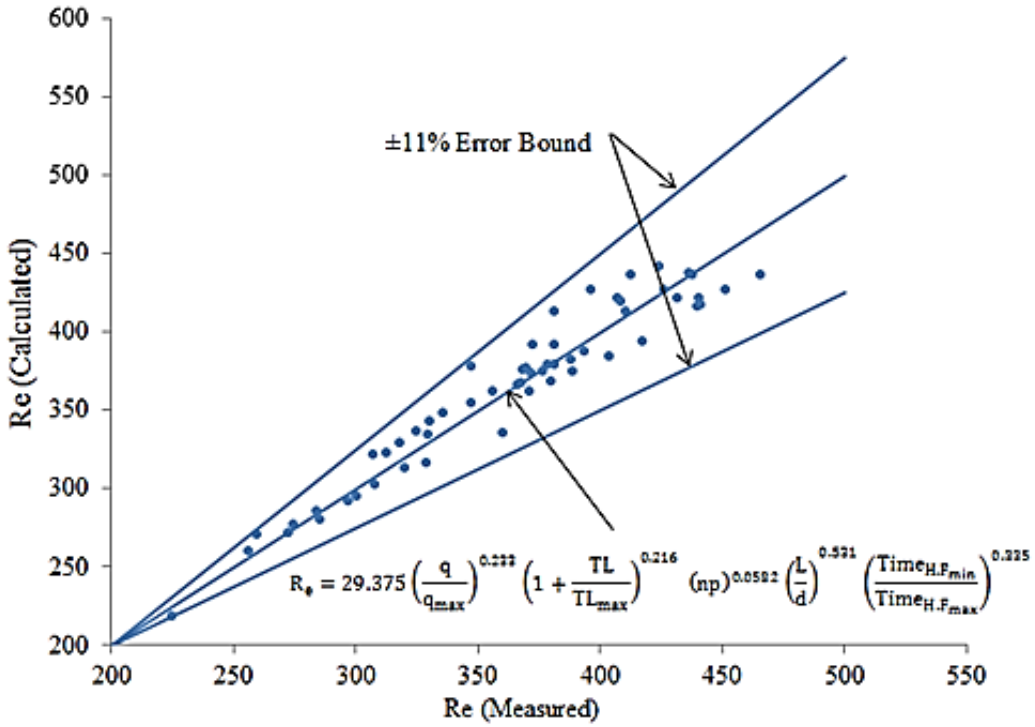

Figure 5-51 Reynolds number variations

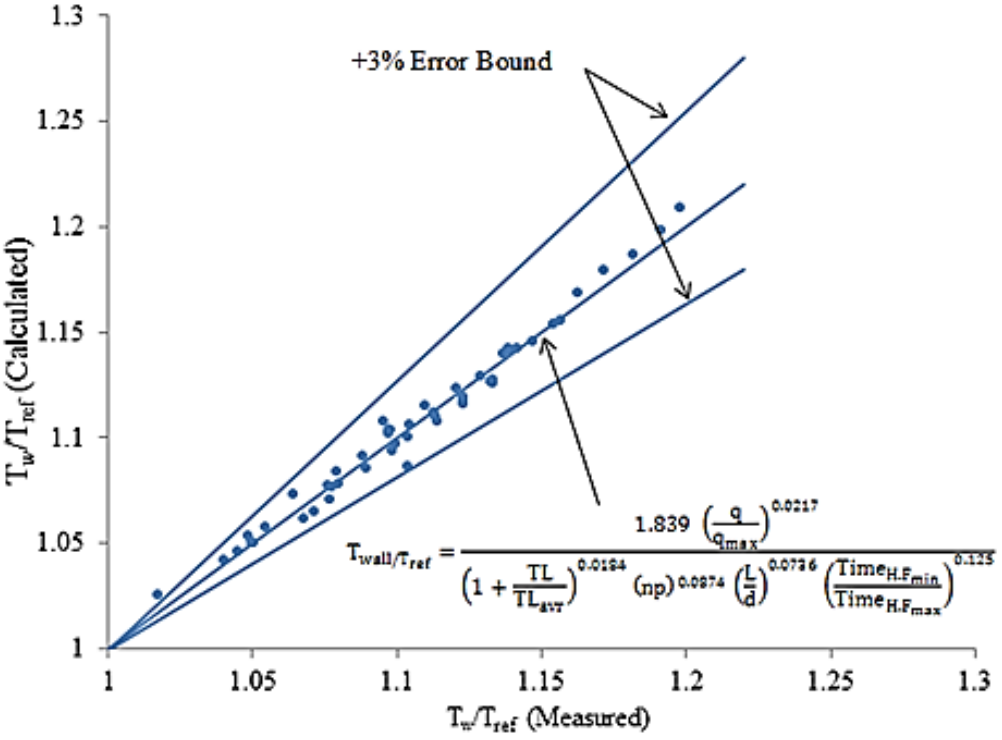

Figure 5-52 Wall temperaure to refrence temperaure ratio variations

5.9. Summary of the Analysis conducted on the Baseline model

Detailed flow behaviour of working fluid within the thermo-syphon system has been revealed in the following results:

- There is a good agreement between experimental results and CFD results. Due to physical models, such as working fluid, model of radiation and Boussinesq approximation approach were not changed and hence the numerical model can be used for further investigation with different configurations
- The mass conservation law has been fulfilled since the sum of the mass flow rates of the working fluid passing through the riser pipes is equal to the mass flow rate of the working fluid through the recirculating pipe. This indicates that there is no recirculation zone in the riser pipe area. Moreover, the assumption of laminar flow has been confirmed, as the calculated Reynolds number is in the laminar zone
- An increase in the number of the riser pipes leads to increase the average velocity of working fluid within the thermo-syphon loop and decrease the wall shear stress within the thermo-syphon loop.
- Moreover, the average velocity of working fluid within the thermo-syphon and wall shear stress increase with increase L/d ratio of the riser pipe
- The thermal loading condition has effect on the thermal performance of thermo-syphon system

This chapter provides information about the natural convection phenomena and behaviour of working fluid within the thermo-syphon loop. In addition, the prediction models have been developed for the Nusselt number, Reynolds number, collector plate's temperature, and inlet, outlet temperature of working fluid, which dictate the design process of the thermo-syphon. Further details regarding the design of the thermo-syphon are presented in Chapter 7. To enhance this performance several models have been used, next chapter provides more details regarding that. The next chapter will provide more details on the results obtained from CFD regarding an enhancement heat transfer within the thermo-syphon loop.

CHAPTER 6

DESIGN MODIFICATIONS

Verification of the numerical model under various operating conditions of the traditional model was carried out in the previous chapter. To obtain the largest amount of solar energy and hence improve the thermal performance of thermo-syphon various models have been developed. This chapter comprises of comparison between various configurations of the riser pipes (traditional, straight, wavy and helical). In addition, an investigation has been conducted, to identify how the amount of working fluid within thermo-syphon loop affects the thermal performance of the system. Moreover, the comparison between new proposed model and baseline model has been conducted based on the experimental results. Furthermore, the manufacturing procedure of this optimum new model has been explained in this chapter.

6.1. Specifications of New Model's Geometry

As it has been mentioned in the previous chapters, one of the focal points of this study is to increase the thermal performance of thermo-syphon solar water system. There are several ways to enhance the amount of heat transfer and hence improve the thermal performance of thermo-syphon. In this study, a technique (modified riser pipe configuration) has been adopted to improve the thermal performance of the system by increasing the surface area to enhance the amount of heat transfer. One of the crucial focal point of this investigation is the amount of working fluid and collector area should remain same for both traditional and proposed model. Therefore, the heat transfer in the system has been improved by increasing the surface area. The increase in the surface area has been achieved by changing the surface of the riser pipe. With this approach, surface area of the riser pipe has been increased by 7.17% with respect to traditional model. In the present study, three thermo-syphon configurations have been developed: comprising of a closed tube within the riser pipes, wavy tube within the riser pipes, and helical tube within the riser pipes as shown in Figure 6-1. These models have been developed to increase the surface area of the riser pipe. The model consists of several inclined riser pipes connected at the top to the upriser and at the bottom to the downcomer. The performance characteristics of the new suggested models are quantified and compared with the traditional baseline model.
The specifications of the straight model are

1- Diameter of a closed pipe is 15mm, 2- Length of a closed pipe is 1170mm

The specifications of the wavy model are

1- Diameter of a closed pipe is 15mm, 2- The wavy pipe angle with the horizontal plane is 10^{o}

The specifications of the helical model are

1- Diameter of coil is 15mm, 2- Number of turns is 55, 3- Pitch is 22.5mm and 4- Diameter pipe is 5mm

Dimensions of the riser pipe for all models are

1- Length is 1.3m, 2- Diameter is (inner 20.2mm) and (outer 22.0mm)

The inner diameter of the condenser is 20.2mm, with thickness of 0.9mm, which is also kept constant for all the models. The whole model is made with a 53º inclination which is the latitude of Huddersfield city.

As mentioned in chapter three these dimensions are considered based on standard dimensions of UK copper pipe. Furthermore, the diameter and thickness for upriser and downcomer were kept constant for all the models. Varying the upriser and downcomer diameter from the riser pipe will increase the amount of losses in the flow such as reducer loss and friction loss (between inner surface and working fluid). The contribution of these losses will reduce the thermal performance of the thermo-syphon loop. In this work, to avoid these losses and for better comparison between the models, upriser and downcomer diameters and thicknesses were kept as same as riser pipe.

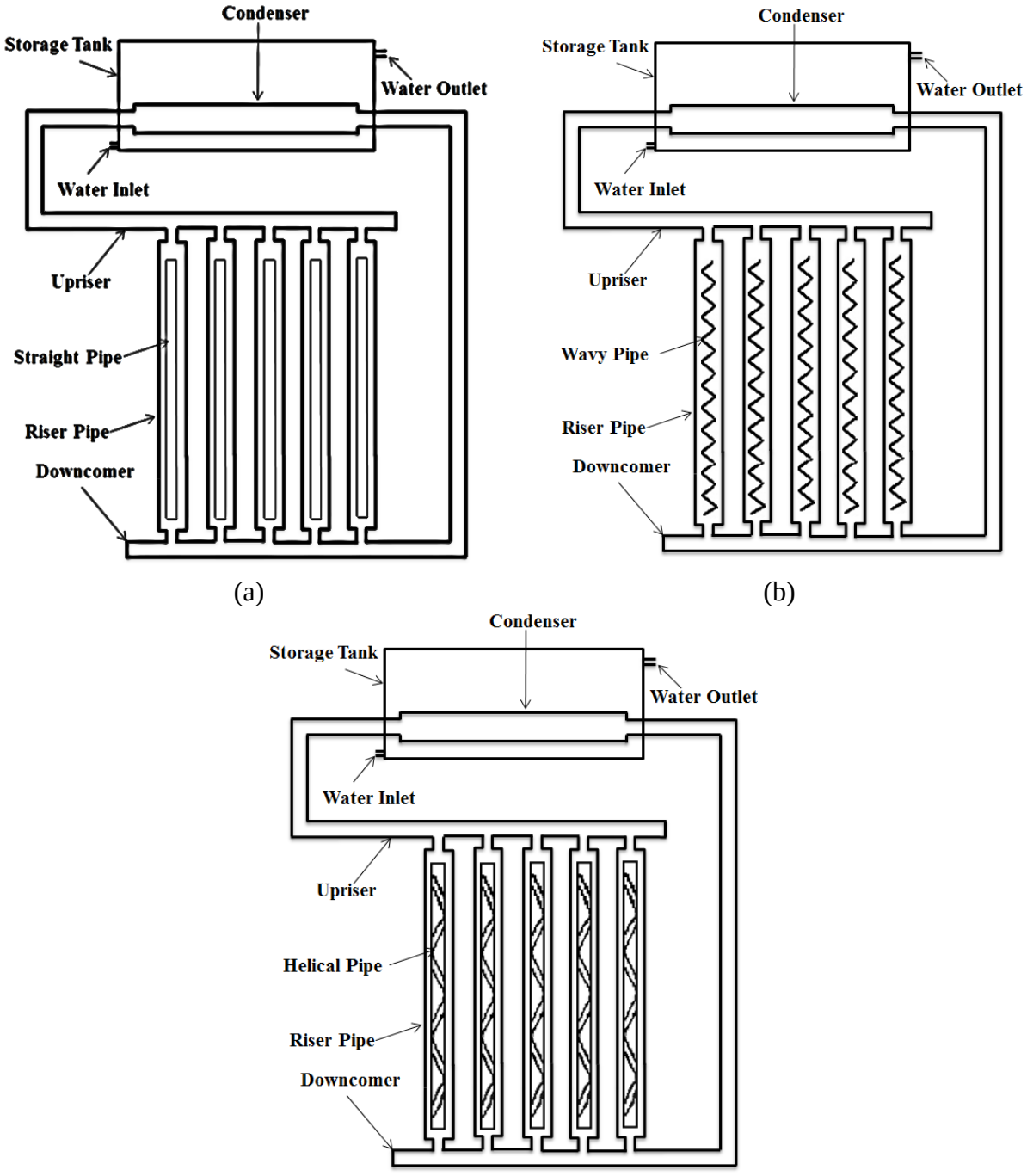

Figure 6-1The geometry of the thermo-syphon (a) new design (closed tube) (b) new design (wavy tube) and (c) new design (helical tube)

6.2. Performance Analysis

In order to depict the natural convection phenomena, the temperature and velocity profile of working fluid within thermo-syphon loop and water within the storage tank for all models, a numerical analysis has been conducted on thermo-syphon. The analysed thermo-syphon model consists of five riser pipes with an L/d (length to diameter ratio) of 100 at an inclination angle of 53º. This configuration is chosen based upon the conclusion of the previous chapter. In the previous chapter, it was concluded that the length to diameter ratio has more significant impact on the thermal performance of the thermo syphon. Since the scope of the study considers only three L/d values, henceforth the highest L/d value (100) has been considered for further investigation, in the following chapters. Moreover, another conclusion from the previous chapter was that the numbers of riser pipes have a small effect on the storage tank temperature. Henceforth, to reduce the computation time and complexity of the geometry, five riser pipes have been chosen. In addition, the inclination angle of 53º has been chosen which represents the latitude of Huddersfield (53.6458°N, 1.7850°W). Furthermore, in order to make the comparison conclusive the amount of the working fluid was kept constant for all models.

Figure 6-2 depicts the velocity distribution of the working fluid within thermo-syphon loop and water within the storage water tank for (a) traditional model, (b) straight model, (c) helical model and (d) wavy model at a heat flux corresponding to15th March under thermal loading condition of weekday. It can be seen clearly that the working fluid attains the highest velocity at the upriser and downcomer for all models. Furthermore, the velocity of working fluid within thermo-syphon loop is higher for traditional model as compared to all new models. The average velocity of working fluid within thermo-syphon loop for traditional, straight, helical and wavy models was 0.0151m/s, 0.0074m/s, 0.0066m/s and 0.0072m/s respectively. This velocity drop in the new model is the result of increment of the inner surface area, which increases the friction between working fluid and inner surface of the riser pipe. It can be evidenced in Figure 6-3 form of measured wall shear stress within thermo-syphon loop.

Figure 6-3 depicts wall shear stress variations within thermosyphon loop for (a) traditional model, (b) straight model, (c) helical model and (d) wavy model at a heat flux corresponding to 15th March under thermal loading condition of weekday. It can be clearly seen that the wall shear stress for traditional model is less as compared to other models. The average wall shear stress for traditional, straight, helical and wavy model was 0.01021Pa, 0.01182Pa, 0.01257Pa and 0.01216Pa respectively.

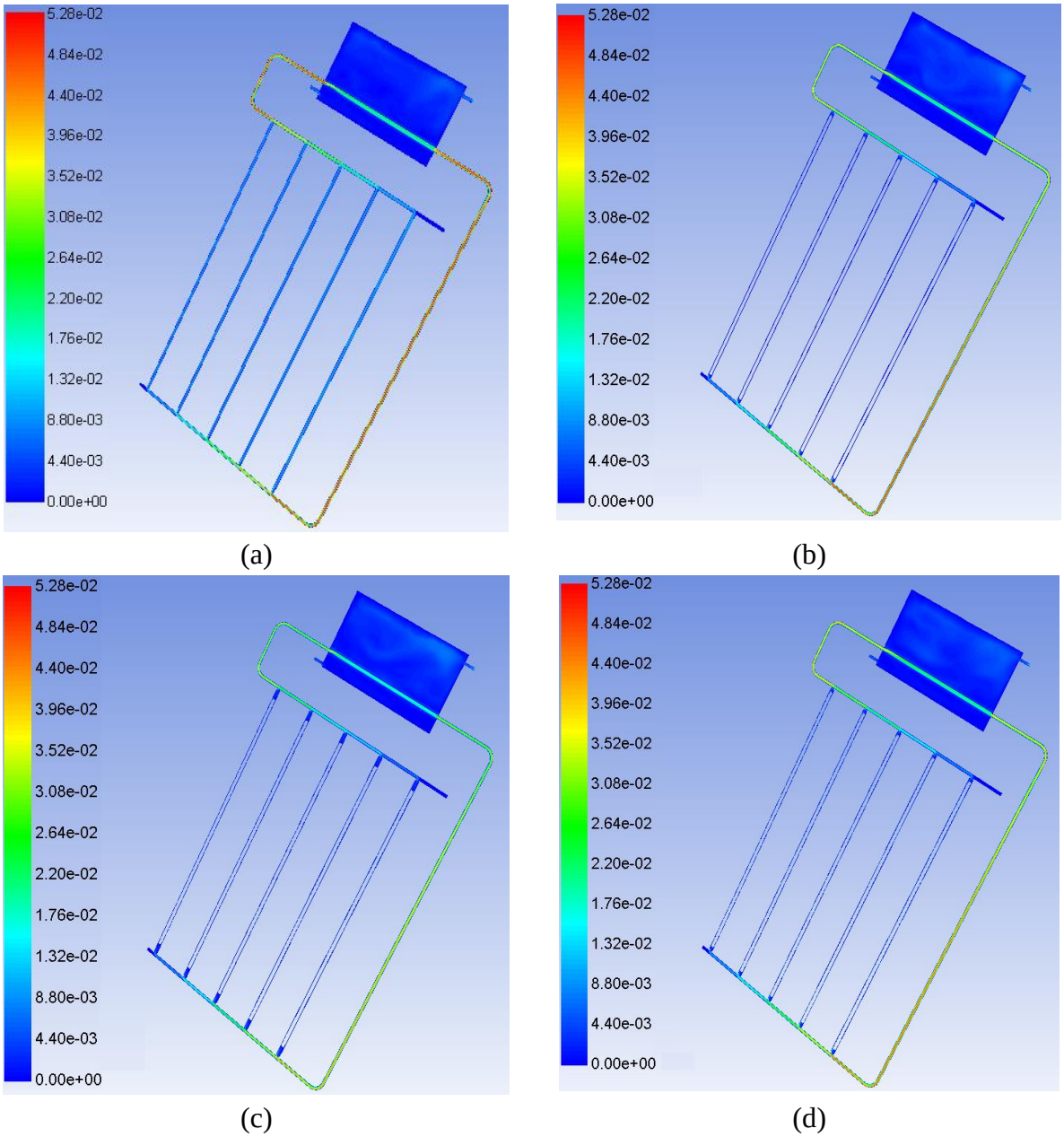

Figure 6-2 Flow velocity variations of the working fluid within thermo-syphon loop and water within the storage tankon for (a) traditional model (b) straight model (c) helical model and (d) wavy model on 15th March under thermal weekday loading

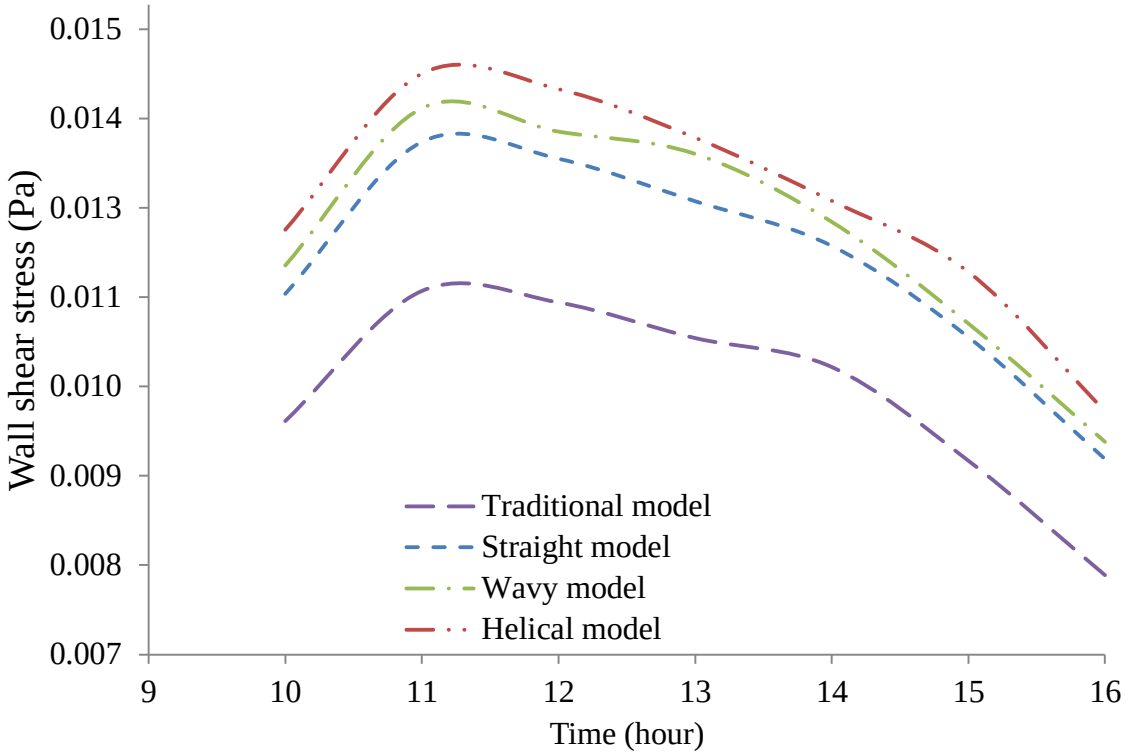

Figure 6-3 Wall shear stress variations within thermo-syphon loop for all models on 15th March under thermal weekday loading

Figure 6-4 further depicts the temperature distribution of the working fluid within thermo-syphon loop and water within the storage water tank for (a) traditional model, (b) straight model, (c) helical model and (d) wavy model at a heat flux corresponding to 15th March at 12 O'clock (midday) under weekday thermal loading condition. It can be seen clearly that the temperature of working fluid within thermo-syphon loop is higher for straight model as compared to other models. This increase in the temperature is the result of surface area increment, which is exposed to solar radiation leading to more heat transfer to the working fluid within the thermo-syphon loop. The average temperature of working fluid within thermo-syphon loop with traditional, straight, helical and wavy models was 52.01ºC 58.46ºC, 57.02ºC and 57.42ºC respectively. Furthermore, the highest temperature of working fluid is observed at the junction of the riser pipes and the upriser for all models.

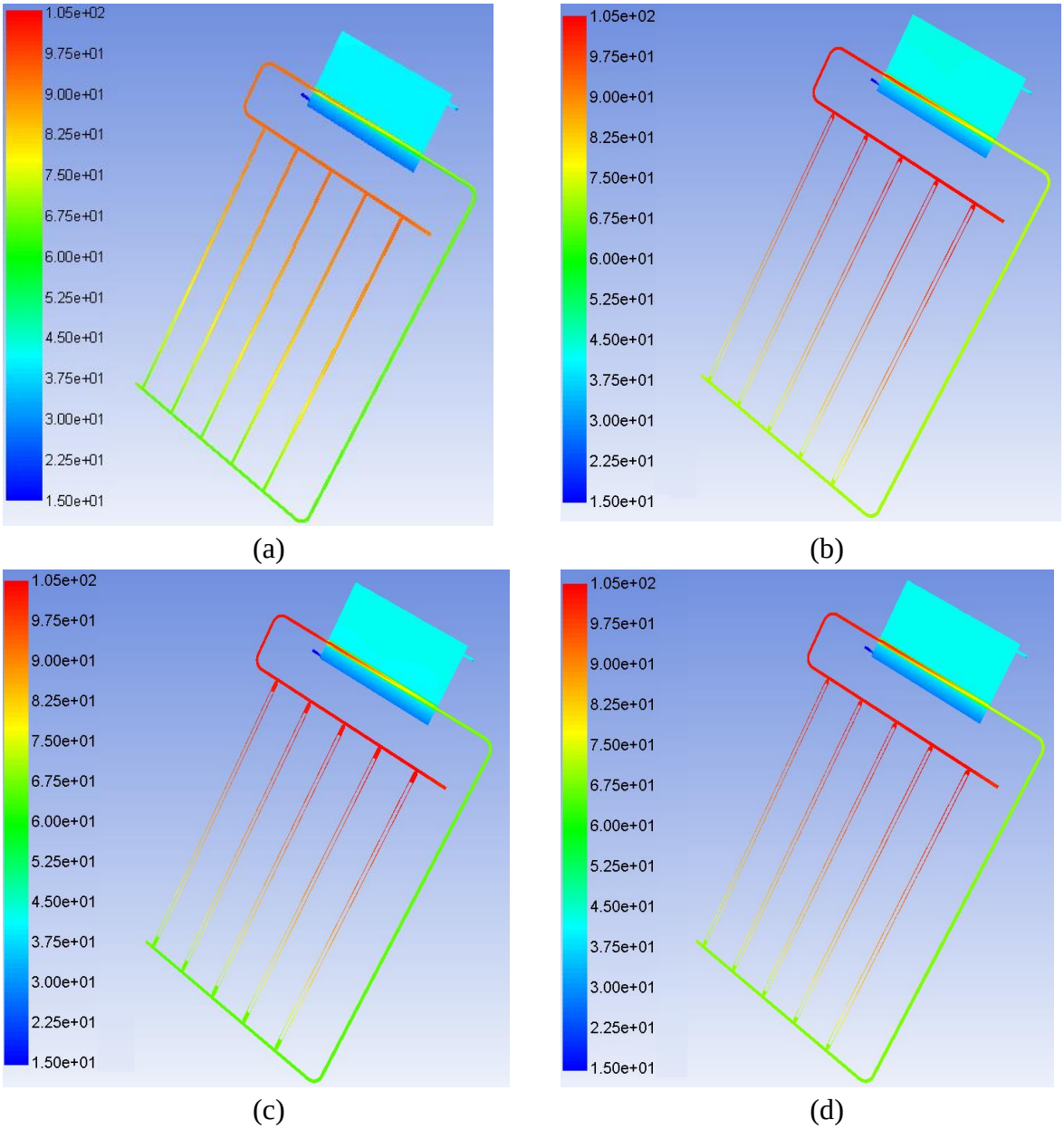

Figure 6-4 Static temperature distribution of the working fluid within thermo-syphon loop and water within the storage tank for (a) traditional model (b) straight model (c) helical model and (d) wavy model on 15th March under thermal weekday loading

To evaluate the thermal performance of thermo-syphon and hence to determine the optimum model heat gain in the storage tank, useful heat gain in the collector, water temperature within the storage tank and heat transfer coefficient of working fluid have been considered as determining parameters.

Amount of useful heat gain in the storage tank can be determined for both a new and tradition model by the equation below:

$$H.G_{tank} = \frac{m_w Cp_w (T_{wo} - T_{wi})}{n * 3600} + \sum_{t=1}^{t=n} \dot{m} Cp_w (T_{ot} - T_{it}) \quad (6.1)$$

where $H.G_{tank}$, m_w, Cp_w, T_{wo} T_{wi}, n, t, $\dot{m}$, T_{ot} and T_{it} denotes the heat gain in the storage tank, amount of water within the tank, specific heat of water, final temperature of water, initial temperature of water, number of hours, time, mass flow rate of working fluid, temperature of water at outlet of the tank, temperature of water at inlet of the tank, respectively.

Figure 6-5 depicts the variation in heat gain in the storage tank for (a) traditional model, (b) straight model, (c) helical model and (d) wavy model at a heat flux corresponding to 15th March under thermal loading condition of weekday. It can be seen clearly that the amount of heat gain within the storage tank is higher for straight model as compared to other models. Furthermore, it is noted that the maximum heat gain takes place at maximum heat flux condition, which is at 12 O'clock (midday). Findings show that maximum heat gain for traditional, straight, helical and wavy model was 525.38W, 625.01W, 621.82W and 616.14W respectively.

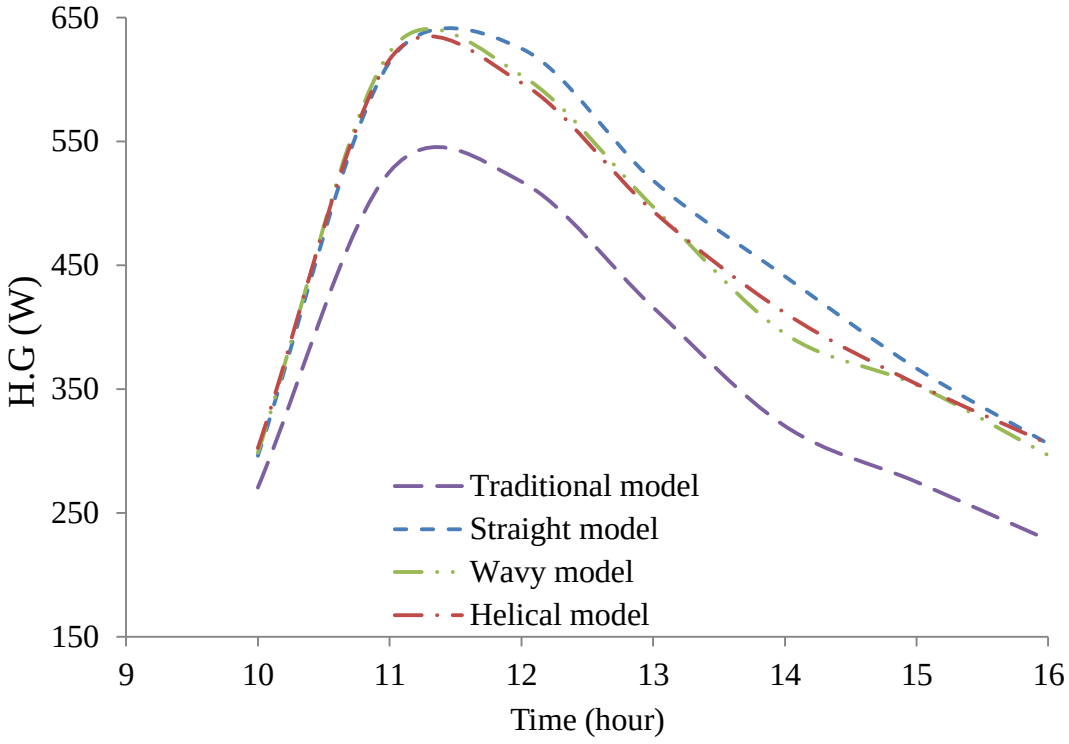

Figure 6-5 Heat gain variations within the storage tank for all models on 15th March under thermal weekday loading

Figure 6-6 depicts total heat gain in the storage tank for traditional model and three proposed models (straight, wavy and helical) with different riser pipe configuration on 15th March under thermal loading condition of the weekday. It can be seen clearly that the amount of heat gain within the storage tank is less for the traditional model as compared to the other models. The difference in the heat gain between the traditional model and the proposed models with straight, helical and wavy pipes in the riser pipes are 12.27%, 10.92% and 9.41% respectively. Moreover, it can be seen clearly that the amount of heat gain within the storage tank is higher for a straight model as compared to wavy and helical model by 1.22% and 2.61% respectively. Furthermore, it can be concluded that all models can be used to improve the thermal performance as compared to traditional model. However, the model with straight pipe in the riser pipe is better as compared with others models although there are no big differences between them regarding the heat gain.

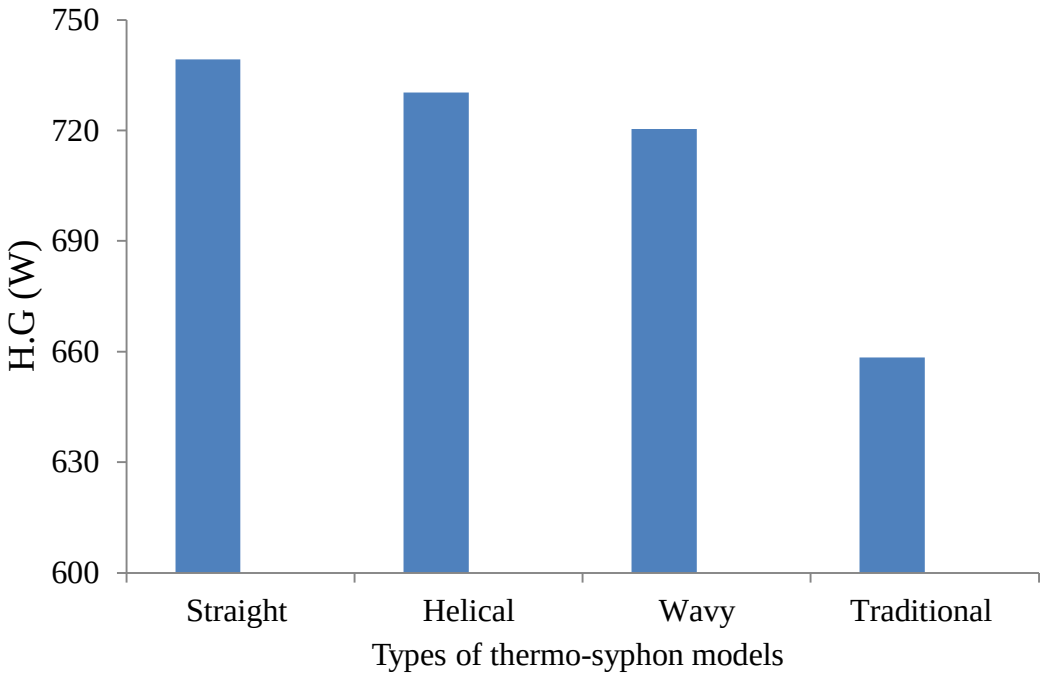

Figure 6-6 Total heat gains within the storage tank for various models of thermo-syphon on 15th March under thermal weekday loading

In order to calculate the useful heat gain in the collector, the following expression can be used

$$H.G_{collector} = \dot{m}Cp_{W.F}(T_o - T_i) \quad (6.2)$$

where $H.G_{collector}$, $Cp_{W.F}$, $\dot{m}$, T_o and T_i denotes the heat gain in the collector, specific heat of working fluid, mass flow rate of working fluid, the inlet and outlet temperature of working fluid at collector respectively.

Figure 6-7 depicts the variation in heat gain in the collector for (a) traditional model, (b) straight model, (c) helical model and (d) wavy model at a heat flux corresponding to 15th March under thermal loading condition of weekday. It can be seen that the amount of useful heat within the collector is higher for a new model as compared to the traditional model. This increase is due to an increase in the exposed surface area to solar radiation, which enhances the rate of heat transfer to the working fluid within the thermo-syphon loop. It can be seen that the amount of useful heat within the collector is approximately same for new models. However, the useful heat is higher for straight model as compared to other models. The maximum heat gain for traditional, straight, helical and wavy model happen at 12 O'clock and the values them were 578W, 618W, 604W and 615.9W respectively. Therefore It can be concluded that an increase of surface area of the riser pipe has a significant effect on the heat gain and hence on the performance of a closed loop thermo-syphon solar water heating system.

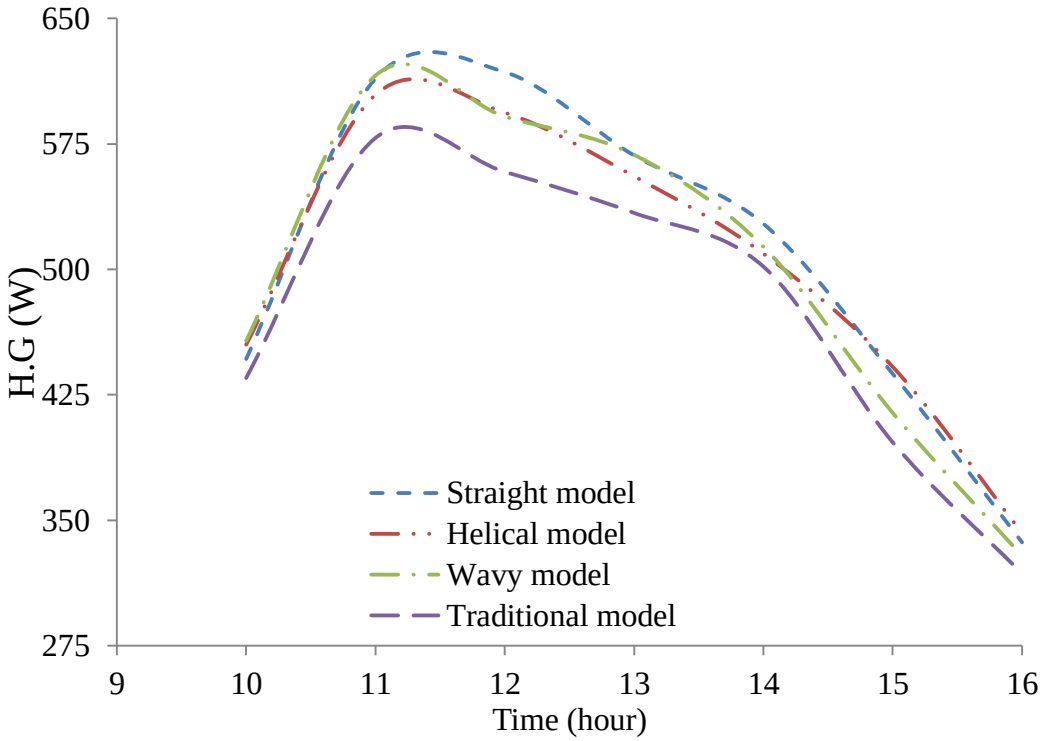

Figure 6-7 Heat gains variations within collector for all models on 15th March under thermal weekday loading

Figure 6-8 depicts the variation in mass flow rate of working fluid within the thermo-syphon loop for (a) traditional model, (b) straight model, (c) helical model and (d) wavy model at a heat flux corresponding to 15th March under thermal loading condition of the weekday. All models show a similar trend on the mass flow variation under transient heat flux. The result illustrates that the mass flow rate is dependent for heat flux. The heat flux changes throughout the day. For the first

three hours, the heat flux increases and hence, the mass flow rate increases along with it. On the other hand, after mid-day, the heat flux starts to decrease leading to a reduction in the mass flow rate as well. However, it can be seen clearly that the average mass flow rate is higher for a traditional model as compared to all new model although the amount of heat absorbed by the working fluid is higher for a new models than the traditional model. The reason behind that is increasing the pressure difference between inlet and outlet of collector increases friction between the working fluid and surface area of riser pipes. It can be illustrated from the Eq. (6.3) and Eq. (6.4) [132]. It can, therefore, be concluded that increasing the inner surface area of the riser pipe without change amount of working fluid will decrease the mass flow rate within thermo-syphon.

$$\tau_w = \frac{A*\Delta p}{s} = \frac{D*\Delta p}{4l} \tag{6.3}$$

$$\Delta p = \frac{2fl\rho u^2}{D} \tag{6.4}$$

where τ_w, s, Δ p, A, f, l, D, ρ and u denotes wall shear stress, surface area, pressure drop, cross-section area, friction factor, length of pipe, pipe diameter, density of fluid and the flow velocity respectively.

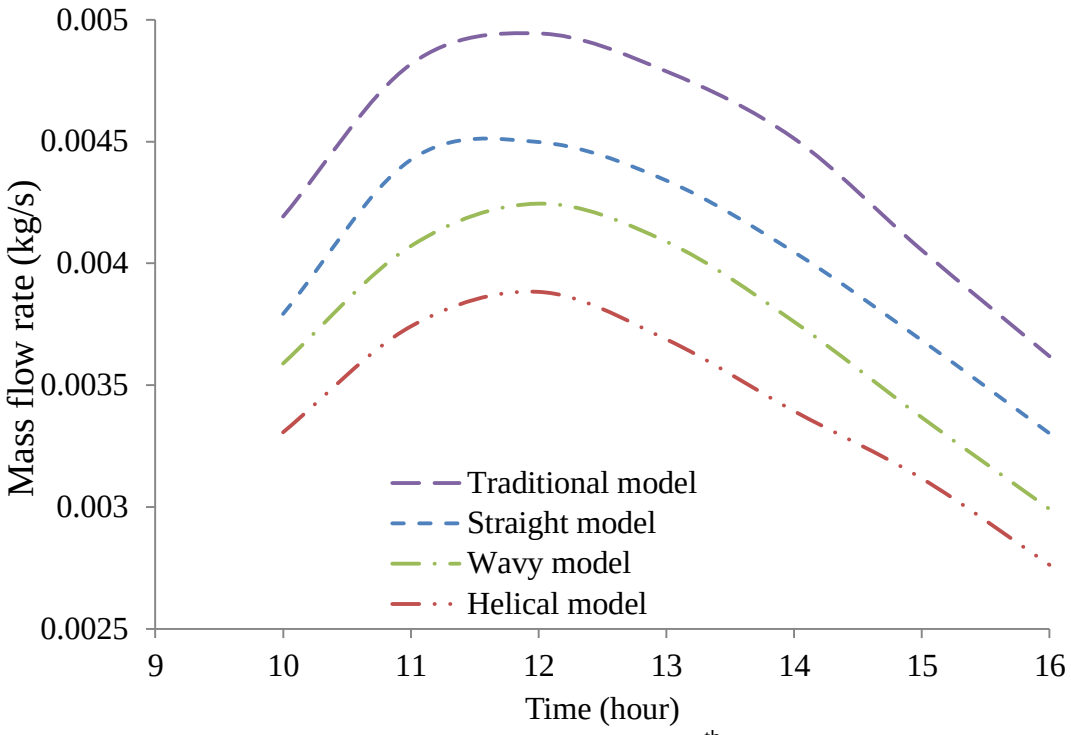

Figure 6-8 Circulating mass flow rate for all models on 15th March under thermal weekday loading

Figure 6-9 depicts the pressure difference between inlet and outlet of a collector for (a) traditional model, (b) straight model, (c) helical model and (d) wavy model at a heat flux corresponding to 15th March under thermal loading condition of the weekday. It can be observed that the pressure difference in the collector is highest for all new models, as compared to the traditional model. The average pressure difference for traditional model, straight model, helical model and wavy model is 55.33Pa, 56.647Pa, 58.51Pa and 58.74Pa respectively. This is because increase in surface area leads to increase in wall shear stress and hence increase the friction between working fluid and the inner surface of thermo-syphon loop. This consequently increases the pressure difference between inlet and outlet of a collector.

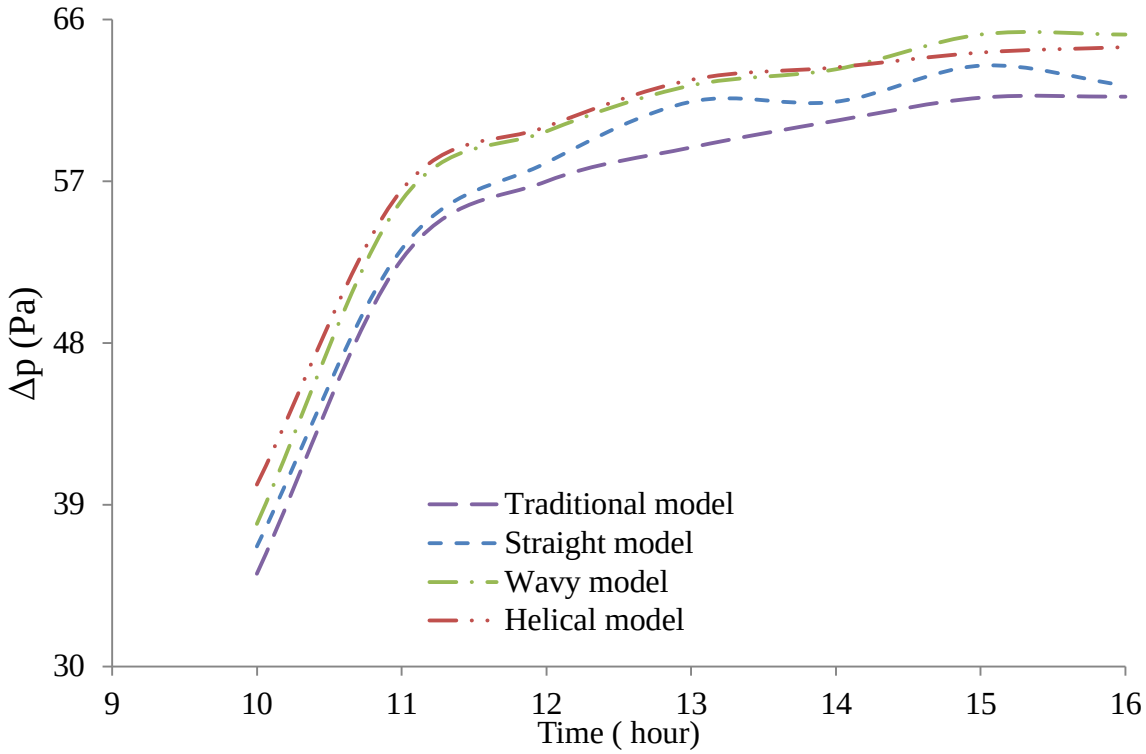

Figure 6-9 Pressure difference between inlet and outlet of a collector for all models on 15th March under thermal weekday loading

Figure 6-10 depicts the variations of heat transfer coefficient of working fluid within thermo-syphon loop for (a) traditional model, (b) straight model, (c) helical model and (d) wavy model at a heat flux corresponding to 15th March under thermal loading condition of weekday. It is evident from the figure that the heat transfer coefficient of working fluid for traditional model is less as compared to proposed models. In addition, the heat transfer coefficient of working fluid for straight model is higher, as compared to wavy and helical model. An increase in the surface area of riser pipe increases the amount of heat transfer to working fluid. This increased heat transfer increases the working fluid temperature and reduces the temperature difference between the

surface and working fluid, leading to an increment in heat transfer coefficient. Furthermore, increasing the surface area by 7.17% respect to traditional model increases the heat transfer coefficient by 19.60%.

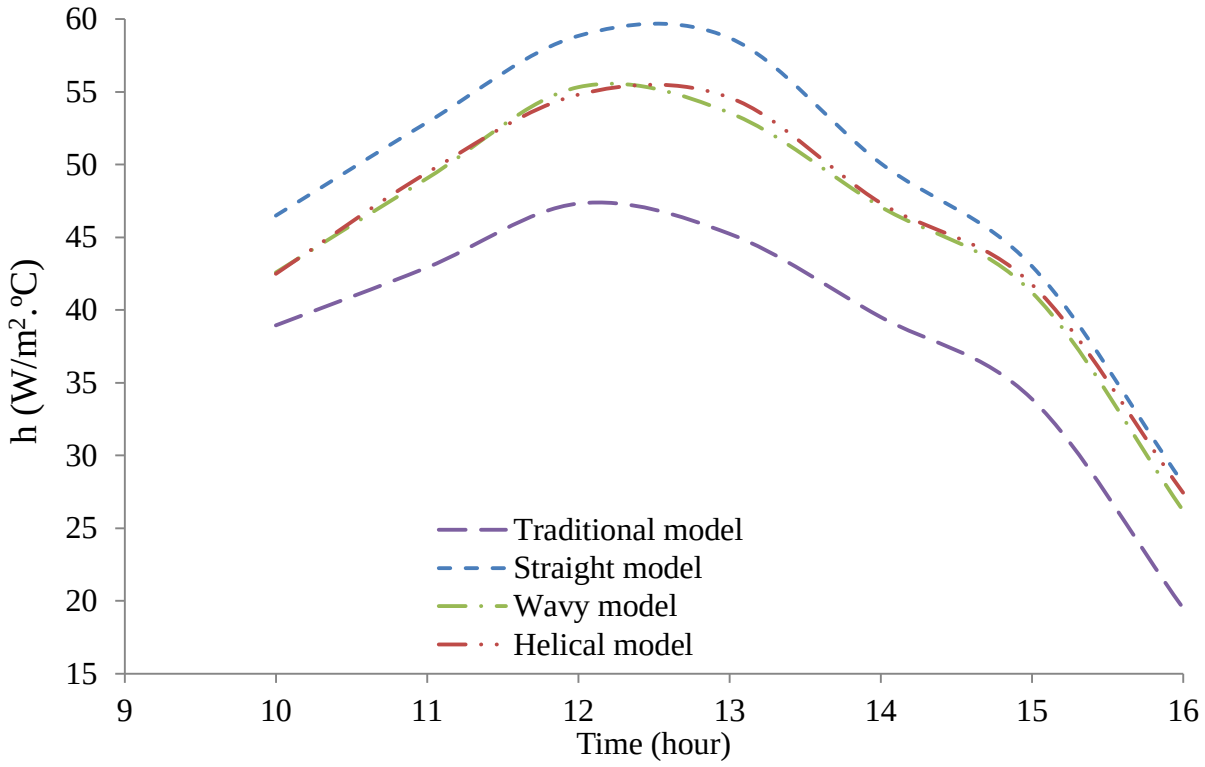

Figure 6-10 Heat transfer coefficient variations within thermo-syphon loop for all models on 15th March under thermal weekday loading

Figure 6-11 depicts the variation in water's temperature at the centre of the storage tank for (a) traditional model, (b) straight model, (b) helical model and (c) wavy model at a heat flux corresponding to 15th March under thermal loading condition of the weekday. It can be seen that, due to an increase of exposed surface area to the heat flux, in the new models the temperature of the water in storage tank has been increased compare to the traditional model. Furthermore, it can be seen that the temperature of water within the storage tank is higher for straight model as compared to other new models having helical and wavy inserts. Moreover, it can be noticed that the final tank temperature at the end is around 53.01ºC, 57.12ºC, 55.68ºC and 55.58ºC for traditional, straight, helical and wavy models respectively. The exposed surface area has been increased by 7.17% with respect to the traditional model. This has caused the temperature of water in the storage tank to increase by 13.33% compare to the traditional model respect to straight model. Based on these aforementioned observations it can be concluded that, an increment in the surface area of the riser pipe will increase the temperature of working fluid within thermo-syphon

loop. This leads to more heat transfer between working fluid and water within the storage tank by the heat coil, which is inside the tank and therefore improve the thermal performance of thermo-syphon.

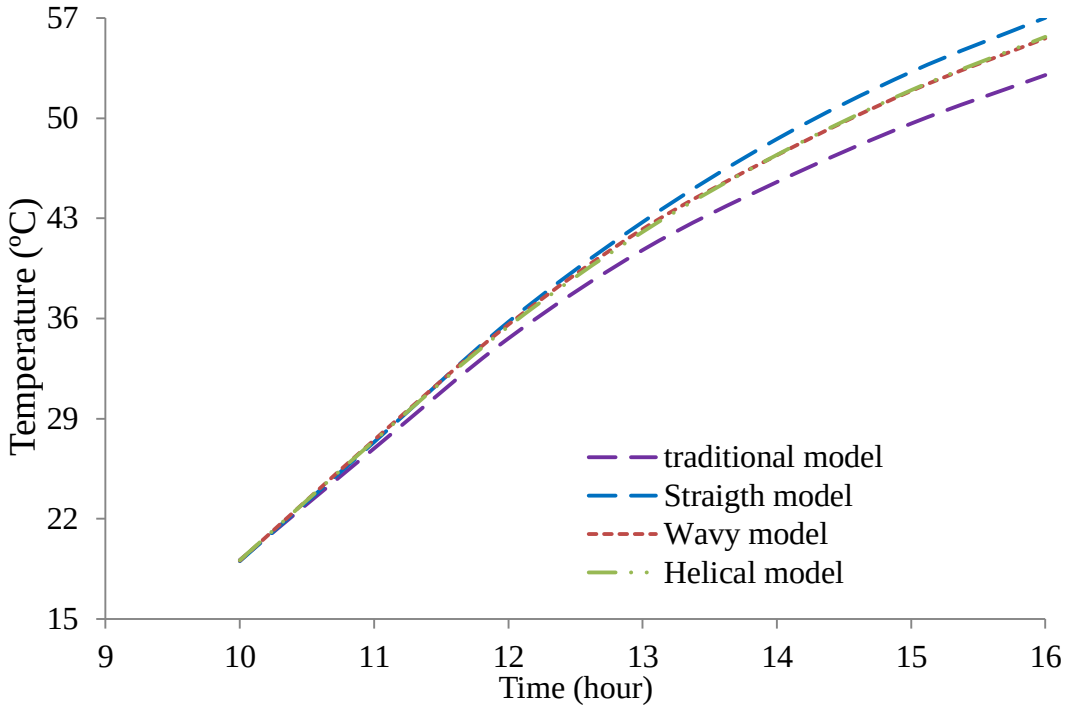

Figure 6-11 Temperature variations within the storage tank for all models on 15th March under thermal weekday loading

Furthermore, in order to understand the behaviour of working fluid within the riser pipes, velocity and temperature distributions have been analysed for all models.

Figure 6-12 depicts the cross-sectional view of flow velocity variations taken along the length in the middle riser pipe at a heat flux corresponding to 15th March, for (a) traditional model, (b) straight model, (b) helical model and (c) wavy model. The corresponding thermal loading condition that has been specified is that of the weekday. The scale of the contours has been kept constant for effective comparison purposes. It can be clearly seen that the flow velocity is considerably higher on the upper section of the riser pipe for the traditional model whereas, high velocity profile has been observed at the mean path for the new models. This is because, with the addition of heat, the temperature of the fluid increases and hence decreases the density. Therefore, fluid moves upward at the upper section of the pipe and then propagates towards the upriser. It can be clearly seen that the velocity of working fluid within the riser pipe is higher for traditional model as compared to new models. Furthermore, it can be seen that the velocity of working fluid within the riser pipe is higher for straight model as compared to other new models. The percentage

decrease of average working fluid velocity for helical and wavy models with respect to the straight model was approximately 34.1% and 10.5% respectively. Whilst the percentage decrease of average working fluid velocity between traditional and straight model was approximately 25.0%. It can therefore be concluded that, increasing surface area of the riser pipe has negative effect on the velocity of working fluid within the riser pipe.

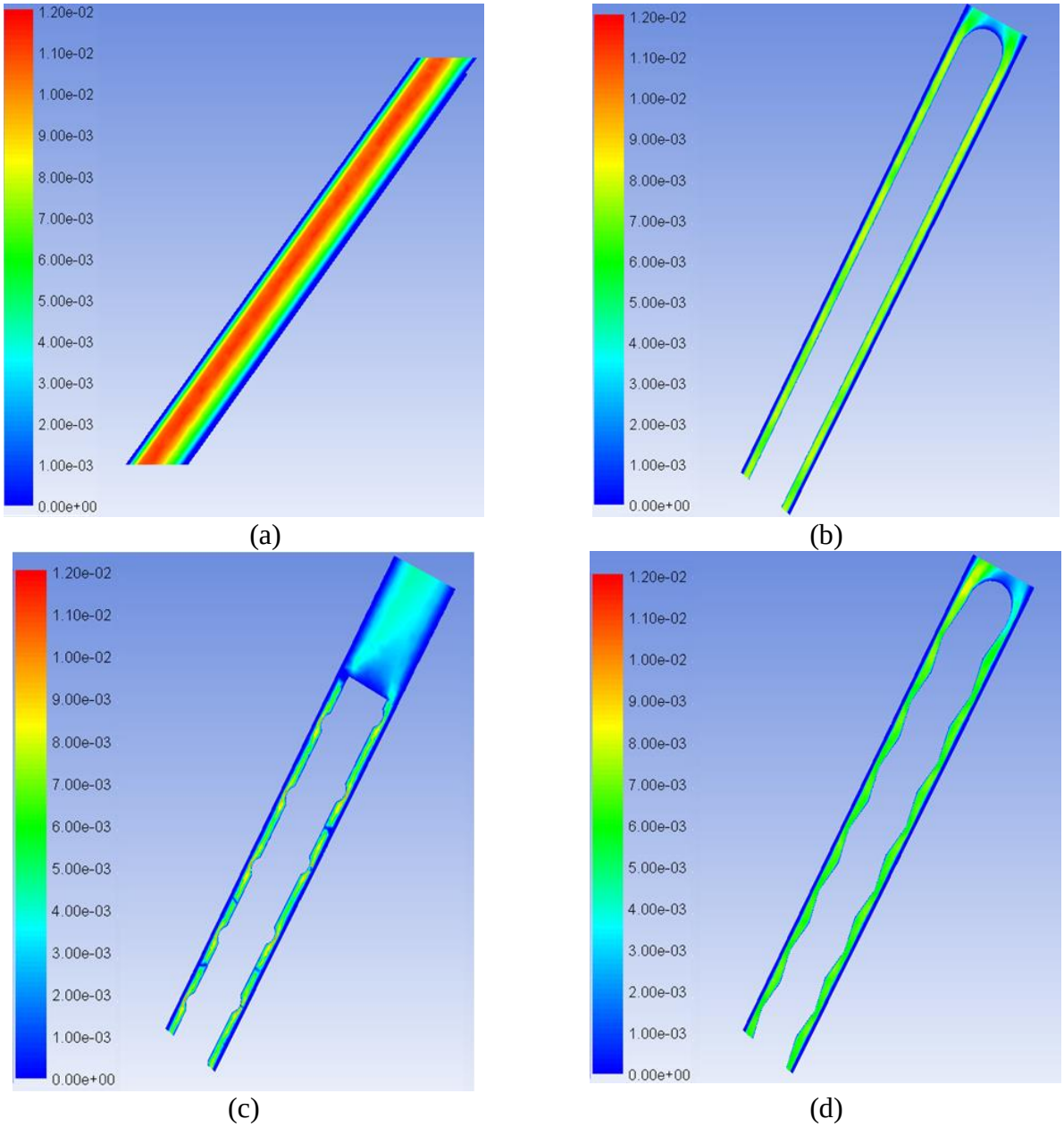

Figure 6-12 Flow velocity variations in the middle riser pipe for (a) traditional model (b) straight model (c) helical model and (d) wavy model on 15th March under thermal weekday loading

Figure 6-13 depicts the velocity profiles of the working fluid taken at a cross-section within the middle riser pipe at a heat flux corresponding to 15th March, for all models considered in the present study. The corresponding thermal loading condition that has been specified is that of the weekday. This analysis has been conducted on a cross-sectional plane located at a length of y/Y=0.9 of the riser pipe to capture the maximum values. The scale of the profile has been kept constant for effective comparison purposes. It can be clearly seen that the velocity of working fluid within the riser pipe is higher for traditional model compared to the new models. Furthermore, it can be seen that the velocity of working fluid within the riser pipe is higher for straight model as compared to other new models. The maximum velocity of working fluid within the riser pipe for all models takes place at 12 O'clock (midday). The maximum velocity of working fluid within the riser pipe for traditional model, straight model, helical model and wavy model was 0.65m/min, 0.36m/min, 0.34m/min and 0.28m/min respectively. There are two reasons that cause the reduction in the flow velocity within the riser pipe. The first one is the presence of pipe inside the riser pipe that increases the resistance in fluid flow. The second being an increased inner surface area of riser pipe. In the new proposed models, the inner surface area have been nearly doubled compared to the traditional model. This increment of the inner surface area has raised the wall shear stress as shown in figure 6-3 and hence decreased flow velocity of working fluid.

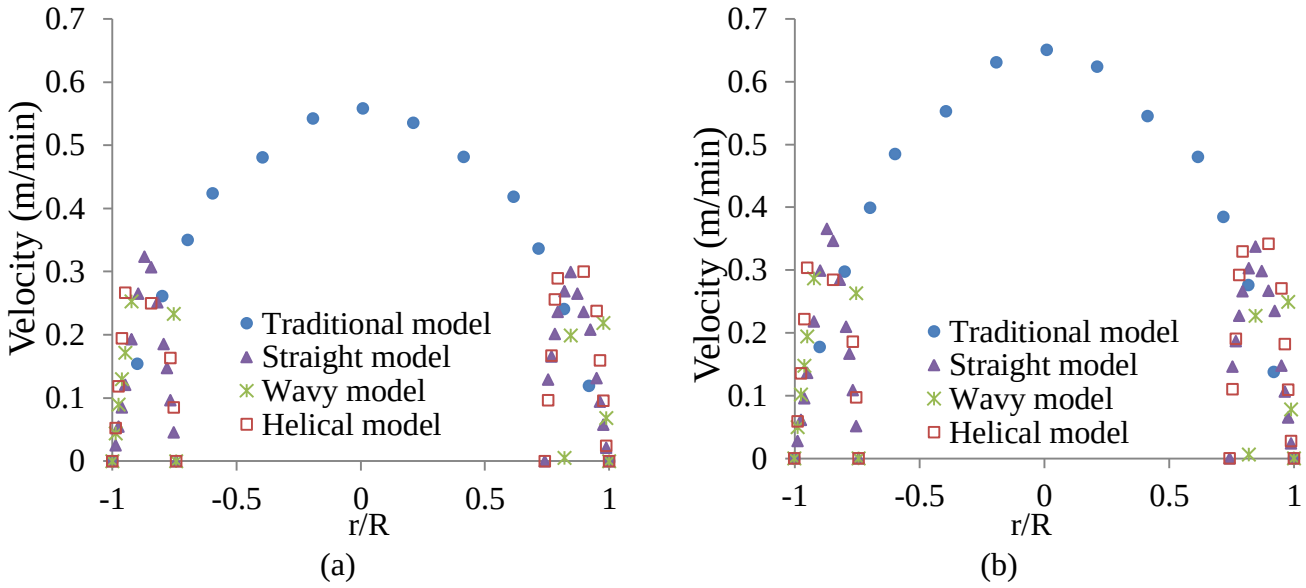

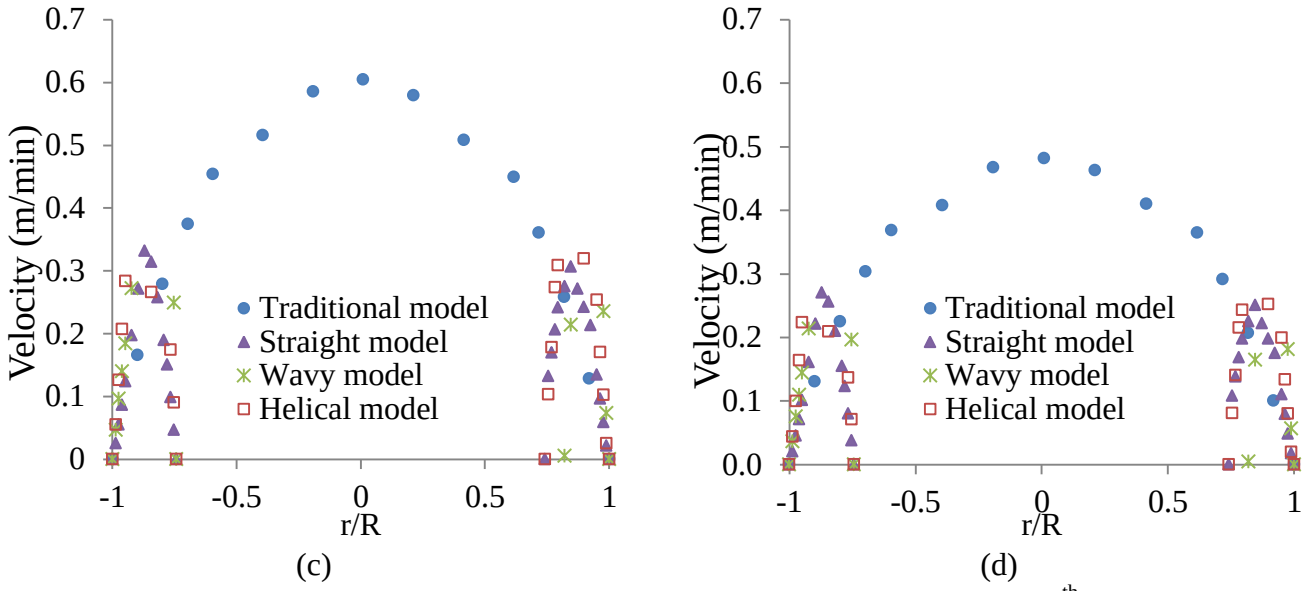

Figure 6-13 Velocity profiles within the middle riser pipe for all models on 15th March under thermal weekday loading for (a) 10 O'clock (b) 12 O'clock (c) 14 O'clock and (d) 16 O'clock

Figure 6-14 depicts variation in static temperature of the working fluid within the cross-section taken along the length of the middle riser pipe at a heat flux corresponding to 15th March, for (a) traditional model, (b) straight model, (b) helical model and (c) wavy model. The corresponding thermal loading condition that has been specified is that of the weekday. The scale of the contours has been kept constant for effective comparison purposes. It can be clearly seen that the working fluid temperature is considerably higher on the upper section of the riser pipe. The reason behind that is an increment in working fluid temperature, which leads to decrease in the density and hence the hot working fluid concentrates on upper section of the riser pipe. It can be further noticed that the temperature of working fluid within the riser pipe is higher for straight model as compared to other models. The percentage decrease of average working fluid temperature for helical and wavy model with respect to straight model was approximately 1.3% and 1.0% respectively. The percentage increase of average temperature of working fluid between traditional and straight model was approximately 7.1%.

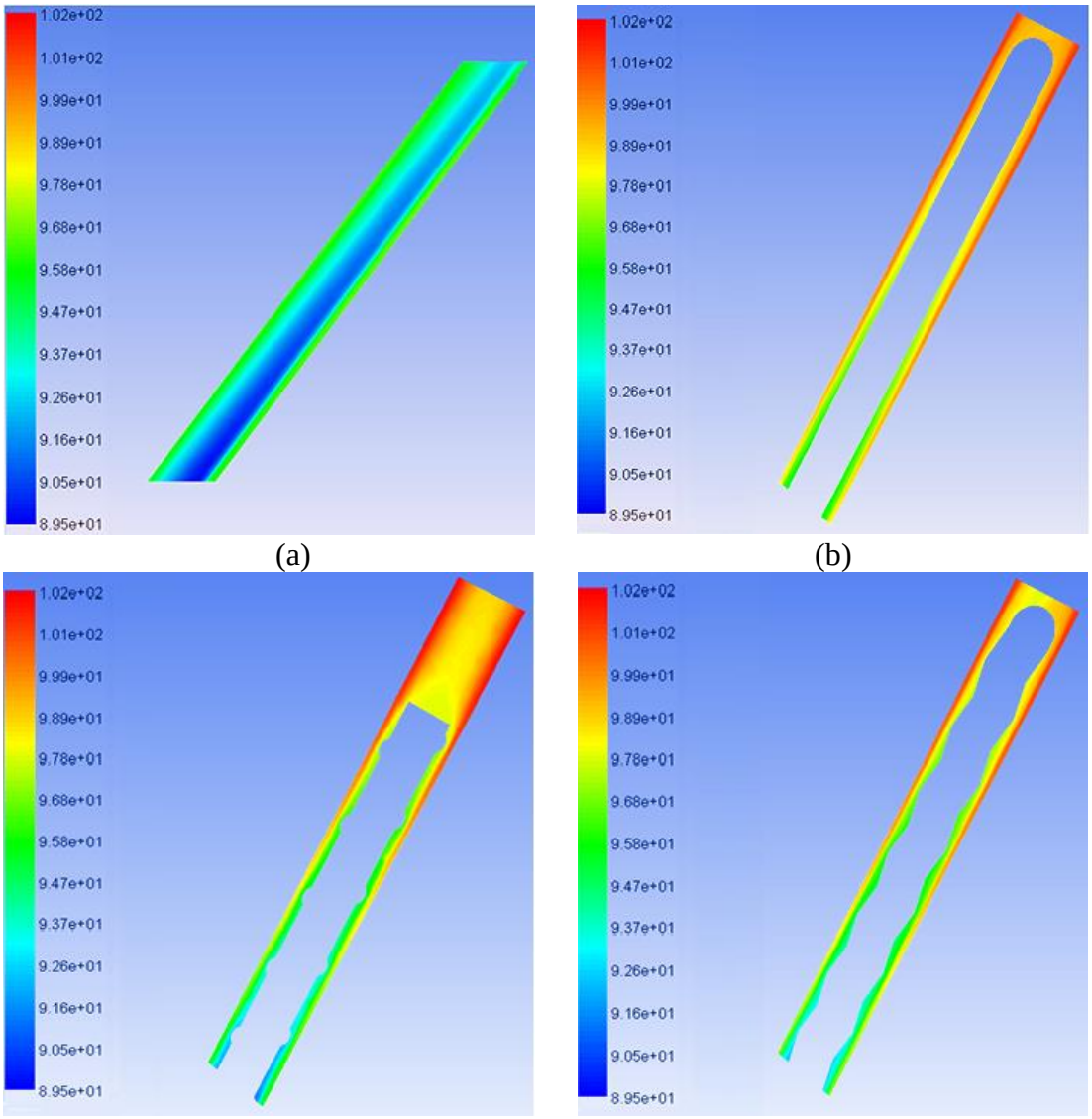

Figure 6-14 Static temperature distributions within the middle riser for (a) traditional model (b) straight model (c) helical model and (d) wavy model on 15th March under thermal weekday loading

Figure 6-15 depicts the static temperature profiles of the working fluid taken at a cross section within the middle riser pipe at a heat flux corresponding to 15th March, for (a) traditional model, (b) straight model, (b) helical model and (c) wavy model. The corresponding thermal loading condition that has been specified is that of the weekday. This analysis has been conducted on a cross-sectional plane located at a length of 0.9 of the riser pipe length to capture the maximum values. It can be seen that the temperature of working fluid within the riser pipe is higher for straight model as compared to other new models. The maximum temperature of the working fluid

within the riser pipe for traditional, straight, helical and wavy models is 94.60ºC, 101.56ºC, 98.60ºC and 99.21ºC respectively. The increased surface area exposed to heat flux, increases the amount of heat transfer to working fluid within the riser pipe and thus raise the working fluid temperature. From this, it can be established that only by increasing the inner surface area of riser pipe the temperature of working fluid can be increased and hence the performance of a closed loop thermo-syphon solar water heating system, while the amount of working fluid remains constant. Findings show that a raise in the surface area of 7.17% can increase the working fluid temperature by 7.98% for same amount of working fluid.

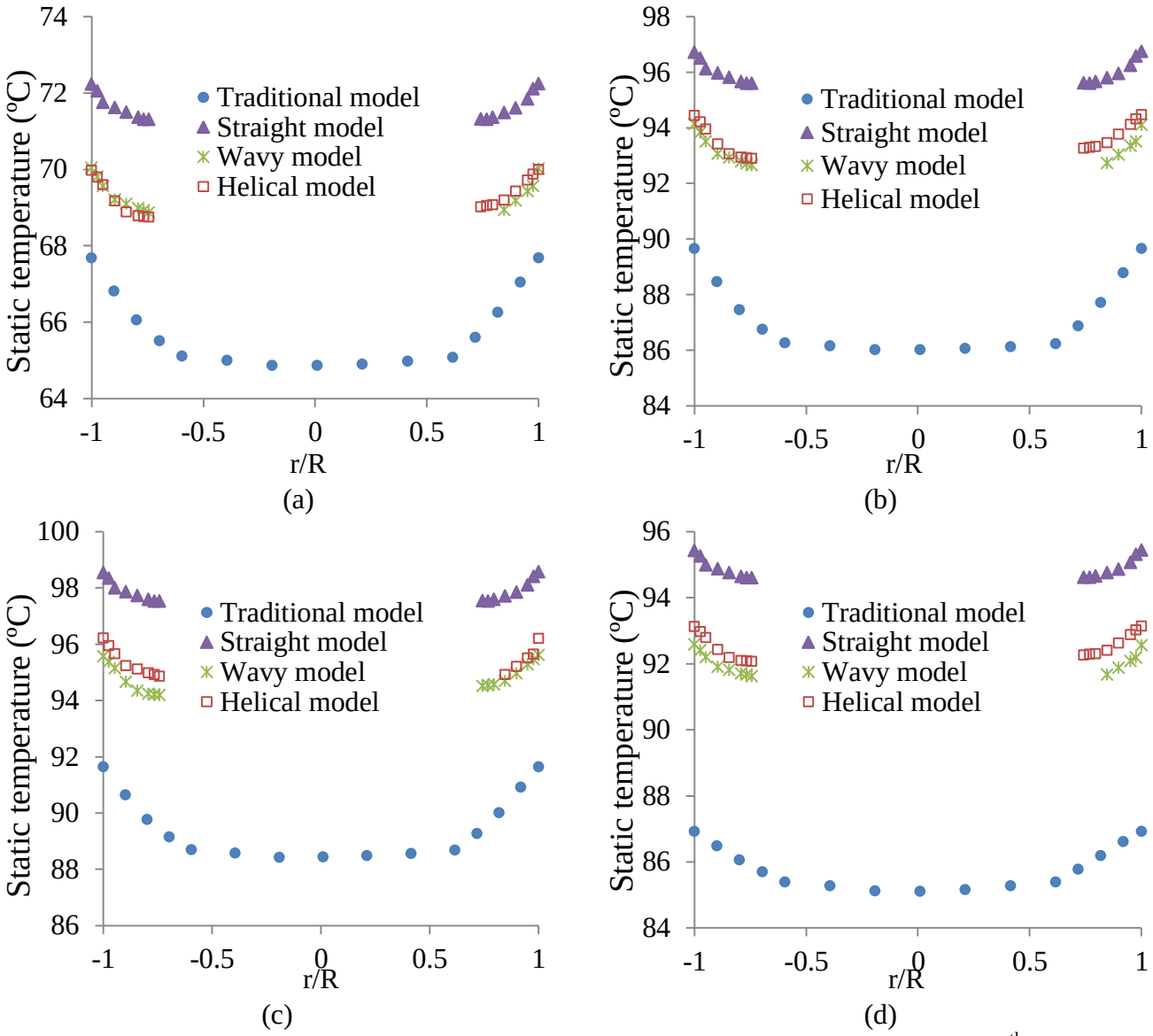

Figure 6-15 Static temperature within the middle riser pipe on different models o 15th March under thermal weekday loading for (a) 10 O'clock (b) 12 O'clock (c) 14 O'clock and (d) 16 O'clock

Based on aforementioned analysis of effect of all models on various parameters quantifying heat transfer effectiveness can be represented as follows:

Table 6-1 The effect of different models on various parameters

Types of models	Heat gain within the storage tank (W)	Heat gain within the collector (W)	Wall shear stress (Pa)	Heat transfer coefficient of working fluid ($W/m^2.^oC$)
Traditional model	658.4	558.3	0.01133	47.31
Straight model	739.2	617.9	0.01310	58.84
Helical model	730.3	593.7	0.01390	54.81
Wavy model	720.4	591.3	0.01340	55.32

From the Table 6-1 it can be concluded that the performance of the thermo-syphon with new configuration of riser pipe have been improved. Although, the performance of these models do not vary much, the model with straight pipe has better thermal performance characteristics compare to other models. Moreover, the straight model has simple geometry and it is cost effective. Henceforth, this model (straight tube) has been chosen for further investigation to improve the thermal performance of thermo-syphon. Henceforth, this new model (straight model) has ability to improve the thermal performance of thermo-syphon by 12.3% as compared to traditional model.

After the previous conclusion, next step is to study the effect of amount of working fluid within the thermo-syphon loop for the better thermal performance of the system. In the present study, the performance of chosen model (straight tube) has been investigated under three conditions by varying the amount of working fluid as compared with the traditional model. The volume of working fluid has been varied against that in the traditional model, by having working fluid as similar, larger, and smaller in volume. The percentage variation in the amount of working fluid was 3.0%. These variations have been achieved by changing the dimensions of inside tube.

Figure 6-16 depicts total heat gain in the storage tank for various amount of working fluid within thermo-syphon loop (same amount, larger amount and smaller amount) at a heat flux corresponding to 15^{th} March under thermal loading condition of the weekday. It can be clearly seen that the amount of heat gained within the storage tank is higher for the similar volume in comparison with the larger and smaller volume by 2.8% and 2.3% respectively. It can be concluded that the same amount of working fluid is better as compared with others. Furthermore, it can be concluded that the amount of working fluid has effect on the heat transfer along with other parameters such as surface area. Henceforth, based on these findings the straight model with same amount of working fluid will be considered for further investigation to improve the thermal performance of thermo-syphon.

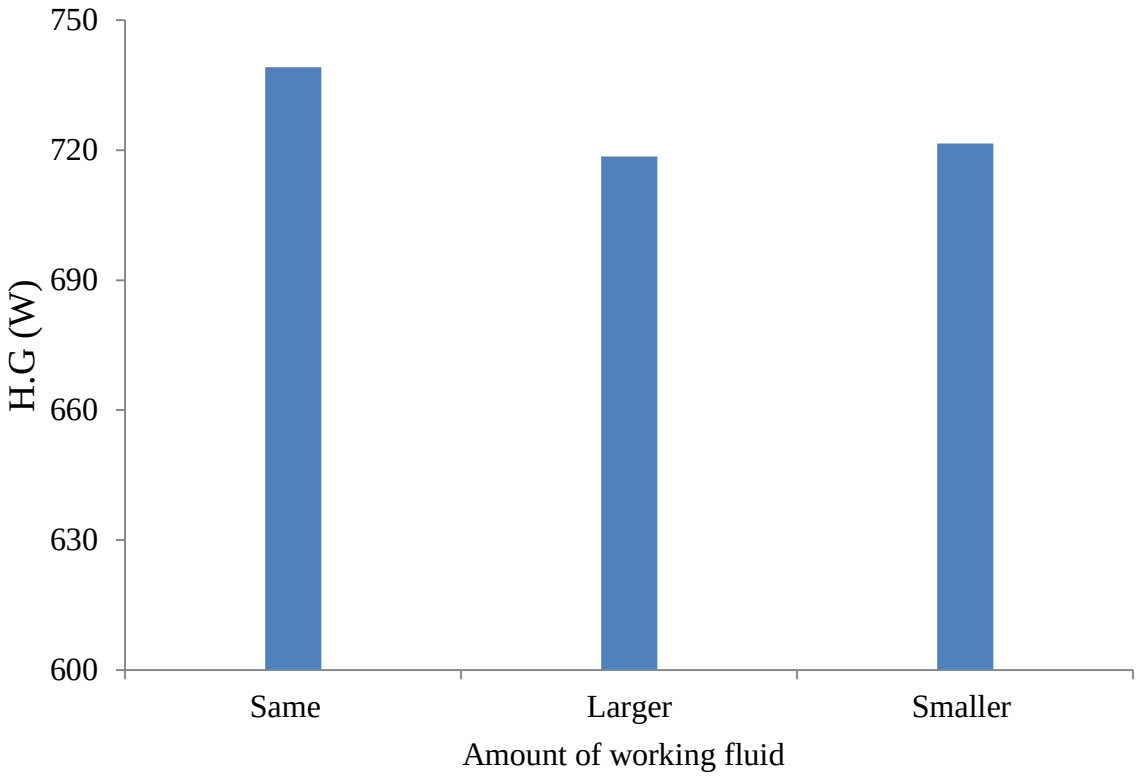

Figure 6-16 Total heat gains within the storage tank for various amount of working fluid on 15th March under thermal weekday loading

To investigate the effect of the new model (straight model with same amount of working fluid) on the thermal performance of thermo-syphon, a comparison between the traditional model and the chosen model has been conducted both experimentally and numerically which is explained in the next sections.

6.3. Benchmark Tests

Based on results from previous sections, it can be concluded that the straight model is better model among other models. A new model has been manufactured in the laboratory with dimensions as shown in Figure 6-17.

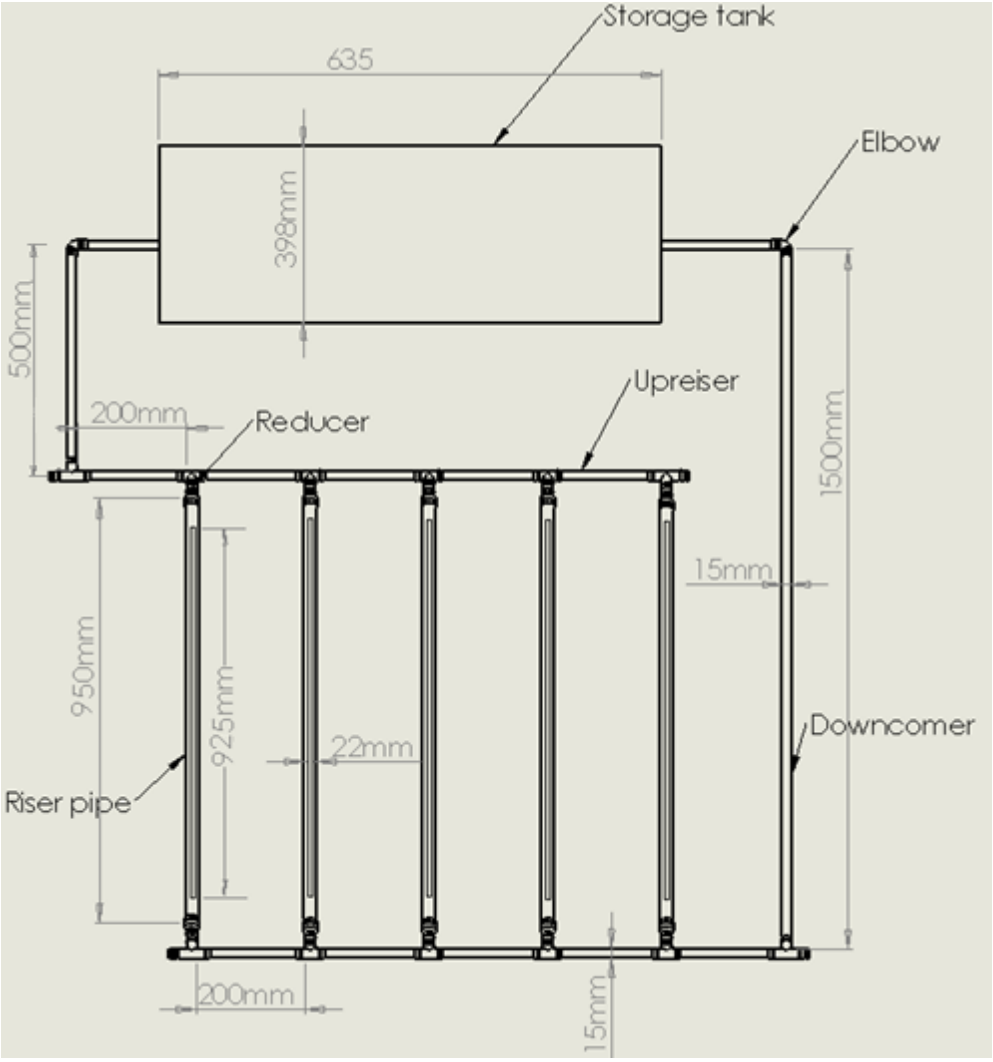

Figure 6-17 Schematic of the new model

The new model can be manufactured by following the procedure mentioned below:

1. To increase the surface area of riser pipe, a hollow copper pipe with external diameter of 22mm has been chosen, which has a wall thickness of 0.9mm. (Standard dimension)
2. Another hollow copper pipe with external diameter of 15mm and 925mm length has been chosen for the inside pipe. However, the dimensions of the condenser, upriser and downcomer remained the same as in traditional model, to keep the same amount of working fluid within the thermo-syphon loop. These dimensions above have been calculated to maintain the same amount working fluid as the traditional model in the new proposed model
3. The both end of the inside pipe is closed by plastic stopper

4. To align the inside pipe with the centre of the riser, create a hole at the centre of the plastic stopper closing the inside pipe and the Equal Tee
5. Link these two holes by a screw which location on the pipe is fixed by bolts. The dimensions of the bolts used in this study are 75mm length and 3.5mm diameter
6. Figure 6-18 (a) shows the exploded view of the riser pipe connection whereas the Figure 6-18 (b) depicts the full-assembled riser pipe configuration

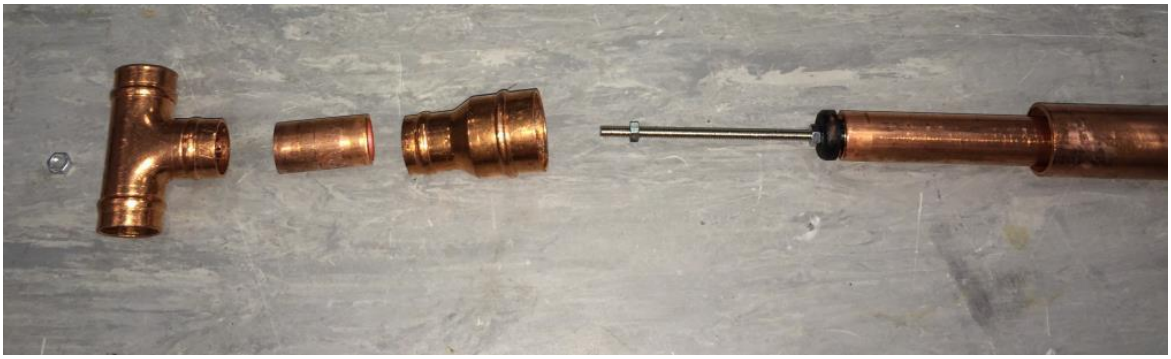

(a)

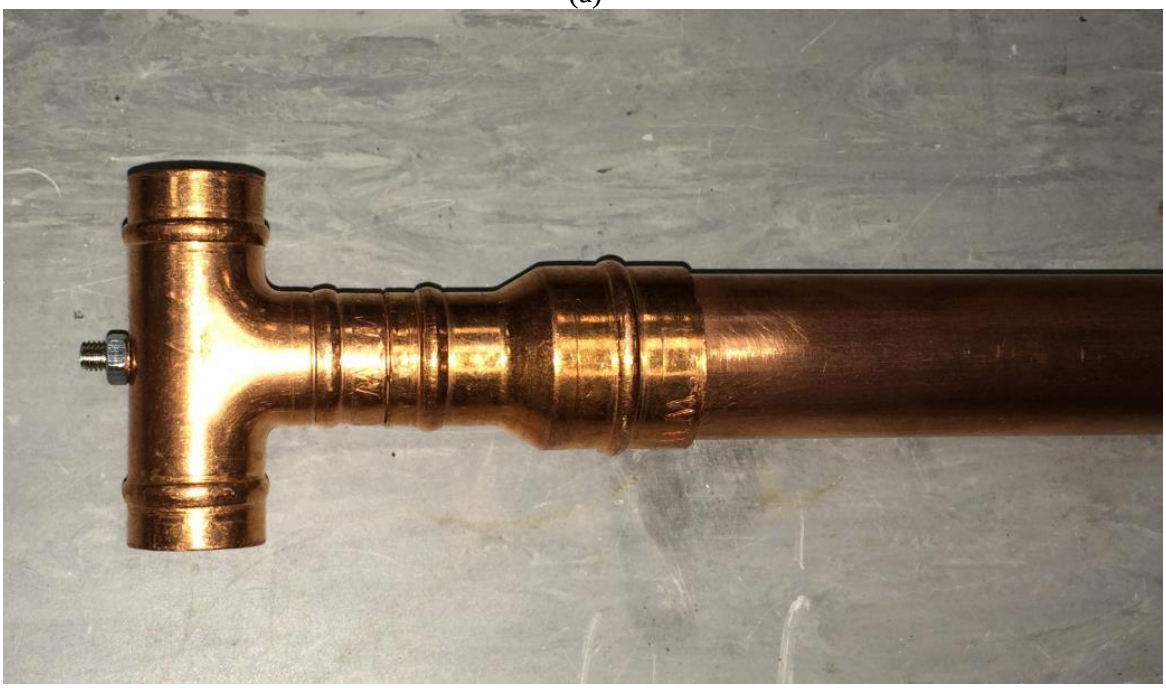

(b)

Figure 6-18 New model

To check the thermal performance of the chosen model experimentally, the temperature of water within the storage tank, the inlet and outlet temperature of working fluid within the thermo-syphon loop has been measured and compared with the traditional model. In this study, two types of investigations have been carried out based on heat flux condition. The first condition was

constant heat flux. However, to simulate real life condition, the later part of this investigation has been carried out on transient heat flux conditions. Table 6-2 contains the dimensions and characteristics of chosen model, which is used in experimental work.

Table 6-2 Test rig specifications of new model of thermo-syphon

Height of casing	1.2	m
Width of casing	1.1	m
Depth of casing	0.18	m
Tilt angle of collector	53º	º
Number of riser pipe	5	
Length of the riser pipe	0.95	m
Inside riser pipe diameter	0.02	m
Outside riser pipe diameter	0.022	m
Riser pipe material	Copper	
Length of inside tube	0.9	m
Diameter of inside tube	0.015	m
inside tube material	Copper	
Absorber plate length	1	m
Absorber plate width	1	m
Absorber plate thickness	0.0007	m
Absorber plate material	Copper	
Diameter of tank	0.398	m
Height of tank	0.635	m
Material of tank	Plastic	
Inside diameter of condenser	0.0202	m
outside diameter of condenser	0.022	m
Length of condenser	0.6	m
Condenser material	Copper	

6.3.1. Constant Heat Flux

In this section, the new proposed model has been compared against the traditional model experimentally, and the parameters used for the comparison are water temperature within the storage tank, temperature of working fluid at the inlet and outlet of collector, as well as the mass flow rate of working fluid within the thermo-syphon loop under constant heat flux.

Figure 6-19 depicts the comparison between the temperature of water within the storage tank and temperature of working fluid at outlet and inlet of collector for both models for five hours of operation, with constant heat flux of 177.7W/m^2 under no loading from the storage tank. It can be clearly seen that there are a good improvement with both temperature of water and working fluid, which indicates an increase in the performance of thermo-syphon. Furthermore, increase in heat gain within the storage tank was (16±1.53)%, while the increase in heat gain within the collector

was (12±1.32)%. It can be further concluded that increasing the surface area of the riser pipe without changing amount of working fluid leads to improvement in the thermal performance of a closed loop thermo-syphon solar water heating system. Therefore, this proposed model can be used to enhance heat transfer in a closed loop thermo-syphon solar water heating system.

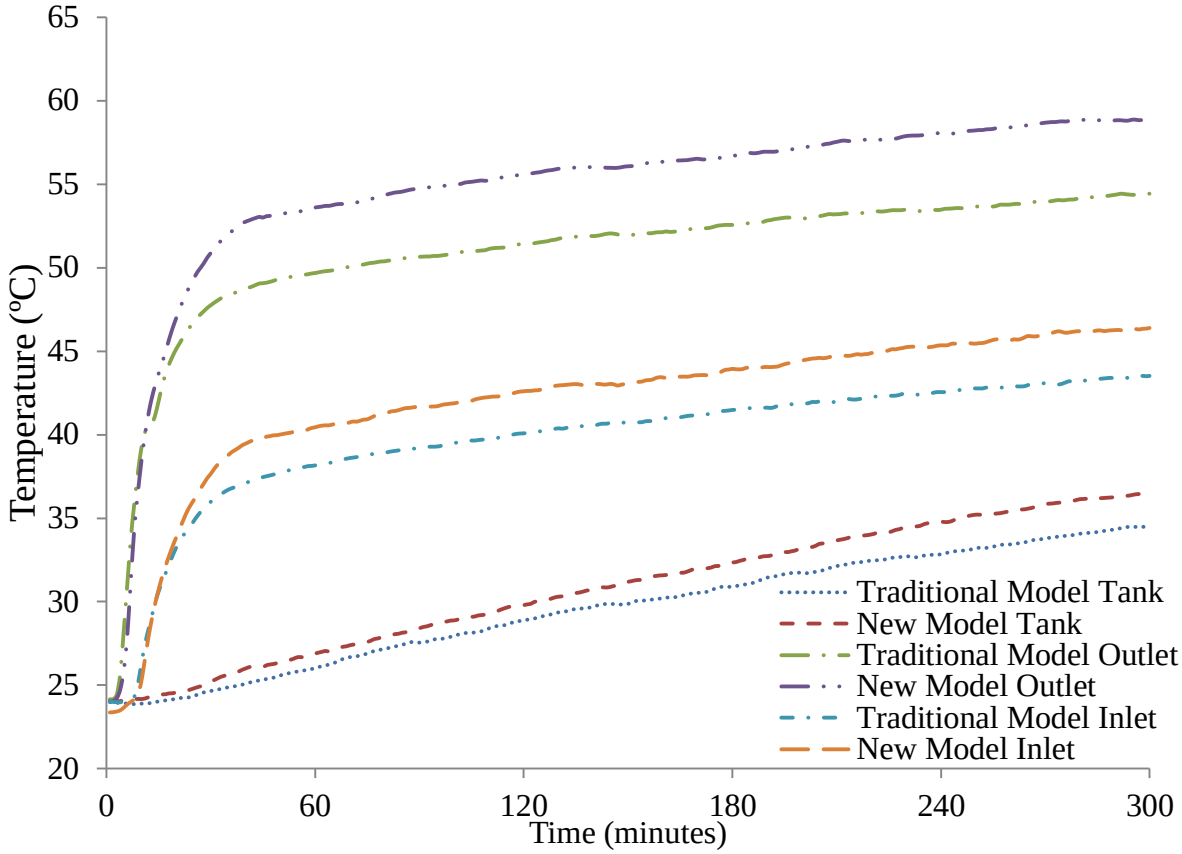

Figure 6-19 Variation in temperature of water within the storage tank and working fluid at the inlet and outlet of collector for different models

6.3.2. Various Heat Flux

For further investigation, the temperature has been measured at the aforementioned locations for both traditional and proposed model at various heat flux conditions. The heat flux was varied by controlling the heat flux source. In this case, the heat flux was applied by a system of halogen lamps. When the halogen lamp was turned on, a constant amount of heat flux was applied on to the collector. The variation in the heat flux was controlled by turning on/off the lamp. This type of heat input arrangement has been chosen to analyse the behaviour of working fluid and to confirm the relation between the mass flow rate of working fluid and heat input. Table 6-3 summarises the range of heat fluxes parameter used during the experimental period, which were considered in experimental work.

Table 6-3 Range of heat fluxes

Time (minutes)	0-90	90-105	105-195	195-210	210-300	300-315	315-405	405-420
Heat flux (W/m^2)	on	off	on	off	on	off	on	off

where,
on is the heat flux at ($177.7W/m^2$)
off is heat flux at ($0W/m^2$)

Figure 6-20 depicts a comparison of water temperature variation within the storage tank between the new proposed model and traditional model for seven hours of operation with various heat fluxes, which is shown in table 6.3. The temperature has been measured at the centre of tank. According to the Figure 6-20 it can be seen that when collector was exposed to a constant heat flux of $177.7W/m^2$ for 90 minutes, the temperature of water in the new proposed model has increased from 22.40ºC to 28.25ºC with a gradient of 0.065ºC/min. While in the traditional model, the temperature of water has increased from 22.86ºC to 27.06ºC, with a gradient of 0.047ºC/min. After 90minutes of constant heat flux, the lamp was turned off for 15 minutes. The storage tank was insulated properly hence, for a short period of time (15minutes) the water temperature did not decrease, instead, it has increased. After 15 minutes the measured temperature of water was 28.48ºC and 27.23ºC having a gradient of 0.0153ºC/min and 0.011ºC/min for both new and traditional models respectively. This is due to the fact that, the temperature of the working fluid after 105 minutes remained higher than the storage water temperature, which means that the storage water is still gaining heat from the working fluid. Moreover, the temperature difference between the storage tank water and the ambient was comparatively low. In addition, since the temperature was measured at the centre of the storage tank, the temperature variation at the centre is expected to be low, which is revealed in Figure 6-20. Furthermore, the final temperature of water within the storage tank after seven hours of operation for new and traditional models was 37.85ºC and 35.13ºC respectively. The total temperature increase for the new model and traditional model was 15.45ºC and 12.27ºC, illustrating a (20±1.53)% increment in storage water temperature by new proposed model.

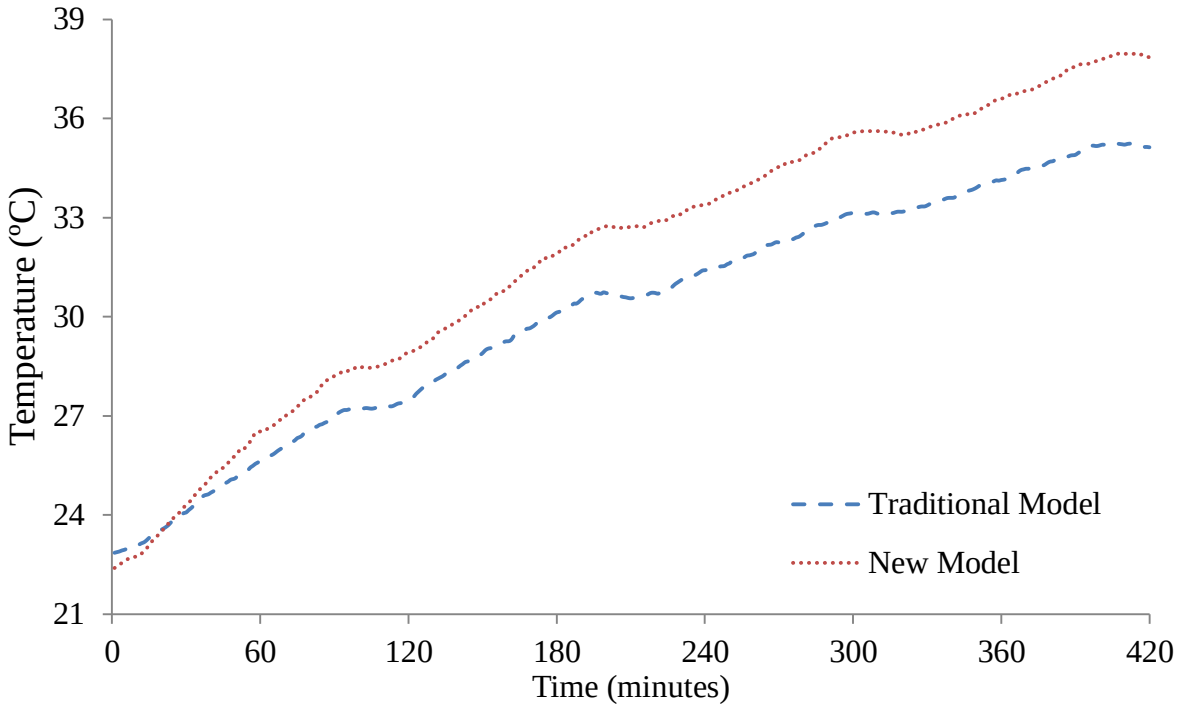

Figure 6-20 Experimental result for temperature of water within the storage tank for a constant heat flux with on-off fluctuations under no loading for different models

Figure 6-21 and Figure 6-22 depict working fluid temperature at inlet and outlet of collector for seven hours of operation with various heat fluxes, which is shown in Table 6-3. According to the Figure 6-21 during first 90 minutes of constant heat flux of 177.7W/m^2, the temperature of working fluid at the inlet of the collector has increased from 22.20ºC to 41.37ºC and from 22.21ºC to 38.45ºC for new proposed model and traditional model respectively, illustrating an (18±1.53)% increase in working fluid temperature by new proposed model. Subsequently during the 15 minutes of removed heat flux, the temperature of working fluid at inlet has decreased from 41.37ºC to 33.92ºC and from 38.45ºC to 31.74ºC for new and traditional models respectively.

Figure 6-22 illustrates that during the first 90 minutes of constant heat flux the working fluid temperature at the outlet of collector of new and traditional models has increased from 22.37ºC to 55.29ºC and from 22.44ºC to 49.44ºC correspondingly, illustrating a (21±1.53)% increment in working fluid temperature by new proposed model. In addition, during the latter 15 minutes (90-105minutes) with no heat flux, the temperature of working fluid at the outlet has decreased from 55.29ºC to 39.03ºC and from 49.44ºC to 35.23ºC for new and traditional models respectively. The new proposed model has increased the working fluid temperature at the inlet and outlet of the collector by (17±1.32)% and (13.8±1.32)% correspondingly with respect to the traditional model.

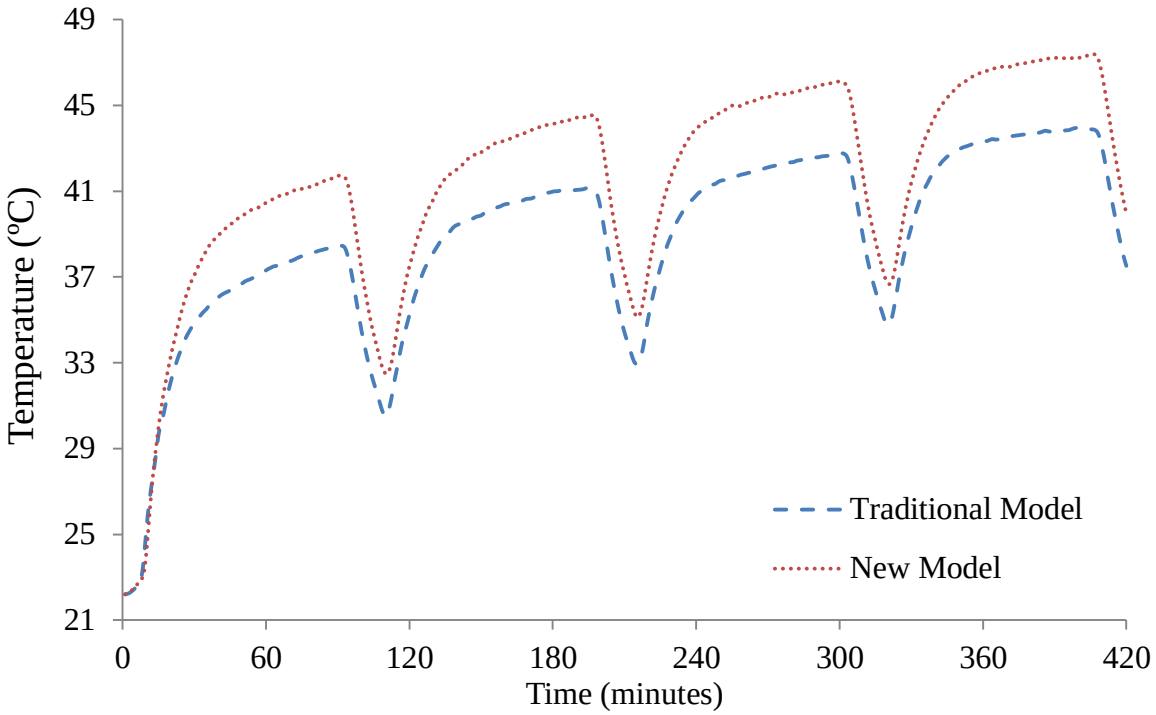

Figure 6-21 Experimental result for temperature of the working fluid at the inlet of the collector for a constant heat flux with on-off fluctuations under no loading for different models

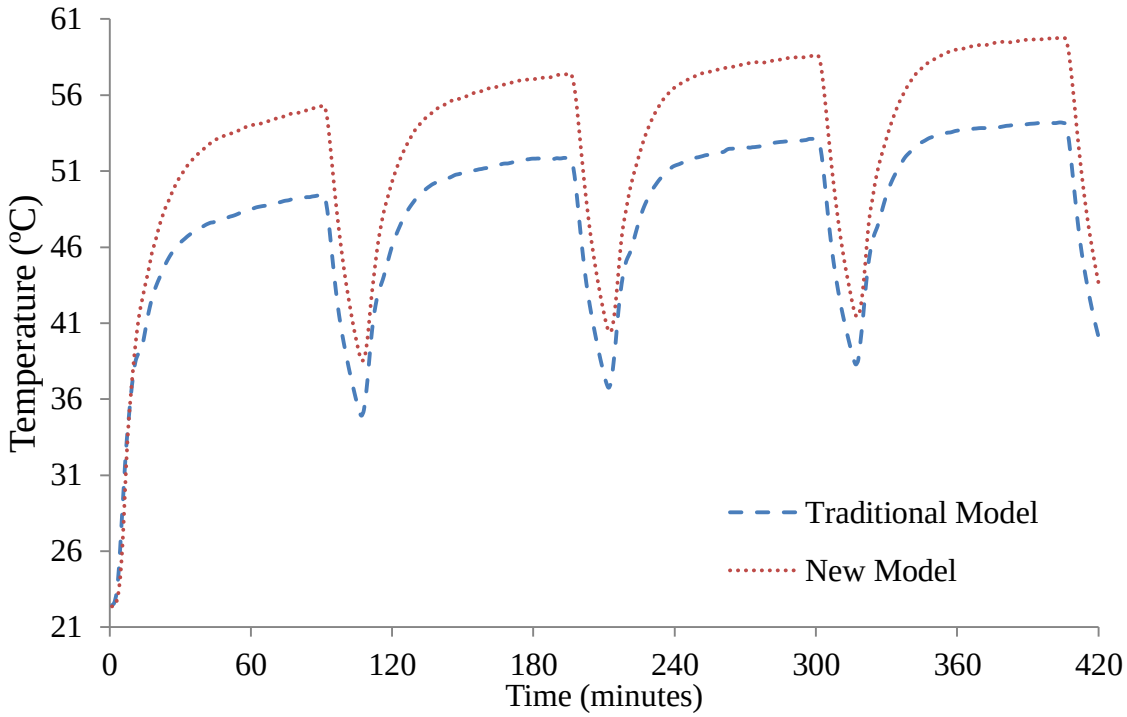

Figure 6-22 Experimental result for temperature of the working fluid at outlet of the collector for a constant heat flux with on-off fluctuations under no loading for different models

Figure 6-23 depicts the variation in mass flow rate of the working fluid within the closed loop thermo-syphon solar water heating for both traditional and new proposed model. It can be seen that the mass flow rate increased instantaneously as the heat flux is applied. Within a short period after the heat flux is added the mass flow rate reaches the maximum, after which it stabilise up to a limit. Subsequently, when the heat flux is removed, the mass flow rate starts to decrease. The rate of mass flow rate change during the heat flux addition is higher compared to the heat flux removal. Furthermore, the average mass flow rate for the traditional model is higher as compared to the new model by 17.1%.

It can be concluded that the heat flux has a significant effect on temperature and mass flow rate of the working fluid within thermo-syphon loop. Hence, it has effect on temperature of water within the storage tank and thermal performance of the system. Moreover, based on the analysis conducted before, it can be noted that the methodology implemented in the new proposed model has improved the thermal performance of thermo-syphon for both constant and transient heat flux condition.

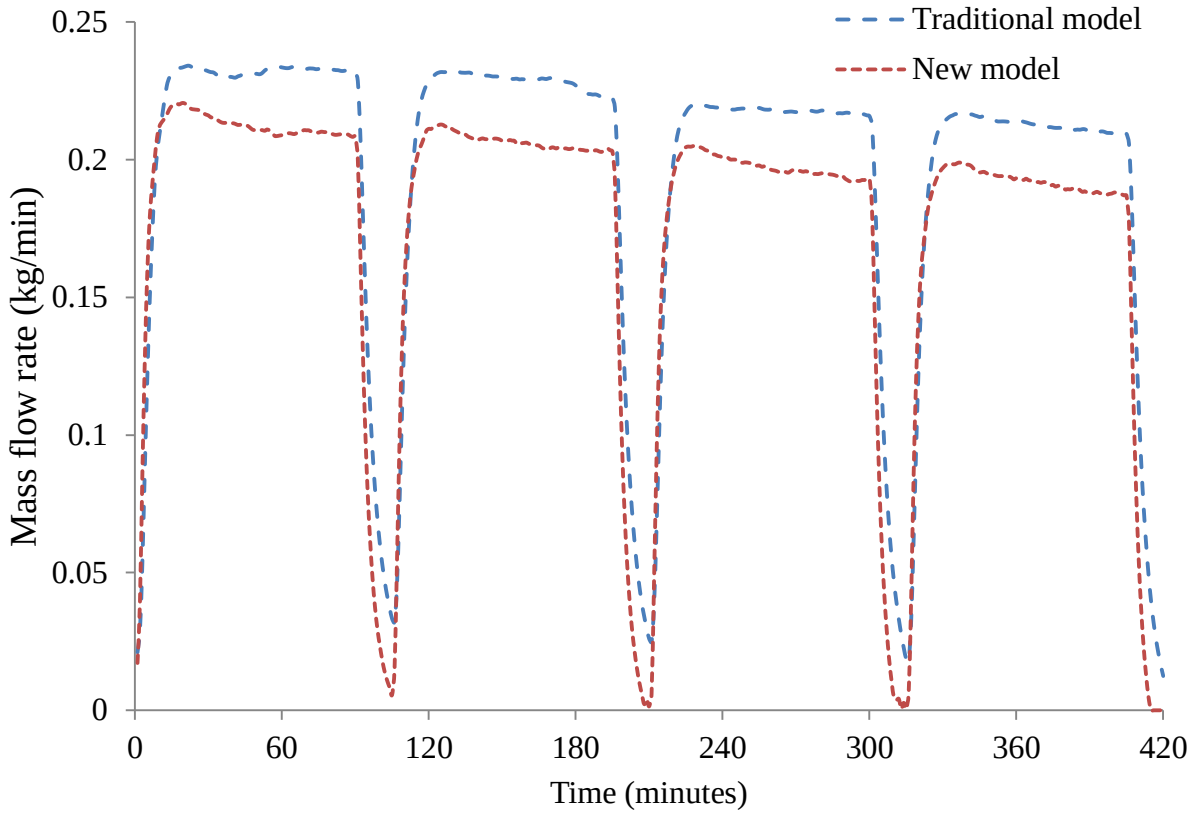

Figure 6-23 Compares the experimental results between traditional model and new model for mass flow rate of the working fluid within thermo-syphon loop for a constant heat flux with on-off fluctuations under no loading for different models

6.4. Summary of the Design Modification of the Thermo-Syphon

Throughout this chapter a novel geometric configuration for thermo-syphon has been presented. This novel geometric configuration was arrived at by careful numerical analysis of a variety of models with different heat transfer enhancement methods. The analysis revealed that pipe-in-pipe model has best heat transfer characteristics. To further strengthen the numerical design an experimental programme of work was designed and it has been conclusively proven that pipe-in-pipe model is better than conventional thermo-syphon model. The manufacturing details of such model have also been presented. Some important observations that have been made during the numerical and experimental investigations are listed below.

- The model with the straight inner pipe model and with same amount of working fluid as the traditional model shows better thermal performance compared to the other models that have been considered at the beginning of this study. Hence, the model with the straight inner pipe model and with same amount of working fluid can be considered as the optimum one
- The average velocity of working fluid within the thermo-syphon is lower for new models as compared to traditional model. This is the resultant of higher wall shear stress in new models caused by the increase of friction between the fluid and the inner surface wall
- Pressure difference between the inlet and outlet of collector is less for the traditional model as compared to the new models due to the increase of friction between working fluid and inner surface area of the riser pipe
- The quantity of heat gain in collector and the storage tank has been improved in the new models as compared to traditional model
- The thermal performance of system is higher for new model (straight model) as compared to traditional model by 12.3%

This chapter has provided information about the effectiveness of the heat enhancement device used within the thermo-syphon loop. The flow behaviour in the new models has been analysed for various characteristic parameters. Based on this analysis, in next chapter a user friendly and reliable methodology for designing a thermo-syphon has been proposed. A detailed description of this methodology has been documented in following chapter (DESIGN MODELLING).

CHAPTER 7

DESIGN MODELLING

In this chapter, a new methodology to design a closed loop thermo-syphon solar water heating system has been presented. This methodology provides a detailed investigation regarding geometrical parameters of thermo-syphon loop, thermal and flow parameters of working fluid within thermo-syphon loop. Furthermore, a new design approach based on the developed correlations has been described.

7.1. Description of the main equations to be used in the design methodology

According to the results, which have been obtained in chapter five from numerical investigations, a new methodology has been created to carry out design analysis of a closed loop thermo-syphon solar water heating system. This methodology depends on semi-empirical correlations for the prediction of Nusselt number, Reynolds number, temperature of plate and working fluid temperature at the inlet and outlet of collector, and these relations have been developed by using multiple variable regression analysis.

7.1.1. Heat Load Required

In order to determine the required amount of heat to meet the demand, several parameters should be considered such as number of persons using hot water, the inlet, and outlet temperature of water. The load on the water heating system can be represented as [133]:

$$LH = N_p V_p \rho C_p (T_{ot} - T_{it}) \tag{7.1}$$

where N_p denotes the number of persons, V_p the volume of hot water used by each person, T_{ot} the required hot water temperature and T_{it} the initial water temperature.

As the amount of water usage varies enormously person to person, it is difficult to quantify the precise amount of water use. Therefore, based on reviewed literature an average of 7.5-15L [134] water usage per day for each person has been considered in this present study.

7.1.2. Area of the Collector

The required collector area can be estimated as in Eq. (7.2).

$$\eta_c = \frac{Q_u}{A_c I_T} \tag{7.2}$$

In this case Q_u denotes the useful heat, which is similar to the heat load (LH) as in previous equation. η_c is the efficiency of the collector, I_T the solar intensity, and A_c the collector area. According to [7], the value η_c lies between (40% and 60%). In addition, the collector area depends on the number of riser pipes (np), length of riser pipes (L) and the distance between centre to centre of pipes (w), which can be represented as:

$$A_c = np * L * w \tag{7.3}$$

7.1.3. The Mean and Collector Wall Temperature

To calculate collector plate's temperature, Eq. (7.4) can be used.

$$T_{wall} = \frac{1.839\,(T_{ref})\left(\frac{q}{q_{max}}\right)^{0.0217}}{\left(1+\frac{TL}{TL_{avr}}\right)^{0.0184}(np)^{0.0874}\left(\frac{L}{d}\right)^{0.0736}\left(\frac{Time_{H.F_{min}}}{Time_{H.F_{max}}}\right)^{0.125}} \tag{7.4}$$

where T_{ref} is the mean temperature of working fluid and can be computed as:

$$T_{ref} = \frac{T_i+T_o}{2} \tag{7.5}$$

To estimate the inlet (T_i) and outlet (T_o)temperature of working fluid, Eq. (7.6) and (7.7) which have been obtained from multiple variable regression analysis in chapter five can be used.

$$\frac{T_o-T_i}{T_o-T_{in}} = \frac{0.816\left(\frac{q}{q_{max}}\right)^{0.309}\left(1+\frac{TL}{TL_{avr}}\right)^{0.5091}\left(\frac{Time_{H.F_{min}}}{Time_{H.F_{max}}}\right)^{2.403}}{(np)^{0.0089}\left(\frac{L}{d}\right)^{0.084}} \tag{7.6}$$

$$\frac{T_o+T_i}{T_o+T_{in}} = \frac{1.178(np)^{0.0023}\left(\frac{L}{d}\right)^{0.0255}}{\left(\frac{q}{q_{max}}\right)^{0.1316}\left(1+\frac{TL}{TL_{avr}}\right)^{0.3033}\left(\frac{Time_{H.F_{min}}}{Time_{H.F_{max}}}\right)^{1.004}} \tag{7.7.}$$

Assume

$$x = \frac{0.816\left(\frac{q}{q_{max}}\right)^{0.309}\left(1+\frac{TL}{TL_{avr}}\right)^{0.5091}\left(\frac{Time_{H.F_{min}}}{Time_{H.F_{max}}}\right)^{2.403}}{(np)^{0.0089}\left(\frac{L}{d}\right)^{0.084}}$$

$$y = \frac{1.178(np)^{0.0023}\left(\frac{L}{d}\right)^{0.0255}}{\left(\frac{q}{q_{max}}\right)^{0.1316}\left(1+\frac{TL}{TL_{avr}}\right)^{0.3033}\left(\frac{Time_{H.F_{min}}}{Time_{H.F_{max}}}\right)^{1.004}}$$

so,

$$T_i = \frac{(x+y-2xy)\,T_{in}}{(2-x-y)} \tag{7.8}$$

and

$$T_o = \frac{(y-x)T_{in}}{(2-x-y)} \tag{7.9}$$

While designing a thermo-syphon system the following parameters should be considered carefully:

q_{max}= maximum heat flux during the day
q=minimum heat flux during day
TL=maximum thermal loading during day
TL_{ave}=average thermal loading during day
$Time_{H.F_{min}}$= time of minimum heat flux occurrence
$Time_{H.F_{max}}$= time of maximum heat flux occurrence

7.1.4. Specifications of the Collector

In order to estimate Nusselt number, Eq. (7.10) can be used which has been obtained from multiple variable regression analysis according the results, which have been obtained from chapter five by CFD technique.

$$N_u = \frac{0.136\left(\frac{q}{q_{max}}\right)^{0.469}(np)^{0.911}\left(\frac{L}{d}\right)^{0.123}\left(\frac{Time_{H.F_{min}}}{Time_{H.F_{max}}}\right)^{0.0597}}{\left(1+\frac{TL}{TL_{avr}}\right)^{0.0213}} \tag{7.10}$$

Nu is Nusselt number and can be calculated by the following expression:

$$Nu = \frac{h\,D}{k} \tag{7.11}$$

where h is the heat transfer coefficient, calculated using the following expression:

$$h = \frac{q}{(T_{wall}-T_{ref})} \tag{7.12}$$

The riser pipe diameter can be equated by combining the above-mentioned Eq. (7.11), (7.12), and (7.10).

$$D = \frac{(T_{wall} - T_{ref})K}{q}\left[\frac{0.136\left(\frac{q}{q_{max}}\right)^{0.469}(np)^{0.911}\left(\frac{L}{d}\right)^{0.123}\left(\frac{Time_{H.F_{min}}}{Time_{H.F_{max}}}\right)^{0.0597}}{\left(1+\frac{TL}{TL_{avr}}\right)^{0.0213}}\right] \quad (7.13)$$

According to the ratio of length to diameter, the length of riser pipe can be calculated by the following form:

$$L = \frac{L}{d} * D \quad (7.14)$$

7.1.5. Mass Flow Rate

The mass flow rate of the working fluid within the thermo-syphon loop can be estimated by using the following expression:

$$\dot{m} = \frac{D\mu\pi R_e}{4} \quad (7.15)$$

where R_e is Reynolds number that can calculate by Eq. (7.16) which, has been developed in chapter five.

$$R_e = 29.375\left(\frac{q}{q_{max}}\right)^{0.233}\left(1+\frac{TL}{TL_{max}}\right)^{0.216}(np)^{0.0582}\left(\frac{L}{d}\right)^{0.531}\left(\frac{Time_{H.F_{min}}}{Time_{H.F_{max}}}\right)^{0.335} \quad (7.16)$$

7.1.6. Collector Heat Removal Factor

The heat removal factor can be calculated as:

$$F_R = \frac{Q_u}{A_c[I_T\tau_g\alpha_p - U(T_i - T_a)]} \quad (7.17)$$

The value of the solar radiation intensity (I_T) and the overall heat losses of collector (U) can be estimated by equations (Chapter one).

Eq. (7.18) can be used to predict the collector efficiency factor.

$$\acute{F} = \frac{1/U}{w\left\{\frac{1}{U[D+(w-D)F]}+\frac{1}{C_b}+\frac{1}{\pi Dh_f}\right\}} \quad (7.18)$$

where

$$C_b = \frac{k_b b}{\gamma} \pi r^2 \tag{7.19}$$

The efficiency of fin (F) is calculated as:

$$F = \frac{\tanh\left[\frac{M(w-D)}{2}\right]}{\frac{M(w-D)}{2}} \tag{7.20}$$

$$M = \sqrt{\frac{U}{k_t \delta}} \tag{7.21}$$

The net energy (useful heat) achieved by the working fluid from the solar energy, can be calculated as:

$$Q_u = \dot{m} C_p (T_o - T_i) \tag{7.22}$$

7.2. Design Procedure

The design process in the present work endeavours to track the thermal performance of a closed loop thermo-syphon solar water heating system. This process enables the designer to invetigate all possible configurations of the system numerically, which reduces the experimental work, saves money and time.

7.2.1. Assumptions used in the Design Methodology

1. Frictional pressure losses in the pipes are neglected because the loop pipe lengths are short, the mass flow rate is low, and the dominated pressure gradient is gravitation which is several orders of magnitude greater than the friction pressure drop
2. The upriser and downcomer are assumed to be well insulated and the thermal losses from these components are ignored
3. Through-out the thermo-syphon loop, the saturation temperature is constant

7.2.2. Design Steps

In order to calculate the theoretical value of useful energy (Q_U), various parameters should be calculated. The following section describes the steps and the sequence of this calculation procedure. The required parameters that need to be considered to obtain the useful energy, are the overall heat transfer coefficient (U), the heat transfer coefficient (h), the mass flow rate of working fluid within the thermo-syphon loop ($\dot{m}$), diameter of riser pipe (D), inlet (T_i), and outlet (T_o) temperatures of the working fluid, mean temperature of the working fluid (T_{ref}), temperature of the plate (T_{wall}), area of the collector (A_c) and the distance between two riser pipes (w).

The design procedure is explained in the following steps:

1. The number of persons who will be using the facility is an input.
2. The initial temperature of water within the storage tank is an input, which will depend on the weather, and determines the final temperature of water (required water's temperature).
3. Calculate the total heat load by using Eq. (7.1)
4. The number of days in the year (N), geographic characteristics of location ($\phi, lst, lioc$), tilt angle of collector (β), and standard time (ST) are defined
5. The given operating conditions air temperature (T_a), velocity of air (V), the initial temperature of working fluid (T_{in}) are also known.
6. System properties ($\varepsilon_p, \varepsilon_g, k_s, l_s, c_p, k_f, \alpha_p, k_p, \delta$) are defined
7. Calculated solar radiation intensity (I_T) by using set of equations presented in section 1.8.1
8. Calculate the heat fluxes at each hour by using Eq. (3.21)
9. Assume the value of the efficiency of thermo-syphon (0.4 – 0.6) and then keep it constant
10. Calculate area of collector (A_c) by using Eq. (7.2)
11. Calculate the useful heat Q_1 in (W) based on minimum the heat flux (step 8) and collector area (step 10)
12. Assume the riser pipe number and L/d ratio
13. Calculate the inlet (T_i) and outlet (T_o) temperatures by using Eq. (7.8) and (7.9) respectively and hence calculate the mean temperature of working fluid (T_{ref}) by using Eq. (7.5). After that, calculate the mean temperature of the absorber plate (T_{wall}) by using (7.4). Then calculate the diameter of riser pipe (D) and Reynolds number (Re) by using Eq. (7.13) and (7.16) respectively. Hence, calculate the mass flow rate of working fluid ($\dot{m}$) within the thermo-syphon loop using Eq. (7.15)
14. Calculate the heat transfer coefficient by using Eq. (7.11) and (7.12)
15. Calculated the heat loss coefficient (U) using set of equations presented in section 1.8.3
16. Calculate the length of the riser pipe and the distance between any two riser pipe (W) using Eq. (7.2), (7.14) and (7.3) respectively
17. Calculate width of collector based on collector area and length of the riser pipe
18. Calculate the useful heat gain at collector Q_2 based on different combination of riser pipe number and L/d ratio by using Eq. (7.22)
19. Compare between the useful heat gain Q_2 (step 18) and the useful heat Q_1 (step 11)
20. Record and save all cases cover the useful heat gain at the collector

Figure 7-1 shows a flow chart regarding the design methodology adopted in this study.

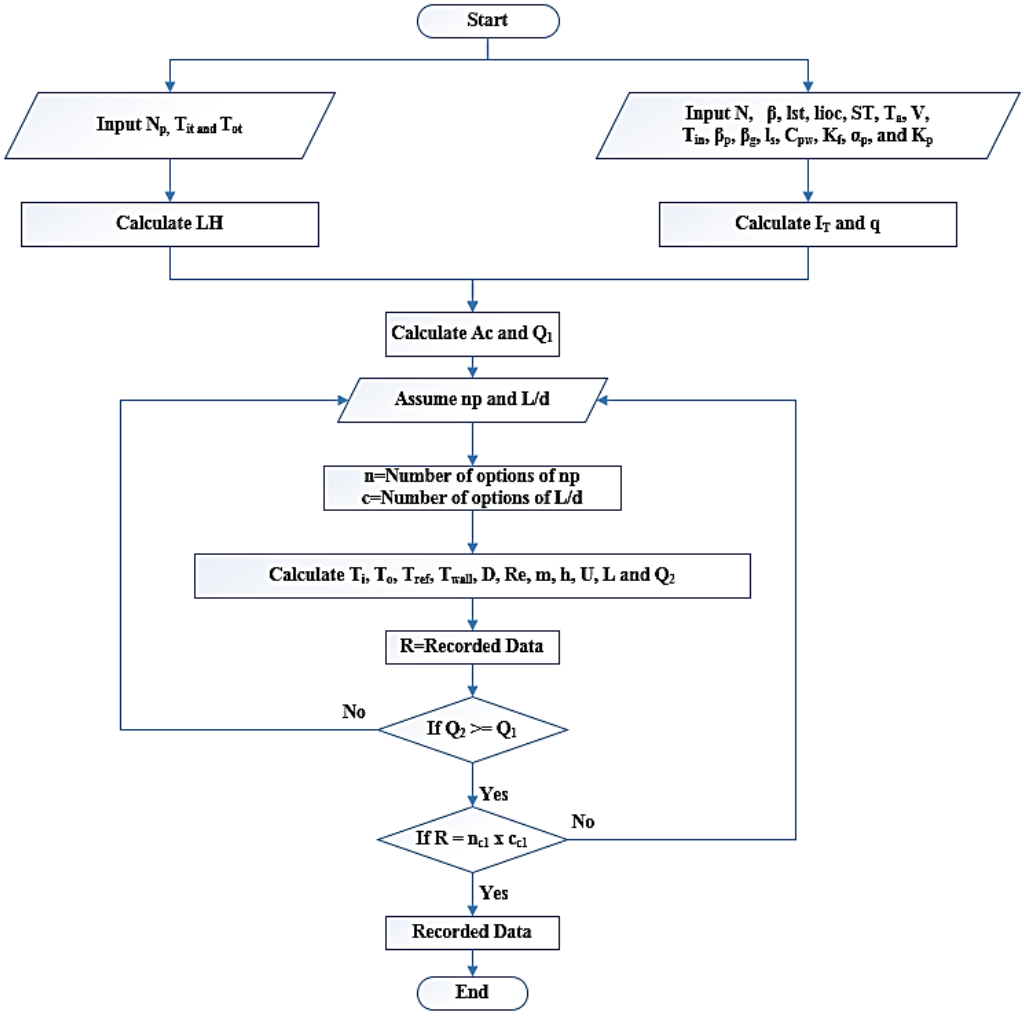

Figure 7-1 Flow chart of the design methodology

7.3. The Cost model for the thermo-syphon

The total cost of (system) a closed loop thermo-syphon solar water heating system consists of three main parts: manufacturing cost, operation cost and maintenance cost.

$$C_{Total} = C_{Manufacturing+}C_{Operation} + C_{Maintenance} \quad (7.23)$$

Being a closed loop thermo-syphon solar water heating system does not have external devices like pump and it depends on solar energy, which is completely free, therefore the operation cost and maintenance cost can be assumed to be negligible. Hence, the total cost will be equal to manufacturing cost as shown in below:

$$C_{Total} = C_{Manufacturing} \quad (7.24)$$

Generally, manufacturing cost consists of two parts: the cost of parts of thermo-syphon and personal cost as shown in Eq. (7.25).

$$C_{Manufacturing} = C_{Parts} + C_{Personal} \quad (7.25)$$

As mentioned in section 1.4 thermo-syphon solar water heating system consists of a storage tank, working fluid, and thermo-syphon loop. The common working fluid within thermo-syphon loop is water and it is inexpensive. Therefore, the cost of the working fluid can be ignored. Thus, cost for the component can be written as:

$$C_{Parts} = C_{thermo-syphon\,loop} + C_{tank} \quad (7.26)$$

Thermo-syphon loop commonly consists of three sections namely solar collector, condenser, and connecting pipe (upriser and downcomer). Solar collector mainly consists of; riser pipes, absorber plate, glazing cover and insulation. All these components are assembled in a proper encasement.

$$C_{collector} = C_{pipes} + C_{absorber\,plate} + C_{insulation} + C_{casing} \quad (7.27)$$

7.3.1. Cost of the Pipe

The pipe cost can be estimated, by Eq. (7.28) which is given by [135]. This equation uses the dimension of the pipe to calculate the cost.

$$C_{pipe} = \rho * \pi * (D - t) * t * L * C_1 \quad (7.28)$$

where D, is the outer diameter of pipe (mm), t is thickness of pipe (mm), L is the total length of pipes (km), ρ is density of material and C_1 is cost of pipe material (£/ton).

7.3.2. Cost of Absorber Plate

Absorber plate cost depended on volume and material. Most of the absorber plate comprises of copper due it's higher conductivity. The absorber plate cost can be calculated by using the formula below.

$$C_{absorber\,plate} = \rho * l * w * t * C_2 \quad (7.29)$$

where l, w, t and C_2 denotes the length of plate, width of plate, thickness of plate ρ is density of material and the unit of cost is £/ton.

7.3.3. Cost of Insulation

The insulation cost can be calculated from the equation formulated below, which is a function of insulation volume:

$$C_{insulation} = l * w * t * C_3 \quad (7.30)$$

where C_3 denotes the insulation cost per one cubic meter.

7.3.4. Cost of the Casing

The aluminium is used as the casing material for a closed loop thermo-syphon solar water heating system for several reasons such as inexpensive, light, higher resistance and easy manufacturing. Eq. (7.31) denotes an equation that can be implemented to estimate the cost for aluminium per volume.

$$C_{casing} = l * w * t * C_4 \quad (7.31)$$

where C_4 denotes the aluminium cost per one cubic meter.

7.3.5. Cost of the Tank

Based on the capacity and material, the cost for the storage tank can be determined. To estimate the cost of tank, the formula below can be used, which depended on capacity and material of tank.

$$C_{tank} = C_p * C_5 \quad (7.32)$$

where C_p and C_5 denotes the capacity of tank and the cost of tank per 60L capacity.

7.4. The Optimisation Model

Design optimisation of thermo-syphon is very important in order to make it an efficient and commercially available device. The following section of this chapter includes the process to define the optimised model. The thermo-syphon will be designed based on the useful heat that covers the minimum heat flux in the collector and the lowest manufacturing costs as well. In order to obtain the optimised case certain steps need to be followed, which are mentioned below:

1. Input all cases that cover the useful heat gain at the collector
2. Calculate the total length of pipes
3. Calculate the cost of pipes by using Eq. (7.28)
4. Estimate the capacity of the storage tank based on number of persons
5. Calculate the storage tank cost by using Eq. (7.32)

6. Calculate width of collector based on collector area and length of the riser pipe
7. Calculate the cost of plate, insulation, casing by using Eq.(7.29), (7.30) and (7.31) respectively
8. Calculate the total cost for all cases that cover the useful heat gain
9. Choose case which has minimum total cost as optimal case

Figure 7-2 shows a flow chart regarding the optimisation model displayed in this study.

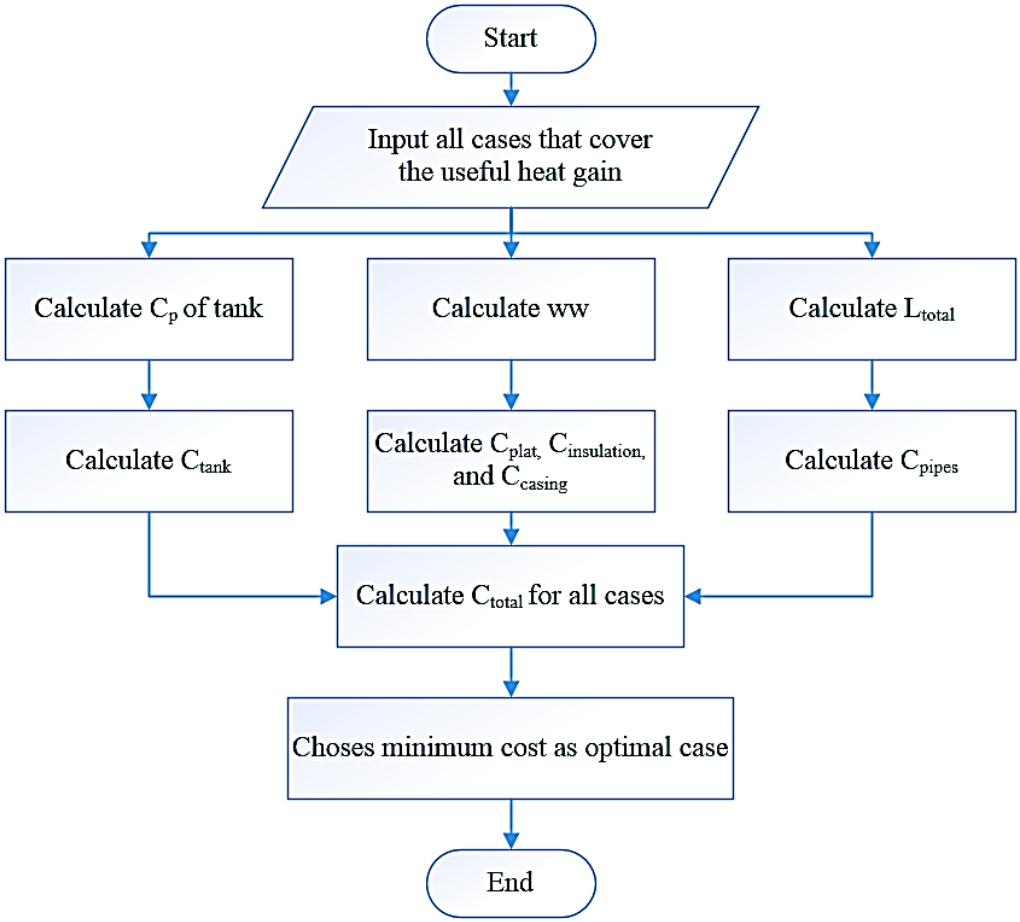

Figure 7-2 Flow chart of the optimisation model

7.5. Design Example for a Closed Loop Thermo-Syphon System

This section will illustrate the procedure and the steps of designing a thermo-syphon system for a small family with five persons living in Huddersfield. Two calculations will be shown for both traditional and new model. In addition, the cost for each model will be estimated for comparison purpose. Following parameters have been assumed for this sample calculation.

Assume, the total solar radiation intensity (I_T) value is 5600W/m^2.day, the initial water temperature is 20^{o}C, required water temperature is 60ºC, the collector efficiency is 50% and the initial temperature of working fluid is 15ºC. Moreover, the total solar radiation intensity can also be calculated by the equation and MATLAB code provided in the APPENDIX B. Heat fluxes and thermal loading are presented in the table below for different time.

Time (hour)	9-10	10-11	11-12	12-13	13-14	14-15	15-16
Heat flux (w/m^2)	196	313	401	433	401	313	196
Thermal loading (W)	4.25	3.75	3.4	2.5	2.5	3.25	3.25

Solution:

7.5.1. Traditional Model

1. From Eq. (7.1) can be calculated the amount of heat to heat the water within the storage tank

$$\mathrm{LH} = (5 * 15 * 4.185 * (60 - 15))/3.6$$

$$\mathrm{LH} = 3923\mathrm{W/day}$$

From Eq. (7.2) can be calculated collector area.

$$\mathrm{A_c} = \frac{\mathrm{Q_u}}{\eta_c \mathrm{I_T}}$$

$$\mathrm{A_c} = \frac{3923}{0.5*5600} = 1.403\mathrm{m}^2$$

2. Calculate the useful heat Q_1 in (W) based on minimum heat flux and collector area as below:

$$\mathrm{Q_1} = 196 * 1.403 = 274.98\mathrm{W}$$

3. Assume number of riser pipes =6, and the L/d ratio of riser pipes =100

4. From Eq. (7.8) and (7.9), the temperature of the working fluid at inlet and outlet of the collector can be calculated

$$x = \frac{0.816\left(\frac{196}{433}\right)^{0.309}\left(1+\frac{4.25}{3.24}\right)^{0.5091}\left(\frac{10}{12}\right)^{2.403}}{(6)^{0.0089}(100)^{0.084}} = 0.4217$$

$$y = \frac{1.178(6)^{0.0023}\,(100)^{0.0255}}{\left(\frac{196}{433}\right)^{0.1316}\left(1+\frac{4.25}{3.24}\right)^{0.3033}\left(\frac{10}{12}\right)^{1.004}} = 1.3752$$

$$T_i = \frac{(1.3752+0.4217-2*0.4217*1.3752)*15}{(2-0.4217-1.3752)} = 47.04^oC$$

$$T_o = \frac{(1.3752-0.4217)T_{in}}{(2-0.4217-1.3752)} = 70.4^oC$$

By using Eq. (7.5) can be evaluated that the reference temperature of working fluid

$$T_{ref} = \frac{47.04+70.4}{2} = 58.72^oC$$

5. From Eq. (7.4) can be estimated that the plate temperature of collector will be

$$T_{wall} = \frac{1.839\,(58.72)\left(\frac{196}{433}\right)^{0.0217}}{\left(1+\frac{4.25}{3.24}\right)^{0.0184}(6)^{0.0874}(100)^{0.0736}\left(\frac{10}{12}\right)^{0.125}} = 64.68^oC$$

6. From Eq. (7.13) can be estimated that the inner diameter of the riser pipe will be

$$D = \frac{(64.68-58.72)*0.6}{196}\left[\frac{0.136\left(\frac{196}{433}\right)^{0.469}(6)^{0.911}(100)^{0.123}\left(\frac{10}{12}\right)^{0.0597}}{\left(1+\frac{4.25}{3.24}\right)^{0.0213}}\right] = 0.0162m$$

7. From Eq.(7.14) can be calculated that the length of riser pipe is:

$$L = \frac{L}{d} * D$$

$$L = 100 * 0.0162 = 1.62m$$

8. From Eq. (7.13) can be estimated that the distance from centre to centre of riser pipe is:

$$1.403 = 6 * 1.62 * w$$

$$w = 0.144m$$

9. From Eq. (7.16) can be estimated that the Reynolds number is:

$$R_e = 29.375\left(\frac{196}{433}\right)^{0.233}\left(1+\frac{4.25}{3.24}\right)^{0.216}(6)^{0.0582}(100)^{0.531}\left(\frac{10}{12}\right)^{0.335}=352.48$$

10. By using Eq. (7.15) can be calculated that the mass flow rate of working fluid within the thermo-syphon loop as:

$$\dot{m} = \frac{0.0162*0.00103*3.14*352.4}{4} = 0.0046 \text{Kg/s}$$

11. From Eq. (7.12) can be calculated that the heat transfer coefficient is:

$$h = \frac{196}{(64.68-58.72)} = 32.88 \text{ W/m}^2.^o\text{C}$$

12. Calculate the useful heat gain in collector by using Eq. (7.22)

$$Q_2 = 0.0046 * 4185 * (70.4 - 47.04) = 449.703\text{W}$$

13. Repeat all the steps above for all options of the number of the riser pipes and L/d ratio
14. Take just the cases which are covered the useful heat Q_1
15. In order to estimate the cost of thermo-syphon system, the following steps can be used

According to the current market, components prices of thermo-syphon listed in Table 7-1

Table 7-1 Various costs of thermo-syphon components

Components	Price
Copper	6300£/ton
Sheet aluminium	13654£/m^3
Insulation	347£/m^3

To estimate the cost of pipe, total length of thermo-syphon loop should be calculated first. In this case, the total length of pipes can be calculated as below:

The total pipes length= (1.62*6) + (1.36*2) +0.5+2.12+0.866=15.92m

Figure 7-3 depicts the dimensions of thermo-syphon loop and by using Eq. (7.28), the cost of pipes can be calculated assuming that the pipe has a thickness of 0.9mm.

$$C_{pipe} = (8.95 * 3.14 * (18 - 0.9) * 0.9 * 0.01592 * 6300)/1000 = £43.37$$

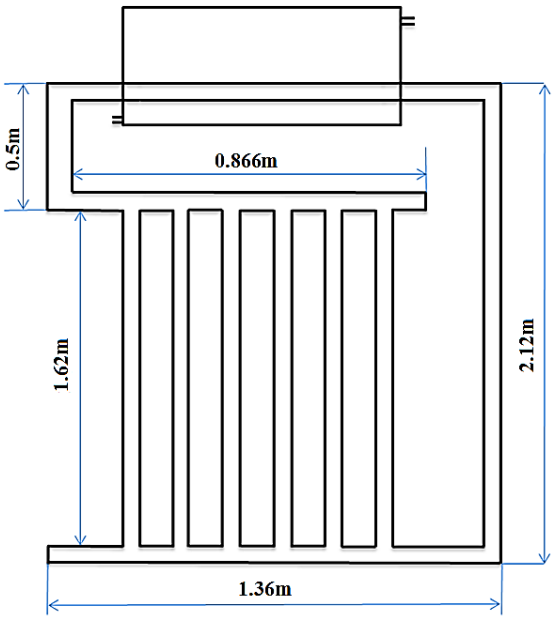

Figure 7-3 The dimensions of thermo-syphon loop (traditional model)

By using Eq. (7.29), absorber plate cost can be calculated.

$$C_{\text{absorber plate}} = (8.95 * 1.62 * 0.866 * 0.0007 * 6300)/1000$$

$$=£55.372$$

To estimate cost of insulation, Eq. (7.30) can be used.

$$C_{\text{insulation}} = (((1.62 * 0.866) + ((2 * 0.866) + (1.62 * 2)) * 0.18) * 0.05) * 347$$

$$=£39.869$$

By using Eq. (7.31) the casing cost can be evaluated.

$$C_{\text{casing}} = (((1.62 * 0.866) + ((2 * 0.866) + (1.62 * 2)) * 0.18) * 0.003) * 13654$$

$$=£94.13$$

While, to calculate the storage tank cost, Eq. (7.32) can be used.

$$C_{\text{tank}} = 75 * 0.75$$

$$=£56.25$$

Assume that the personal cost of £50.
Finally, the total cost for the system is £338.991, which can produce 449.703W. Therefore the cost for per unit heat is 0.754£/W.

Repeat the above steps to calculate the total cost for all cases. The optimum case has been chosen with two prior conditions. The first condition is the useful heat gain should be close to the heat achieved from the Sun rays to attain best thermal performance. The second condition is the cost for the system should be less. Table 7-2 summarises the total cost of thermo-syphon per watt thermal output for various combinations of riser pipes number and length to diameter ratio of the riser pipe. It can be clearly seen that the case with 6 riser pipes and L/d ratio of 100 is the optimum case.

Table 7-2 The cost per watt for different number of pipes and L/d ratio

L/d	np					
	5	6	7	8	9	10
50	0.8709	0.8281	0.8032	0.7899	0.7849	0.7861
60	0.8283	0.7957	0.7790	0.7731	0.7749	0.7829
70	0.8000	0.7756	0.7660	0.7666	0.7751	0.7902
80	0.7808	0.7635	0.7604	0.7675	0.7830	0.8061
90	0.7679	0.7572	0.7603	0.7741	0.7974	0.8300
100	0.7597	0.7450	0.7646	0.7857	0.8179	0.8624
110	0.7594	0.7564	0.7726	0.8019	0.8449	0.9046
120	0.7620	0.7606	0.7841	0.8228	0.8791	0.9586
130	0.7746	0.7902	0.8229	0.8733	0.9462	1.0518
140	0.7771	0.7993	0.8408	0.9042	0.9980	1.1401
150	0.7813	0.8107	0.8622	0.9415	1.0626	0.0000
Minimum value	0.7594	0.7550	0.7603	0.7666	0.7749	0.0000
Optimum value		0.7450				

7.5.2. A design example for the novel Model

A new design proposed to increase surface area of the riser pipe without changing amount of working fluid within the thermo-syphon loop is presented here. The diameter of riser pipe is very important in this case, hence equality of the volume of working fluid within the thermo-syphon loop, can be used to calculate the diameter for new model from the constraint as shown below:

$$V_{trad.} = V_{new} \tag{7.21}$$

1. Assume the length of riser pipe for new model is equal to 0.95 of length of riser pipe for traditional model. While, length of a closed tube is equal to 0.9 of length of riser pipe for traditional and the diameter is equal to the diameter of riser pipe for traditional model

$$V_{trad.} = \frac{\pi}{4}(D_{trad.})^2 * l$$

$$V_{trad.} = \frac{\pi}{4}(0.0162)^2 * 1.62$$

$$V_{trad.} = 0.00033391 m^3$$

$$V_{new.} = \frac{\pi}{4}(D_{new})^2 * 0.95 * l - \frac{\pi}{4}(D_i)^2 * 0.9 * l$$

$$V_{new} = V_{trad.}$$

$$\frac{\pi}{4}(D_{new})^2 * 0.95 * l - \frac{\pi}{4}(D_i)^2 * 0.9 * l = 0.00033391 m^3$$

$$(\frac{\pi}{4}(D_{new})^2 * 0.95 * 1.62) - (\frac{\pi}{4}(0.0162)^2 * 0.9 * 1.62) = 0.00033391 m^3$$

$$D_{new} = 0.0229 m$$

2. To calculate the inner diameter of the riser pipe for new model, first step is calculated hydraulic diameter, as bellow:

$$D_H = D_{new} - D_i = 0.0229 - 0.0162 = 0.0067 m$$

3. Calculate Reynolds number by using Eq. (7.16) based on hydraulic diameter, then calculate mass flow rate of working fluid by using Eq. (7.15)

$$R_e = \frac{37.94\left(\frac{196}{433}\right)^{0.206}(230)^{0.531}}{\left(1+\frac{4.25}{3.24}\right)^{0.147}(6)^{0.942}} = 548.48$$

$$\dot{m} = \frac{0.0067 * 0.00103 * 3.14 * 548.48}{4} = 0.00297 kg/s$$

4. Calculate temperature of working fluid at inlet and outlet of collector by using Eq. (7.8) and (7.9) based on hydraulic diameter

$$x = \frac{0.4113\left(\frac{196}{433}\right)^{0.2085}\left(1+\frac{4.25}{3.24}\right)^{0.5801}}{(6)^{0.0497}(230)^{0.2403}} = 0.4217$$

$$y = \frac{1.6106(6)^{0.0654}\,(230)^{0.3024}}{\left(\frac{196}{433}\right)^{0.245}\left(1+\frac{4.25}{3.24}\right)^{0.733}} = 1.3752$$

$$T_i = \frac{(2xy-x-y)\,15}{(2-x-y)} = 47.04^oC$$

$$T_o = \frac{(x-y)15}{(2-x-y)} = 70.4^oC$$

5. By using Eq. (7.5) can be evaluated that the reference temperature of working fluid is:

$$T_{ref} = \frac{51.48+75.1}{2} = 63.29^oC$$

6. Calculate temperature of collector plate by using Eq. (7.4) based on hydraulic diameter

$$T_{wall} = \frac{1.672\,(59.66)\left(\frac{196}{433}\right)^{0.0317}\left(1+\frac{4.25}{3.24}\right)^{0.117}}{(6)^{0.0874}(230)^{0.0741}} = 64.68^oC$$

7. From Eq. (7.12) can be calculated that the heat transfer coefficient is:

$$h = \frac{196}{(65.86-63.29)} = 76.26\ W/m^2.^oC$$

8. In order to estimate the cost of thermo-syphon system, the steps are shown below:

As mention in previous section that to estimate the cost of pipes, first total length of pipes for the thermo-syphon loop should be calculated. Since, there are two pipes with different diameter; length of each type of diameter should be calculated separately.

The total length for 16.2mm diameter pipes

$$= (1.45 * 6) + (1.36 * 2) + 0.5 + 2.12 + 0.866 = 14.9m$$

The total length for 22.9mm diameter pipes $= (1.53 * 6) = 9.18m$

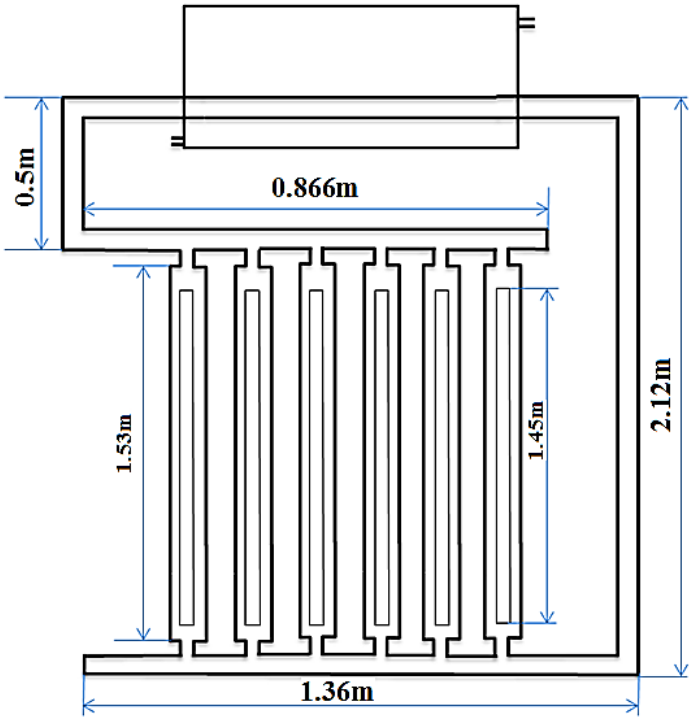

Figure 7-4 The dimensions of thermo-syphon loop (new model)

From Eq. (7.28), the cost of pipes can be calculated.

$$C_{pipe} = (8.95 * 3.14 * (18 - 0.9) * 0.9 * 0.0149 * 6300)/1000 = £40.59$$

$$C_{pipe} = (8.95 * 3.14 * (25 - 1) * 1 * 0.00918 * 6300)/1000 = £39$$

$$C_{total\ pipes} = £79.59$$

By using Eq. (7-29), absorber plate cost can be calculated.

$$C_{absorber\ plate} = (8.95 * 1.62 * 0.886 * 0.0007 * 6300)/1000$$

$$= £55.372$$

To estimate cost of insulation, Eq. (7.30) can be used.

$$C_{insulation} = (((1.62 * 0.866) + ((2 * 0.866) + (1.62 * 2)) * 0.18) * 0.05) * 347$$

$$= £39.869$$

By using Eq. (7-31), the casing cost can be evaluated.

$$C_{casing} = (((1.62 * 0.866) + ((2 * 0.866) + (1.62 * 2)) * 0.18) * 0.003) * 13654$$

$$=£94.13$$

While, to calculate the storage tank cost, Eq. (7-32) can be used.

$$C_{tank} = 75 * 0.75$$

$$=£56.25$$

Assume that the personal cost of £50.

Finally, the total cost is £375.211.

Based on aforementioned analysis of cost and the heat gain in the storage tank for both a new model and the traditional model can be explained as below.

1- The total cost of traditional model is £338.991while the total cost of the new model is £375.211. That the total cost for new model has increased by 10.6% in comparison to traditional model
2- Based on results from previous chapter the heat gain in the storage tank for new model is higher as compared to traditional model by 12.3%. That means that the thermal performance of the new model is higher than as compared to the traditional model
3- It can be concluded that although the cost of new model is higher than traditional model but the output from the new model is higher than output of traditional model

7.6. Design Charts for Designing Thermo-syphons

In order to make the design of thermo-syphon more easer, designing charts of thermo-syphon configuration have been generated. The following sections show the evaluated design parameters and the performance parameters of a closed loop thermo-syphon solar water heating system for various combinations of geometrical and operational parameters. These results represent the case of Huddersfield location with 15th of March's heat flux and thermal loading of a weekday. All charts have been created based on the assumptions below

q_{max}= maximum heat flux during day
q=minimum heat flux during day
TL=maximum thermal loading during day
TL_{ave}=average thermal loading during day

$Time_{H.F_{min}}$ = time of minimum heat flux occurrence
$Time_{H.F_{max}}$ = time of maximum heat flux occurrence

7.6.1. Geometrical Parameters

Figure 7-5 depicts the variation in collector area with respect to the number of hot water users. According to the figure, the required collector area increases as the number of water users increased. Moreover, it can be seen that if the number of users and efficiency of collector remains constant, higher output temperature can be gained by increasing the collector area. Moreover, the collector area requirement is a function of number of users. It increases from 1.24m^2 to 3.32m^2 when the number of users increased from three to eight. Furthermore, the demand output temperature has a significant effect on the collector area. At demand output temperature of 60ºC for 8 persons with the efficiency of 50%, the collector area was 2.41m^2 while it was 3.02m^2 at demand output temperature of 70ºC. It can further be concluded that the demand output temperature has more effect on the collector area as compared to number of users.

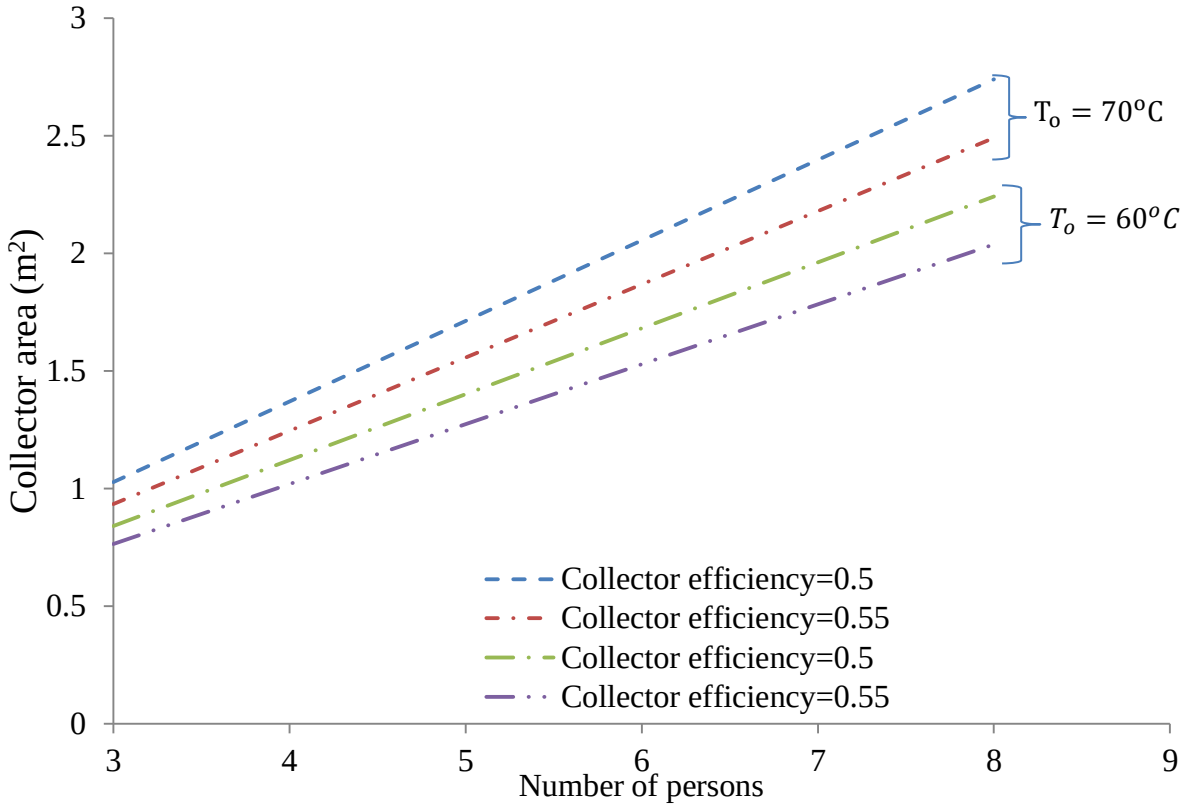

Figure 7-5 Collector area variations against number of people for various efficiency of collector and different required temperature

After determining the collector area from figure 7-5 based on the number of persons and required water temperature, the next step is to calculate the useful heat gain in collector based on minimum heat flux.

$$H.G_{collector} = q_{min} * A_c \quad (7.22)$$

From Figure 7-6 and based on the value of useful heat gain in collector which is calculated from Eq. (7.22), the number of riser pipes and L/d ratio can be defined. The number of riser pipes and L/d ratio determine geometrical parameters of thermo-syphon such as the diameter, length of the riser pipes etc. Furthermore, the number of the riser pipes and L/d ratio can also be used to determine the thermal parameters such as Reynolds number and heat transfer coefficient.

Figure 7-6 depicts the variation in heat gains within collector for various L/d ratios of the riser pipes at a heat flux corresponding to 15th March under thermal loading condition of weekday. It can be seen that the both of L/d and number of riser pipe have a significant effect on useful heat. However, the effect of L/d ratio of riser pipe on useful heat is higher as compared to number of riser pipes. For example, increase in L/d ratio from 50 to 100 at number of riser pipe of 5, the useful heat will increase by 41%, while incresing number of riser pipe from 5 to 9 at L/d=50 the useful heat will increase by 23%. From this investigation, it can be concluded that the length to diameter ratio of riser pipe has more significant impact on the increase of collector's area in comparison with the number of pipes. Therefore, increasing the length to diameter ratio of the riser pipes will help to increase the surface area of the collector and improve the useful heat gain of the system. From this chart, useful heat within collector can be obtained based on number of riser pipe and length to diameter ratio of riser pipe.

Figure 7-7 depicts the variation in diameter of riser pipe for a various L/d ratios of the riser pipes at a heat flux corresponding to 15th March under thermal loading condition of the weekday. It can be seen that the diameter of the riser pipe increases with an increase in the number of the riser pipes for L/d less than 70, which is the average value of L/d values (50-100). However, for L/d more than 70, the diameter of riser pipe starts to increase with an increase of riser pipe number and after a certain riser pipe number it (diameter) starts to decrease. Furthermore, increase in L/d leads to decrease in the diameter of riser pipe for any number of riser pipes. This happens in order to keep the same collector area, for example, with an increase in L/d from 50 to 100 at a constant number of the riser pipes 9, the diameter will decrease from 0.016m to 0.012m. This leads to decrease in distance between pipe to pipe and increase in length of the riser pipe. It can be concluded that the L/d ratio has a significant effect on diameter value of the riser pipe as compared to the number of riser pipe. From this chart, the diameter of riser pipe can be obtained based on number of riser pipe and length to diameter ratio.

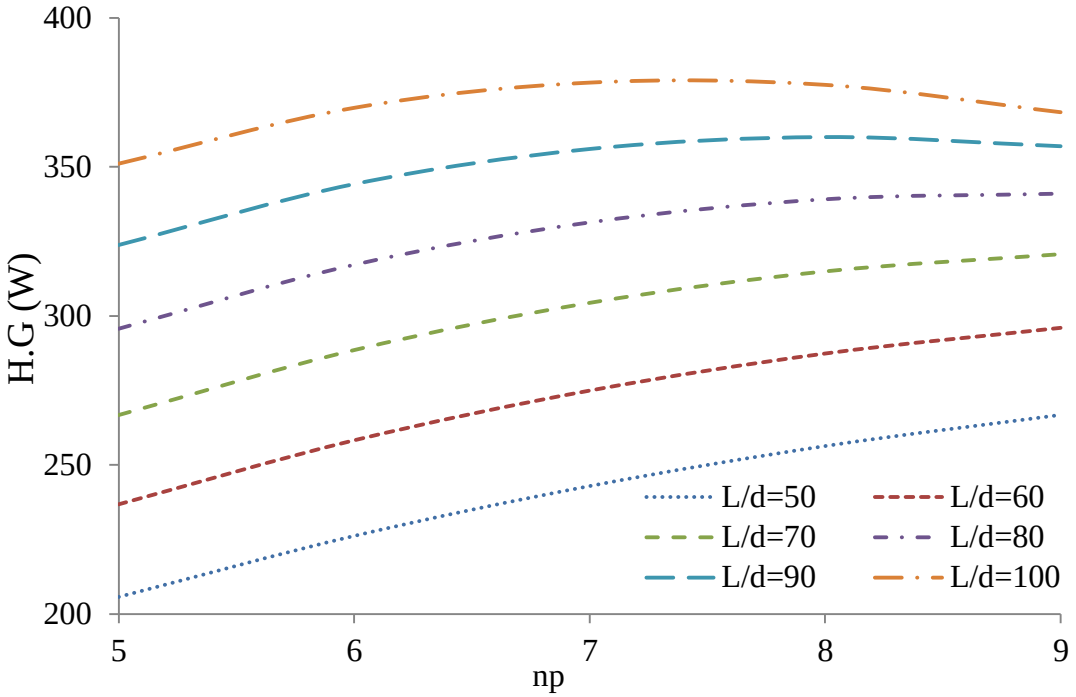

Figure 7-6 Heat gains variations within collector against number of riser pipe for various L/d ratios on 15th March

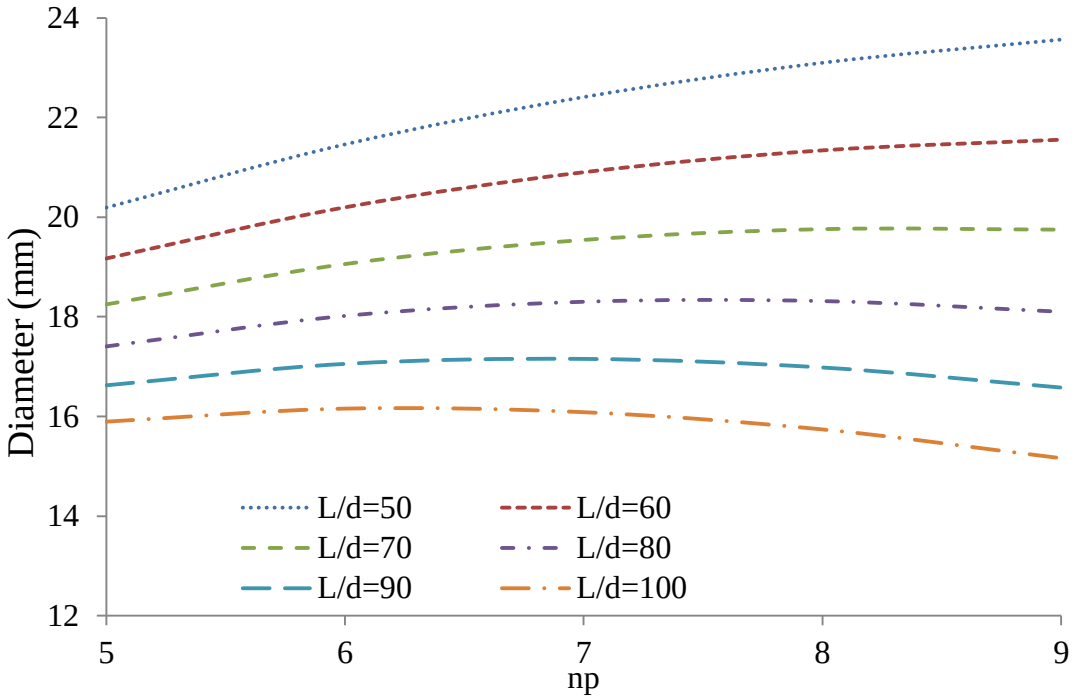

Figure 7-7 Diameter of riser pipe against number of riser pipe for various L/d ratios at minimum heat flux on 15th March

Eq. (7.3) depicts that the collector area is a function of riser pipe's length, numbers of riser pipes and distances between two riser pipes. Therefore, it is important to estimate the riser pipe length to define the collector length. Figure 7-8 depicts the variation in the length of riser pipe for various L/d ratios of the riser pipes at a heat flux corresponding to 15th March under thermal loading condition of the weekday to meet the useful heat requirement. It can be seen that the length of riser pipe increases with increase in L/d value. From this chart, the length of riser pipe can be obtained based on number of riser pipe and length to diameter ratio.

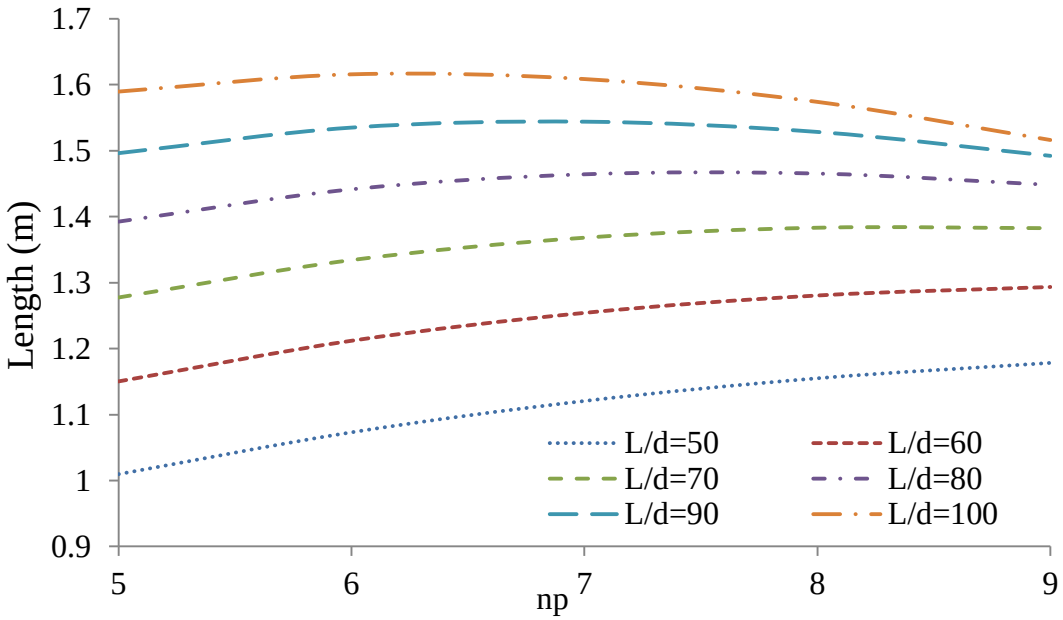

Figure 7-8 Length of riser pipe against number of riser pipe for various L/d ratios on 15th March

According to the Eq. (7.3), the distance between two neighbouring riser pipes is another important parameter to define the collector area, which indicates the performance of thermo-syphon. The effect of number of riser pipes and L/d of the riser pipes on the distance between pipes for a fixed collector area has been investigated in this sector and is shown in the Figure 7-9. This investigation has been conducted for various L/d ratios of the riser pipes at a heat flux corresponding to 15th March under thermal loading condition of the weekday. The distance between the centres of two adjacent riser pipes have been represented as fins. According to the findings, the number of riser pipes has a significant effect on the distance between two adjacent riser pipes. While, the length to diameter ratio of riser pipes have very small impact on the distance between the centres of two adjacent pipes. The distance between two neighbouring riser pipes decreases from 0.177m to 0.109m when the number of riser pipes increases from 5 to 9 for L/d of 100 and collector area of 1.401m^2. At the same time, an increase in L/d from 50 to 100 leads to an increase in the distance between the riser pipes from 0.175m to 0.177m. From this chart, the distance between centres of pipe-to-pipe can be obtained based on number of riser pipe and length to diameter ratio.

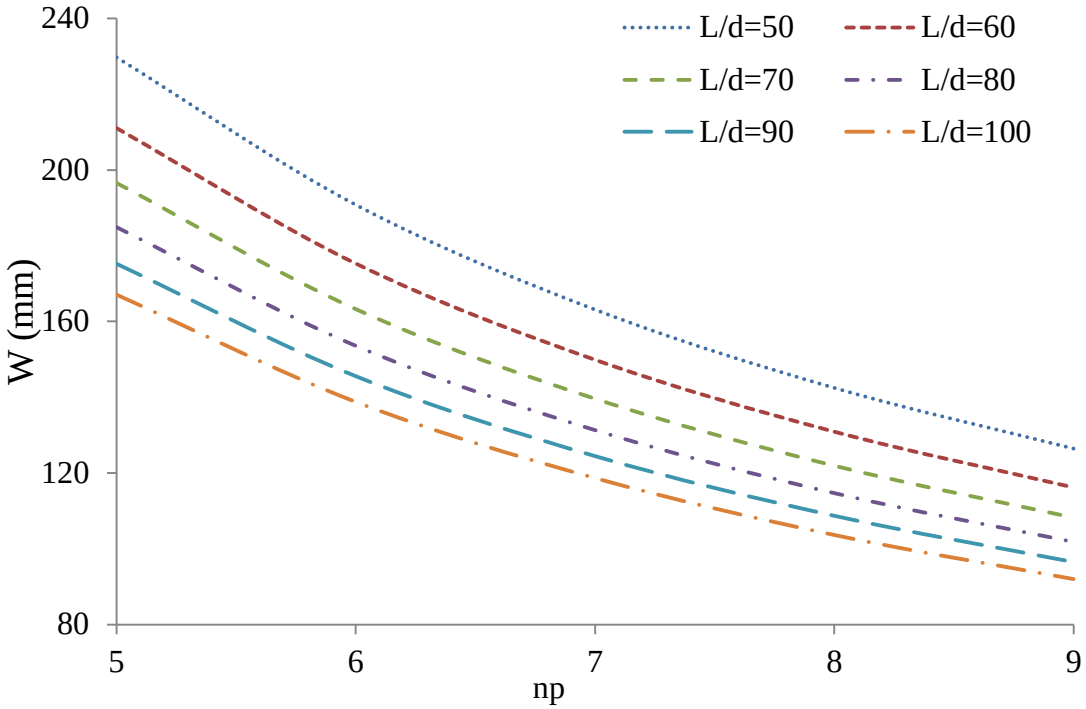

Figure 7-9 Distance between pipe-to-pipe against number of riser pipe for various L/d ratios on 15th March

7.6.2. Thermal and Flow Parameters of the Working Fluid

Figure 7-10 depicts the Reynolds number variations within thermo-syphon loop for various L/d ratios of riser pipes at a heat flux corresponding to 15th March under thermal loading condition of the weekday. It can be seen that the Reynolds number of working fluid within upriser pipe increases with an increases in L/d and the number of riser pipes. However, the effect of L/d on the Reynolds number of the working fluid in the upriser is more significant as compared to the number of riser pipes. From the following chart, Reynolds number of working fluid can be obtained based on number of riser pipes and length to diameter ratio of riser pipes.

Figure 7-11 depicts the variation in plate temperature of collector for various L/d ratios of the riser pipes at a heat flux corresponding to 15th March under thermal loading condition of the weekday. It can be seen that the length to diameter ratio of riser pipe has a significant effect on temperature of plate, whilst the number of riser pipes has a small effect on plate temperature. It is obvious from the fact that more riser pipes lead to increased amount of working fluid within the thermo-syphon loop with same collector area. From this chart, temperature of the absorber plate can be obtained based on number of riser pipes and length to diameter ratio of riser pipe.

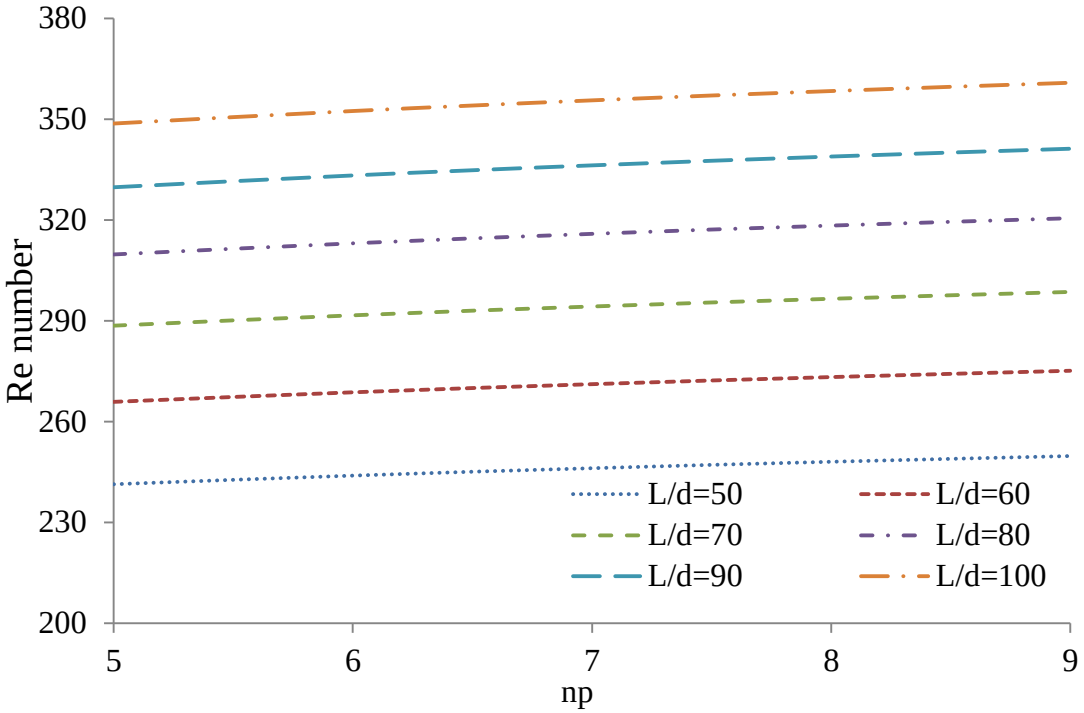

Figure 7-10 Reynolds number variations against number of riser pipe for various L/d ratios on15th March

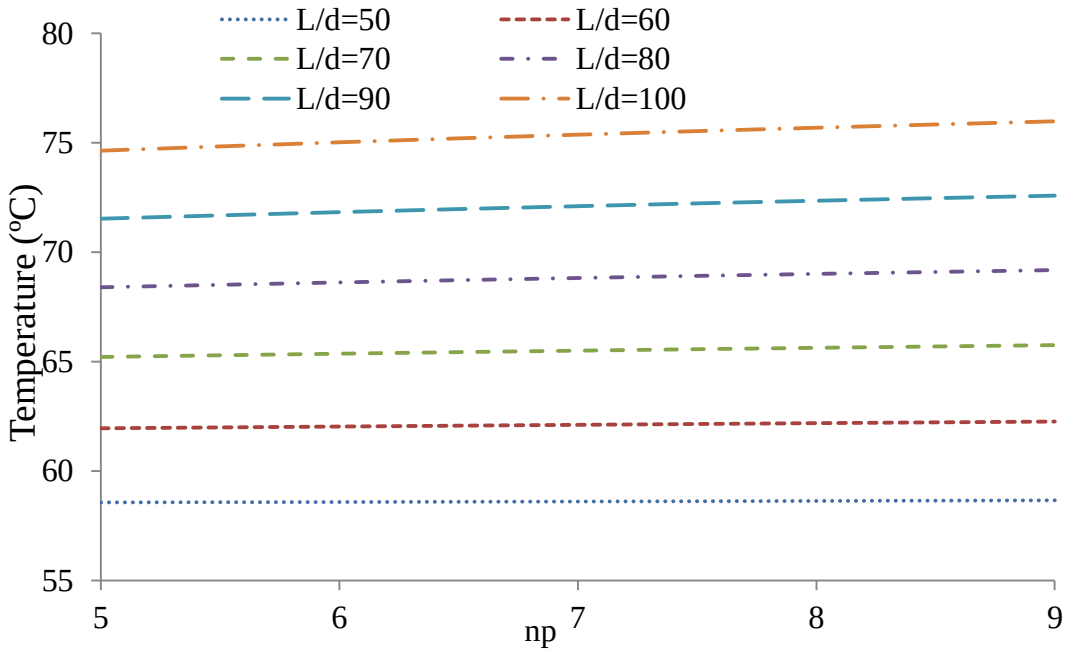

Figure 7-11 Static temperature of plate of collector against number of riser pipes for various L/d ratios on 15th March

Figure 7-12 depicts the variation of overall heat transfer coefficient of collector for various L/d ratios of riser pipes at a heat flux corresponding to 15th March under thermal loading condition of the weekday. It can be seen that the length to diameter ratio of riser pipe has a significant effect on overall heat transfer, whilst the number of riser pipe have a small effect on plate temperature. One of the most important parameters to predict the heat loss from collector is the overall heat transfer. It is obvious from the fact that increase in the length of riser pipe leads to increase of overall heat transfer coefficient. From this chart, overall heat transfer coefficient of the absorber plate can be obtained based on number of riser pipe and length to diameter ratio of riser pipe.

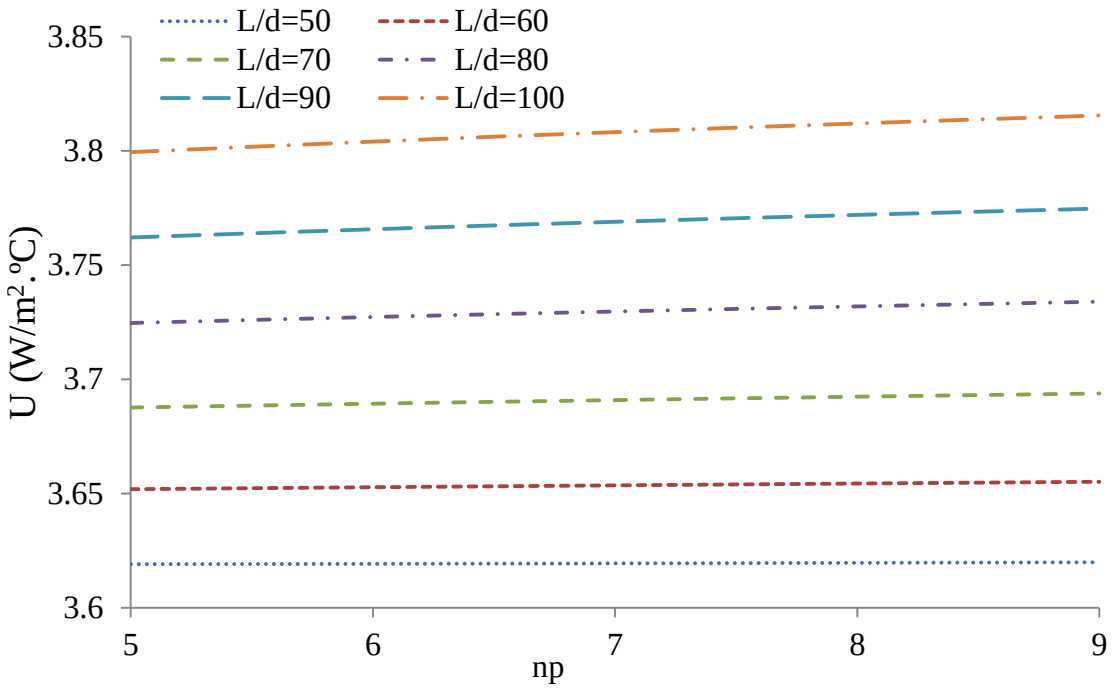

Figure 7-12 Overall heat loss cofficient of collector against number of riser pipe for various L/d ratios on 15th March

Figure 7-13 depicts the variation in heat transfer coefficient of working fluid within collector for various L/d ratios of riser pipes at a heat flux corresponding to 15th March under thermal loading condition of the weekday. It can be seen that the heat transfer coefficient of working fluid increases with an increase in both L/d and number of riser pipes. One of the most important parameters to predict the thermal performance of collector and hence predict the performance of the thermo-syphon system is heat transfer coefficient. From this chart, heat transfer coefficient within collector can be obtained based on number of riser pipe and length to diameter ratio of riser pipe.

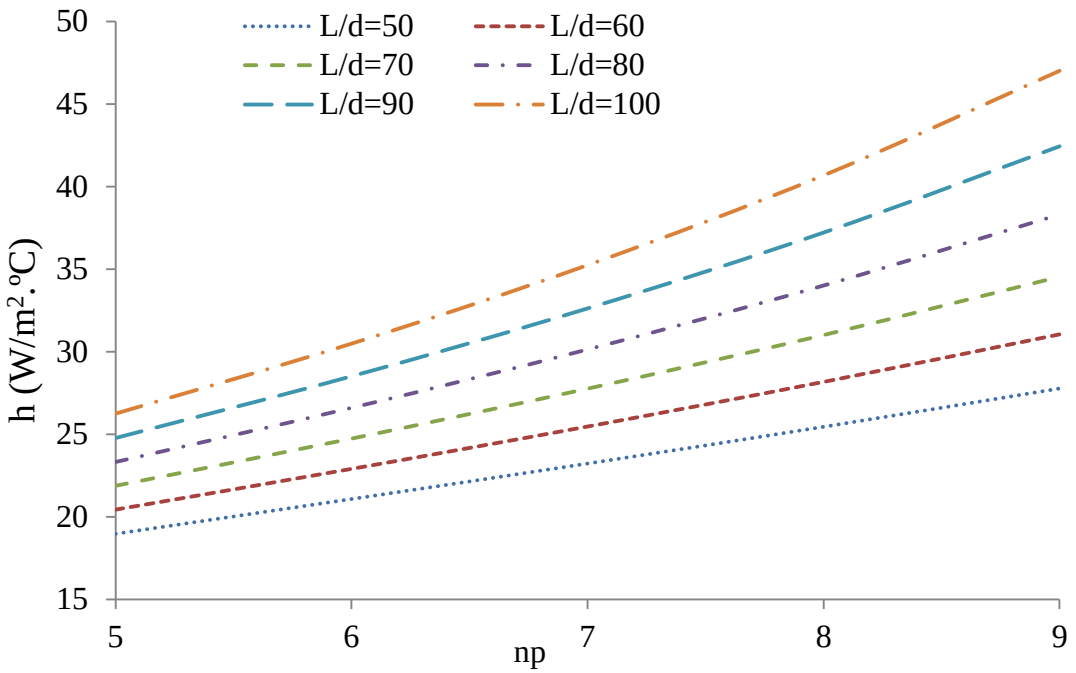

Figure 7-13 Variation in heat transfer coefficient within collector against the number of riser pipe for various L/d ratios on 15th March

Figure 7-14 depicts the variation in outlet temperature of working fluid within collector for various L/d ratios of the riser pipes at a heat flux corresponding to 15th March under thermal loading condition of the weekday. It can be seen that the temperature of working fluid at outlet of collector increase with increases L/d is higher as compared to increase number of riser pipe. The temperature of working fluid provide an indication about the thermal performance of collector and hence the performance of system. Furthermore, to determine the properties of working fluid we should know the reference temperature, which is equal to the average temperature between temperature at inlet and outlet of the collector. From this chart, outlet temperature of working fluid can be obtained based on number of riser pipes and length to diameter ratio of riser pipe.

Figure 7-15 depicts the variation in inlet temperature of working fluid within collector for a various L/d ratios of the riser pipes at a heat flux corresponding to 15th March under thermal loading condition of the weekday. It can be seen that the L/d has more significant impact on the temperature of working fluid at inlet of collector as compared to the number of riser pipe. From this chart, inlet temperature of working fluid can be obtained based on number of riser pipe and length to diameter ratio of riser pipe.

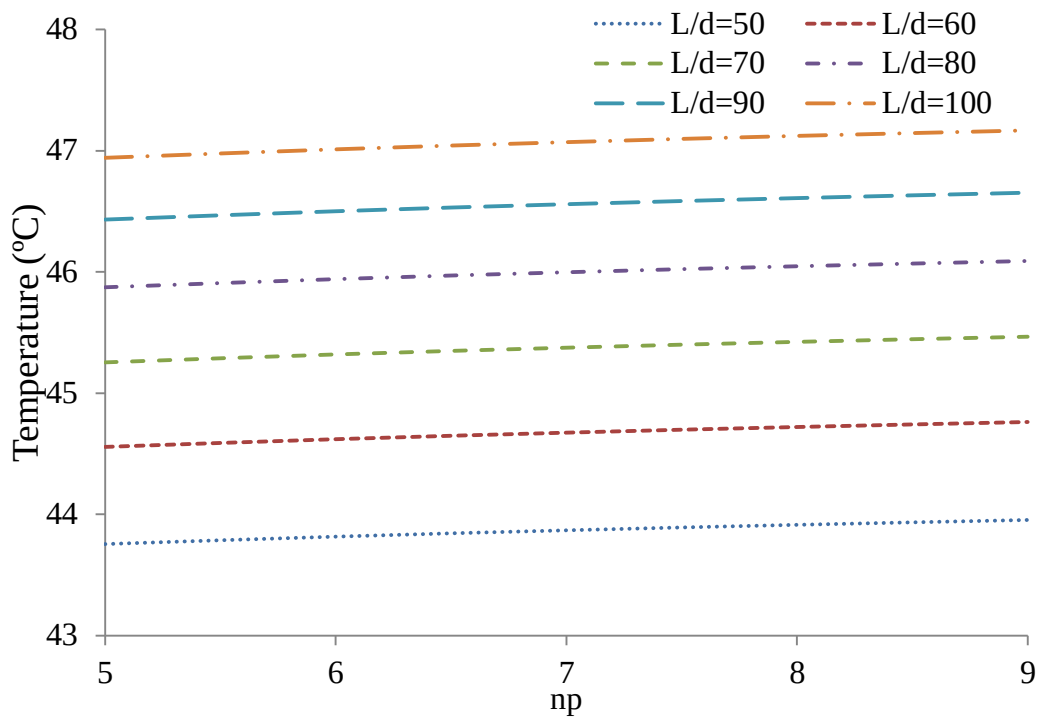

Figure 7-14 Variation in outlet temperature within collector with number of riser pipe for various L/d ratios as obtained on 15th March

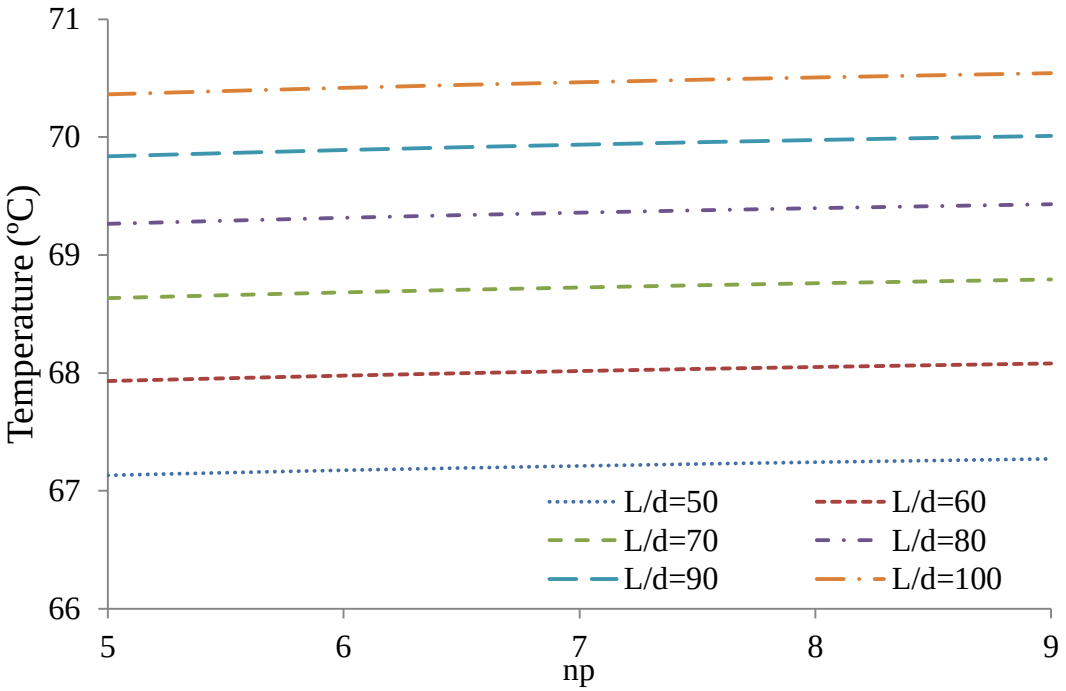

Figure 7-15 Variation in inlet temperature within collector with number of riser pipe for various L/d ratios as obtained on 15th March

7.6.3. The Design Steps

The following section shows the design steps for a closed loop thermo-syphon solar water heating system using charts.

1- Based on number of persons and required temperature, collector's area can be calculated from figure (7-5)
2- Based on the area of collector and minimum heat flux, the useful heat gain at the collector can be calculated from Eq. (7.22)
3- Number of riser pipes and L/d can be estimated based on the useful heat gain at the collector and figure (7-6)
4- Based on number of the riser pipes and L/d, the diameter of the riser pipe can be determined from figure (7-7)
5- Based on number of the riser pipes and L/d from figure(7-8), the length of the riser pipe can be estimated
6- The distance between the two neighbouring pipes can be estimated from figure (7-9) based on number of riser pipes and L/d
7- From figure (7-10) and with defined number of the riser pipes and L/d, Reynolds number of working fluid can be estimeted. Hence, the mass flow rate of working fluid can be calculated using the estimted Reynold number
8- Based on number of the riser pipes, L/d and figure (7-11), the temperature of plate of collector can be evaluated
9- The overall heat loss cofficient of collector can be evaluated from figure (7-12), and the number of riser pipes and L/d
10- For certain number of the riser pipes, L/d, the heat transfer coefficient can be estimated from figure (7-13)
11- The inlet and outlet temperature of working fluid can be defined from the figure (7-15) and figure (7-14) for a predefined number of the riser pipes and L/d

7.7. Summary of Design process development for the Thermo-syphon

A novel design methodology has been presented that can be used to design thermos-syphons for practical use. Design charts have also been presented that can be used to design a thermos-syphon system for a given set of requirements. Based on parametric investigations the following outcomes are presented:

- The demand output temperature has more effect on the collector area as compared to number of users
- The riser pipe number has more significant effect on the pipe to pipe distance as compared to L/d ratio

- A collector area of 1.403m^2 was required to heat 75L of water from 15^oC to 60^oC on a clear day in Huddersfield on 15th March
- The heat transfer coefficient of working fluid within thermo-syphon loop for a new model was approximately double as compared to the traditional model
- The cost for new model was more than the cost for traditional model due to bigger diameter of the riser pipe and secondary straight pipe inside the riser pipe in the new model

Furthermore, based on the numerical analysis conducted in Chapter 5, a design methodology has been proposed to ease the thermo-syphon designing process. In addition, this design methodology can be used by a closed loop thermo-syphon system designers with reasonable accurcy as illustrated above in the design example.Furthermore, in this chapter, an optimisation approach has been suggested to reduce the cost and improve the thermal performance of system.

CHAPTER 8

CONCLUSIONS

This chapter concludes the thesis by summarising the achievements of this research. In this thesis, experimental and numerical investigations have been conducted on a thermo-syphon system to analyse the flow of working fluid within the thermo-syphon loop and storage tank. Moreover, a design methodology for a closed loop thermo-syphon solar water heating system has been developed. Furthermore, requirements for future work in the field of a closed loop thermo-syphon solar water heating system have been defined.

8.1. Research Problem Synopsis

In recent decades, the use of solar energy to produce hot water has become more significant globally due to reasons, such as unlimited resource of solar energy and depletion of fossil fuels. Several studies have reported that use of solar technology has increased. Since 1980, implementation of this technology has increased dramatically [136] with about 70 million houses are now using solar energy in order to heat water for their daily use [137]. Although, there are many research studies conducted in the area of thermo-syphon, most of these studies lacked the detailed analysis on several important parameters (heat transfer coefficient, heat gain in collector and heat gain in the storage tank), which have significant impact on the thermal performance of thermo-syphon. Furthermore, majority of these studies did not consider the flow behaviour of working fluid like temperature distribution and velocity profile within thermo-syphon loop.
According to literature review in chapter two, number of objectives have been formulated, which determines the scope the present research study. The objectives and scope of this research are to predict the flow behaviour within the thermo-syphon more accurately. The main aims of this study and the major achievements and contributions that have been achieved during this study have been presented in a summary form in the following sections of this chapter.

8.2. Research Aims and Major Achievements

Based on extensive literature review regarding thermo-syphon solar water heating, the main aims of the thesis are given below with a summary of how these aims have been achieved.

Research Aim # 1: Parametric investigation on various geometrical and flow variables of a thermo-syphon

Achievement # 1: A commercial CFD package has been used to create a virtual domain of the working fluid within the thermo-syphon. The model makes use of the control volume numerical technique for solving the governing equations of mass and heat transfer. The numerical model has been verified against the experimental result, which shows a good agreement. Subsequently, similar approach has been taken to analyse other cases with various geometrical and characteristics parameters. The model has been tested for various length to diameter ratios of connecting pipes (L/d =50, 75 and 100) for different heat flux obtained on 15th March, 15th Jun and 15th September respectively being applied to the riser pipes, simulating the effect of the solar rays on these pipes. The whole model is made with an inclination of 53^{o} to capture the natural convection phenomena occurring in the thermo-syphon. In order to analyse the effect of the number of riser pipes on the performance output of the thermo-syphon, five, seven and nine riser pipes have been modelled separately in the thermo-syphon model. It has been assumed that the thermo-syphon is in operation under transient load condition of working day and weekend.

The temperature and velocity distributions of working fluid within the thermo-syphon loop and water within the storage tank have been analysed qualitatively and quantitatively. Qualitative analysis has been used to show the velocity and temperature profile of water and working fluid within the storage tank and thermo-syphon loop respectively. While, the quantitative analyses have been conducted to illustrate the temperature, mass flow rate and heat transfer coefficient distributions of working fluid within the thermo-syphon loop. In addition, the temperature distributions of water within the storage tank have been presented to depict the heat transfer phenomena inside the storage tank. Since, the main parameters for designing a thermo-syphon system are geometrical parameters, heat flux and thermal loading, Nusselt number, Reynolds number, plate and working fluid temperature, various cases have been studied by changing these parameters. Based on the findings from these numerical studies some semi-empirical correlations have been developed, to improve the designing process of thermo-syphon system. The major achievement of first aim of the present study is the development of the correlations for Nusselt number, Reynolds number, plate's temperature, and temperature of working fluid at inlet and outlet of the collector. These prediction models are the function of geometric parameters of thermo-syphon loop, heat fluxes, and thermal loading. Furthermore, it can be shown that prediction models generated in this study have a good accuracy with respect to the numerical results.

Research Aim # 2: Parametric investigation on various design modifications and flow variables of a thermo-syphon

Achievement # 2: The main purpose of design modification is to enhance the heat transfer. The main objective to use heat transfer enhancement methods is to improve the thermal performance of a closed loop thermo-syphon solar water heating system. In this present study, heat transfer enhancement has been achieved by increasing the surface area of the riser pipe. In this work, three new geometrical configurations of the riser pipe have been investigated to improve the thermal performance of thermo-syphon. These three models consist of straight pipe inside the riser pipe, wavy pipe inside the riser pipe and helical pipe inside the riser pipe. In addition, to investigate the effect of the working fluid amount, three conditions have been chosen by varying the amount of working fluid. The amount of working fluid has been varied against the amount of working fluid in a traditional model. The results depicted in chapter six have shown that the straight pipe inside the riser pipe with same amount of working fluid has better performance characteristics as compared to other models that have been considered in this study. In order to demonstrate the effect of new models on the performance output of the thermo-syphon, a comparison between new models and traditional model have been conducted. A commercial CFD package has been used to create a virtual domain of the working fluid within the thermo-syphon. The models make use of the control volume using numerical technique for solving the governing equations of mass conservation, momentum conservation and heat transfer. These models have been tested at a heat flux corresponding to 15th March being applied to the riser pipes, simulating the effect of the solar

rays on these pipes. It has been assumed that the thermo-syphon is in operation under transient load condition of working day hot water use. The models are made inclined by 53º to capture the natural convection phenomena occurring in the thermo-syphon.
The temperature and velocity distributions of working fluid within thermo-syphon loop and water within the storage tank for new and traditional models have been analysed qualitatively and quantitatively. Qualitative analysis has been used to show the effect of heat transfer enhancement methods on the velocity and temperature distributions of water and working fluid within the storage tank and thermo-syphon loop respectively. While, the quantitative analysis has been used to show temperature, mass flow rate, heat transfer coefficient, shear stress, pressure drop, heat gain in the collector and water storage tank distributions within the thermo-syphon system. The major achievement of the present study is development of a novel thermo-syphon which provides better performance as compared to traditional thermos-syphon.

Research Aim # 3: Development of a model for design of thermo-syphon

Achievement # 3: In the present study, an optimal design methodology of a closed loop thermo-syphon solar heating system has been developed, which is easy to use and reliable. In this methodology, the semi-empirical correlations have been developed for predicting Nusselt number, Reynolds number, temperature of working fluid at the inlet and outlet of collector and plate's temperature within thermo-syphon. The parameters that affect the performance of thermo-syphon and hence the design of a closed loop thermo-syphon solar water heating system have been included into the developed model, which is one of the most important achievements of this study. Moreover, the inputs to a model that has been developed for optimal design in this study require only altitude and tilt angle of collector. The optimisation methodology provides the geometrical parameters such as diameter, length and number of the riser pipes and hence the collector area. Furthermore, the optimisation model provides relevant parameters such as the flow rate of working fluid within the thermo-syphon loop, useful heat, and heat transfer coefficient etc. The design methodology is quite robust and can be used with confidence to design thermos-syphon system for a variety of operating conditions.

8.3. Thesis Conclusions

An inclusive study has been carried out to support the existing literature regarding a single phase closed loop thermo-syphon and to provide novel additions to improve the current understanding of the design process, operational characteristics, geometry related effects and optimization methodology. The major conclusions from each facet of this research study are summarized as follows:

1. To determine the effect of number of riser pipes on the performance of thermo-syphon

From the investigations regarding the effect of the geometrical parameters on the performance of thermo-syphon, carried out in this study, it can be concluded that an increase in the number of riser pipes increases the temperature of the working fluid within the condenser and hence increases the temperature within storage water tank by absorbing more solar energy. Furthermore, increase in number of riser pipe decreases the velocity of working fluid within riser pipe. The results provided in this study regarding the effect of the number of riser pipes on the performance of a closed loop thermo-syphon solar water heating system can be used to design optimal thermo-syphon systems optimally.

2. To establish the effect of length to diameter ratio (L/d) of the riser pipes on the performance of thermo-syphon

From the investigations regarding the effect of the geometrical parameters on the performance of thermo-syphon, carried out in this study, it can be concluded that an increase in the L/d of riser pipe increases the temperature of working fluid within the condenser and hence increases the temperature within storage water tank by absorbing more solar energy. Increase in L/d ratio of the riser pipe increases the velocity of working fluid within riser pipes. Furthermore, length to diameter ratio of riser pipes has more significant effect on working fluid's temperature and hence on the performance of the thermo-syphon as compared to the effect of number of riser pipes. For example, an increase in the number of riser pipes from five to nine, increases the temperature of water within the storage tank by 11.75%, while an increase in L/d ratio of the riser pipe from 50 to 100 increase water temperature by 69.21%. The results provided in this study regarding the effect of L/d of riser pipes on the performance of a closed loop thermo-syphon solar water heating system can be used to design optimal thermo-syphon systems.

3. To analyse the effect of transient heat fluxes on the performance of thermo-syphon

From the investigations regarding the effect of solar irradiation on any day of that year (and hence heat flux) on the performance of a closed loop thermo-syphon system, carried out in this study, it can be concluded that day of the year and hence corresponding heat flux has significant effect on the performance of thermo-syphon. The temperature within the condenser hence within the storage water tank increases significant in the hot months as compared with cold months. It is obvious from the fact that more heat flux provided to the riser pipes heats up the working fluid more. Furthermore, an increase in solar heat flux leads to increase in the mass flow rate within thermo-syphon. The maximum average mass flow rate for all cases of solar heat flux has been achieved at local solar noon time. The results provided in this study regarding the effect of the day of that year (heat flux) on the performance of a closed loop thermo-syphon system can be used to design the thermo-syphon systems optimally for a given heating requirement.

4. To establish the effect of transient thermal loading conditions on the performance of thermo-syphon

From the investigations regarding the effect of thermal loading on the performance of a closed loop thermo-syphon system, carried out in this study, it can be concluded that an increase in the thermal loading decreases the temperature of working fluid within thermo-syphon because of loss of more heat energy in the condenser. The results provided in this study regarding the effect of the thermal loading on the performance of a closed loop thermo-syphon can be used to design optimal thermo-syphon systems.

5. To determine the effect of a closed wavy tube inside the riser pipe on the performance of thermo-syphon

The numerical investigation has been conducted to depict the effect of wavy pipes within the riser pipe on the performance of a closed loop thermo-syphon system. The investigations revealed that the heat gain in the storage tank is lower for the wavy pipe as compared to the straight pipe. The results provided in this study regarding the effect of new model on the performance of a closed loop thermo-syphon solar water heating system can be used to improve the performance of thermo-syphon systems.

6. To determine the effect of a helical tube inside the riser pipe on the performance of thermo-syphon

The numerical investigation has been conducted to depict the effect of helical pipe inside the riser pipe on the performance of a closed loop thermo-syphon system. The investigation depicts that the heat gain in the storage tank is lower for the helical pipe model as compared to the straight pipe model. The results provided in this study regarding the effect of new model on the performance of a closed loop thermo-syphon solar water heating system can be used to improve the performance of thermo-syphon system.

7. To determine the effect of a closed straight tube inside the riser pipe on the performance of thermo-syphon with same amount of working fluid (model 1)

A detailed numerical investigation has been carried out regarding the effect of closed straight tube within the riser pipe on the performance of a closed loop thermo-syphon system, with same amount of working fluid as traditional model. The investigations indicate that the temperature of water within the tank, heat gain in the collector and heat gain in the storage tank are higher for new model as compared to the traditional model. Hence, the performance of thermo-syphon is higher for the new model as compared to the traditional model. However, the average mass flow rate is less for the new model as compared to the traditional model. The results provided in this

study regarding the effect of new model on the performance of a closed loop thermo-syphon solar water heating system can be used to improve the performance of thermo-syphon systems.

8. To formulate the effect of a closed straight tube inside the riser pipe on the performance of thermo-syphon with larger amount of working fluid (model 2)

A numerical investigation has been conducted to depict the effect of an increase in the working fluid amount on the thermal performance of thermo-syphon with respect to the model 1, for a configuration, which has a straight closed tube within the riser pipe. The investigation shows that, heat gain in the storage tank is lower for this model in comparison with the previous model. Hence, the performance of thermo-syphon is lower for the new model (model 2) as compared to the previous model (model 1). The results provided in this study regarding the effect of new model on the performance of a closed loop thermo-syphon solar water heating system can be used to improve the performance of thermo-syphon systems.

9. To formulate the effect of a closed straight tube inside the riser pipe on the performance of thermo-syphon with smaller amount of working fluid (model 3)

A numerical investigation has been conducted to depict the effect of smaller amount of working fluid on the thermal performance of thermo-syphon with respect to the model 1, for a configuration, which has a straight closed tube within the riser pipe. The investigation shows that, heat gain in the storage tank is lower for this model in comparison with the model 1. Hence, the performance of thermo-syphon is lower for the new model (model 3) as compared to the model 1. The results provided in this study regarding the effect of new model on the performance of a closed loop thermo-syphon solar water heating system can be used to improve the performance of thermo-syphon systems.

10. Development of semi-empirical correlations for the Nusselt number, Reynolds number, plate temperature and temperature of working fluid at inlet and outlet of the collector

Based on the numerical results obtained in the present study and after analysing the effects of various parameters, which are considered in this study, semi-empirical relationships have been developed for Nusselt number, Reynolds number, temperature plate of collector, inlet, and outlet temperature of working fluid within thermo-syphon loop. Multiple regression analysis has been used for the evaluation of effects of various parameters on the performance of a closed loop thermo-syphon solar water heating system.

11. Development of a design methodology for a thermo-syphon system based on optimum thermal performance and cost consideration

Based on semi-empirical relationships, which have been developed in the present work, a methodology of design of a closed loop thermo-syphon solar water heating system has been developed. This methodology provides a detailed investigation regarding geometrical parameters of thermo-syphon loop, thermal and flow parameters of working fluid within thermo-syphon loop. Furthermore, this methodology of design can be widely used to estimate the geometrical parameters of thermo-syphon loop solar water heater system. Design charts have also been provided which can be easily used to design a closed loop thermo-syphon system.

12. To analyse the experimental results on the performance of thermo-syphon

The experimental investigations have been conducted to measure the temperature of water, temperature of working fluid and mass flow rate within the thermo-syphon loop. The mesured parameters shows similar trend for both traditional and new models. In addition, according to the experiment results the performance of the new model has been improved compared to traditional model. Furthermore, the experimental results have been used to verify the numerical results, which show a good agreement with the CFD results with a considerable amount of accuracy. Hence, Computational Fluid Dynamics can be used as an effective tool to analyse the performance of a thermo-syphon with reasonable accuracy.

8.4. Thesis Contributions

The major contributions of this research study are summarised below in which novelties of this research are described.

Contribution # 1:

The first contribution of the present study is a comprehensive investigation on local and global flow characteristics for working fluid within a closed loop thermo-syphon system. The available literature regarding the velocity and temperature distributions of working fluid within the riser pipes of thermo-syphon are severely limited. Hence, a Computational Fluid Dynamics code has been used to carry out extensive investigations on velocity and temperature distributions within the thermo-syphon system. Effects of various parameters such as, number of riser pipe and length to diameter ratio of riser pipe, transient heat flux, and thermal loadings have been enumerated. Furthermore, based on these parameters, new mathematical prediction models have been suggested for Nusselt number, Reynolds number, plate temperature, and temperature of working fluid at inlet and outlet of collector. The mathematical models have been developed based on the data generated from the extensive numerical investigations, which were validated through

experimental measurements. Hence, these equations can be used to estimate the thermal performance of thermo-syphon for wide range of geometrical parameters and operating conditions such as various heat fluxes, different thermal loadings, and time. Furthermore, these prediction models are a novel contribution to the knowledge that can be used to design a closed loop thermo-syphon solar water heating system.

Contribution # 2:

The significant contribution of this study is the enhancement of the thermal performance of a thermo-syphon by increasing surface area of riser pipe. An attempt has been made to justify the improvement in thermal characteristics of the new geometries by keeping working fluid volume to be same so that only geometric effects are considered in the analysis. In this study, an extensive study has been conducted on the velocity and temperature distributions within the thermo-syphon for various riser pipe configurations and volumes of working fluid, using CFD code. Investigations on various riser pipe configurations and amounts of working fluid have been conducted by comparing the performance of the proposed models with the traditional model to develop an optimised thermo-syphon model. The experimental results obtained on the proposed model confirm the numerical findings. Findings of this investigation on design modifications are novel contribution to the knowledge that can be used to enhance the amount of heat transfer and hence improve the thermal performance of a closed loop thermo-syphon solar water heating system.

Contribution # 3:

A closed loop thermo-syphon solar water heating system is becoming more popular to supply hot water. According to studies available in literature review, design methodology of thermo-syphon relies on many of the assumptions. In this study, a design methodology for a closed loop thermo-syphon solar water heating system has been developed in order to reduce the number of assumptions and ease the designing process. This methodology is reliable for providing various geometrical parameters based on the input of the user such as, collector area, the diameter and the length of riser pipe and the distance between the centre to centre of riser pipes. Furthermore, this methodology is user friendly, robust and reliable to provide an optimal solution, for designing a closed loop thermo-syphon solar water heating system. Furthermore, this methodology can be adapted for both the traditional and the new model, which have been considered in this study.

8.5. Thesis Novelties

The main novielites of the current study are presented below:

1. Semi-empirical relationships have been developed for Nu number, Re number, Tp, Tin, and Tout

2. Enhancement in the thermal performance of thermo-syphon has been achieved by increasing the surface area of riser pipes maintaining the same amount of working fluid and collector area as in the traditional model
3. Development of a novel design methodology has been accomplished for a thermo-syphon based on optimum thermal performance and optimum cost of system

8.6. Recommendations for Future Work

In order to bridge the knowledge gaps, which have been identified in the literature review section, operation and design of a closed loop thermo-syphon has been conducted in the current study. From the current investigations it has become obvious that there is a huge potential for further research and studies in the field of thermo-syphon. For further analysis in the design and improvement of the performance of thermo-syphon, following future works have been suggested.

Recommendation # 1: A detailed investigation on the effect of using a closed pipe within the riser pipe on the performance of an active thermo-syphon system. Hence, a comparison between the passive and active systems can be carried out to develop a new optimum system.

Recommendation # 2: To improve the performance of the thermo-syphon system, a study on the effect of different pipe materials and pipe locations within the riser pipe on the performance of thermo-syphon can be carried out.

Recommendation # 3: A study of the effect on performance of thermo-syphon by implementing PCM within a closed pipe of riser pipe can potentially help to develop a new range of thermo-syphons. The main aim of utilizing PCM is to store the heat during peak heat flux, which can be used later when there is shortage of heat flux.

Recommendation # 4: A detailed investigation on the effects of using different working fluids on the thermal performance of thermo-syphon within a closed pipe within the riser pipe output can be carried out.

REFERENCES

1. Khan, B.A., et al., Performance improvement of solar hot water system by reducing solar irradiation from solar collector and solar tank, 2011, BRAC University.

2. Brown, E.W., An Introduction to Solar Energy. Online posting, 1988. **12**.

3. Office, M. Solar Energy. 2014 [cited 2016; Available from: http://www.metoffice.gov.uk/renewables/solar.

4. Duffie, J.A. and W.A. Beckman, Solar engineering of thermal processes. Vol. 3. 1980: Wiley New York etc.

5. Energy, k., Thermosiphon, 2015.

6. Gordon, J., Solar energy: the state of the art: ISES position papers2001: Earthscan.

7. Smith, C., Revisiting solar power's past. Technology Review, 1995. **98**(5): p. 38-47.

8. Society, K.S.E. Kentucky Solar Energy Society 2014 [cited 2013; Available from: http://www.kyses.org/.

9. Programme, I.S.H.C., 2001 Annual Report, 2002.

10. 212, T. Flat-Plate Collectors. 2016; Available from: http://www.powerfromthesun.net/Book/chapter06/chapter06.html#6.2Advantages.

11. TUTORIAILS, A.E. Solar Flat Plate Collectors. Solar Flat Plate Collectors: the Cheapest Way to Your Heat Water 2016; Available from: http://www.alternative-energy-tutorials.com/energy-articles/solar-flat-plate-collectors.html.

12. Solar, B.I. Welcome To Build-It-Solar. 2013; Available from: http://www.builditsolar.com/index.htm.

13. Kalogirou, S.A., Solar thermal collectors and applications. Progress in energy and combustion science, 2004. **30**(3): p. 231-295.

14. Dwivedi, V., Thermal Modelling and Control of Domestic Hot Water Tank. Master of Science in Energy Systems and the Environment, 2009.

15. Samanci, A. and A. Berber, Experimental investigation of singlephase and two phase closed thermosyphon solar water heater systems. Scientific Research and Essays, 2011. **6**(4): p. 688-693.

16. Soin, R., et al., Performance of flat plate solar collector with fluid undergoing phase chance. Solar Energy, 1979. **23**(1): p. 69-73.

17. Sabharwall, P., Engineering design elements of a two-phase thermosyphon to transfer nuclear thermal energy to a hydrogen plant2009.

18. Federation, E.s.T.I. SOLAR DOMESTIC HOT WATER PREPARATION (SDHW). 2016; Available from: http://www.estif.org/st_energy/technology/solar_domestic_hot_water_heating_sdhw/.

19. Climate, S., Facility, 2015.

20. Franco, A. and S. Filippeschi, Closed loop two-phase thermosyphon of small dimensions: a review of the experimental results. Microgravity Science and Technology, 2012. **24**(3): p. 165-179.

21. Tuma, P.E., Indirect Thermosyphons For Cooling Electronic Devices, 2006.

22. LEPTEN, 2015.

23. Lienhard, J.H., A heat transfer textbook2013: Courier Corporation.

24. engr.colostate. Heat Transfer Mechanisms. 2016; Available from: http://www.engr.colostate.edu/~allan/heat_trans/page4/page4f.html.

25. Ibrahim, D., Optimum tilt angle for solar collectors used in Cyprus. Renewable energy, 1995. **6**(7): p. 813-819.

26. Hsieh, J.S., Solar energy engineering. 1986.

27. La Gennusa, M., et al., A model for managing and evaluating solar radiation for indoor thermal comfort. Solar Energy, 2007. **81**(5): p. 594-606.

28. Sukhatme, S.P. and J. Nayak, Principles of thermal collection and storage. Solar Energy, 3rd Edition, Tata McGraw Hill Publishing company, New Delhi, 2008.

29. Yeh, H., C. Ho, and C. Yeh, Effect of aspect ratio on the collector efficiency of sheet-and-tube solar water heaters with the consideration of hydraulic dissipated energy. Renewable energy, 2003. **28**(10): p. 1575-1586.

30. Thianpong, C., et al., Compound heat transfer enhancement of a dimpled tube with a twisted tape swirl generator. International Communications in Heat and Mass Transfer, 2009. **36**(7): p. 698-704.

31. Sivashanmugam, P. and S. Suresh, Experimental studies on heat transfer and friction factor characteristics of laminar flow through a circular tube fitted with regularly spaced helical screw-tape inserts. Experimental Thermal and Fluid Science, 2007. **31**(4): p. 301-308.

32. Sivashanmugam, P. and P. Nagarajan, Studies on heat transfer and friction factor characteristics of laminar flow through a circular tube fitted with right and left helical screw-tape inserts. Experimental Thermal and Fluid Science, 2007. **32**(1): p. 192-197.

33. Promvonge, P. and S. Eiamsa-ard, Heat transfer behaviors in a tube with combined conical-ring and twisted-tape insert. International Communications in Heat and Mass Transfer, 2007. **34**(7): p. 849-859.

34. Kongkaitpaiboon, V., K. Nanan, and S. Eiamsa-ard, Experimental investigation of heat transfer and turbulent flow friction in a tube fitted with perforated conical-rings. International Communications in Heat and Mass Transfer, 2010. **37**(5): p. 560-567.

35. Sheikholeslami, M., M. Gorji-Bandpy, and D.D. Ganji, Review of heat transfer enhancement methods: Focus on passive methods using swirl flow devices. Renewable and Sustainable Energy Reviews, 2015. **49**: p. 444-469.

36. Varol, Y. and H.F. Oztop, A comparative numerical study on natural convection in inclined wavy and flat-plate solar collectors. Building and Environment, 2008. **43**(9): p. 1535-1544.

37. Sivakumar, P., et al., Performance improvement study of solar water heating system. ARPN Journal of Engineering and Applied Sciences, 2012. **7**(1): p. 45-9.

38. Subramanian, J., S. Tamilkozhndu, and T. Selvam. Experimental Studies on Variable Header Solar Water Heating System. in 2nd International Conference on Mechanical, Production and Automobile. 2012.

39. Amori, K. and N. Jabouri, Thermal performance of solar hot water systems using a flat plate collector of accelerated risers. The Journal of Engineering Research, 2012. **9**(1): p. 1-10.

40. El-Din, S.H.S., Heat transfer characteristics of an inclined single-phase toroidal thermosyphon. Alexandria Engineering Journal, 2005. **44**(2): p. 157-171.

41. Kundu, B., Performance analysis and optimization of absorber plates of different geometry for a flat-plate solar collector: a comparative study. Applied Thermal Engineering, 2002. **22**(9): p. 999-1012.

42. Shelke, V.G. and C.V. Patil, Analyze the Effect of Variations in Shape of Tubes for Flat Plate Solar Water Heater.

43. Hussein, H., M. Mohamad, and A. El-Asfouri, Optimization of a wickless heat pipe flat plate solar collector. Energy Conversion and Management, 1999. **40**(18): p. 1949-1961.

44. Hasan, A., Thermosyphon solar water heaters: effect of storage tank volume and configuration on efficiency. Energy Conversion and Management, 1997. **38**(9): p. 847-854.

45. Sato, A., V. Scalon, and A. Padilha. Numerical analysis of a modified evacuated tubes solar collector. in International Conference on Renewable Energies and Power Quality (ICREPQ'12) Santiago de Compostela (Spain), 28th to 30th March. 2012.

46. AlShamaileh, E., Testing of a new solar coating for solar water heating applications. Solar Energy, 2010. **84**(9): p. 1637-1643.

47. Zerrouki, A., A. Boumedien, and K. Bouhadef, The natural circulation solar water heater model with linear temperature distribution. Renewable energy, 2002. **26**(4): p. 549-559.

48. Rehim, Z.S.A. A new design of solar water heater. in Proceedings of the Indian Academy of Sciences-Chemical Sciences. 1998. Springer.

49. Koffi, P.M.E., et al., Thermal performance of a solar water heater with internal exchanger using thermosiphon system in Côte d'Ivoire. Energy, 2014. **64**: p. 187-199.

50. Hussein, H., Optimization of a natural circulation two phase closed thermosyphon flat plate solar water heater. Energy Conversion and Management, 2003. **44**(14): p. 2341-2352.

51. Mathioulakis, E. and V. Belessiotis, A new heat-pipe type solar domestic hot water system. Solar Energy, 2002. **72**(1): p. 13-20.

52. TSIRIGOTIS, G. and G. Iordanou, Computational Fluid Dynamics (CFD) investigations of the effect of placing a metallic mesh in the channels of a passive solar collector model. Elektronika ir Elektrotechnika, 2012. **121**(5): p. 69-74.

53. Sandhu, G., K. Siddiqui, and A. Garcia, Experimental study on the combined effects of inclination angle and insert devices on the performance of a flat-plate solar collector. International Journal of Heat and Mass Transfer, 2014. **71**: p. 251-263.

54. Razavi, J., M. Riazi, and M. Mahmoodi, Rate of heat transfer in polypropylene tubes in solar water heaters. Solar Energy, 2003. **74**(6): p. 441-445.

55. Ramasamy, S. and P. Balashanmugam, Thermal Performance Analysis of the Solar Water Heater with Circular and Rectangular Absorber Fins.

56. Kumar, A. and B. Prasad, Investigation of twisted tape inserted solar water heaters—heat transfer, friction factor and thermal performance results. Renewable energy, 2000. **19**(3): p. 379-398.

57. Hobbi, A. and K. Siddiqui, Experimental study on the effect of heat transfer enhancement devices in flat-plate solar collectors. International Journal of Heat and Mass Transfer, 2009. **52**(19): p. 4650-4658.

58. Martín, R.H., et al., Simulation of an enhanced flat-plate solar liquid collector with wire-coil insert devices. Solar Energy, 2011. **85**(3): p. 455-469.

59. Jaisankar, S., T. Radhakrishnan, and K. Sheeba, Experimental studies on heat transfer and thermal performance characteristics of thermosyphon solar water heating system with helical and left–right twisted tapes. Energy Conversion and Management, 2011. **52**(5): p. 2048-2055.

60. Viyaykumar, S., Enhancement of heat transfer rate in a solar flat plate collector using twisted tapes and wire coiled turbulators. International journal of mechanical aerospace, industrial and mechatronics engineering, 2014. **8**.

61. Esen, M. and H. Esen, Experimental investigation of a two-phase closed thermosyphon solar water heater. Solar Energy, 2005. **79**(5): p. 459-468.

62. Lin, M.-C., et al., Thermal performance of a two-phase thermosyphon energy storage system. Solar Energy, 2003. **75**(4): p. 295-306.

63. Fanney, A. and C. Terlizzi, Testing of refrigerant-charged solar domestic hot water systems. Solar Energy, 1985. **35**(4): p. 353-366.

64. Abreu, S.L. and S. Colle, An experimental study of two-phase closed thermosyphons for compact solar domestic hot-water systems. Solar Energy, 2004. **76**(1): p. 141-145.

65. Riahi, A. and H. Taherian, Experimental investigation on the performance of thermosyphon solar water heater in the South Caspian Sea. Thermal Science, 2011. **15**(2): p. 447-456.

66. Belessiotis, V. and E. Mathioulakis, Analytical approach of thermosyphon solar domestic hot water system performance. Solar Energy, 2002. **72**(4): p. 307-315.

67. Rikoto, I.I., et al., Design, Construction and Installation of 250-Liter Capacity Solar Water Heating System at Danjawa Renewable Energy Model Village. Int. j. eng. sci, 2015. **4**(3): p. 39-44.

68. Agbo, S. and G. Unachukwu, Design and Performance Features of a Domestic Thermosyphon Solar Water Heater for an Average-Sized Family in Nsukka Urban. Trends in Applied Sciences Research, 2007. **2**(3): p. 224-230.

69. Versteeg, H. and W. Malalasekera, An Introduction to Computational Fluid Dynamics (Harlow: Longman Scientific and Technical), 1995, Wiley (US).

70. Cebeci, T., et al., Computational fluid dynamics for engineers: from panel to navier-stokes methods with computer programs. 2005.

71. Blazek, J., Computational fluid dynamics: principles and applications2015: Butterworth-Heinemann.

72. Lomax, H., T.H. Pulliam, and D.W. Zingg, Fundamentals of computational fluid dynamics2013: Springer Science & Business Media.

73. Hoffmann, K.A. and S.T. Chiang, Computational fluid dynamics. 2000.

74. Munson, B.R., D.F. Young, and T.H. Okiishi, Fundamentals of Fluid Mechanics, John Wiley & Sons. Inc., New York, 1994. **2**.

75. Barth, T.J. and D.C. Jespersen, The design and application of upwind schemes on unstructured meshes. 1989.

76. Batinat, J.T., U.A. Branch, and H.T. Yangi, Spatial adaption procedures on unstructured meshes for accurate unsteady aerodynamic flow computation. 1991.

77. Menter, F.R., Two-equation eddy-viscosity turbulence models for engineering applications. AIAA journal, 1994. **32**(8): p. 1598-1605.

78. Patankar, S.V. and D.B. Spalding, A calculation procedure for heat, mass and momentum transfer in three-dimensional parabolic flows. International Journal of Heat and Mass Transfer, 1972. **15**(10): p. 1787-1806.

79. Venkatakrishnan, V., 'On the Accuracy of Limiters and Convergence to Steady State Solutions,' AIAA Paper 93-0880, Jan. 1993.

80. ANSYS, ANSYS Fluent User's Guide, 2012.

81. Heck, D.,Hybrid meshing for CFD-analysis, in Hybrid meshing for CFD-analysis2015.

82. Hu, J., et al. Overlay Grid Based Geometry Cleanup. in IMR. 2002.

83. Alizadehdakhel, A., M. Rahimi, and A.A. Alsairafi, CFD modeling of flow and heat transfer in a thermosyphon. International Communications in Heat and Mass Transfer, 2010. **37**(3): p. 312-318.

84. Neale, A., et al., CFD calculation of convective heat transfer coefficients and validation–Part 2: Turbulent flow, 2006, Annex.

85. Zhang, T., H. Zhou, and S. Wang, An adjustment to the standard temperature wall function for CFD modeling of indoor convective heat transfer. Building and Environment, 2013. **68**: p. 159-169.

86. Mmhtl. Fluid Properties Calculator. 1997; Available from: http://www.mhtl.uwaterloo.ca/old/onlinetools/airprop/airprop.html.

87. ANSYS, Heat Transfer Modeling: Introductory FLUENT Training, 2006. p. 7-22.

88. FLUENT, A., 13.3.1 Overview and Limitations, 2006.

89. Lee, H.G. and J. Kim, A comparison study of the Boussinesq and the variable density models on buoyancy-driven flows. Journal of Engineering Mathematics, 2012. **75**(1): p. 15-27.

90. Han, J. and G. Tryggvason, Secondary breakup of axisymmetric liquid drops. I. Acceleration by a constant body force. Physics of Fluids (1994-present), 1999. **11**(12): p. 3650-3667.

91. Jacqmin, D., Calculation of two-phase Navier–Stokes flows using phase-field modeling. Journal of Computational Physics, 1999. **155**(1): p. 96-127.

92. Liu, C. and J. Shen, A phase field model for the mixture of two incompressible fluids and its approximation by a Fourier-spectral method. Physica D: Nonlinear Phenomena, 2003. **179**(3): p. 211-228.

93. Vladimirova, N., Model flames in the Boussinesq limit: Rising bubbles. Combustion Theory and Modelling, 2007. **11**(3): p. 377-400.

94. Vladimirova, N. and R. Rosner, Model flames in the Boussinesq limit: the effects of feedback. Physical Review E, 2003. **67**(6): p. 066305.

95. Vladimirova, N. and R. Rosner, Model flames in the Boussinesq limit: the case of pulsating fronts. Physical Review E, 2005. **71**(6): p. 067303.

96. Young, Y.-N., et al., On the miscible Rayleigh–Taylor instability: two and three dimensions. Journal of Fluid Mechanics, 2001. **447**: p. 377-408.

97. Qin, L., Analysis, modeling and optimum design of solar domestic hot water systems. 1999.

98. Kudela, H., Hydraulic losses in pipes.

99. Dr PA Sleigh, D.I.M.G., Section 1: Fluid Flow in Pipes, 2008: leeds.

100. EDUR Pipe Friction Losses. Fundamental Principles for Project Work, 2014.

101. efm.leeds. Boundary Layers. 2016; Available from: http://www.efm.leeds.ac.uk/CIVE/CIVE1400/Section4/boundary_layer.htm.

102. Hobson, P., Thermosyphon solar water heaters: validated numerical simulation and design correlations. 1988.

103. Franco, A. and S. Filippeschi, Experimental analysis of closed loop two phase thermosyphon (CLTPT) for energy systems. Experimental Thermal and Fluid Science, 2013. **51**: p. 302-311.

104. Joudi, K.A. and A.A. Al-Tabbakh, A Theoretical Procedure for Estimating Saturation Temperature Inside Solar Two-Phase Loops. Journal of Engineering and Development, 2015. **19**(4).

105. Aung, N.Z. and S. Li, Numerical investigation on effect of riser diameter and inclination on system parameters in a two-phase closed loop thermosyphon solar water heater. Energy Conversion and Management, 2013. **75**: p. 25-35.

106. Handbook, A., 1985 Fundamentals. American Society of Heating, Refrigerating, and Air Conditioning Engineers, Inc., Atlanta, Georgia, 1985.

107. Sen, Z., Solar energy fundamentals and modeling techniques: atmosphere, environment, climate change and renewable energy2008: Springer Science & Business Media.

108. Easy, E. F-Test. 2016 [cited 2016 2/11/2016]; Available from: http://www.excel-easy.com/examples/f-test.html.

109. Rawlings, J.O., S.G. Pantula, and D.A. Dickey, Applied regression analysis: a research tool2001: Springer Science & Business Media.

110. Runkel, P., What Are T Values and P Values in Statistics?

111. De Smith, M., STATSREF: Statistical Analysis Handbook-a web-based statistics.". 2015.

112. Preacher, K.J. Calculation for the Chi-Square Test. [cited 2016 15/01/2016]; An interactive calculation tool for chi-square tests of goodness of fit and independence]. Available from: http://www.quantpsy.org/chisq/chisq.htm.

113. Fluent, A., Single-Precision and Double-Precision Solvers, 2006.

114. Fluent, A., Solver setting, 2006.

115. Fluent, A., ANSYS Fuent 6.3 user's Guide, 2006.

116. Fluent, A., FLUENT 6.3 Tutorial Guide. 2006.

117. Fluent, A., Solver Settings, 2016.

118. Singh, S. and S. Kumar, New approach for thermal testing of solar dryer: Development of generalized drying characteristic curve. Solar Energy, 2012. **86**(7): p. 1981-1991.

119. Standard, A., STANDARD 41.1-1986 (RA 91) Standard Method for temperature Measurement. Atlanta USA, 1991.

120. physics.stackexchange.com, Lux and W/m2 relationship?, 2016.

121. Iordanou, G., Flat-plate solar collectors for water heating with improved heat transfer for application in climatic conditions of the Mediterranean region, 2009, Durham University.

122. Hollands, K., et al., Free convective heat transfer across inclined air layers. Journal of Heat Transfer, 1976. **98**(2): p. 189-193.

123. Bell, S., Measurement Good Practice Guide No. 11 (Issue 2). A Beginner's Guide to Uncertainty of Measurement. National Physical Laboratory Teddington, Middlesex, United Kingdom, 2001.

124. Castrup, S. and H. Castrup, Measurement uncertainty analysis principles and methods. National Aeronautics and Space Administration, 2010.

125. Index, C. Temperature Effects on Density. 2016; Available from: http://butane.chem.uiuc.edu/pshapley/GenChem1/L21/2.html.

126. Idowu, O.S., O.M. Olarenwaju, and O.I. Ifedayo, Determination of optimum tilt angles for solar collectors in low-latitude tropical region. International Journal of Energy and Environmental Engineering, 2013. **4**(1): p. 1-10.

127. Ahmad, M.J. and G. Tiwari, Optimization of tilt angle for solar collector to receive maximum radiation. The Open Renewable Energy Journal, 2009. **2**(1): p. 19-24.

128. belkacem Ihya, A.M., Rachid Tadili, Mohammed Najib Bargach, Optimal tilt angles for solar collectors facing south at Fez city. Journal of Natural Sciences Research, 2014. **4**(10).

129. Yakup, M.A.b.H.M. and A. Malik, Optimum tilt angle and orientation for solar collector in Brunei Darussalam. Renewable energy, 2001. **24**(2): p. 223-234.

130. Benghanem, M., Optimization of tilt angle for solar panel: Case study for Madinah, Saudi Arabia. Applied Energy, 2011. **88**(4): p. 1427-1433.

131. Elminir, H.K., et al., Optimum solar flat-plate collector slope: case study for Helwan, Egypt. Energy Conversion and Management, 2006. **47**(5): p. 624-637.

132. Kudela, H., Viscous flow in pipe.

133. Sheng, H.J., Solar energy engineering, 1986, Prentice Hall Inc., New Jersey.

134. Humanitarian Charter and Minimum Standards in Humanitarian Response. Water supply standard 1: Access and water quantity; Available from: http://www.spherehandbook.org/en/water-supply-standard-1-access-and-water-quantity/.

135. Menon, E.S., Gas pipeline hydraulics2005: CRC Press.

136. Langniss, O. and D. Ince, Solar water heating: a viable industry in developing countries. Refocus, 2004. **5**(3): p. 18-21.

137. Energy, R., Key Facts and Figures for Decision Makers. Global status report, 2010.

138. Mendenhall, W., T. Sincich, and N.S. Boudreau, A second course in statistics: regression analysis. Vol. 5. 1996: Prentice Hall Upper Saddle River^ eNew Jersey New Jersey.

APPENDIX A

1- Heat flux of 15th of March and thermal loading of weekday

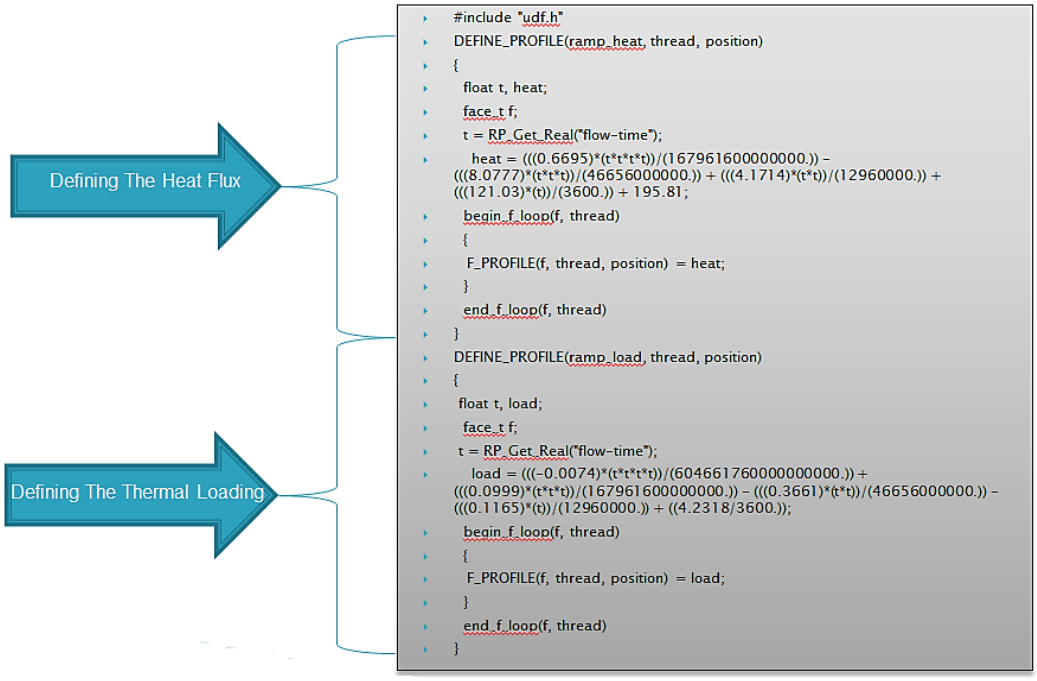


```
#include "udf.h"
DEFINE_PROFILE(ramp_heat, thread, position)
{
  float t, heat;
  face_t f;
  t = RP_Get_Real("flow-time");
    heat = (((0.6695)*(t*t*t*t))/(167961600000000.)) -
(((8.0777)*(t*t*t))/(46656000000.)) + (((4.1714)*(t*t))/(12960000.)) +
(((121.03)*(t))/(3600.)) + 195.81;
  begin_f_loop(f, thread)
  {
   F_PROFILE(f, thread, position)  = heat;
  }
  end_f_loop(f, thread)
}
DEFINE_PROFILE(ramp_load, thread, position)
{
 float t, load;
  face_t f;
 t = RP_Get_Real("flow-time");
    load = (((-0.0074)*(t*t*t*t))/(604661760000000000.)) +
(((0.0999)*(t*t*t))/(167961600000000.)) - (((0.3661)*(t*t))/(46656000000.)) -
(((0.1165)*(t))/(12960000.)) + ((4.2318/3600.));
  begin_f_loop(f, thread)
  {
   F_PROFILE(f, thread, position)  = load;
  }
  end_f_loop(f, thread)
}
```

2- Heat flux of 15th of June and thermal loading of weekday

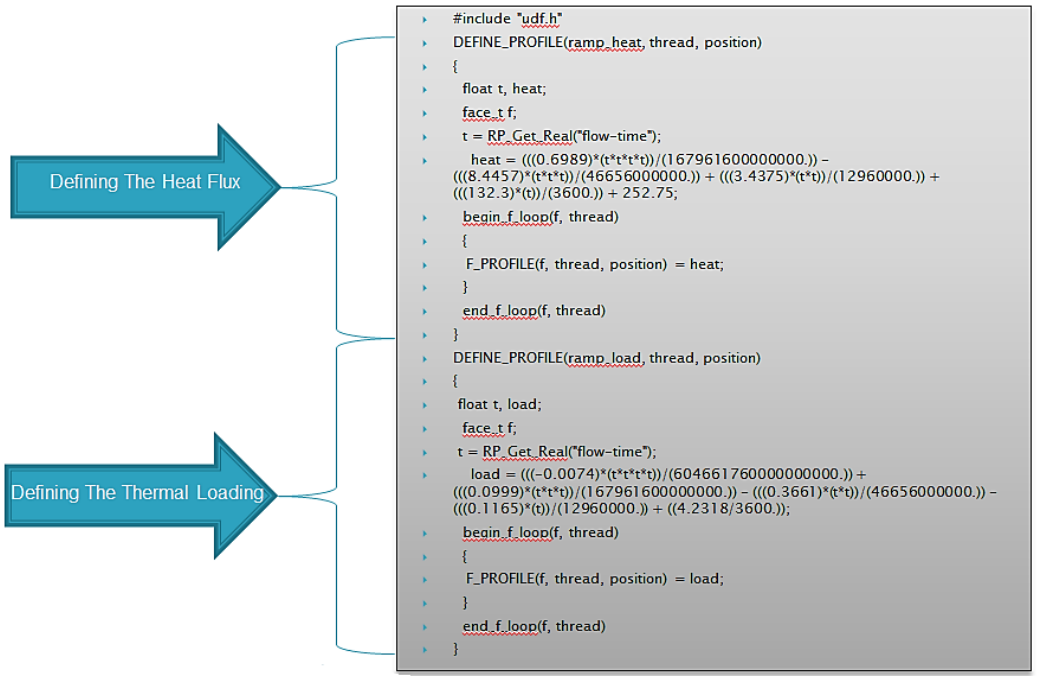


```
#include "udf.h"
DEFINE_PROFILE(ramp_heat, thread, position)
{
  float t, heat;
  face_t f;
  t = RP_Get_Real("flow-time");
    heat = (((0.6989)*(t*t*t*t))/(167961600000000.)) -
(((8.4457)*(t*t*t))/(46656000000.)) + (((3.4375)*(t*t))/(12960000.)) +
(((132.3)*(t))/(3600.)) + 252.75;
  begin_f_loop(f, thread)
  {
   F_PROFILE(f, thread, position)  = heat;
  }
  end_f_loop(f, thread)
}
DEFINE_PROFILE(ramp_load, thread, position)
{
 float t, load;
  face_t f;
 t = RP_Get_Real("flow-time");
    load = (((-0.0074)*(t*t*t*t))/(604661760000000000.)) +
(((0.0999)*(t*t*t))/(167961600000000.)) - (((0.3661)*(t*t))/(46656000000.)) -
(((0.1165)*(t))/(12960000.)) + ((4.2318/3600.));
  begin_f_loop(f, thread)
  {
   F_PROFILE(f, thread, position)  = load;
  }
  end_f_loop(f, thread)
}
```

3- Heat flux of 15th of September and thermal loading of weekday

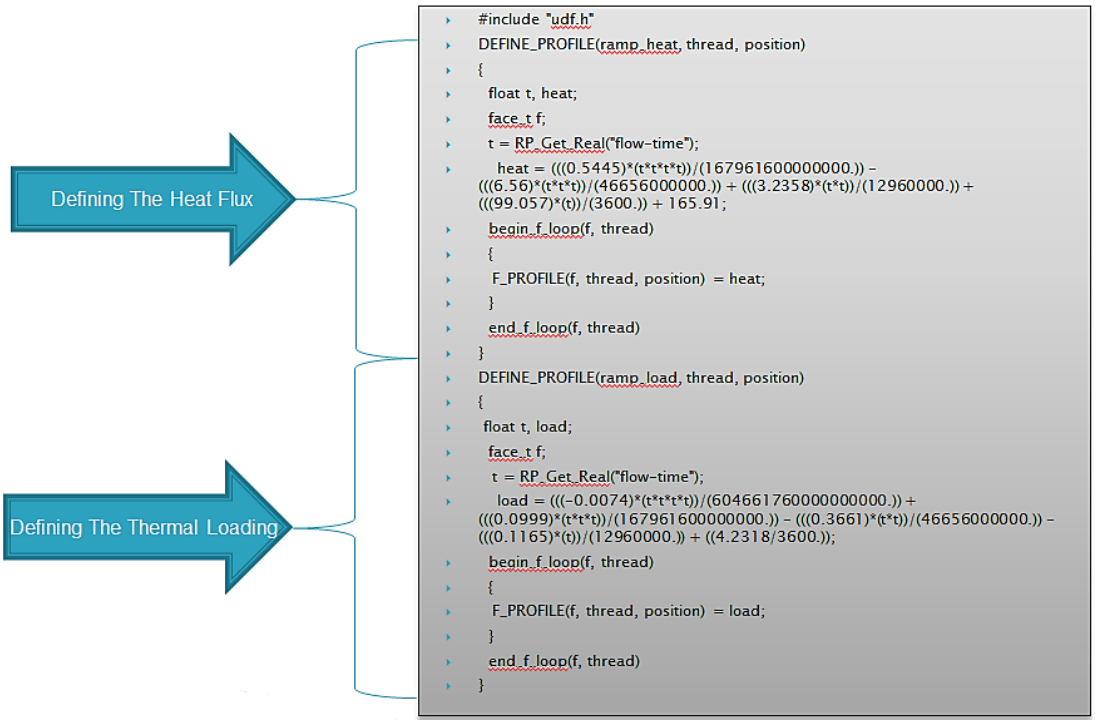


```
#include "udf.h"
DEFINE_PROFILE(ramp_heat, thread, position)
{
  float t, heat;
  face_t f;
  t = RP_Get_Real("flow-time");
    heat = (((0.5445)*(t*t*t*t))/(167961600000000.)) -
(((6.56)*(t*t*t))/(46656000000.)) + (((3.2358)*(t*t))/(12960000.)) +
(((99.057)*(t))/(3600.)) + 165.91;
  begin_f_loop(f, thread)
  {
   F_PROFILE(f, thread, position) = heat;
  }
  end_f_loop(f, thread)
}
DEFINE_PROFILE(ramp_load, thread, position)
{
 float t, load;
  face_t f;
   t = RP_Get_Real("flow-time");
    load = (((-0.0074)*(t*t*t*t))/(604661760000000000.)) +
(((0.0999)*(t*t*t))/(167961600000000.)) - (((0.3661)*(t*t))/(46656000000.)) -
(((0.1165)*(t))/(12960000.)) + ((4.2318/3600.));
  begin_f_loop(f, thread)
  {
   F_PROFILE(f, thread, position) = load;
  }
  end_f_loop(f, thread)
}
```

4- Heat flux of 15th of March and thermal loading of weekend

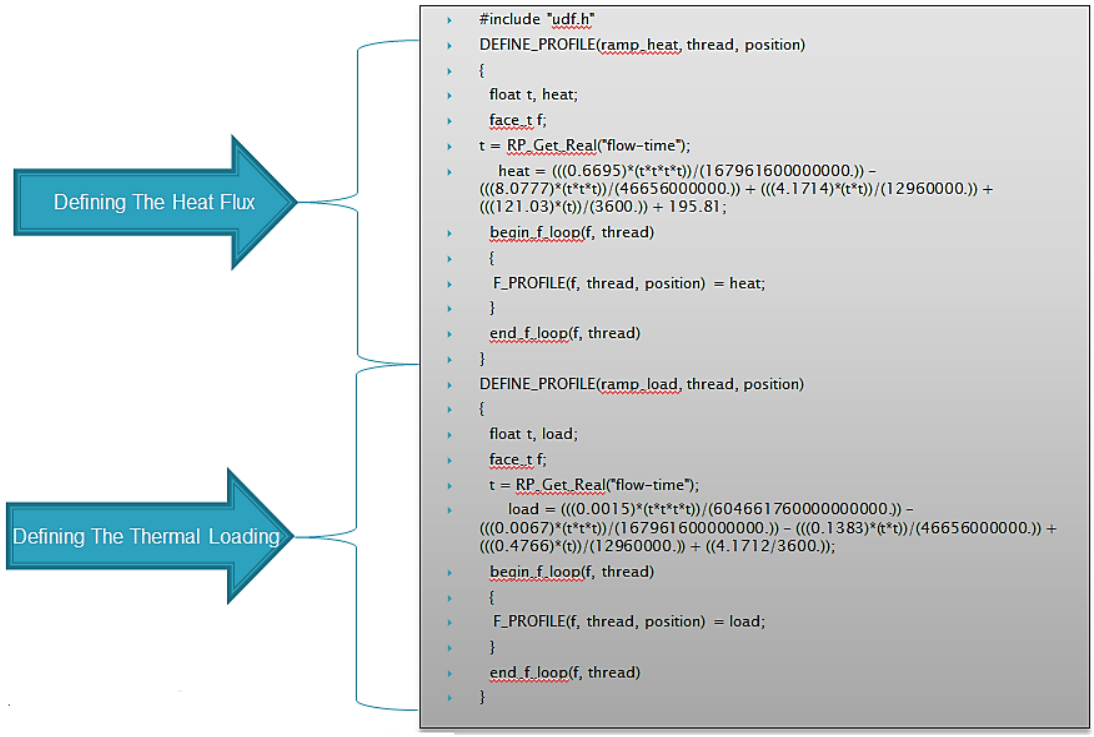


```
#include "udf.h"
DEFINE_PROFILE(ramp_heat, thread, position)
{
  float t, heat;
  face_t f;
t = RP_Get_Real("flow-time");
    heat = (((0.6695)*(t*t*t*t))/(167961600000000.)) -
(((8.0777)*(t*t*t))/(46656000000.)) + (((4.1714)*(t*t))/(12960000.)) +
(((121.03)*(t))/(3600.)) + 195.81;
  begin_f_loop(f, thread)
  {
   F_PROFILE(f, thread, position) = heat;
  }
  end_f_loop(f, thread)
}
DEFINE_PROFILE(ramp_load, thread, position)
{
  float t, load;
  face_t f;
  t = RP_Get_Real("flow-time");
     load = (((0.0015)*(t*t*t*t))/(604661760000000000.)) -
(((0.0067)*(t*t*t))/(167961600000000.)) - (((0.1383)*(t*t))/(46656000000.)) +
(((0.4766)*(t))/(12960000.)) + ((4.1712/3600.));
  begin_f_loop(f, thread)
  {
   F_PROFILE(f, thread, position) = load;
  }
  end_f_loop(f, thread)
}
```

APPENDIX B

```
N=input('input the number of day N= ');
M=input('input the site latitude M= ');
AN=input('input the tilt angle AN= ');
ST=input('input standard time ST= ');
T=input('input atmospheric transmittance T= ');
y=(360/365)*(N-81);
E=9.87*sin(2*y*pi/180)-7.53*cos(y*pi/180)-1.5*sin(y*pi/180)
W=abs((ST-12)*15)
H=23.45*sin(((360/365)*(284+N))*pi/180)
cosq2=sin((M-AN)*pi/180)*sin(H*pi/180)+cos((M-AN)*pi/180)*cos(H*pi/180)*cos(W*pi/180);
q1=acosd(cosq2)
sina=cos(M*pi/180)*cos(H*pi/180)*cos(W*pi/180)+sin(M*pi/180)*sin(H*pi/180);
a1=asind(sina);
A=1158*(1+ 0.066*cos((360/370)*N*pi/180));
B=0.175*(1-0.2*cos(0.9*N*pi/180))-0.0045*(1-cos(1.86*N*pi/180));
C=0.0965*(1-0.42*cos((360/370)*N*pi/180))-0.0075*(1-cos(1.95*N*pi/180));
IBN=A/exp(B/sin(a1*pi/180));
IB=IBN*cos(q1*pi/180);
ID=IBN*C*(((1+cos(AN*pi/180))/2));
q2=asind(sin(q1*pi/180)/1.52);
R1=(sin((q2*pi/180)-q1*pi/180))^2/(sin((q1*pi/180)+q2*pi/180)^2);
R2=(tan((q2*pi/180)-q1*pi/180)^2)/(tan((q1*pi/180)+q2*pi/180)^2);
R=(R1+R2)/2;
IR=R*IBN*(sin(a1*pi/180)+C)*((1-cos(AN*pi/180))/2);
IT=IB+ID+IR
s=(1+0.033*cos((pi/180)*(360*N/365)))
q=IT*s*T*((sin(H*pi/180)*sin((M-AN)*pi/180))+((cos(H*pi/180)*cos((M-
AN)*pi/180))*cos(W*pi/180)))
```

APPENDIX C

1- **F-value**

In this thesis the F-value test is used to check whether the analytical data, experimental data and CFD against regression model results comes from populations with equal variance [138].

2- **Durbin-Watson statistic,**

It is used to check if the residual has an autocorrelation or not. For a precise mode, residuals should be a white noise which has a normal distribution [109].

3- **Standard error,**

The standard error of the estimate is a measure of the accuracy of predictions. Recall that the regression line is the line that minimizes the sum of squared deviations of prediction (also called the sum of squares error) [138].

4- **T-Test value**

The t-test assesses whether the means of two groups are statistically different from each other [111].

5- **Lilliefors test**

Test the normality of the residual (t.e the difference between the analytical data, experimental data and CFD against regression model results) [111].

APPENDIX D

	Thermometer	Thermocouple			Inlet collector	Outlet collector	Tank
		Inlet collector	Outlet collector	Tank			
	97.5	97.72	97.75	97.78			
	97	97.21	97.24	97.28			
	96.5	96.38	96.33	96.32			
	95.7	95.41	95.39	95.35			
	95	94.88	94.81	94.84			
	94.5	94.41	94.47	94.43			
	94.3	94.28	94.25	94.22			
	93.6	93.41	93.51	93.46			
	93.1	92.91	92.87	92.85			
	92.4	92.31	92.28	92.25			
Average value	94.96	94.892	94.89	94.87	0.0716	0.0737	0.0863
	91	91.12	91.15	91.11			
	90.6	90.81	90.85	90.87			
	90	90.11	90.18	90.21			
	89.7	89.77	89.81	89.73			
	88.6	88.55	88.4	88.45			
	87.8	87.87	87.93	87.91			
	87.2	87.16	87.18	87.12			
	86.8	86.61	86.63	86.64			
	85.8	85.57	85.59	85.57			
	85.3	84.53	84.43	84.63			
Average value	88.28	88.21	88.215	88.224	0.0792	0.0736	0.0634
Percentage error					0.0754	0.0736	0.0748

APPENDIX E

1- After conducting parameters effect investigation by using the proposed CFD model, the acquired results have been classified according to the level of their effectives as shown in Appendix G.

2- The above classification has been employed to obtain dimensionless equations through using several forms for the depended and independent variables, such as Nu, Re, q/q_{max}, L/d ...etc.

3- In order to calculate the indices and factors for each term in the equation, different mathematical approaches that are adopted in the regression have been used such as $\log_{10}$, power, line ...etc. However it was found that $\log_{10}$ is the most accurate way as R^2 scored the highest value in this case among the others.

4- Microsoft excel was used as a tool to conduct the regression. The steps below explain how it can be used.

- On the Data tab, click Data Analysis as shown in figure below

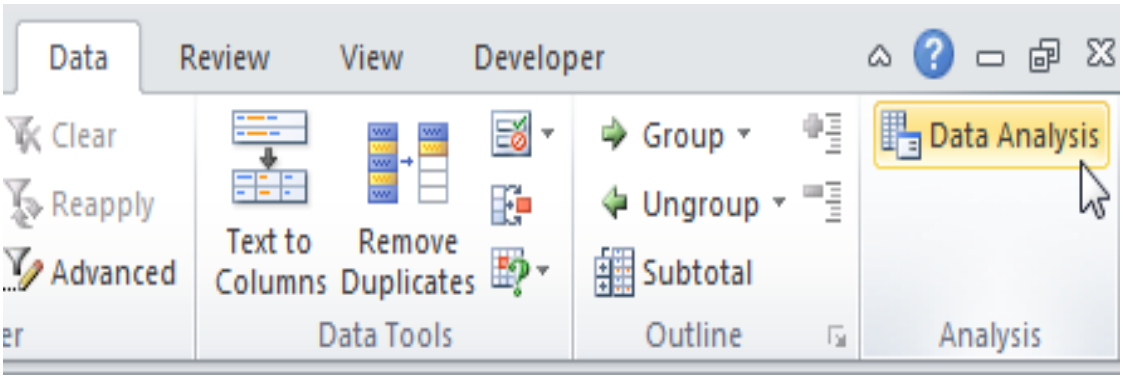

- Select Regression and click OK as shown below

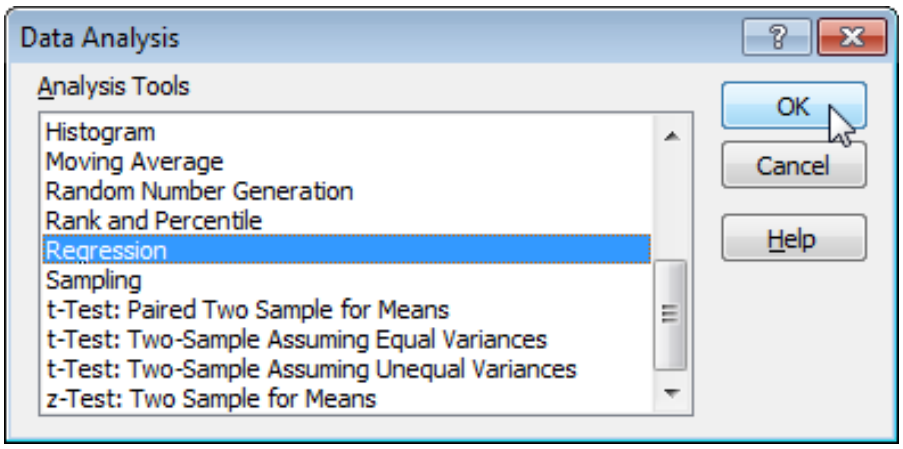

- Select the Y Range, which is the dependent variable or predictor variable
- Select the X Ranges which are independent variables
- Check Labels
- Chose an Output Range
- Click OK

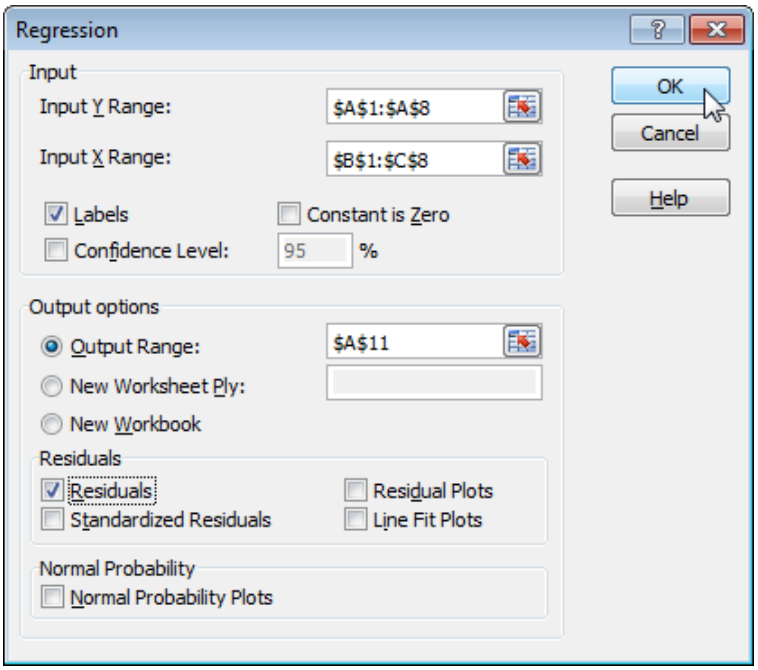

APPENDIX F

Test No.1 traditional model with constant heat flux (five hours)

Time (minutes)	Outlet °C	Inlet °C	Tank °C	Average wall °C
0	24.16	24.01	23.99	25.055
1	24.17	24	23.99	26.565
2	24.45	23.98	23.95	31.01
3	25.71	23.98	23.94	36.365
4	28.29	24.04	23.91	41.36
5	31.02	24.08	23.9	45.605
6	33.73	24.09	23.87	49.06
7	35.84	24.29	23.87	51.88
8	37.63	25.01	23.89	54.205
9	39.12	26.22	23.9	56.065
10	40.09	27.35	23.89	57.59
11	40.44	28.27	23.91	58.945
12	40.61	29.09	23.95	59.97
13	41.15	29.92	24	60.905
14	42	30.61	24.02	61.73
15	42.89	31.15	24.06	62.415
16	43.62	31.69	24.09	63.045
17	44.2	32.21	24.13	63.545
18	44.68	32.74	24.15	63.95
19	45.1	33.2	24.18	64.32
20	45.45	33.6	24.23	64.635
21	45.8	33.94	24.24	64.895
22	46.13	34.21	24.24	65.135
23	46.44	34.48	24.29	65.265
24	46.71	34.79	24.35	65.515
25	46.96	35.09	24.42	65.68
26	47.19	35.35	24.49	65.925
27	47.39	35.59	24.57	66.02
28	47.59	35.81	24.58	66.2
29	47.75	35.98	24.65	66.31
30	47.9	36.15	24.71	66.43
31	48.04	36.31	24.74	66.54
32	48.17	36.45	24.78	66.615
33	48.26	36.58	24.82	66.75
34	48.37	36.7	24.88	66.835

35	48.45	36.79	24.93	67
36	48.5	36.86	24.94	67.01
37	48.58	36.95	24.99	66.955
38	48.68	37.03	25.03	67.005
39	48.76	37.11	25.09	67.06
40	48.81	37.18	25.15	67.17
41	48.88	37.24	25.2	67.14
42	48.97	37.33	25.26	67.24
43	49.05	37.41	25.28	67.23
44	49.07	37.46	25.33	67.325
45	49.1	37.51	25.37	67.315
46	49.15	37.56	25.39	67.36
47	49.21	37.61	25.45	67.455
48	49.28	37.68	25.49	67.495
49	49.32	37.73	25.58	67.575
50	49.37	37.78	25.66	67.585
51	49.4	37.84	25.7	67.62
52	49.45	37.89	25.74	67.635
53	49.5	37.93	25.79	67.73
54	49.53	37.99	25.82	67.805
55	49.56	38.04	25.87	67.825
56	49.58	38.07	25.89	67.85
57	49.61	38.12	25.92	67.98
58	49.65	38.13	25.97	68.075
59	49.68	38.16	26.02	68.01
60	49.72	38.19	26.09	68.035
61	49.76	38.24	26.13	67.945
62	49.79	38.27	26.19	67.91
63	49.81	38.31	26.23	67.835
64	49.84	38.34	26.29	67.9
65	49.88	38.39	26.38	67.9
66	49.92	38.44	26.48	67.91
67	49.98	38.51	26.57	68
68	50.02	38.56	26.62	68.025
69	50.05	38.6	26.68	68.095
70	50.06	38.63	26.7	68.07
71	50.1	38.66	26.73	68.17
72	50.16	38.72	26.79	68.26
73	50.19	38.76	26.83	68.31
74	50.24	38.8	26.9	68.28
75	50.28	38.82	26.97	68.165
76	50.3	38.86	27.05	68.115
77	50.34	38.87	27.12	68.16

78	50.37	38.87	27.13	68.21
79	50.38	38.91	27.16	68.235
80	50.42	38.96	27.22	68.26
81	50.44	39	27.27	68.29
82	50.47	39.03	27.32	68.31
83	50.49	39.06	27.37	68.32
84	50.53	39.1	27.43	68.32
85	50.58	39.11	27.47	68.295
86	50.62	39.13	27.55	68.335
87	50.63	39.16	27.59	68.295
88	50.62	39.17	27.57	68.31
89	50.65	39.19	27.55	68.365
90	50.66	39.2	27.57	68.405
91	50.67	39.25	27.6	68.36
92	50.67	39.28	27.66	68.255
93	50.7	39.28	27.74	68.155
94	50.7	39.29	27.75	68.225
95	50.72	39.32	27.76	68.33
96	50.75	39.37	27.8	68.385
97	50.78	39.41	27.83	68.45
98	50.83	39.45	27.9	68.475
99	50.84	39.49	27.96	68.535
100	50.88	39.54	28.02	68.655
101	50.92	39.57	28.08	68.725
102	51	39.6	28.12	68.71
103	51.02	39.62	28.13	68.57
104	51.02	39.65	28.14	68.395
105	51	39.65	28.16	68.345
106	51.01	39.68	28.19	68.46
107	51.03	39.7	28.24	68.5
108	51.05	39.71	28.3	68.585
109	51.12	39.72	28.4	68.455
110	51.16	39.73	28.48	68.475
111	51.18	39.77	28.53	68.605
112	51.19	39.84	28.56	68.695
113	51.2	39.89	28.58	68.735
114	51.24	39.94	28.62	68.79
115	51.29	39.98	28.7	68.815
116	51.34	40.01	28.77	68.71
117	51.39	40.05	28.85	68.745
118	51.39	40.07	28.84	68.67
119	51.38	40.08	28.87	68.68
120	51.39	40.1	28.92	68.765

121	51.43	40.12	28.96	68.87
122	51.46	40.12	29	68.86
123	51.5	40.16	29.03	68.845
124	51.53	40.22	29.11	68.845
125	51.56	40.25	29.15	68.89
126	51.59	40.27	29.19	68.965
127	51.65	40.32	29.25	68.99
128	51.67	40.35	29.3	69.01
129	51.73	40.38	29.36	68.98
130	51.77	40.36	29.38	68.94
131	51.78	40.39	29.42	68.94
132	51.79	40.46	29.45	68.975
133	51.82	40.51	29.52	69.035
134	51.85	40.54	29.57	69.09
135	51.89	40.51	29.58	69.08
136	51.91	40.51	29.6	69.105
137	51.9	40.48	29.61	68.98
138	51.9	40.49	29.65	68.995
139	51.89	40.51	29.72	68.86
140	51.91	40.58	29.77	68.98
141	51.94	40.64	29.81	69.09
142	51.99	40.66	29.86	69.145
143	52.03	40.66	29.85	69.09
144	52.05	40.73	29.86	68.94
145	52.03	40.76	29.86	68.94
146	51.99	40.76	29.85	68.89
147	51.94	40.73	29.83	68.86
148	51.91	40.72	29.83	68.925
149	51.93	40.73	29.87	69.15
150	51.95	40.73	29.93	69.245
151	52	40.72	30.02	69.115
152	52.06	40.74	30.07	68.985
153	52.08	40.75	30.06	69.005
154	52.08	40.8	30.08	69.045
155	52.06	40.82	30.1	69.02
156	52.07	40.81	30.13	69.025
157	52.11	40.87	30.14	69.13
158	52.12	40.93	30.18	69.14
159	52.13	40.97	30.21	69.2
160	52.17	40.99	30.26	69.225
161	52.14	40.98	30.23	69.225
162	52.15	40.99	30.25	69.195
163	52.17	41	30.29	69.255

164	52.21	41.04	30.32	69.375
165	52.23	41.08	30.39	69.415
166	52.26	41.12	30.42	69.42
167	52.31	41.14	30.48	69.49
168	52.31	41.15	30.52	69.48
169	52.31	41.15	30.54	69.57
170	52.32	41.17	30.52	69.515
171	52.36	41.21	30.56	69.445
172	52.37	41.23	30.61	69.52
173	52.41	41.28	30.68	69.535
174	52.47	41.3	30.79	69.585
175	52.52	41.36	30.86	69.57
176	52.54	41.41	30.89	69.56
177	52.56	41.43	30.89	69.505
178	52.56	41.45	30.89	69.435
179	52.56	41.48	30.9	69.475
180	52.58	41.49	30.92	69.565
181	52.59	41.51	30.99	69.525
182	52.62	41.54	31	69.535
183	52.65	41.58	31.05	69.62
184	52.66	41.59	31.08	69.56
185	52.68	41.57	31.13	69.59
186	52.69	41.56	31.21	69.325
187	52.71	41.56	31.29	69.06
188	52.75	41.6	31.35	69.07
189	52.82	41.62	31.44	69.23
190	52.85	41.6	31.48	69.275
191	52.9	41.64	31.51	69.405
192	52.93	41.72	31.55	69.49
193	52.96	41.77	31.6	69.57
194	52.99	41.78	31.65	69.52
195	53	41.77	31.67	69.485
196	52.99	41.82	31.72	69.48
197	52.98	41.85	31.74	69.46
198	53	41.85	31.74	69.395
199	52.97	41.86	31.72	69.455
200	52.95	41.87	31.7	69.58
201	52.97	41.89	31.73	69.65
202	53.01	41.96	31.78	69.715
203	53.05	41.95	31.78	69.76
204	53.08	41.99	31.81	69.77
205	53.12	42	31.88	69.78
206	53.17	41.99	31.95	69.685

207	53.21	41.97	32.02	69.555
208	53.19	41.95	32.07	69.6
209	53.2	41.99	32.13	69.6
210	53.21	42.04	32.17	69.675
211	53.24	42.09	32.21	69.575
212	53.25	42.14	32.24	69.545
213	53.24	42.12	32.3	69.58
214	53.26	42.1	32.33	69.455
215	53.27	42.12	32.34	69.475
216	53.27	42.15	32.37	69.555
217	53.29	42.18	32.43	69.555
218	53.34	42.2	32.44	69.45
219	53.37	42.23	32.46	69.54
220	53.38	42.28	32.47	69.585
221	53.37	42.3	32.49	69.525
222	53.36	42.33	32.52	69.525
223	53.38	42.33	32.53	69.575
224	53.41	42.33	32.57	69.635
225	53.44	42.33	32.63	69.655
226	53.44	42.34	32.65	69.51
227	53.44	42.38	32.66	69.46
228	53.45	42.44	32.71	69.49
229	53.48	42.44	32.73	69.505
230	53.46	42.4	32.7	69.395
231	53.46	42.44	32.68	69.38
232	53.4	42.41	32.66	69.395
233	53.39	42.38	32.73	69.45
234	53.4	42.37	32.76	69.44
235	53.43	42.41	32.75	69.375
236	53.46	42.46	32.8	69.425
237	53.46	42.52	32.81	69.41
238	53.45	42.55	32.8	69.395
239	53.47	42.55	32.85	69.38
240	53.52	42.55	32.89	69.485
241	53.53	42.58	32.94	69.535
242	53.54	42.6	32.99	69.57
243	53.56	42.65	33.02	69.615
244	53.57	42.67	33.03	69.64
245	53.56	42.68	33.05	69.725
246	53.58	42.71	33.08	69.735
247	53.6	42.74	33.11	69.725
248	53.62	42.78	33.14	69.675
249	53.65	42.77	33.2	69.675

250	53.67	42.77	33.23	69.63
251	53.65	42.77	33.21	69.67
252	53.67	42.82	33.22	69.6
253	53.67	42.82	33.25	69.65
254	53.66	42.82	33.3	69.58
255	53.7	42.82	33.33	69.655
256	53.77	42.81	33.38	69.745
257	53.77	42.84	33.43	69.77
258	53.77	42.89	33.44	69.745
259	53.78	42.93	33.43	69.8
260	53.81	42.93	33.47	69.855
261	53.82	42.89	33.49	69.725
262	53.81	42.89	33.51	69.685
263	53.83	42.9	33.54	69.77
264	53.86	42.97	33.62	69.875
265	53.89	43.01	33.66	69.88
266	53.94	43.01	33.71	69.865
267	53.96	43.04	33.72	69.86
268	53.98	43.07	33.75	69.9
269	53.98	43.07	33.78	69.845
270	53.97	43.02	33.82	69.825
271	53.99	42.99	33.84	69.82
272	54.03	43.01	33.86	69.8
273	54.05	43.01	33.93	69.765
274	54.03	43.06	33.94	69.855
275	54.05	43.14	33.94	69.795
276	54.08	43.2	33.97	69.81
277	54.08	43.13	33.99	69.905
278	54.12	43.12	34.02	70.02
279	54.19	43.17	34.07	70.02
280	54.2	43.22	34.09	69.965
281	54.21	43.26	34.11	70
282	54.21	43.29	34.13	69.935
283	54.23	43.32	34.15	69.905
284	54.26	43.32	34.17	69.97
285	54.27	43.35	34.2	69.95
286	54.29	43.37	34.24	69.98
287	54.3	43.39	34.28	69.92
288	54.33	43.4	34.3	70.02
289	54.36	43.37	34.32	69.88
290	54.4	43.37	34.37	69.825
291	54.43	43.36	34.41	69.755
292	54.4	43.4	34.45	69.545

293	54.38	43.4	34.48	69.665
294	54.36	43.37	34.47	69.725
295	54.37	43.43	34.48	69.765
296	54.39	43.49	34.47	69.855
297	54.43	43.52	34.48	69.865
298	54.43	43.5	34.49	69.81
299	54.43	43.52	34.49	69.98

Test No.2 traditional model with constant heat flux (four hours)

Time (minutes)	Outlet °C	Inlet °C	Tank °C	Average wall °C
0	25.81	23.72	25.16	25.55
1	25.81	23.78	25.16	26.515
2	26.02	23.91	25.18	30.23
3	27.05	24.06	25.2	35.195
4	29.19	24.28	25.21	40.065
5	31.47	24.5	25.22	44.36
6	33.84	24.72	25.27	47.885
7	35.85	25.03	25.29	50.735
8	37.5	25.73	25.34	53.065
9	38.82	26.87	25.39	54.87
10	39.83	27.91	25.41	56.395
11	40.46	28.75	25.44	57.695
12	40.84	29.54	25.46	58.78
13	41.32	30.43	25.49	59.73
14	42.09	31.15	25.53	60.535
15	42.91	31.67	25.57	61.28
16	43.64	32.22	25.59	61.845
17	44.26	32.76	25.64	62.36
18	44.77	33.27	25.7	62.825
19	45.2	33.74	25.75	63.21
20	45.59	34.19	25.78	63.595
21	45.96	34.58	25.84	63.89
22	46.3	34.91	25.88	64.205
23	46.62	35.18	25.92	64.455
24	46.96	35.46	25.98	64.67
25	47.21	35.71	26.04	64.86
26	47.42	35.97	26.07	65.065
27	47.64	36.2	26.09	65.27
28	47.84	36.42	26.14	65.435
29	48.03	36.63	26.23	65.665

30	48.2	36.81	26.3	65.76
31	48.35	36.96	26.35	65.9
32	48.47	37.09	26.37	66.005
33	48.58	37.2	26.39	66.08
34	48.69	37.32	26.45	66.16
35	48.8	37.42	26.49	66.23
36	48.9	37.51	26.54	66.455
37	48.98	37.59	26.58	66.47
38	49.06	37.69	26.63	66.605
39	49.12	37.74	26.68	66.715
40	49.2	37.82	26.69	66.75
41	49.32	37.93	26.79	66.785
42	49.37	37.99	26.81	66.77
43	49.43	38.06	26.89	66.84
44	49.5	38.14	26.92	66.925
45	49.52	38.18	26.94	66.985
46	49.55	38.22	26.97	66.97
47	49.62	38.28	27.02	66.95
48	49.67	38.35	27.08	66.995
49	49.7	38.38	27.12	67.04
50	49.76	38.42	27.17	67.16
51	49.8	38.46	27.19	67.065
52	49.86	38.52	27.27	67.09
53	49.87	38.53	27.27	67.13
54	49.88	38.56	27.29	67.185
55	49.91	38.63	27.36	67.33
56	49.95	38.66	27.4	67.28
57	50.01	38.68	27.44	67.26
58	50.06	38.72	27.48	67.37
59	50.07	38.74	27.5	67.355
60	50.07	38.77	27.52	67.32
61	50.09	38.81	27.56	67.35
62	50.13	38.86	27.63	67.395
63	50.16	38.91	27.66	67.43
64	50.18	38.93	27.67	67.39
65	50.19	38.97	27.72	67.37
66	50.19	38.94	27.77	67.465
67	50.29	38.99	27.83	67.57
68	50.36	39.06	27.89	67.65
69	50.41	39.11	27.91	67.565
70	50.39	39.12	27.94	67.535
71	50.4	39.14	27.98	67.525
72	50.36	39.14	28	67.475

73	50.4	39.18	28.05	67.475
74	50.42	39.21	28.11	67.595
75	50.46	39.27	28.17	67.645
76	50.48	39.28	28.22	67.76
77	50.48	39.28	28.22	67.72
78	50.5	39.31	28.28	67.735
79	50.51	39.32	28.3	67.755
80	50.51	39.34	28.37	67.855
81	50.55	39.37	28.39	67.825
82	50.61	39.42	28.48	67.735
83	50.64	39.44	28.48	67.685
84	50.69	39.48	28.53	67.73
85	50.67	39.47	28.56	67.825
86	50.65	39.47	28.57	67.86
87	50.7	39.51	28.63	67.96
88	50.7	39.53	28.62	67.93
89	50.73	39.58	28.67	67.94
90	50.8	39.64	28.71	67.835
91	50.82	39.67	28.77	67.825
92	50.86	39.73	28.82	67.86
93	50.9	39.78	28.85	67.94
94	50.92	39.81	28.89	68.06
95	50.97	39.83	28.97	68.035
96	51.01	39.83	28.99	67.99
97	51.06	39.87	29.03	68
98	51.08	39.9	29.07	67.99
99	51.13	39.96	29.14	67.94
100	51.17	39.99	29.19	67.95
101	51.18	40	29.22	67.945
102	51.15	39.96	29.22	67.915
103	51.13	39.96	29.21	68.08
104	51.14	39.98	29.23	68.015
105	51.11	39.99	29.22	67.95
106	51.11	39.97	29.26	68.04
107	51.12	39.98	29.27	68.135
108	51.15	40.02	29.31	68.225
109	51.17	40.03	29.3	68.095
110	51.17	40.04	29.35	68.03
111	51.23	40.09	29.41	68.105
112	51.28	40.12	29.49	68.125
113	51.34	40.17	29.57	67.975
114	51.41	40.25	29.61	68.015
115	51.43	40.27	29.67	68.145

116	51.44	40.29	29.73	68.1
117	51.5	40.37	29.79	68.175
118	51.53	40.42	29.81	68.19
119	51.55	40.47	29.84	68.41
120	51.59	40.49	29.87	68.46
121	51.61	40.52	29.88	68.265
122	51.68	40.54	29.94	68.38
123	51.7	40.56	29.98	68.44
124	51.71	40.59	30.05	68.32
125	51.71	40.6	30.05	68.17
126	51.69	40.61	30.07	68.265
127	51.69	40.62	30.11	68.255
128	51.71	40.65	30.15	68.365
129	51.76	40.68	30.19	68.43
130	51.78	40.72	30.22	68.41
131	51.84	40.76	30.25	68.54
132	51.89	40.81	30.3	68.615
133	51.88	40.81	30.33	68.64
134	51.91	40.84	30.42	68.64
135	51.98	40.88	30.47	68.565
136	52.03	40.93	30.51	68.525
137	52.03	40.95	30.53	68.61
138	52.04	40.96	30.56	68.75
139	52.07	41	30.59	68.675
140	52.11	41.02	30.67	68.635
141	52.14	41.02	30.71	68.64
142	52.17	41.03	30.75	68.72
143	52.18	41.05	30.77	68.86
144	52.2	41.12	30.79	68.89
145	52.18	41.14	30.79	68.885
146	52.19	41.17	30.8	68.685
147	52.2	41.18	30.82	68.5
148	52.23	41.2	30.87	68.525
149	52.28	41.22	30.94	68.61
150	52.26	41.2	30.97	68.63
151	52.26	41.23	30.99	68.705
152	52.28	41.26	31.04	68.625
153	52.31	41.3	31.03	68.655
154	52.3	41.32	31.06	68.815
155	52.28	41.31	31.06	68.96
156	52.27	41.29	31.08	68.925
157	52.34	41.36	31.16	68.96
158	52.41	41.4	31.19	69.045

159	52.43	41.43	31.19	69.01
160	52.39	41.46	31.2	68.92
161	52.4	41.47	31.25	68.725
162	52.39	41.48	31.31	68.595
163	52.39	41.51	31.35	68.6
164	52.38	41.52	31.38	68.58
165	52.42	41.5	31.39	68.62
166	52.44	41.52	31.45	68.805
167	52.48	41.51	31.51	68.84
168	52.47	41.51	31.53	68.715
169	52.51	41.53	31.56	68.72
170	52.51	41.53	31.58	68.855
171	52.56	41.59	31.61	68.845
172	52.56	41.63	31.61	68.915
173	52.6	41.67	31.65	68.945
174	52.63	41.7	31.69	69.055
175	52.64	41.69	31.72	68.94
176	52.68	41.73	31.77	68.96
177	52.7	41.75	31.8	69.025
178	52.69	41.78	31.82	69.02
179	52.68	41.78	31.83	69.05
180	52.69	41.8	31.86	69.035
181	52.7	41.83	31.87	69.135
182	52.73	41.83	31.93	69.135
183	52.74	41.84	31.98	69.255
184	52.79	41.87	32	69.185
185	52.8	41.9	32.01	69.04
186	52.84	41.93	32.04	69.025
187	52.88	41.96	32.1	69.125
188	52.91	41.98	32.16	69.145
189	52.95	42	32.2	68.96
190	52.99	42.06	32.24	69.005
191	52.98	42.06	32.27	69.03
192	52.95	42.05	32.26	68.995
193	52.94	42.05	32.26	68.925
194	52.97	42.1	32.31	68.915
195	53	42.15	32.35	68.93
196	52.96	42.14	32.32	68.915
197	52.96	42.13	32.33	68.915
198	52.99	42.16	32.36	69.05
199	53.01	42.19	32.39	69.005
200	53.04	42.2	32.4	68.935
201	53.06	42.18	32.44	68.81

202	53.08	42.2	32.49	68.705
203	53.11	42.22	32.55	68.74
204	53.11	42.29	32.6	68.84
205	53.1	42.32	32.64	69.135
206	53.1	42.29	32.65	69.28
207	53.1	42.25	32.62	69.325
208	53.15	42.28	32.68	69.095
209	53.16	42.28	32.73	68.91
210	53.19	42.32	32.76	68.94
211	53.25	42.36	32.82	68.92
212	53.23	42.37	32.83	68.945
213	53.19	42.38	32.82	69.04
214	53.19	42.41	32.8	69.185
215	53.22	42.43	32.85	69.34
216	53.25	42.45	32.9	69.295
217	53.29	42.5	32.9	69.205
218	53.3	42.51	32.93	69.31
219	53.31	42.5	33.01	69.275
220	53.3	42.51	32.98	69.32
221	53.28	42.5	32.98	69.46
222	53.3	42.51	32.99	69.34
223	53.34	42.53	33.03	69.305
224	53.37	42.57	33.1	69.38
225	53.36	42.58	33.13	69.35
226	53.39	42.63	33.16	69.28
227	53.41	42.69	33.18	69.33
228	53.42	42.71	33.21	69.25
229	53.43	42.72	33.23	69.29
230	53.48	42.74	33.28	69.3
231	53.49	42.74	33.3	69.255
232	53.5	42.72	33.35	69.41
233	53.54	42.72	33.36	69.375
234	53.55	42.76	33.38	69.25
235	53.54	42.8	33.38	69.36
236	53.52	42.81	33.39	69.355
237	53.55	42.82	33.45	69.445
238	53.62	42.81	33.5	69.445
239	53.64	42.82	33.5	69.49
240	53.59	42.82	33.46	69.58

Test No.3 traditional model with various heat fluxes (seven hours)

Time (minutes)	Inlet °C	Outlet °C	Tank °C	Average wall °C
0	22.21	22.44	22.86	26
1	22.23	22.61	22.88	27.29
2	22.28	23.3	22.9	31.225
3	22.37	24.95	22.93	36.095
4	22.47	27.55	22.95	40.665
5	22.64	30.19	22.98	44.56
6	22.8	32.71	23	47.675
7	23.1	34.5	23.02	50.135
8	24.03	36.16	23.02	52.085
9	25.32	37.53	23.06	53.68
10	26.39	38.48	23.11	55.015
11	27.21	38.92	23.15	56.105
12	27.96	39.13	23.18	57.11
13	28.78	39.6	23.24	57.915
14	29.64	40.38	23.31	58.66
15	30.13	41.25	23.36	59.295
16	30.55	42	23.42	59.835
17	31.07	42.61	23.46	60.37
18	31.6	43.12	23.52	60.825
19	32.06	43.54	23.56	61.175
20	32.46	43.91	23.6	61.475
21	32.83	44.26	23.65	61.795
22	33.19	44.62	23.71	62.095
23	33.49	44.96	23.79	62.3
24	33.79	45.25	23.83	62.43
25	34.06	45.51	23.88	62.655
26	34.29	45.74	23.94	62.955
27	34.49	45.95	24	62.99
28	34.68	46.14	24.06	63.07
29	34.85	46.29	24.08	63.235
30	35.01	46.43	24.15	63.44
31	35.13	46.56	24.21	63.555
32	35.27	46.7	24.28	63.475
33	35.39	46.82	24.34	63.535
34	35.5	46.94	24.39	63.43
35	35.64	47.06	24.5	63.57
36	35.78	47.17	24.58	63.885
37	35.87	47.24	24.61	63.87
38	35.95	47.3	24.63	64.015

39	36.05	47.39	24.68	64.02
40	36.14	47.48	24.72	63.98
41	36.21	47.55	24.77	64.17
42	36.27	47.61	24.82	64.385
43	36.32	47.63	24.86	64.38
44	36.38	47.69	24.9	64.495
45	36.46	47.76	24.97	64.52
46	36.53	47.8	25.01	64.6
47	36.6	47.84	25.07	64.68
48	36.64	47.87	25.09	64.64
49	36.7	47.93	25.12	64.7
50	36.78	48	25.2	64.78
51	36.84	48.04	25.25	64.84
52	36.88	48.09	25.28	65.055
53	36.93	48.15	25.33	65.175
54	36.99	48.22	25.36	65.3
55	37.06	48.3	25.44	65.4
56	37.13	48.34	25.49	65.355
57	37.2	48.4	25.55	65.415
58	37.25	48.44	25.59	65.455
59	37.31	48.5	25.64	65.45
60	37.38	48.54	25.68	65.435
61	37.43	48.6	25.72	65.445
62	37.49	48.64	25.78	65.575
63	37.51	48.67	25.8	65.635
64	37.56	48.7	25.83	65.7
65	37.59	48.72	25.88	65.725
66	37.6	48.75	25.94	65.76
67	37.64	48.82	25.99	65.855
68	37.71	48.87	26.04	65.87
69	37.74	48.9	26.12	65.975
70	37.77	48.91	26.14	65.99
71	37.82	48.94	26.19	66.05
72	37.88	48.98	26.22	66.16
73	37.93	49.03	26.26	66.045
74	37.97	49.06	26.33	65.975
75	38	49.08	26.36	65.995
76	38.05	49.13	26.41	66.115
77	38.08	49.18	26.5	66.26
78	38.11	49.21	26.52	66.22
79	38.16	49.22	26.56	66.145
80	38.18	49.25	26.6	66.135
81	38.22	49.25	26.66	66.125

82	38.25	49.27	26.68	66.175
83	38.28	49.29	26.73	66.11
84	38.31	49.29	26.75	66.13
85	38.33	49.33	26.79	66.2
86	38.36	49.35	26.82	66.19
87	38.39	49.38	26.86	66.29
88	38.42	49.42	26.96	66.475
89	38.46	49.51	27.04	66.445
90	38.45	49.44	27.06	65.54
91	38.45	48.9	27.11	61.95
92	38.36	47.75	27.15	57.53
93	38.06	46.25	27.18	53.455
94	37.6	44.73	27.18	49.98
95	37.04	43.31	27.2	47.11
96	36.41	42.06	27.21	44.745
97	35.75	41.01	27.22	42.775
98	35.1	40.1	27.2	41.11
99	34.47	39.28	27.19	39.71
100	33.93	38.51	27.2	38.515
101	33.4	37.77	27.23	37.445
102	32.93	37.1	27.24	36.52
103	32.49	36.42	27.23	35.645
104	32.1	35.79	27.22	34.875
105	31.74	35.23	27.23	34.87
106	31.37	34.91	27.25	37.585
107	30.99	35.27	27.26	41.83
108	30.66	36.43	27.26	46.045
109	30.52	38.03	27.26	49.69
110	30.7	39.79	27.31	52.675
111	31.1	41.18	27.3	55.04
112	31.67	42.18	27.29	56.985
113	32.31	42.92	27.31	58.6
114	32.84	43.41	27.35	59.8
115	33.43	43.84	27.38	60.795
116	33.96	44.38	27.39	61.585
117	34.39	44.96	27.42	62.245
118	34.81	45.54	27.48	62.875
119	35.23	46.06	27.53	63.43
120	35.64	46.52	27.54	64.02
121	36.04	46.92	27.57	64.44
122	36.37	47.28	27.66	64.875
123	36.68	47.63	27.73	65.195
124	37	47.97	27.8	65.52

125	37.29	48.25	27.86	65.77
126	37.53	48.51	27.88	65.985
127	37.76	48.74	27.96	66.235
128	37.94	48.95	28.01	66.37
129	38.13	49.16	28.03	66.65
130	38.31	49.36	28.09	66.795
131	38.49	49.52	28.13	66.79
132	38.67	49.65	28.17	66.9
133	38.81	49.77	28.21	67.08
134	38.95	49.9	28.27	67.24
135	39.04	50.01	28.33	67.33
136	39.13	50.12	28.38	67.36
137	39.27	50.2	28.4	67.355
138	39.37	50.27	28.42	67.355
139	39.43	50.33	28.46	67.415
140	39.47	50.37	28.52	67.44
141	39.51	50.43	28.57	67.44
142	39.57	50.51	28.63	67.525
143	39.61	50.55	28.65	67.61
144	39.64	50.61	28.69	67.65
145	39.7	50.69	28.76	67.725
146	39.75	50.76	28.8	67.765
147	39.81	50.79	28.82	67.8
148	39.84	50.83	28.85	67.85
149	39.87	50.88	28.9	67.875
150	39.95	50.95	28.98	67.865
151	40.02	50.99	29.03	67.865
152	40.09	51	29.05	67.87
153	40.13	51.02	29.06	67.99
154	40.15	51.05	29.08	67.985
155	40.2	51.08	29.14	68.02
156	40.26	51.12	29.17	68.045
157	40.29	51.14	29.2	68.05
158	40.35	51.18	29.25	68.065
159	40.39	51.2	29.26	68.08
160	40.41	51.23	29.27	68.115
161	40.42	51.25	29.34	68.185
162	40.45	51.31	29.46	68.245
163	40.48	51.37	29.5	68.305
164	40.51	51.43	29.57	68.355
165	40.5	51.44	29.57	68.38
166	40.54	51.48	29.6	68.36
167	40.6	51.5	29.64	68.41

168	40.64	51.5	29.65	68.415
169	40.65	51.53	29.69	68.365
170	40.66	51.57	29.74	68.5
171	40.71	51.63	29.81	68.51
172	40.76	51.66	29.86	68.53
173	40.79	51.68	29.88	68.495
174	40.81	51.7	29.89	68.45
175	40.86	51.75	29.96	68.435
176	40.91	51.77	29.98	68.47
177	40.93	51.78	30.02	68.48
178	40.95	51.81	30.08	68.455
179	40.98	51.82	30.13	68.34
180	41	51.82	30.15	68.32
181	41	51.83	30.18	68.18
182	41.03	51.81	30.21	68.125
183	41.06	51.79	30.23	68.015
184	41.06	51.78	30.28	67.905
185	41.06	51.76	30.34	67.905
186	41.04	51.77	30.4	67.925
187	41.03	51.78	30.4	67.985
188	41.05	51.81	30.45	68
189	41.06	51.85	30.52	67.955
190	41.07	51.83	30.56	68
191	41.08	51.84	30.57	68.015
192	41.1	51.87	30.59	67.89
193	41.14	51.86	30.63	67.855
194	41.14	51.86	30.68	67.95
195	41.12	51.79	30.73	67.2
196	41.1	51.21	30.71	63.475
197	40.98	50.03	30.7	59.025
198	40.69	48.56	30.74	54.905
199	40.19	47.01	30.72	51.395
200	39.59	45.54	30.7	48.49
201	38.9	44.22	30.66	46.065
202	38.21	43.11	30.67	44.09
203	37.54	42.15	30.65	42.425
204	36.92	41.28	30.63	41
205	36.33	40.47	30.62	39.755
206	35.79	39.7	30.6	38.685
207	35.28	38.96	30.59	37.78
208	34.84	38.28	30.57	36.955
209	34.42	37.63	30.56	36.23
210	34.05	37.07	30.57	36.2

211	33.71	36.75	30.58	38.835
212	33.37	37.11	30.6	42.98
213	33.06	38.3	30.62	47.235
214	32.94	39.83	30.63	50.865
215	33.04	41.59	30.66	53.79
216	33.34	43.01	30.68	56.075
217	33.85	44.07	30.72	57.96
218	34.53	44.84	30.73	59.43
219	35.13	45.29	30.72	60.545
220	35.66	45.61	30.7	61.415
221	36.17	46.09	30.73	62.34
222	36.62	46.67	30.76	63.135
223	37.01	47.23	30.78	63.72
224	37.43	47.75	30.8	64.295
225	37.81	48.24	30.85	64.765
226	38.17	48.65	30.92	65.15
227	38.51	49	30.99	65.49
228	38.79	49.31	31.04	65.795
229	39.07	49.62	31.09	66.055
230	39.35	49.89	31.13	66.23
231	39.59	50.11	31.12	66.37
232	39.79	50.33	31.14	66.525
233	39.98	50.52	31.19	66.675
234	40.16	50.67	31.22	66.765
235	40.32	50.82	31.26	66.985
236	40.45	50.99	31.3	67.07
237	40.57	51.13	31.35	67.13
238	40.68	51.27	31.4	67.14
239	40.8	51.35	31.41	67.12
240	40.92	51.41	31.42	67.18
241	40.99	51.46	31.42	67.255
242	41.07	51.53	31.48	67.36
243	41.11	51.57	31.48	67.43
244	41.2	51.64	31.49	67.515
245	41.25	51.69	31.52	67.585
246	41.31	51.73	31.53	67.615
247	41.34	51.81	31.54	67.7
248	41.42	51.88	31.59	67.765
249	41.48	51.91	31.62	67.79
250	41.51	51.95	31.68	67.825
251	41.52	51.99	31.7	67.79
252	41.57	52.04	31.69	67.755
253	41.59	52.06	31.72	67.885

254	41.6	52.07	31.76	67.95
255	41.66	52.11	31.8	68.005
256	41.7	52.17	31.85	67.985
257	41.74	52.19	31.86	67.995
258	41.78	52.21	31.88	68.045
259	41.8	52.24	31.91	68.02
260	41.83	52.28	31.98	68.12
261	41.86	52.39	32.06	68.09
262	41.88	52.46	32.12	68.025
263	41.91	52.47	32.16	68
264	41.96	52.48	32.17	67.995
265	41.97	52.49	32.18	68.085
266	42.01	52.51	32.19	68.075
267	42.04	52.54	32.23	68.12
268	42.08	52.55	32.26	68.14
269	42.11	52.55	32.25	68.135
270	42.14	52.56	32.26	68.13
271	42.17	52.54	32.27	68.17
272	42.19	52.57	32.26	68.15
273	42.21	52.58	32.29	68.165
274	42.24	52.6	32.33	68.15
275	42.27	52.62	32.36	68.13
276	42.29	52.65	32.4	68.195
277	42.31	52.66	32.42	68.24
278	42.34	52.7	32.47	68.355
279	42.35	52.75	32.53	68.44
280	42.37	52.81	32.61	68.445
281	42.42	52.85	32.67	68.38
282	42.44	52.88	32.72	68.415
283	42.46	52.9	32.73	68.395
284	42.51	52.92	32.76	68.48
285	42.53	52.93	32.78	68.5
286	42.54	52.95	32.78	68.505
287	42.56	52.95	32.8	68.53
288	42.56	52.97	32.83	68.535
289	42.58	52.98	32.86	68.6
290	42.58	52.98	32.88	68.57
291	42.61	52.99	32.91	68.58
292	42.63	53.01	32.92	68.59
293	42.64	53.01	32.96	68.605
294	42.65	53.03	33.02	68.615
295	42.64	53.05	33.06	68.555
296	42.66	53.11	33.1	68.39

297	42.69	53.12	33.12	68.495
298	42.72	53.12	33.13	68.57
299	42.77	53.12	33.15	68.525
300	42.77	53.04	33.16	67.745
301	42.74	52.48	33.15	64.155
302	42.63	51.32	33.15	59.78
303	42.32	49.85	33.13	55.755
304	41.84	48.32	33.12	52.32
305	41.27	46.88	33.12	49.445
306	40.66	45.61	33.14	47.045
307	40.03	44.51	33.16	45.06
308	39.39	43.55	33.15	43.395
309	38.77	42.67	33.12	41.99
310	38.18	41.87	33.13	40.79
311	37.66	41.15	33.13	39.745
312	37.19	40.48	33.15	38.805
313	36.76	39.83	33.17	37.975
314	36.37	39.21	33.16	37.245
315	35.99	38.63	33.14	37.225
316	35.63	38.28	33.16	39.885
317	35.29	38.58	33.18	44.05
318	34.95	39.86	33.18	48.26
319	34.8	41.33	33.18	51.875
320	34.86	43.07	33.2	54.9
321	35.15	44.53	33.23	57.28
322	35.7	45.62	33.25	59.135
323	36.33	46.4	33.26	60.665
324	36.97	46.91	33.3	61.91
325	37.51	47.29	33.31	62.88
326	38.02	47.78	33.33	63.74
327	38.5	48.36	33.34	64.425
328	38.91	48.92	33.34	64.925
329	39.31	49.43	33.37	65.355
330	39.71	49.88	33.41	65.815
331	40.06	50.25	33.45	66.225
332	40.39	50.59	33.47	66.52
333	40.71	50.89	33.49	66.82
334	40.98	51.19	33.52	67.06
335	41.21	51.44	33.53	67.195
336	41.42	51.7	33.56	67.45
337	41.64	51.93	33.59	67.67
338	41.81	52.1	33.6	67.825
339	41.95	52.25	33.6	67.885

340	42.11	52.41	33.61	67.915
341	42.25	52.56	33.66	67.985
342	42.39	52.68	33.71	68.095
343	42.5	52.8	33.74	68.21
344	42.61	52.9	33.76	68.26
345	42.68	52.98	33.79	68.255
346	42.75	53.07	33.82	68.33
347	42.83	53.16	33.84	68.295
348	42.89	53.22	33.87	68.285
349	42.96	53.27	33.91	68.39
350	43.01	53.32	33.96	68.44
351	43.06	53.36	34.01	68.405
352	43.09	53.4	34.02	68.515
353	43.13	53.45	34.03	68.545
354	43.17	53.49	34.05	68.62
355	43.21	53.53	34.07	68.665
356	43.21	53.54	34.1	68.765
357	43.25	53.58	34.13	68.815
358	43.3	53.63	34.12	68.8
359	43.31	53.66	34.14	68.83
360	43.33	53.68	34.15	68.735
361	43.35	53.67	34.17	68.7
362	43.4	53.68	34.2	68.645
363	43.43	53.71	34.23	68.715
364	43.41	53.73	34.28	68.715
365	43.41	53.75	34.32	68.8
366	43.42	53.79	34.39	68.795
367	43.45	53.8	34.44	68.72
368	43.49	53.82	34.46	68.615
369	43.52	53.83	34.48	68.65
370	43.56	53.83	34.48	68.66
371	43.57	53.83	34.5	68.635
372	43.58	53.85	34.53	68.69
373	43.6	53.87	34.54	68.725
374	43.61	53.87	34.55	68.65
375	43.63	53.86	34.57	68.68
376	43.64	53.85	34.58	68.645
377	43.66	53.89	34.62	68.68
378	43.69	53.92	34.67	68.745
379	43.69	53.95	34.7	68.855
380	43.66	53.98	34.71	68.895
381	43.67	53.99	34.76	68.82
382	43.72	54.01	34.79	68.795

383	43.74	54.01	34.8	68.805
384	43.78	54.02	34.83	68.86
385	43.82	54.04	34.85	68.84
386	43.8	54.04	34.85	68.855
387	43.78	54.07	34.88	68.82
388	43.8	54.07	34.89	68.825
389	43.77	54.09	34.9	68.95
390	43.77	54.11	34.95	68.87
391	43.81	54.12	34.99	68.855
392	43.83	54.13	35.01	68.92
393	43.83	54.15	35.05	68.91
394	43.84	54.17	35.08	68.93
395	43.85	54.19	35.12	68.935
396	43.89	54.19	35.18	68.935
397	43.93	54.18	35.17	68.835
398	43.95	54.16	35.17	68.69
399	43.95	54.16	35.19	68.7
400	43.94	54.16	35.21	68.825
401	43.92	54.16	35.21	68.81
402	43.93	54.19	35.25	68.825
403	43.93	54.2	35.23	68.66
404	43.89	54.17	35.22	68.74
405	43.88	54.1	35.24	68.045
406	43.85	53.5	35.24	64.465
407	43.73	52.34	35.23	60.045
408	43.43	50.87	35.22	56.005
409	42.96	49.38	35.21	52.57
410	42.41	47.96	35.23	49.705
411	41.78	46.66	35.24	47.365
412	41.17	45.55	35.24	45.43
413	40.55	44.58	35.23	43.75
414	39.97	43.71	35.19	42.335
415	39.42	42.89	35.16	41.135
416	38.88	42.13	35.15	40.1
417	38.38	41.41	35.14	39.205
418	37.91	40.76	35.14	38.405
419	37.52	40.13	35.13	37.67

Test No.4 traditional model with various heat fluxes (five hours)

Time (minutes)	Outlet °C	Inlet °C	Tank °C	Average wall °C
0	22.22	22.06	22.89	22.425
1	22.25	22.09	22.92	23.46
2	22.36	22.14	22.96	27.21
3	23.18	22.19	23	32.5
4	25.21	22.26	23.04	37.825
5	28.1	22.38	23.08	42.455
6	30.88	22.6	23.12	46.26
7	33.41	22.78	23.14	49.315
8	35.41	23.18	23.15	51.77
9	37.13	24.27	23.18	53.7
10	38.42	25.58	23.22	55.285
11	39.22	26.66	23.23	56.675
12	39.54	27.52	23.28	57.805
13	39.87	28.36	23.32	58.755
14	40.53	29.22	23.4	59.6
15	41.43	29.9	23.48	60.415
16	42.32	30.46	23.52	61.105
17	43.03	31.02	23.54	61.64
18	43.63	31.6	23.6	62.17
19	44.15	32.15	23.71	62.63
20	44.57	32.63	23.8	62.96
21	44.94	33.07	23.87	63.355
22	45.33	33.48	23.93	63.7
23	45.69	33.82	23.99	64
24	46.02	34.14	24.05	64.295
25	46.35	34.46	24.09	64.405
26	46.6	34.71	24.16	64.525
27	46.84	34.94	24.23	64.7
28	47.05	35.17	24.31	64.885
29	47.25	35.37	24.4	64.985
30	47.41	35.54	24.45	65.21
31	47.6	35.71	24.52	65.395
32	47.73	35.87	24.6	65.57
33	47.87	36.03	24.62	65.625
34	47.99	36.18	24.66	65.715
35	48.11	36.3	24.73	65.815
36	48.22	36.4	24.79	65.895
37	48.33	36.51	24.88	65.855
38	48.48	36.63	25	65.79

39	48.59	36.71	25.06	65.755
40	48.67	36.8	25.12	65.815
41	48.71	36.89	25.16	66.055
42	48.74	36.93	25.19	66.16
43	48.76	36.97	25.2	66.195
44	48.8	37.03	25.2	66.24
45	48.86	37.09	25.29	66.465
46	48.94	37.13	25.32	66.46
47	49	37.19	25.34	66.35
48	49.05	37.25	25.38	66.215
49	49.09	37.31	25.44	66.185
50	49.11	37.37	25.52	66.3
51	49.11	37.37	25.57	66.32
52	49.17	37.44	25.61	66.41
53	49.26	37.52	25.67	66.505
54	49.28	37.55	25.7	66.635
55	49.31	37.56	25.75	66.73
56	49.38	37.61	25.82	66.73
57	49.38	37.63	25.84	66.695
58	49.41	37.67	25.9	66.635
59	49.45	37.73	25.95	66.49
60	49.47	37.79	26.01	66.48
61	49.49	37.82	26.03	66.575
62	49.47	37.81	26.05	66.73
63	49.47	37.82	26.09	66.8
64	49.54	37.9	26.14	66.93
65	49.59	37.95	26.23	66.845
66	49.6	37.99	26.29	66.74
67	49.66	38.05	26.35	66.725
68	49.66	38.08	26.37	66.865
69	49.7	38.11	26.43	67.095
70	49.72	38.11	26.49	67.04
71	49.79	38.13	26.53	67.005
72	49.86	38.18	26.58	67.08
73	49.9	38.2	26.63	67.175
74	49.92	38.23	26.67	67.165
75	49.95	38.28	26.73	67.13
76	50.02	38.35	26.79	67.33
77	50.08	38.4	26.85	67.445
78	50.13	38.43	26.9	67.355
79	50.16	38.51	26.92	67.19
80	50.2	38.58	26.97	67.14
81	50.24	38.63	27.03	67.12

82	50.24	38.64	27.07	67.125
83	50.27	38.67	27.12	67.12
84	50.28	38.69	27.16	67.285
85	50.31	38.73	27.22	67.26
86	50.3	38.77	27.28	67.225
87	50.32	38.75	27.32	67.355
88	50.38	38.73	27.36	67.465
89	50.45	38.78	27.45	67.39
90	50.49	38.83	27.49	67.435
91	50.48	38.85	27.51	67.435
92	50.48	38.9	27.51	67.32
93	50.54	39	27.6	67.375
94	50.58	39.06	27.66	67.355
95	50.6	39.07	27.65	67.305
96	50.61	39.1	27.68	67.345
97	50.63	39.1	27.69	67.44
98	50.67	39.12	27.74	67.595
99	50.7	39.11	27.77	67.56
100	50.71	39.15	27.81	67.495
101	50.73	39.19	27.84	67.475
102	50.74	39.24	27.87	67.475
103	50.76	39.28	27.93	67.515
104	50.78	39.32	28.02	67.565
105	50.83	39.33	28.11	67.73
106	50.86	39.33	28.15	67.845
107	50.86	39.33	28.17	67.97
108	50.9	39.35	28.23	68.01
109	50.91	39.37	28.25	67.95
110	50.94	39.43	28.27	68.065
111	50.97	39.44	28.33	68.205
112	51	39.44	28.38	68.215
113	51.04	39.46	28.42	68.075
114	51.07	39.52	28.47	67.89
115	51.08	39.56	28.46	67.915
116	51.13	39.62	28.51	67.96
117	51.15	39.65	28.56	67.955
118	51.17	39.67	28.58	67.88
119	51.18	39.69	28.59	67.835
120	51.22	39.74	28.61	67.885
121	51.23	39.76	28.65	68.04
122	51.25	39.78	28.74	67.985
123	51.27	39.8	28.78	68.12
124	51.28	39.79	28.86	68.085

125	51.28	39.8	28.91	68.065
126	51.3	39.83	28.92	68
127	51.32	39.85	28.96	68.065
128	51.35	39.87	29.05	68.15
129	51.4	39.91	29.07	68.32
130	51.44	39.96	29.08	68.425
131	51.47	40.02	29.1	68.49
132	51.49	40.07	29.13	68.59
133	51.54	40.11	29.2	68.59
134	51.54	40.16	29.24	68.76
135	51.58	40.19	29.27	68.835
136	51.61	40.21	29.32	68.8
137	51.65	40.23	29.37	68.69
138	51.7	40.28	29.42	68.585
139	51.75	40.31	29.44	68.57
140	51.76	40.36	29.44	68.4
141	51.78	40.38	29.47	68.375
142	51.8	40.41	29.5	68.48
143	51.78	40.4	29.53	68.53
144	51.78	40.41	29.51	68.565
145	51.8	40.43	29.57	68.795
146	51.83	40.45	29.61	68.855
147	51.84	40.46	29.66	68.925
148	51.88	40.5	29.72	68.785
149	51.91	40.52	29.76	68.88
150	51.9	40.55	29.75	68.955
151	51.91	40.61	29.8	68.995
152	51.98	40.66	29.89	69.125
153	52.02	40.67	29.94	69.015
154	52.05	40.73	29.99	69.025
155	52.1	40.79	30.02	69.13
156	52.11	40.78	30.04	69.115
157	52.11	40.76	30.07	69.22
158	52.1	40.76	30.09	69.165
159	52.12	40.82	30.12	69.115
160	52.14	40.88	30.16	69.105
161	52.18	40.93	30.22	69.19
162	52.23	40.95	30.26	69.145
163	52.28	40.98	30.32	69.07
164	52.31	41.03	30.35	69.23
165	52.35	41.07	30.38	69.335
166	52.39	41.12	30.41	69.305
167	52.41	41.13	30.42	69.34

168	52.41	41.17	30.47	69.415
169	52.44	41.19	30.5	69.39
170	52.45	41.21	30.55	69.335
171	52.49	41.25	30.63	69.445
172	52.53	41.27	30.67	69.465
173	52.57	41.3	30.74	69.465
174	52.56	41.32	30.75	69.5
175	52.58	41.31	30.79	69.525
176	52.59	41.29	30.79	69.54
177	52.62	41.34	30.85	69.54
178	52.68	41.4	30.89	69.47
179	52.7	41.47	30.92	69.49
180	52.73	41.47	30.92	69.535
181	52.74	41.49	30.93	69.53
182	52.75	41.54	30.98	69.57
183	52.77	41.54	31.04	69.565
184	52.8	41.55	31.1	69.5
185	52.81	41.59	31.16	69.525
186	52.83	41.63	31.16	69.53
187	52.82	41.67	31.18	69.465
188	52.85	41.69	31.24	69.49
189	52.87	41.69	31.28	69.57
190	52.88	41.71	31.27	69.5
191	52.89	41.72	31.26	69.63
192	52.91	41.75	31.28	69.65
193	52.89	41.75	31.3	69.72
194	52.91	41.78	31.36	69.715
195	52.96	41.8	31.44	69.78
196	52.99	41.81	31.5	69.795
197	53.04	41.85	31.57	69.795
198	53.08	41.89	31.59	69.815
199	53.12	41.92	31.6	69.745
200	53.15	41.95	31.64	69.79
201	53.16	41.99	31.66	69.825
202	53.11	41.93	31.66	69.695
203	53.1	41.91	31.64	69.715
204	53.13	41.94	31.65	69.73
205	53.12	41.97	31.68	69.665
206	53.11	41.99	31.73	69.56
207	53.12	41.99	31.77	69.6
208	53.11	42	31.81	69.695
209	53.17	42.07	31.87	69.66
210	53.23	42.12	31.93	69.78

211	53.27	42.14	31.98	69.9
212	53.28	42.15	32.01	69.98
213	53.29	42.19	32.04	69.845
214	53.32	42.19	32.09	69.82
215	53.34	42.22	32.09	69.8
216	53.34	42.22	32.1	69.715
217	53.39	42.22	32.11	69.79
218	53.39	42.25	32.14	69.845
219	53.42	42.29	32.22	70.04
220	53.43	42.33	32.24	69.97
221	53.47	42.37	32.28	69.85
222	53.47	42.38	32.3	69.865
223	53.48	42.36	32.33	69.88
224	53.47	42.38	32.34	69.985
225	53.45	42.4	32.31	69.935
226	53.47	42.43	32.33	69.905
227	53.49	42.46	32.36	69.945
228	53.51	42.47	32.38	69.96
229	53.51	42.48	32.42	69.88
230	53.51	42.49	32.45	69.865
231	53.52	42.54	32.47	69.96
232	53.54	42.56	32.51	70.02
233	53.54	42.56	32.54	70.03
234	53.6	42.59	32.61	70.075
235	53.65	42.62	32.68	70.01
236	53.69	42.63	32.73	69.975
237	53.72	42.67	32.76	69.94
238	53.75	42.7	32.77	70.07
239	53.7	42.67	32.76	70.165
240	53.7	42.65	32.73	70.02
241	53.63	42.59	32.73	69.11
242	53.02	42.56	32.77	65.38
243	51.73	42.45	32.77	60.92
244	50.18	42.18	32.86	56.77
245	48.64	41.71	32.95	53.185
246	47.12	41.07	32.89	50.13
247	45.84	40.38	32.88	47.61
248	44.76	39.73	32.89	45.53
249	43.78	39.08	32.9	43.805
250	42.93	38.45	32.95	42.32
251	42.1	37.85	32.95	41.04
252	41.32	37.33	32.92	39.95
253	40.58	36.84	32.9	38.96

254	39.93	36.39	32.92	38.105
255	39.26	35.93	32.89	37.34
256	38.59	35.47	32.83	36.655
257	38.01	35.1	32.83	36.05
258	37.47	34.75	32.83	35.495
259	36.94	34.42	32.81	34.965
260	36.45	34.11	32.77	34.49
261	36.01	33.82	32.73	34.04
262	35.59	33.54	32.7	33.645
263	35.21	33.28	32.66	33.25
264	34.88	33.04	32.64	32.91
265	34.56	32.82	32.63	32.59
266	34.25	32.61	32.6	32.265
267	34	32.43	32.59	31.995
268	33.76	32.26	32.61	31.74
269	33.53	32.1	32.62	31.51
270	33.31	31.93	32.61	31.29
271	33.07	31.74	32.57	31.06
272	32.88	31.58	32.55	30.855
273	32.72	31.41	32.54	30.66
274	32.61	31.25	32.53	30.505
275	32.5	31.1	32.52	30.345
276	32.37	30.92	32.52	30.175
277	32.24	30.73	32.5	30.01
278	32.11	30.55	32.49	29.85
279	32.03	30.39	32.51	29.72
280	31.96	30.21	32.51	29.59
281	31.89	30.03	32.5	29.48
282	31.8	29.84	32.47	29.345
283	31.7	29.64	32.44	29.205
284	31.62	29.5	32.46	29.115
285	31.53	29.33	32.46	29.01
286	31.41	29.16	32.44	28.87
287	31.3	29	32.42	28.76
288	31.21	28.87	32.42	28.68
289	31.1	28.76	32.42	28.61
290	31.02	28.65	32.41	28.545
291	30.94	28.55	32.42	28.47
292	30.81	28.41	32.38	28.36
293	30.7	28.31	32.37	28.285
294	30.61	28.22	32.35	28.205
295	30.52	28.12	32.35	28.145
296	30.47	28.07	32.37	28.09

297	30.39	27.98	32.35	28.015
298	30.31	27.9	32.35	27.955
299	30.23	27.82	32.35	27.9

Test No.5 new model with constant heat fluxes (five hours)

Time (minutes)	Inlet °C	Outlet °C	Tank °C	Average wall °C
0	23.37	24.03	24.05	24.565
1	23.39	24.06	24.05	26.4
2	23.43	24.23	24.04	31.79
3	23.5	24.76	24.05	37.835
4	23.66	25.88	24.09	43.235
5	23.85	27.96	24.1	47.745
6	24	31.21	24.11	51.475
7	24.15	34.29	24.15	54.475
8	24.42	36.42	24.18	56.88
9	25.18	38.29	24.17	58.905
10	26.45	39.87	24.2	60.555
11	27.76	41.13	24.27	62.005
12	28.9	42.15	24.31	63.345
13	29.86	42.94	24.33	64.555
14	30.72	43.65	24.41	65.595
15	31.47	44.29	24.45	66.405
16	32.12	44.97	24.46	67.19
17	32.73	45.69	24.51	67.875
18	33.29	46.35	24.52	68.49
19	33.81	46.94	24.56	69.045
20	34.33	47.5	24.57	69.52
21	34.83	48	24.61	69.935
22	35.31	48.47	24.66	70.305
23	35.71	48.91	24.73	70.645
24	36.04	49.29	24.8	70.83
25	36.4	49.68	24.87	71.065
26	36.75	49.97	24.93	71.3
27	37.07	50.26	25	71.545
28	37.4	50.6	25.16	71.765
29	37.65	50.87	25.23	71.83
30	37.95	51.14	25.31	72.03
31	38.21	51.39	25.41	72.27
32	38.43	51.62	25.51	72.46
33	38.61	51.83	25.57	72.68

34	38.77	52	25.69	72.965
35	38.95	52.17	25.76	73.18
36	39.08	52.32	25.79	73.25
37	39.21	52.51	25.82	73.305
38	39.36	52.65	25.92	73.335
39	39.46	52.75	26	73.42
40	39.56	52.83	26.08	73.405
41	39.65	52.91	26.12	73.39
42	39.75	52.98	26.11	73.455
43	39.81	53.04	26.09	73.52
44	39.79	53	26.09	73.495
45	39.88	53.08	26.19	73.47
46	39.91	53.1	26.24	73.54
47	39.96	53.16	26.27	73.555
48	39.97	53.21	26.32	73.415
49	40.01	53.24	26.4	73.345
50	40.05	53.25	26.46	73.455
51	40.09	53.27	26.5	73.46
52	40.12	53.3	26.53	73.405
53	40.18	53.35	26.6	73.45
54	40.21	53.37	26.68	73.54
55	40.19	53.38	26.68	73.64
56	40.23	53.41	26.68	73.65
57	40.32	53.45	26.74	73.68
58	40.4	53.52	26.8	73.765
59	40.44	53.6	26.89	73.795
60	40.5	53.63	26.95	73.825
61	40.54	53.66	27	73.815
62	40.56	53.7	27.05	73.85
63	40.56	53.7	27.02	73.795
64	40.61	53.74	27.09	73.81
65	40.65	53.79	27.18	73.79
66	40.65	53.81	27.24	73.795
67	40.64	53.81	27.3	73.745
68	40.67	53.78	27.33	73.615
69	40.74	53.82	27.39	73.655
70	40.79	53.86	27.43	73.74
71	40.78	53.91	27.46	73.73
72	40.84	53.95	27.49	73.775
73	40.9	54	27.53	73.98
74	40.92	54.04	27.59	74.125
75	41.01	54.1	27.66	74.245
76	41.11	54.17	27.76	74.255

77	41.16	54.21	27.8	74.28
78	41.19	54.29	27.86	74.315
79	41.27	54.34	27.93	74.285
80	41.33	54.4	27.99	74.325
81	41.4	54.45	28	74.445
82	41.42	54.5	28.06	74.47
83	41.47	54.52	28.08	74.5
84	41.53	54.55	28.14	74.56
85	41.59	54.6	28.17	74.61
86	41.6	54.65	28.25	74.7
87	41.63	54.69	28.3	74.825
88	41.66	54.71	28.36	74.845
89	41.69	54.76	28.41	74.9
90	41.69	54.78	28.48	74.92
91	41.7	54.81	28.52	74.925
92	41.68	54.81	28.58	74.885
93	41.69	54.81	28.65	74.865
94	41.7	54.83	28.74	74.78
95	41.75	54.88	28.78	74.795
96	41.81	54.9	28.79	74.885
97	41.83	54.92	28.82	74.985
98	41.86	54.95	28.87	75.065
99	41.88	54.97	28.88	75.045
100	41.92	54.99	28.93	74.99
101	41.95	55.02	29.02	74.92
102	41.99	55.09	29.02	74.99
103	42.01	55.12	29.08	75.155
104	42.03	55.14	29.09	75.11
105	42.11	55.17	29.12	75.005
106	42.16	55.2	29.18	75.01
107	42.2	55.22	29.2	75.015
108	42.23	55.2	29.23	75.07
109	42.25	55.23	29.27	75.195
110	42.28	55.27	29.33	75.215
111	42.28	55.3	29.4	75.18
112	42.3	55.37	29.49	75.3
113	42.33	55.41	29.57	75.39
114	42.38	55.46	29.64	75.425
115	42.44	55.5	29.7	75.445
116	42.48	55.5	29.69	75.475
117	42.54	55.53	29.71	75.52
118	42.58	55.54	29.74	75.635
119	42.6	55.56	29.79	75.675

120	42.62	55.58	29.84	75.59
121	42.62	55.63	29.87	75.56
122	42.65	55.67	29.98	75.48
123	42.66	55.7	30.03	75.42
124	42.7	55.73	30.06	75.535
125	42.76	55.78	30.1	75.65
126	42.83	55.82	30.13	75.715
127	42.89	55.84	30.19	75.735
128	42.92	55.88	30.26	75.695
129	42.95	55.92	30.3	75.645
130	42.96	55.94	30.32	75.585
131	42.98	55.94	30.38	75.585
132	43	55.95	30.45	75.575
133	43.02	55.97	30.5	75.55
134	43.03	56	30.52	75.57
135	43.01	55.99	30.55	75.495
136	42.97	55.98	30.6	75.405
137	42.97	56.01	30.66	75.505
138	43.03	56.02	30.7	75.55
139	43.06	56.03	30.76	75.43
140	43.04	56.02	30.79	75.355
141	43.03	56.02	30.86	75.405
142	43	56	30.86	75.435
143	43.01	55.98	30.85	75.495
144	43.04	55.98	30.89	75.5
145	43.01	55.97	30.94	75.425
146	42.94	55.98	30.94	75.315
147	42.99	56.01	31.05	75.26
148	43.03	56.05	31.12	75.25
149	43.07	56.07	31.19	75.245
150	43.06	56.08	31.23	75.28
151	43.11	56.1	31.28	75.335
152	43.16	56.12	31.3	75.395
153	43.18	56.15	31.31	75.445
154	43.25	56.22	31.37	75.46
155	43.27	56.3	31.46	75.48
156	43.3	56.35	31.52	75.525
157	43.39	56.36	31.54	75.535
158	43.44	56.33	31.57	75.455
159	43.43	56.34	31.58	75.475
160	43.39	56.35	31.6	75.495
161	43.42	56.34	31.6	75.485
162	43.45	56.38	31.64	75.545

163	43.49	56.41	31.69	75.56
164	43.47	56.42	31.73	75.63
165	43.48	56.43	31.74	75.635
166	43.47	56.44	31.8	75.62
167	43.5	56.47	31.88	75.655
168	43.55	56.5	31.95	75.65
169	43.56	56.52	31.95	75.685
170	43.57	56.49	31.94	75.645
171	43.57	56.48	31.98	75.62
172	43.56	56.5	32.01	75.535
173	43.58	56.54	32.05	75.47
174	43.66	56.57	32.13	75.56
175	43.68	56.55	32.14	75.6
176	43.79	56.62	32.22	75.695
177	43.88	56.67	32.22	75.77
178	43.9	56.7	32.29	75.75
179	43.94	56.73	32.35	75.79
180	43.92	56.71	32.37	75.795
181	43.91	56.74	32.44	75.795
182	43.93	56.79	32.49	75.805
183	44	56.85	32.55	75.92
184	44.01	56.87	32.57	75.935
185	43.95	56.85	32.6	75.965
186	43.96	56.86	32.61	75.93
187	43.99	56.9	32.67	75.98
188	44.05	56.94	32.72	75.955
189	44.05	56.94	32.73	75.935
190	44.05	56.94	32.76	75.82
191	44.06	56.94	32.84	75.76
192	44.08	56.97	32.94	75.85
193	44.15	57.01	32.98	75.885
194	44.22	57.02	32.98	75.935
195	44.27	57.05	32.97	75.985
196	44.3	57.08	33.02	76.08
197	44.34	57.12	33.06	76.055
198	44.39	57.16	33.14	76.02
199	44.44	57.2	33.19	76.045
200	44.48	57.21	33.23	76.19
201	44.52	57.25	33.26	76.18
202	44.56	57.26	33.28	76.155
203	44.57	57.3	33.35	76.185
204	44.6	57.35	33.46	76.265
205	44.58	57.36	33.49	76.24

206	44.6	57.41	33.58	76.145
207	44.65	57.43	33.61	76.08
208	44.69	57.49	33.65	76.07
209	44.69	57.53	33.67	76.055
210	44.7	57.58	33.71	76.105
211	44.73	57.61	33.75	76.175
212	44.72	57.59	33.8	76.2
213	44.73	57.58	33.86	76.155
214	44.78	57.61	33.87	76.085
215	44.82	57.63	33.91	76.12
216	44.79	57.63	33.93	76.215
217	44.82	57.66	33.97	76.24
218	44.83	57.65	33.99	76.18
219	44.89	57.67	34.03	76.3
220	44.9	57.64	34.08	76.26
221	44.95	57.65	34.16	76.23
222	44.97	57.67	34.15	76.28
223	45	57.68	34.15	76.31
224	45.05	57.7	34.16	76.35
225	45.12	57.72	34.22	76.405
226	45.11	57.73	34.3	76.38
227	45.16	57.78	34.34	76.39
228	45.19	57.84	34.41	76.42
229	45.24	57.88	34.41	76.385
230	45.26	57.9	34.43	76.39
231	45.27	57.91	34.46	76.425
232	45.24	57.91	34.51	76.405
233	45.21	57.92	34.54	76.38
234	45.21	57.94	34.63	76.285
235	45.23	57.97	34.69	76.32
236	45.25	57.99	34.72	76.375
237	45.28	58.03	34.74	76.455
238	45.33	58.05	34.76	76.355
239	45.35	58.04	34.79	76.235
240	45.35	58.03	34.77	76.235
241	45.36	58.01	34.77	76.28
242	45.44	58.03	34.82	76.37
243	45.45	58.04	34.91	76.405
244	45.44	58.07	34.97	76.505
245	45.42	58.1	35.02	76.545
246	45.44	58.15	35.09	76.605
247	45.48	58.19	35.14	76.63
248	45.46	58.2	35.18	76.55

249	45.45	58.22	35.21	76.515
250	45.48	58.24	35.21	76.48
251	45.49	58.24	35.2	76.455
252	45.54	58.28	35.22	76.485
253	45.61	58.29	35.26	76.515
254	45.67	58.31	35.26	76.62
255	45.71	58.36	35.28	76.645
256	45.72	58.4	35.3	76.69
257	45.7	58.4	35.34	76.62
258	45.66	58.39	35.38	76.68
259	45.65	58.4	35.39	76.69
260	45.71	58.45	35.44	76.765
261	45.69	58.46	35.5	76.745
262	45.73	58.48	35.52	76.72
263	45.82	58.5	35.53	76.795
264	45.91	58.53	35.57	76.895
265	45.89	58.54	35.61	76.87
266	45.88	58.58	35.67	76.845
267	45.91	58.61	35.7	76.87
268	45.96	58.65	35.77	76.835
269	46.01	58.68	35.83	76.81
270	46.02	58.7	35.87	76.83
271	46.09	58.72	35.88	76.865
272	46.16	58.72	35.91	76.8
273	46.19	58.75	35.93	76.87
274	46.14	58.76	35.95	76.905
275	46.1	58.75	35.95	76.925
276	46.13	58.79	36	76.915
277	46.16	58.8	36.04	76.85
278	46.19	58.8	36.09	76.68
279	46.2	58.82	36.14	76.67
280	46.23	58.85	36.15	76.84
281	46.22	58.82	36.16	76.905
282	46.18	58.79	36.08	76.845
283	46.2	58.8	36.14	76.88
284	46.24	58.82	36.18	76.85
285	46.24	58.83	36.2	76.795
286	46.2	58.81	36.21	76.81
287	46.23	58.82	36.23	76.74
288	46.25	58.8	36.24	76.735
289	46.26	58.82	36.27	76.72
290	46.27	58.83	36.33	76.775
291	46.25	58.82	36.32	76.77

292	46.23	58.8	36.34	76.74
293	46.28	58.81	36.35	76.8
294	46.34	58.86	36.39	76.86
295	46.33	58.86	36.43	76.825
296	46.3	58.83	36.45	76.72
297	46.34	58.85	36.49	76.73
298	46.35	58.89	36.51	76.745
299	46.39	58.89	36.55	76.745

Test No.6 new model with constant heat fluxes (seven hours)

Time (minutes)	Inlet °C	Outlet °C	Tank °C	Average wall °C
0	23.64	23.98	24.04	26.71
1	23.65	24.04	24.06	28.755
2	23.71	24.33	24.09	34.715
3	23.78	25.02	24.14	40.86
4	23.83	26.42	24.17	46.06
5	23.95	29.26	24.2	50.315
6	24.09	32.74	24.21	53.735
7	24.22	35.58	24.22	56.445
8	24.67	37.78	24.22	58.665
9	25.68	39.57	24.24	60.6
10	27.05	40.99	24.28	62.23
11	28.35	42.05	24.33	63.645
12	29.47	42.9	24.38	64.895
13	30.43	43.64	24.43	65.99
14	31.26	44.33	24.46	66.905
15	31.96	45.04	24.46	67.765
16	32.6	45.68	24.5	68.405
17	33.17	46.39	24.54	69.04
18	33.76	47.16	24.62	69.7
19	34.28	47.75	24.67	70.03
20	34.73	48.26	24.72	70.48
21	35.22	48.74	24.79	70.825
22	35.65	49.14	24.84	71.23
23	36.04	49.49	24.9	71.595
24	36.4	49.87	24.98	71.92
25	36.77	50.22	25.04	72.21
26	37.12	50.55	25.09	72.43
27	37.42	50.83	25.13	72.645
28	37.68	51.09	25.2	72.8

29	37.9	51.33	25.25	72.94
30	38.09	51.68	25.3	73.055
31	38.25	52.03	25.36	73.07
32	38.38	52.16	25.41	73.12
33	38.56	52.31	25.47	73.23
34	38.7	52.45	25.53	73.395
35	38.83	52.58	25.62	73.58
36	38.96	52.71	25.71	73.64
37	39.1	52.79	25.75	73.7
38	39.19	52.81	25.75	73.715
39	39.29	52.85	25.78	73.765
40	39.4	52.91	25.82	73.855
41	39.49	53.01	25.95	74.04
42	39.54	53.11	26.03	74.065
43	39.61	53.2	26.13	74.035
44	39.67	53.29	26.14	74.015
45	39.75	53.35	26.21	74.035
46	39.81	53.39	26.31	74.13
47	39.86	53.45	26.32	74.155
48	39.89	53.52	26.34	74.15
49	39.92	53.6	26.42	74.19
50	40.02	53.79	26.47	74.185
51	40.11	53.8	26.53	74.21
52	40.17	53.79	26.62	74.27
53	40.21	53.83	26.67	74.31
54	40.22	53.83	26.71	74.29
55	40.25	53.87	26.75	74.305
56	40.27	53.9	26.83	74.355
57	40.3	53.94	26.89	74.375
58	40.33	53.95	27.01	74.435
59	40.37	53.94	27.03	74.51
60	40.37	54	27.08	74.525
61	40.38	54	27.12	74.59
62	40.39	54.05	27.16	74.6
63	40.43	54.13	27.24	74.62
64	40.47	54.15	27.3	74.605
65	40.43	54.18	27.35	74.63
66	40.47	54.31	27.4	74.635
67	40.52	54.39	27.43	74.635
68	40.55	54.44	27.48	74.65
69	40.6	54.53	27.58	74.535
70	40.63	54.51	27.63	74.645
71	40.69	54.52	27.7	74.745

72	40.73	54.58	27.7	74.825
73	40.74	54.62	27.83	74.875
74	40.75	54.68	27.89	74.885
75	40.78	54.69	27.9	74.91
76	40.85	54.75	27.95	74.935
77	40.87	54.74	28.01	74.96
78	40.86	54.78	28.05	75.075
79	40.85	54.83	28.1	75.135
80	40.88	54.88	28.15	75.155
81	40.94	54.93	28.2	75.175
82	40.97	54.99	28.24	75.125
83	40.97	55.01	28.31	75.095
84	40.97	54.98	28.35	75.025
85	40.95	54.93	28.35	74.995
86	40.96	54.96	28.38	75.02
87	40.99	55.02	28.36	75.075
88	41.07	55.09	28.47	75.155
89	41.14	55.11	28.52	75.215
90	41.19	55.18	28.62	75.19
91	41.23	55.22	28.66	75.205
92	41.27	55.23	28.72	75.285
93	41.33	55.27	28.72	75.315
94	41.37	55.33	28.74	75.37
95	41.42	55.38	28.84	75.245
96	41.44	55.39	28.92	75.25
97	41.47	55.47	28.99	75.355
98	41.49	55.49	29.06	75.43
99	41.53	55.54	29.11	75.425
100	41.58	55.54	29.13	75.33
101	41.63	55.56	29.18	75.265
102	41.68	55.63	29.24	75.345
103	41.72	55.66	29.3	75.405
104	41.7	55.67	29.32	75.475
105	41.72	55.69	29.38	75.575
106	41.76	55.76	29.47	75.61
107	41.81	55.82	29.53	75.595
108	41.83	55.88	29.58	75.62
109	41.85	55.87	29.66	75.755
110	41.87	55.89	29.69	75.805
111	41.92	55.92	29.69	75.83
112	41.96	55.94	29.74	75.915
113	41.99	55.98	29.81	75.975
114	42.05	55.95	29.8	75.95

115	42.11	56.02	29.85	75.98
116	42.12	56.05	29.91	75.985
117	42.14	56.09	30.01	76.03
118	42.17	56.14	30.05	76.03
119	42.17	56.14	30.1	76
120	42.16	56.14	30.09	75.99
121	42.2	56.16	30.12	75.995
122	42.25	56.16	30.23	75.96
123	42.28	56.19	30.24	76.015
124	42.32	56.22	30.28	76.045
125	42.38	56.29	30.35	76.11
126	42.41	56.3	30.38	76.135
127	42.44	56.35	30.43	76.15
128	42.46	56.41	30.49	76.13
129	42.49	56.4	30.48	76.125
130	42.52	56.42	30.55	76.23
131	42.59	56.43	30.59	76.21
132	42.62	56.41	30.64	76.215
133	42.64	56.44	30.71	76.22
134	42.66	56.43	30.7	76.19
135	42.69	56.35	30.74	76.265
136	42.71	56.34	30.81	76.3
137	42.73	56.37	30.85	76.195
138	42.71	56.48	30.92	76.13
139	42.71	56.56	30.96	76.125
140	42.74	56.59	31.03	76.15
141	42.74	56.64	31.03	76.1
142	42.75	56.7	31.07	76.11
143	42.78	56.73	31.1	76.14
144	42.8	56.73	31.15	76.165
145	42.84	56.74	31.23	76.21
146	42.87	56.75	31.29	76.275
147	42.89	56.78	31.29	76.4
148	42.94	56.83	31.35	76.405
149	43.01	56.79	31.38	76.305
150	43.07	56.84	31.4	76.385
151	43.09	56.89	31.43	76.47
152	43.13	56.91	31.48	76.495
153	43.15	56.95	31.55	76.495
154	43.18	56.99	31.6	76.46
155	43.21	57.01	31.65	76.47
156	43.23	57.03	31.68	76.47
157	43.21	57.04	31.69	76.5

158	43.2	57.05	31.69	76.5
159	43.23	57.08	31.75	76.44
160	43.29	57.09	31.81	76.39
161	43.33	57.08	31.8	76.37
162	43.36	57.08	31.83	76.425
163	43.35	57.19	31.88	76.48
164	43.35	57.24	31.97	76.38
165	43.33	57.26	32.03	76.31
166	43.35	57.28	32.06	76.39
167	43.4	57.3	32.11	76.385
168	43.43	57.32	32.14	76.335
169	43.45	57.35	32.19	76.335
170	43.49	57.36	32.18	76.41
171	43.5	57.38	32.23	76.4
172	43.52	57.38	32.33	76.42
173	43.52	57.39	32.4	76.465
174	43.51	57.4	32.49	76.485
175	43.49	57.34	32.49	76.395
176	43.48	57.27	32.43	76.28
177	43.51	57.27	32.43	76.245
178	43.48	57.24	32.48	76.215
179	43.46	57.24	32.5	76.285
180	43.51	57.28	32.56	76.26
181	43.54	57.3	32.61	76.295
182	43.57	57.3	32.64	76.35
183	43.57	57.3	32.65	76.335
184	43.61	57.32	32.66	76.305
185	43.66	57.37	32.71	76.345
186	43.68	57.42	32.77	76.365
187	43.68	57.46	32.83	76.42
188	43.73	57.5	32.91	76.45
189	43.75	57.52	32.92	76.43
190	43.77	57.54	32.97	76.46
191	43.75	57.54	33.04	76.5
192	43.78	57.57	33.09	76.525
193	43.8	57.58	33.09	76.45
194	43.81	57.6	33.15	76.385
195	43.81	57.61	33.18	76.405
196	43.84	57.62	33.22	76.445
197	43.91	57.62	33.23	76.495
198	43.94	57.65	33.29	76.55
199	43.91	57.65	33.32	76.52
200	43.92	57.68	33.37	76.48

201	43.93	57.66	33.41	76.465
202	43.96	57.65	33.46	76.385
203	44.01	57.66	33.47	76.365
204	44.05	57.65	33.49	76.41
205	44.04	57.65	33.51	76.445
206	44.06	57.68	33.57	76.52
207	44.04	57.66	33.57	76.5
208	44.06	57.7	33.58	76.415
209	44.2	57.82	33.61	76.35
210	44.64	57.51	33.65	76.32
211	44.55	57.5	33.72	76.335
212	44.2	57.71	33.76	76.375
213	44.1	57.92	33.79	76.36
214	44.07	58.08	33.82	76.365
215	44.16	58.23	33.86	76.445
216	44.27	58.32	33.89	76.49
217	44.33	58.3	33.94	76.51
218	44.35	58.28	33.95	76.55
219	44.42	58.3	34.06	76.55
220	44.48	58.35	34.1	76.55
221	44.53	58.37	34.11	76.56
222	44.54	58.4	34.13	76.54
223	44.52	58.42	34.18	76.435
224	44.56	58.46	34.19	76.455
225	44.63	58.51	34.19	76.45
226	44.69	58.56	34.23	76.45
227	44.69	58.58	34.28	76.445
228	44.73	58.55	34.31	76.45
229	44.76	58.6	34.34	76.555
230	44.78	58.6	34.38	76.555
231	44.8	58.63	34.41	76.52
232	44.81	58.64	34.41	76.54
233	44.83	58.66	34.45	76.56
234	44.86	58.69	34.5	76.605
235	44.91	58.68	34.49	76.595
236	44.92	58.7	34.51	76.61
237	44.93	58.73	34.58	76.645
238	44.97	58.79	34.67	76.68
239	44.96	58.82	34.7	76.755
240	44.96	58.86	34.73	76.745
241	45.02	58.89	34.75	76.775
242	45.01	58.87	34.74	76.79
243	45.09	58.89	34.76	76.785

244	45.15	58.9	34.78	76.72
245	45.16	58.9	34.8	76.75
246	45.15	58.97	34.86	76.845
247	45.11	58.96	34.9	76.845
248	45.09	58.94	34.92	76.78
249	45.11	58.96	34.96	76.755
250	45.13	58.97	34.97	76.705
251	45.12	58.99	35.05	76.7
252	45.15	59.08	35.11	76.715
253	45.2	59.11	35.16	76.73
254	45.21	59.12	35.19	76.795
255	45.19	59.07	35.2	76.71
256	45.17	59.05	35.18	76.645
257	45.19	59.09	35.26	76.65
258	45.22	59.11	35.32	76.565
259	45.28	59.16	35.37	76.495
260	45.33	59.15	35.34	76.57
261	45.37	59.17	35.38	76.73
262	45.41	59.19	35.45	76.765
263	45.48	59.23	35.48	76.705
264	45.5	59.24	35.51	76.685
265	45.56	59.25	35.54	76.705
266	45.53	59.2	35.54	76.7
267	45.55	59.22	35.58	76.81
268	45.54	59.27	35.64	76.885
269	45.58	59.3	35.65	76.805
270	45.61	59.31	35.64	76.725
271	45.64	59.28	35.67	76.7
272	45.61	59.28	35.7	76.8
273	45.62	59.3	35.74	76.94
274	45.62	59.34	35.75	76.935
275	45.62	59.34	35.78	77
276	45.66	59.39	35.8	77.09
277	45.74	59.43	35.83	77.065
278	45.78	59.47	35.85	77.035
279	45.81	59.5	35.91	77.14
280	45.84	59.52	35.98	77.175
281	45.85	59.55	35.97	77.22
282	45.88	59.58	36.02	77.315
283	45.89	59.63	36.04	77.28
284	45.9	59.67	36.01	77.225
285	45.92	59.69	36.02	77.24
286	45.97	59.72	36.07	77.27

287	45.98	59.73	36.1	77.29
288	45.98	59.77	36.14	77.385
289	45.95	59.82	36.19	77.35
290	45.96	59.85	36.27	77.275
291	45.99	59.86	36.32	77.325
292	46.01	59.88	36.34	77.37
293	46.06	59.91	36.35	77.475
294	46.13	59.95	36.42	77.52
295	46.18	59.97	36.47	77.55
296	46.15	59.99	36.47	77.485
297	46.16	59.98	36.5	77.45
298	46.16	59.99	36.52	77.51
299	46.16	60.01	36.56	77.515
300	46.21	60.03	36.62	77.565
301	46.26	60.02	36.65	77.545
302	46.3	60.01	36.62	77.56
303	46.3	60.02	36.66	77.575
304	46.27	60.02	36.7	77.43
305	46.27	60.03	36.72	77.285
306	46.32	60.08	36.78	77.27
307	46.36	60.11	36.83	77.255
308	46.36	60.1	36.87	77.255
309	46.36	60.07	36.84	77.26
310	46.37	60.1	36.88	77.245
311	46.42	60.09	36.92	77.075
312	46.43	60.06	36.91	77.07
313	46.42	60.05	36.95	77.16
314	46.44	60.07	36.98	77.28
315	46.47	60.1	37	77.365
316	46.47	60.1	37	77.4
317	46.5	60.15	37.07	77.4
318	46.51	60.19	37.12	77.43
319	46.54	60.22	37.15	77.43
320	46.58	60.23	37.15	77.405
321	46.61	60.26	37.18	77.465
322	46.62	60.27	37.21	77.495
323	46.62	60.28	37.24	77.485
324	46.63	60.28	37.25	77.485
325	46.63	60.3	37.27	77.365
326	46.67	60.3	37.3	77.4
327	46.69	60.3	37.33	77.455
328	46.69	60.32	37.35	77.415
329	46.7	60.35	37.39	77.395

330	46.71	60.37	37.42	77.45
331	46.76	60.39	37.46	77.475
332	46.78	60.42	37.5	77.53
333	46.81	60.43	37.54	77.59
334	46.84	60.45	37.57	77.585
335	46.86	60.48	37.58	77.48
336	46.9	60.52	37.62	77.405
337	46.87	60.55	37.64	77.46
338	46.89	60.58	37.69	77.46
339	46.96	60.53	37.67	77.455
340	47	60.51	37.68	77.455
341	46.99	60.55	37.71	77.46
342	46.95	60.57	37.79	77.485
343	46.96	60.58	37.83	77.52
344	46.98	60.61	37.87	77.515
345	47.05	60.6	37.91	77.49
346	47.07	60.63	37.94	77.54
347	47.09	60.67	37.97	77.575
348	47.12	60.7	37.98	77.645
349	47.12	60.68	38	77.65
350	47.14	60.7	38.04	77.67
351	47.17	60.71	38.05	77.685
352	47.16	60.72	38.06	77.65
353	47.18	60.74	38.09	77.62
354	47.2	60.75	38.12	77.655
355	47.21	60.77	38.09	77.615
356	47.22	60.77	38.1	77.6
357	47.24	60.79	38.12	77.68
358	47.22	60.79	38.15	77.7
359	47.18	60.8	38.21	77.64
360	47.15	60.79	38.29	77.565
361	47.17	60.77	38.28	77.55
362	47.21	60.84	38.26	77.615
363	47.24	60.85	38.27	77.63
364	47.25	60.85	38.3	77.59
365	47.26	60.86	38.37	77.63
366	47.25	60.84	38.39	77.655
367	47.23	60.78	38.4	77.74
368	47.22	60.72	38.38	77.76
369	47.28	60.74	38.39	77.775
370	47.31	60.77	38.41	77.87
371	47.35	60.8	38.45	77.87
372	47.38	60.81	38.47	77.835

373	47.39	60.81	38.49	77.795
374	47.39	60.83	38.51	77.78
375	47.41	60.84	38.54	77.735
376	47.43	60.85	38.54	77.715
377	47.43	60.88	38.56	77.79
378	47.46	60.89	38.58	77.815
379	47.49	60.93	38.66	77.79
380	47.49	60.93	38.69	77.795
381	47.49	60.93	38.67	77.775
382	47.5	60.94	38.68	77.845
383	47.51	60.93	38.69	77.835
384	47.52	60.92	38.67	77.795
385	47.52	60.93	38.68	77.86
386	47.54	60.92	38.74	77.845
387	47.54	60.94	38.76	77.75
388	47.57	60.98	38.78	77.75
389	47.59	61.01	38.82	77.725
390	47.64	61.04	38.82	77.68
391	47.65	61.05	38.84	77.82
392	47.65	61.08	38.92	77.835
393	47.68	61.1	38.97	77.815
394	47.69	61.13	38.99	77.805
395	47.72	61.13	38.96	77.8
396	47.73	61.09	38.96	77.78
397	47.74	61.05	38.97	77.695
398	47.74	61.07	38.97	77.805
399	47.75	61.13	39.01	77.88
400	47.76	61.17	39.04	77.955
401	47.76	61.21	39.09	78
402	47.75	61.22	39.13	78.005
403	47.74	61.22	39.17	77.99
404	47.75	61.26	39.19	77.995
405	47.81	61.29	39.22	78.06
406	47.87	61.27	39.21	78.045
407	47.91	61.24	39.16	78.025
408	47.89	61.25	39.19	78.02
409	47.89	61.23	39.21	78.04
410	47.92	61.22	39.21	78.07
411	47.95	61.24	39.2	78.105
412	47.93	61.24	39.2	78.15
413	47.94	61.26	39.23	78.215
414	47.96	61.32	39.26	78.33
415	47.98	61.35	39.26	78.425

416	48	61.36	39.24	78.51
417	48.02	61.43	39.29	78.525
418	48.05	61.47	39.35	78.495
419	48.09	61.5	39.39	78.39

Test No.7 new model with various heat fluxes (seven hours)

Time (minutes)	Inlet °C	Outlet °C	Tank °C	wall-1 °C
0	22.20	22.37	22.40	24.99
1	22.25	22.41	22.44	28.63
2	22.33	22.71	22.51	35.90
3	22.41	23.54	22.55	42.13
4	22.52	25.20	22.61	47.08
5	22.66	28.01	22.65	50.95
6	22.79	31.47	22.70	53.85
7	22.92	34.27	22.73	56.09
8	23.29	36.22	22.74	57.89
9	24.25	38.03	22.74	59.37
10	25.61	39.60	22.77	60.63
11	26.94	40.90	22.84	61.74
12	28.09	41.92	22.90	62.75
13	29.09	42.65	22.99	63.69
14	29.98	43.42	23.10	64.57
15	30.79	44.10	23.19	65.23
16	31.49	44.84	23.28	65.91
17	32.10	45.64	23.34	66.46
18	32.68	46.16	23.43	66.99
19	33.23	46.72	23.50	67.52
20	33.75	47.32	23.59	67.93
21	34.20	47.82	23.65	68.14
22	34.66	48.28	23.77	68.45
23	35.13	48.70	23.82	68.85
24	35.55	49.02	23.93	69.18
25	35.93	49.40	24.02	69.51
26	36.27	49.75	24.06	69.77
27	36.59	50.09	24.13	69.97
28	36.86	50.39	24.23	70.16
29	37.08	50.64	24.31	70.33
30	37.34	50.88	24.38	70.44
31	37.59	51.12	24.45	70.76
32	37.81	51.35	24.57	70.94

33	38.03	51.54	24.63	70.97
34	38.22	51.72	24.71	71.02
35	38.42	51.90	24.83	71.14
36	38.59	52.06	24.88	71.34
37	38.71	52.18	24.96	71.44
38	38.83	52.30	25.07	71.56
39	38.94	52.46	25.14	71.74
40	39.05	52.61	25.19	71.82
41	39.18	52.74	25.27	71.88
42	39.26	52.85	25.37	72.01
43	39.36	52.97	25.41	72.06
44	39.46	53.07	25.43	72.21
45	39.51	53.13	25.48	72.19
46	39.59	53.18	25.58	72.04
47	39.71	53.27	25.67	72.00
48	39.79	53.35	25.75	72.04
49	39.84	53.41	25.78	72.14
50	39.92	53.47	25.89	72.23
51	39.99	53.48	26.00	72.27
52	40.07	53.52	25.98	72.27
53	40.14	53.60	26.05	72.52
54	40.18	53.69	26.15	72.50
55	40.21	53.76	26.23	72.41
56	40.25	53.80	26.35	72.16
57	40.31	53.92	26.50	72.29
58	40.39	53.95	26.52	72.43
59	40.46	54.01	26.53	72.55
60	40.53	54.04	26.53	72.62
61	40.58	54.05	26.55	72.70
62	40.64	54.11	26.62	72.78
63	40.71	54.12	26.66	72.75
64	40.75	54.16	26.70	72.71
65	40.80	54.20	26.75	72.83
66	40.84	54.28	26.81	72.98
67	40.86	54.29	26.88	73.02
68	40.89	54.33	26.89	73.13
69	40.96	54.42	26.98	73.19
70	41.00	54.47	27.05	73.18
71	41.05	54.54	27.11	73.09
72	41.10	54.54	27.14	73.15
73	41.11	54.60	27.20	73.07
74	41.11	54.69	27.29	73.13
75	41.14	54.72	27.34	73.30

76	41.18	54.77	27.44	73.36
77	41.20	54.80	27.49	73.35
78	41.20	54.80	27.50	73.33
79	41.25	54.83	27.56	73.26
80	41.31	54.86	27.62	73.25
81	41.36	54.88	27.66	73.25
82	41.41	54.95	27.73	73.38
83	41.46	55.03	27.87	73.53
84	41.52	55.09	27.93	73.63
85	41.55	55.09	27.97	73.64
86	41.58	55.17	28.08	73.73
87	41.60	55.22	28.12	73.57
88	41.64	55.25	28.16	73.50
89	41.71	55.27	28.21	73.63
90	41.73	55.29	28.25	72.01
91	41.71	54.87	28.28	65.61
92	41.65	53.77	28.33	59.39
93	41.41	52.22	28.35	54.35
94	40.94	50.64	28.33	50.42
95	40.32	49.08	28.40	47.42
96	39.58	47.69	28.40	44.95
97	38.81	46.40	28.43	42.99
98	38.07	45.21	28.49	41.40
99	37.30	44.08	28.46	40.06
100	36.62	43.11	28.47	38.88
101	36.02	42.18	28.49	37.85
102	35.41	41.29	28.48	36.98
103	34.84	40.47	28.46	36.21
104	34.36	39.74	28.46	35.48
105	33.92	39.03	28.48	36.80
106	33.48	38.55	28.49	42.94
107	33.02	38.60	28.50	48.99
108	32.70	39.32	28.53	53.84
109	32.50	40.67	28.55	57.45
110	32.53	42.37	28.59	60.25
111	32.80	43.75	28.63	62.37
112	33.29	45.05	28.66	63.97
113	33.95	46.25	28.69	65.26
114	34.66	47.16	28.69	66.48
115	35.33	47.98	28.72	67.45
116	35.94	48.65	28.77	68.17
117	36.51	49.21	28.84	68.88
118	37.05	49.76	28.89	69.57

119	37.49	50.30	28.90	70.00
120	37.89	50.78	28.93	70.42
121	38.30	51.22	28.97	70.88
122	38.67	51.62	28.99	71.21
123	39.03	52.01	29.04	71.60
124	39.31	52.34	29.09	71.84
125	39.64	52.66	29.13	72.06
126	39.95	52.96	29.19	72.22
127	40.20	53.24	29.28	72.61
128	40.39	53.50	29.31	72.62
129	40.62	53.76	29.35	72.71
130	40.87	53.94	29.45	72.84
131	41.09	54.13	29.53	73.01
132	41.26	54.30	29.56	73.08
133	41.44	54.46	29.61	73.26
134	41.59	54.59	29.65	73.43
135	41.71	54.72	29.69	73.40
136	41.79	54.84	29.72	73.38
137	41.88	54.99	29.79	73.33
138	41.94	55.10	29.83	73.22
139	42.03	55.19	29.87	73.35
140	42.12	55.25	29.91	73.52
141	42.21	55.34	29.96	73.71
142	42.35	55.44	30.03	73.80
143	42.45	55.53	30.09	73.87
144	42.56	55.61	30.16	73.89
145	42.63	55.68	30.24	74.05
146	42.70	55.76	30.26	74.21
147	42.70	55.76	30.30	74.19
148	42.71	55.75	30.28	74.12
149	42.81	55.81	30.36	74.09
150	42.90	55.88	30.43	74.19
151	42.97	55.95	30.48	74.24
152	43.03	56.00	30.52	74.39
153	43.09	56.08	30.57	74.44
154	43.18	56.16	30.64	74.51
155	43.24	56.22	30.72	74.26
156	43.27	56.24	30.72	74.26
157	43.29	56.26	30.76	74.30
158	43.33	56.30	30.81	74.36
159	43.38	56.38	30.90	74.46
160	43.40	56.44	30.92	74.39
161	43.44	56.43	31.00	74.45

162	43.49	56.46	31.07	74.45
163	43.54	56.52	31.13	74.52
164	43.58	56.57	31.21	74.56
165	43.65	56.63	31.26	74.49
166	43.70	56.67	31.33	74.43
167	43.70	56.71	31.39	74.45
168	43.75	56.75	31.43	74.42
169	43.80	56.79	31.44	74.64
170	43.85	56.83	31.51	74.68
171	43.88	56.87	31.57	74.65
172	43.91	56.90	31.65	74.77
173	43.96	56.95	31.75	74.74
174	44.03	56.99	31.74	74.78
175	44.08	57.02	31.81	74.84
176	44.08	57.01	31.84	74.75
177	44.10	57.03	31.83	74.75
178	44.13	57.03	31.88	74.84
179	44.14	57.04	31.91	74.84
180	44.16	57.07	31.96	74.81
181	44.23	57.13	32.06	74.87
182	44.25	57.14	32.10	74.85
183	44.24	57.14	32.09	74.80
184	44.22	57.14	32.11	74.79
185	44.28	57.15	32.16	74.81
186	44.32	57.16	32.19	74.78
187	44.34	57.21	32.25	74.98
188	44.38	57.27	32.34	75.00
189	44.43	57.32	32.37	74.95
190	44.44	57.33	32.42	74.94
191	44.41	57.33	32.46	75.05
192	44.43	57.34	32.45	75.14
193	44.51	57.37	32.55	75.03
194	44.55	57.41	32.61	75.00
195	44.54	57.40	32.63	73.16
196	44.53	56.89	32.66	66.78
197	44.49	55.85	32.69	60.67
198	44.20	54.40	32.71	55.66
199	43.71	52.81	32.74	51.78
200	43.04	51.24	32.76	48.72
201	42.29	49.74	32.74	46.25
202	41.51	48.42	32.72	44.27
203	40.70	47.14	32.68	42.65
204	39.98	46.07	32.70	41.34

205	39.30	45.04	32.69	40.19
206	38.67	44.10	32.72	39.20
207	38.10	43.22	32.72	38.30
208	37.59	42.40	32.71	37.54
209	37.13	41.65	32.73	36.84
210	36.65	40.94	32.73	37.99
211	36.23	40.47	32.74	44.08
212	35.81	40.46	32.74	50.29
213	35.41	41.12	32.72	55.24
214	35.15	42.41	32.70	58.83
215	35.18	44.12	32.75	61.46
216	35.43	45.90	32.79	63.51
217	35.94	47.23	32.83	65.11
218	36.59	48.12	32.85	66.37
219	37.28	48.98	32.86	67.44
220	37.93	49.77	32.89	68.42
221	38.52	50.42	32.92	69.23
222	39.08	51.01	32.94	69.88
223	39.54	51.53	32.92	70.51
224	39.99	52.09	32.95	71.00
225	40.41	52.59	33.01	71.40
226	40.84	53.10	33.05	71.79
227	41.20	53.52	33.03	72.14
228	41.54	53.92	33.06	72.49
229	41.85	54.28	33.10	72.77
230	42.12	54.61	33.12	72.93
231	42.39	54.91	33.16	73.13
232	42.65	55.19	33.26	73.26
233	42.88	55.42	33.30	73.46
234	43.10	55.68	33.32	73.49
235	43.29	55.86	33.34	73.58
236	43.47	56.04	33.34	73.79
237	43.64	56.23	33.37	73.88
238	43.79	56.39	33.38	74.04
239	43.90	56.49	33.40	74.06
240	44.01	56.60	33.41	74.20
241	44.09	56.71	33.43	74.33
242	44.18	56.79	33.46	74.32
243	44.25	56.89	33.52	74.40
244	44.33	56.98	33.58	74.46
245	44.38	57.04	33.62	74.44
246	44.45	57.11	33.64	74.46
247	44.55	57.19	33.71	74.38

248	44.60	57.27	33.74	74.49
249	44.66	57.35	33.75	74.54
250	44.73	57.41	33.80	74.58
251	44.78	57.44	33.81	74.57
252	44.87	57.48	33.83	74.54
253	44.94	57.50	33.86	74.56
254	44.99	57.54	33.92	74.67
255	45.02	57.57	33.95	74.63
256	45.02	57.61	33.99	74.77
257	44.97	57.66	34.03	74.64
258	44.99	57.70	34.05	74.57
259	45.04	57.74	34.08	74.56
260	45.11	57.77	34.13	74.60
261	45.13	57.80	34.16	74.56
262	45.14	57.83	34.19	74.50
263	45.20	57.85	34.25	74.65
264	45.25	57.87	34.30	74.75
265	45.30	57.92	34.35	74.71
266	45.35	57.97	34.42	74.73
267	45.35	57.98	34.46	74.88
268	45.35	58.02	34.50	74.97
269	45.36	58.06	34.54	75.01
270	45.43	58.08	34.53	74.96
271	45.50	58.12	34.59	75.00
272	45.54	58.16	34.67	75.02
273	45.55	58.16	34.69	75.02
274	45.51	58.16	34.69	74.88
275	45.50	58.13	34.68	74.92
276	45.52	58.13	34.70	74.82
277	45.56	58.14	34.73	74.88
278	45.58	58.17	34.77	74.89
279	45.60	58.19	34.82	74.96
280	45.62	58.24	34.89	75.06
281	45.65	58.27	34.93	75.05
282	45.67	58.29	34.95	75.05
283	45.72	58.31	34.96	75.07
284	45.77	58.34	34.98	75.09
285	45.79	58.38	35.04	75.05
286	45.81	58.40	35.13	75.05
287	45.82	58.43	35.20	75.20
288	45.83	58.45	35.25	75.17
289	45.87	58.46	35.31	75.00
290	45.88	58.47	35.37	74.90

291	45.91	58.50	35.42	74.84
292	45.97	58.51	35.42	74.93
293	46.00	58.50	35.43	74.97
294	46.02	58.48	35.44	74.92
295	46.03	58.50	35.44	74.92
296	46.05	58.53	35.47	75.04
297	46.08	58.57	35.51	75.07
298	46.11	58.60	35.54	75.24
299	46.11	58.62	35.58	75.30
300	46.11	58.59	35.58	73.35
301	46.04	58.05	35.60	66.98
302	45.93	56.93	35.60	60.68
303	45.63	55.49	35.62	55.67
304	45.13	53.91	35.61	51.84
305	44.50	52.35	35.62	48.84
306	43.78	50.88	35.62	46.47
307	43.06	49.56	35.63	44.50
308	42.33	48.31	35.63	42.95
309	41.60	47.16	35.62	41.62
310	40.90	46.13	35.62	40.44
311	40.26	45.18	35.61	39.44
312	39.69	44.30	35.60	38.56
313	39.19	43.51	35.61	37.88
314	38.70	42.72	35.59	37.21
315	38.23	41.97	35.57	38.47
316	37.80	41.50	35.58	44.55
317	37.38	41.48	35.56	50.66
318	36.98	42.04	35.53	55.40
319	36.74	43.26	35.50	58.91
320	36.67	44.95	35.51	61.59
321	36.84	46.85	35.52	63.48
322	37.29	48.26	35.57	65.08
323	37.92	49.12	35.60	66.47
324	38.59	50.10	35.58	67.56
325	39.26	50.88	35.63	68.52
326	39.88	51.55	35.66	69.42
327	40.43	52.11	35.66	70.12
328	40.94	52.63	35.68	70.77
329	41.39	53.16	35.72	71.27
330	41.79	53.67	35.75	71.75
331	42.19	54.14	35.76	72.17
332	42.57	54.58	35.80	72.48
333	42.89	55.00	35.81	72.77

334	43.21	55.37	35.83	73.08
335	43.51	55.72	35.85	73.50
336	43.77	56.02	35.86	73.78
337	44.03	56.32	35.89	73.93
338	44.27	56.61	35.91	74.09
339	44.50	56.86	35.97	74.34
340	44.71	57.07	36.02	74.54
341	44.90	57.29	36.04	74.60
342	45.06	57.50	36.08	74.56
343	45.20	57.65	36.11	74.62
344	45.34	57.77	36.10	74.69
345	45.49	57.91	36.12	74.88
346	45.60	58.05	36.15	75.01
347	45.71	58.15	36.17	74.95
348	45.81	58.22	36.15	75.04
349	45.93	58.33	36.21	75.11
350	46.02	58.42	36.27	75.15
351	46.08	58.48	36.30	75.14
352	46.15	58.58	36.36	75.20
353	46.21	58.69	36.39	75.33
354	46.30	58.75	36.42	75.42
355	46.37	58.81	36.47	75.54
356	46.42	58.89	36.52	75.64
357	46.47	58.96	36.57	75.62
358	46.52	58.99	36.58	75.47
359	46.52	58.97	36.60	75.52
360	46.58	59.00	36.62	75.61
361	46.63	59.04	36.65	75.56
362	46.68	59.07	36.69	75.57
363	46.72	59.13	36.74	75.76
364	46.73	59.17	36.73	75.63
365	46.77	59.20	36.74	75.62
366	46.81	59.25	36.78	75.62
367	46.80	59.26	36.79	75.55
368	46.78	59.28	36.82	75.58
369	46.80	59.30	36.84	75.55
370	46.80	59.28	36.84	75.68
371	46.81	59.28	36.86	75.69
372	46.85	59.32	36.90	75.55
373	46.91	59.35	36.93	75.54
374	46.92	59.38	36.97	75.65
375	46.95	59.44	37.01	75.59
376	46.96	59.48	37.06	75.71

377	46.98	59.50	37.10	75.72
378	47.01	59.50	37.13	75.64
379	47.02	59.50	37.17	75.45
380	47.05	59.50	37.21	75.54
381	47.06	59.49	37.24	75.51
382	47.07	59.46	37.26	75.57
383	47.11	59.47	37.30	75.69
384	47.10	59.51	37.39	75.72
385	47.13	59.56	37.42	75.66
386	47.18	59.61	37.50	75.59
387	47.19	59.62	37.53	75.71
388	47.18	59.63	37.55	75.56
389	47.21	59.63	37.57	75.56
390	47.22	59.62	37.63	75.52
391	47.23	59.65	37.64	75.58
392	47.22	59.66	37.64	75.66
393	47.20	59.67	37.65	75.52
394	47.22	59.66	37.65	75.47
395	47.21	59.67	37.68	75.30
396	47.20	59.68	37.71	75.30
397	47.23	59.71	37.73	75.43
398	47.26	59.73	37.75	75.53
399	47.24	59.68	37.79	75.62
400	47.21	59.68	37.80	75.54
401	47.25	59.73	37.83	75.48
402	47.28	59.76	37.86	75.51
403	47.35	59.77	37.87	75.50
404	47.39	59.77	37.92	75.50
405	47.38	59.70	37.92	73.66
406	47.37	59.18	37.95	67.34
407	47.23	58.10	37.98	61.24
408	46.87	56.67	37.98	56.25
409	46.36	55.12	37.96	52.31
410	45.72	53.54	37.96	49.28
411	45.03	52.07	37.96	46.93
412	44.33	50.68	37.95	45.08
413	43.59	49.40	37.96	43.55
414	42.90	48.25	37.92	42.21
415	42.25	47.19	37.92	41.05
416	41.61	46.24	37.94	40.07
417	41.03	45.34	37.92	39.19
418	40.47	44.48	37.88	38.37
419	39.96	43.69	37.85	37.68

APPENDIX G

To calculate Nussult number, it can be used the equation below

$$Nu = \frac{h\,D}{k}$$

Where D is inner diameter of the riser pipe, k is thermal conductivity of working fluid and h is heat transfer coefficient which calculate as below

$$h = \frac{q}{Tw - Tref}$$

Where q is heat flux, Tw is collector temperature and $Tref$ is reference temperature of working fluid which calculate as below

$$\mathrm{Tref} = \frac{\mathrm{Tin} + \mathrm{Tout}}{2}$$

Where Tin and Tout are temperature of working fluid at the inlet and outlet of collector respectively.

Nu (CFD)	q/qmax	TL/Tlavr	np	L/d	Time/non	Nu (Equation)
0.851845	0.72497	2.409953	5	50	0.833333	0.798595
0.924957	0.92619	2.244076	5	50	0.916667	0.900366
0.966407	1	2.127962	5	50	1	0.937298
0.925486	0.92722	1.829384	5	50	1.083333	0.916824
0.832319	0.725818	1.829384	5	50	1.166667	0.818225
0.631881	0.450903	1.779621	5	50	1.25	0.657431
0.411685	0.194735	1.779621	5	50	1.333333	0.445079
0.869849	0.72497	2.409953	5	75	0.833333	0.839562
0.944056	0.92619	2.244076	5	75	0.916667	0.946553
1.014452	1	2.127962	5	75	1	0.98538
0.968555	0.92722	1.829384	5	75	1.083333	0.963855
0.848052	0.725818	1.829384	5	75	1.166667	0.860199
0.662463	0.450903	1.779621	5	75	1.25	0.691156
0.437938	0.194735	1.779621	5	75	1.333333	0.467911
0.882682	0.72497	2.409953	5	100	0.833333	0.869897
0.972895	0.92619	2.244076	5	100	0.916667	0.980754
1.072501	1	2.127962	5	100	1	1.020983
1.025407	0.92722	1.829384	5	100	1.083333	0.998681
0.859406	0.725818	1.829384	5	100	1.166667	0.891279
0.767968	0.450903	1.779621	5	100	1.25	0.716129

0.44208	0.194735	1.779621	5	100	1.333333	0.484817
1.102705	0.72497	2.409953	7	75	0.833333	1.140791
1.221681	0.92619	2.244076	7	75	0.916667	1.286169
1.330399	1	2.127962	7	75	1	1.338926
1.307273	0.92722	1.829384	7	75	1.083333	1.309679
1.112307	0.725818	1.829384	7	75	1.166667	1.168831
1.012009	0.450903	1.779621	7	75	1.25	0.939138
0.652101	0.194735	1.779621	7	75	1.333333	0.635793
1.311635	0.72497	2.409953	9	75	0.833333	1.434363
1.466941	0.92619	2.244076	9	75	0.916667	1.617154
1.626426	1	2.127962	9	75	1	1.683487
1.611159	0.92722	1.829384	9	75	1.083333	1.646714
1.346156	0.725818	1.829384	9	75	1.166667	1.46962
1.309391	0.450903	1.779621	9	75	1.25	1.180817
1.028859	0.194735	1.779621	9	75	1.333333	0.799409
0.944421	0.747775	2.409953	5	100	0.833333	0.882506
1.047739	0.932345	2.244076	5	100	0.916667	0.983777
1.136692	1	2.127962	5	100	1	1.020983
1.09911	0.933576	1.829384	5	100	1.083333	1.001856
0.928777	0.748849	1.829384	5	100	1.166667	0.904309
0.753129	0.494542	1.779621	5	100	1.25	0.747534
0.551945	0.252317	1.779621	5	100	1.333333	0.546824
0.825947	0.729945	2.409953	5	100	0.833333	0.872666
0.909375	0.927646	2.244076	5	100	0.916667	0.98147
0.985312	1	2.127962	5	100	1	1.020983
0.961265	0.92838	1.829384	5	100	1.083333	0.999261
0.813611	0.730544	1.829384	5	100	1.166667	0.893971
0.677549	0.460631	1.779621	5	100	1.25	0.723266
0.469925	0.209161	1.779621	5	100	1.333333	0.501185
0.883527	0.72497	2.075914	5	100	0.833333	0.881148
0.967261	0.92619	2.154639	5	100	0.916667	0.984196
1.078866	1	2.154639	5	100	1	1.019888
1.030333	0.92722	2.141518	5	100	1.083333	0.985222
0.852524	0.725818	1.970947	5	100	1.166667	0.885576
0.730423	0.450903	1.806935	5	100	1.25	0.71519
0.489832	0.194735	1.695408	5	100	1.333333	0.486846

To calculate Reynolds number, it can be used the equation below

$$R_e = \frac{\rho V D}{\mu} = \frac{4\dot{m}}{\pi \mu D}$$

Where ṁ is mass flow rate of working fluid within the thermo-syphon loop, D is inner diameter of the riser pipe, μ is dynamic viscosity of working fluid

Re	q/qmax	TL/Tlavr	np	L/d	Time/non	Re (Equation)
260.0752	0.72497	2.409953	5	50	0.833333	270.9043
297.0083	0.92619	2.244076	5	50	0.916667	291.6195
308.3416	1	2.127962	5	50	1	302.1865
300.893	0.92722	1.829384	5	50	1.083333	295.1933
284.3843	0.725818	1.829384	5	50	1.166667	285.8301
256.4761	0.450903	1.779621	5	50	1.25	260.2389
225.0523	0.194735	1.779621	5	50	1.333333	218.6559
324.993	0.72497	2.409953	5	75	0.833333	335.8747
371.5053	0.92619	2.244076	5	75	0.916667	361.5579
376.8585	1	2.127962	5	75	1	374.6592
366.4997	0.92722	1.829384	5	75	1.083333	365.9889
347.201	0.725818	1.829384	5	75	1.166667	354.3801
312.9246	0.450903	1.779621	5	75	1.25	322.6514
272.9301	0.194735	1.779621	5	75	1.333333	271.0957
381.2591	0.72497	2.409953	5	100	0.833333	391.2175
440.5178	0.92619	2.244076	5	100	0.916667	421.1326
438.1195	1	2.127962	5	100	1	436.3926
426.3695	0.92722	1.829384	5	100	1.083333	426.2937
410.4011	0.725818	1.829384	5	100	1.166667	412.7721
368.71	0.450903	1.779621	5	100	1.25	375.8153
329.0882	0.194735	1.779621	5	100	1.333333	315.7647
330.228	0.72497	2.409953	7	75	0.833333	342.5192
380.2494	0.92619	2.244076	7	75	0.916667	368.7105
388.3415	1	2.127962	7	75	1	382.0709
372.2348	0.92722	1.829384	7	75	1.083333	373.2291
356.1328	0.725818	1.829384	7	75	1.166667	361.3907
318.5655	0.450903	1.779621	7	75	1.25	329.0343
274.4935	0.194735	1.779621	7	75	1.333333	276.4587
335.7087	0.72497	2.409953	9	75	0.833333	347.5677
388.945	0.92619	2.244076	9	75	0.916667	374.145
393.538	1	2.127962	9	75	1	387.7023
378.4541	0.92722	1.829384	9	75	1.083333	378.7302
367.904	0.725818	1.829384	9	75	1.166667	366.7173
329.7088	0.450903	1.779621	9	75	1.25	333.884
285.4956	0.194735	1.779621	9	75	1.333333	280.5334
417.568	0.747775	2.409953	5	100	0.833333	394.0528
471.9984	0.932345	2.244076	5	100	0.916667	421.7834
465.9522	1	2.127962	5	100	1	436.3926
451.8269	0.933576	1.829384	5	100	1.083333	426.9731

440.2482	0.748849	1.829384	5	100	1.166667	415.7893
404.24	0.494542	1.779621	5	100	1.25	383.9973
360.1413	0.252317	1.779621	5	100	1.333333	335.4234
352.8815	0.729945	2.409953	5	100	0.833333	391.8419
407.0265	0.927646	2.244076	5	100	0.916667	421.2869
413.0555	1	2.127962	5	100	1	436.3926
396.6042	0.92838	1.829384	5	100	1.083333	426.4179
381.2558	0.730544	1.829384	5	100	1.166667	413.3971
347.4916	0.460631	1.779621	5	100	1.25	377.6901
307.1569	0.209161	1.779621	5	100	1.333333	321.0699
381.1717	0.72497	2.075914	5	100	0.833333	378.8125
441.0414	0.92619	2.154639	5	100	0.916667	417.4499
436.4257	1	2.154639	5	100	1	437.5683
424.2619	0.92722	2.141518	5	100	1.083333	441.0463
408.9949	0.725818	1.970947	5	100	1.166667	419.47
369.7997	0.450903	1.806935	5	100	1.25	377.0536
320.3036	0.194735	1.695408	5	100	1.333333	312.4761

To calculate reference temperature of working fluid, it can be used equation below

$$T_{ref} = \frac{T_i + T_o}{2}$$

Where Tin and Tout are temperature of working fluid at the inlet and outlet of collector respectively

Tw/Tref (CFD)	q/qmax	TL/Tlavr	np	L/d	Time/non	Tw/Tref (Equation)
1.20917	0.72497	2.409953	5	50	0.833333	1.197976
1.19795	0.92619	2.244076	5	50	0.916667	1.191634
1.186707	1	2.127962	5	50	1	1.181825
1.179069	0.92722	1.829384	5	50	1.083333	1.171349
1.15383	0.725818	1.829384	5	50	1.166667	1.15434
1.125536	0.450903	1.779621	5	50	1.25	1.133167
1.086768	0.194735	1.779621	5	50	1.333333	1.103668
1.168322	0.72497	2.409953	5	75	0.833333	1.162735
1.155631	0.92619	2.244076	5	75	0.916667	1.156579
1.145727	1	2.127962	5	75	1	1.147059
1.139964	0.92722	1.829384	5	75	1.083333	1.136891
1.123567	0.725818	1.829384	5	75	1.166667	1.120383
1.097161	0.450903	1.779621	5	75	1.25	1.099833
1.065398	0.194735	1.779621	5	75	1.333333	1.071201
1.142202	0.72497	2.409953	5	100	0.833333	1.138361
1.126729	0.92619	2.244076	5	100	0.916667	1.132335

1.11726	1	2.127962	5	100	1	1.123014
1.11174	0.92722	1.829384	5	100	1.083333	1.11306
1.103517	0.725818	1.829384	5	100	1.166667	1.096897
1.070774	0.450903	1.779621	5	100	1.25	1.076778
1.053352	0.194735	1.779621	5	100	1.333333	1.048746
1.129393	0.72497	2.409953	7	75	0.833333	1.129037
1.116287	0.92619	2.244076	7	75	0.916667	1.12306
1.107612	1	2.127962	7	75	1	1.113815
1.100003	0.92722	1.829384	7	75	1.083333	1.103942
1.09129	0.725818	1.829384	7	75	1.166667	1.087912
1.061459	0.450903	1.779621	7	75	1.25	1.067958
1.042078	0.194735	1.779621	7	75	1.333333	1.040155
1.106402	0.72497	2.409953	9	75	0.833333	1.104506
1.093849	0.92619	2.244076	9	75	0.916667	1.098659
1.0855	1	2.127962	9	75	1	1.089615
1.07827	0.92722	1.829384	9	75	1.083333	1.079957
1.072988	0.725818	1.829384	9	75	1.166667	1.064275
1.045934	0.450903	1.779621	9	75	1.25	1.044754
1.025651	0.194735	1.779621	9	75	1.333333	1.017556
1.141293	0.747775	2.409953	5	100	0.833333	1.139129
1.126528	0.932345	2.244076	5	100	0.916667	1.132498
1.11818	1	2.127962	5	100	1	1.123014
1.110368	0.933576	1.829384	5	100	1.083333	1.113225
1.104002	0.748849	1.829384	5	100	1.166667	1.097643
1.083662	0.494542	1.779621	5	100	1.25	1.078946
1.057879	0.252317	1.779621	5	100	1.333333	1.054679
1.141632	0.729945	2.409953	5	100	0.833333	1.138531
1.126577	0.927646	2.244076	5	100	0.916667	1.132374
1.118081	1	2.127962	5	100	1	1.123014
1.110793	0.92838	1.829384	5	100	1.083333	1.11309
1.102242	0.730544	1.829384	5	100	1.166667	1.097052
1.076386	0.460631	1.779621	5	100	1.25	1.077278
1.050343	0.209161	1.779621	5	100	1.333333	1.050379
1.14205	0.72497	2.075914	5	100	0.833333	1.14149
1.127153	0.92619	2.154639	5	100	0.916667	1.133182
1.119399	1	2.154639	5	100	1	1.122756
1.114865	0.92722	2.141518	5	100	1.083333	1.109839
1.108001	0.725818	1.970947	5	100	1.166667	1.095394
1.076993	0.450903	1.806935	5	100	1.25	1.076476
1.050064	0.194735	1.695408	5	100	1.333333	1.049682

LIST OF PUBLICATIONS

- Freegah, B. Asim, T. and Mishra, R. (2013) "Computational Fluid Dynamics based Analysis of a Closed Thermo-Siphon Hot Water Solar System", 26th International Congress of Condition Monitoring and Diagnostic Engineering Management

- Freegah, B. Asim, T. and Mishra, R. (2013) "Effects of condenser volume on the performance of a solar thermo-syphon", Annual Researchers Conference Computing and Engineering 2013 (CEARC'13), December 2013, University of Huddersfield, Huddersfield, UK, pp. 140-145

- Freegah, B. Asim, T. and Mishra, R. (2013) "Numerical Analysis of a Closed Thermo-syphon Hot Water Solar System under Steady and Transient Loading Conditions", 40th National Conference on Fluid Mechanics & Fluid Power FMFP 2013

- Freegah, B. Asim, T. Albarzenji, D. Pradhan, S. and Mishra, R. (2014) "Effect of the shape of connecting pipes on the performance output of a closed-loop hot water solar Thermo-syphon", 3rd International Workshop and Congress on e-Maintenance

- Freegah, B. Asim, T. and Mishra, R. and Zala. K. (2015) "Numerical investigations on the effects of transient heat input and loading conditions on the performance of a single-phase closed-loop thermo-syphon", 42th National Conference on Fluid Mechanics & Fluid Power FMFP 2015

- Freegah, B. Asim, T. and Mishra, R. (2015) "Effect of Solar Heat Flux and Thermal Loading on the Flow Distribution within the Riser Pipes of a Closed-Loop Thermo-syphon Solar Water Heater System", 28th International Congress of Condition Monitoring and Diagnostic Engineering Management